Mathematical modelling of paper degradation in books

Alexander James Nimmo
University College London
Department of Chemical Engineering
Thesis submitted for the degree of Doctor of Philosophy

8th September 2015

I, Alexander James Nimmo, confirm that the work presented in this thesis is my own. Where information has been derived from other sources, I confirm that this has been indicated in the thesis.

_____

Alex Nimmo

Abstract

Paper cannot be prevented from degrading and does not necessarily degrade uniformly across its volume. It has been established that as paper degrades, VOCs (Volatile Organic Compounds) are produced. This body of work studies paper degradation with respect to the role VOCs play.

The thesis investigates how a VOC affecting the paper's acidity can in turn affect the degradation rate and through modelling the VOC concentration profile, the degradation profile is found. To create the model from a chemical engineering perspective, mass transfer fundamentals are explored: diffusion through porous a medium, chemical reaction, and adsorption are utilised.

Current literature highlights acetic acid as a representative VOC in paper due to its presence in all different paper types and is used as the VOC for the model.

To aid simulation of the model, experimentation was carried out for four different paper samples for the porosity, surface area, pore diameter, effective diffusion coefficient and the adsorption coefficient. For adsorption experimentation, propionic acid was used as a substitute for acetic acid due to limitations of measuring devices available.

To run the simulations, gPROMS was used and the results showed how acetic acid negatively affects the degradation rate of paper, how the degradation profile can vary across a paper volume and what measures can be taken to improve the life span of paper. The results also showed how paper with an alkaline reserve can avoid the effects of acetic acid as it is neutralised by the reserve.

The simulations showed how storing paper in a sealed fitted container ensures uniform degradation, but the VOC cannot escape and so increases the degradation rate. Paper stored on a shelf allows the VOC to escape, but can cause noticeable non-uniform degradation across the volume. The simulations displayed the advantage of using the lower temperature and relative humidity.

Acknowledgements

"What an astonishing thing a book is. It's a flat object made from a tree with flexible parts on which are imprinted lots of funny dark squiggles. But one glance at it and you're inside the mind of another person, maybe somebody dead for thousands of years. Across the millennia, an author is speaking clearly and silently inside your head, directly to you. Writing is perhaps the greatest of human inventions, binding together people who never knew each other, citizens of distant epochs. Books break the shackles of time. A book is proof that humans are capable of working magic."

-Carl Sagan

Contents

List of Figures

List of Tables

Nomenclature

$[X]$ The concentration of X in the liquid phase

$\dot{V}_X$ Volumetric flowrate of X

η The Avogadro constant

γ Surface tension

κ The Boltzmann constant

λ The mean free path

$\mathbf{J}_A$ The diffusive flux of A

$\mathbf{N}_A$ The molar flux of A

$\mathbf{n}_A$ The mass flux of A

μ The viscosity

Ω_{AB} Collision integral for use with Lennard-Jones potential

ω_X Volumetric fraction of X

ψ Ratio between porosity and tortuosity

ρ_A The density of A

σ The unit surface area per unit volume

σ_{AB} Lennard-Jones parameter

τ The tortuosity

θ Contact angle

$\tilde{\mathbf{x}}$ The non-dimensionalised length

$\tilde{t}$ The non-dimensionalised time

ε The porosity, or void fraction

φ The dimensionless concentration

A The pre-exponential factor with regards to the Arrhenius equation

A_s Specific surface area

Acc_x The accumulation term for x

C_r The concentration scale

D_{AB} The diffusion coefficient of A through B in a binary mixture

D_{Ae} The effective diffusion coefficient of A

D_A Diffusion coefficient of A

D_{KA}, D_K The Knudsen diffusion coefficient

d_{pore} The pore diameter

E The activation energy with regards to the Arrhenius equation

K_A The (Henry) adsorption equilibrium constant for A

K_{BET} BET constant

k_c The mass transfer coefficient

k_{DP} The degradation reaction rate constant

k_m The mass transfer coefficient relating to mass transfer
from the pore bulk volume to the surface of the pore

Ka The acid dissociation constant

Kn The Knudsen number

L The charateristic length

m mass

$M\{X\}$ The magnitude of X

M_A The molecular weight of A

N Number of monomers in cellulose

n Number of chains of cellulose

P,p Pressure

pKa The logarithm of the acid dissociation equilibrium constant

R The universal gas constant

r radius

r_A The rate of reaction for A

Re The Reynolds number

Sc The Schmidt number

Sh The Sherwood number

T The absolute temperature

t_r The time scale

V_X Volume of X

x_r The length scale

$y(t)$ The mean number of glycosidic bonds in celluose that break per unit time

y_i The mole fraction of component i

$\mathbf{v_A}$ The velocity of A

DMF   Dimethylformamide, a common solvent for chemical reactions

DP   Degree of polymerisation

IAQ   Indoor Air Quality

sccm   Standard Cubic Centimeters per Minute

Chapter 1

Introduction

Degradation, in general terms, is a process by which materials lose their desirable properties over time. The degradation process relies on various factors that influence how quickly this occurs. Therefore, to preserve objects for longer, we need to understand in detail these factors and what measures we can take to eliminate, or at least reduce as much as possible, their effects. For example, outdoor wooden furniture has sealant on it to slow the effect of natural weathering and biological specimens are typically preserved in formaldehyde.

This work is concerned with book degradation, or more particularly with paper degradation and the loss of the paper's properties due to this process.

In our exploration of paper degradation, the factor we are interested in is the role that Volatile Organic Compounds (VOCs) play in the process. VOCs make up the majority of indoor pollutants [Xiong et al., 2012] and it is known that these compounds are present in paper at higher concentrations when the paper has degraded; however, we want to delve further and see how the VOCs participate in the degradation process.

To investigate the VOCs' role in the degradation process from a chemical engineering perspective, we study how VOCs as gases diffuse and react with paper within books, trying to characterise what happens locally within their matrix, which we regard as a porous medium.

To achieve this, we create a model describing a VOC's movement through the paper. In order to solve these models, we use computational tools, such as gPROMS and Matlab or Computational Fluid Dynamics (CFD) software.

1.1 Why preservation and knowledge on degradation are important

As mentioned earlier, when materials degrade they lose their desirable properties. In the case of paper and books, when they have degraded beyond a certain point they become useless, as the information

they held is no longer legible. As the paper degrades, its quality decreases. As users of the paper, we experience this in various ways. For example, the loss of colour in the ink on the paper, the change of colour (typically yellowing) of the paper and the paper becoming more fragile to the touch. We therefore want to prevent or slow down the paper degradation process in order to preserve the content on the paper.

The importance of being able to preserve paper can easily be overlooked when people see how much computers are involved in our life as more and more information is stored and viewed electronically on devices such as the Amazon Kindle, Apple IPad and other e-book readers.

Digital information has not existed for comparatively long and the format in which this information is stored is constantly changing. For example, the most common form of image file format, JPEG [JPEG committee, 2010], has been around since 1992, and there are various other file types (PNG, TIFF and GIF are the most well-known). However, forms of paper have been used, and are still being used, since approximately 2000 years ago.

It is true that historical artefacts can be scanned into a digital format, but how much information can be scanned in will always be limited by the technology. Scanners today can get 600 DPI (Dots Per Inch) for their quality [Fujitsu Europe, 2014]. As scanners improve they can take in more information, but without the original there is no benefit to the improvement.

Assuming it was possible to scan all the information from a historical artefact, collection institutions would still need to account for the costs of digital preservation and the associated problems. In addition to needing the space for storing the digital information, possible problems include [Wright et al., 2008]:

- Technical obsolescence, e.g. digital formats and players

- Hardware failures, e.g. digital storage systems

- Loss of staff, e.g. skilled transfer operators

- Insufficient budget, e.g. digitisation too expensive

- Accidental loss, e.g. human error

- Stakeholder changes, e.g. preservation no longer a priority

- Underestimation of resources or effort

- Fire, flood ...

Figures 1.1 and 1.2 show scanned images the British Library has available on their website, with Figure 1.2 demonstrating the ability to zoom-in. These scanned images can then be viewed without the risk of further damage.

These historical artefacts have a value as pieces of art as well as being a source of information, and so their preservation from this perspective is important, for example keeping Leonardo Da Vinci's notebooks from degrading further, or the sketchbooks of various artists including William Blake and

Figure 1.1: British Library Psalter World Map c.1265 © The British Library Board, BL Add MS 28681 [British Library, 2010b]

Figure 1.2: Zoomed-in view of British Library Psalter World Map c.1265

Vincent van Gogh. Museums, art galleries and library archives all have substantial quantities of paper based materials and are therefore particularly interested in preservation.

Finally, books made between around 1850 and 1990 and newspaper print are under particular threat as they degrade rapidly, not being expected to last more than 100 years in critical cases [Strlic and Kolar, 2005a].

For these reasons, collection institutions want diagnostic tools for evaluating the condition of their artefacts and conservation methods.

1.2   Research aims and objectives

Our work is to analyse the degradation of paper from a chemical engineering perspective. In particular, it intends to investigate the gas-phase mass transfer through the paper of the compounds involved in its degradation process. This is because this process is not necessarily uniform in a book across a page or from one page to the next. This section outlines the goals and objectives of the research project.

Firstly, we will understand the process of degradation of paper and in particular the role played by VOCs.

Then, we will be investigating to see if there are particular VOCs that have a prominent role in the process. This will help make simplifications to the work.

With the VOCs' role having been studied, our work will then aim to model the reactive mass transfer of a VOC within books, describing the concentration profile over time in the gas phase.

We will then be able to link this model to the process of paper degradation, providing a way of predicting the degradation profile of paper across a stack under assigned conditions.

Below is a summary of the aims and objectives of this research project:

- To understand the process of paper degradation, and in particular the role played by VOCs.

- To know which VOCs are most important to the process, in order to focus the work.

- To model the reactive mass transfer of a VOC within books.

- To be able to link this model to the process of paper degradation.

This work has been carried out at the UCL Department of Chemical Engineering, in collaboration with the UCL Centre for Sustainable Heritage.

The resulting model would then be able to benefit managers of archives and libraries, helping them to decide on how to keep their collections. The model will help predict the lifespan and condition of paper materials and, in addition to this, it can be extended to examine the influence one book may have on a neighbouring book's degradation in regards to VOCs being transferred from one to the other. This can be important when considering a large amount of items being kept side by side on shelves or in storage long boxes.

1.3   Thesis outline

In this chapter we have briefly outlined the problem of paper degradation with our intentions and motivations for investigating the issue.

Chapter 2 delves into the composition of paper and its degradation mechanisms as well as how degradation is currently evaluated. The chapter explores how the composition affects paper's degradation in addition to the external effects. We explain the main degradation reactions, how the degradation rate is derived and what part VOCs play in the degradation process.

Chapter 3 describes the mass transfer theory that is to be used in establishing our model. It covers how gases diffuse through a porous material, the relation between a compound in the gas phase and the adsorbed phase and the reactive process in a porous material.

Chapter 4 presents our model. The chapter starts by reviewing other mass transfer models for VOCs available in the literature, considering if and how these are applicable to our case. We then derive our model in general terms, exploring the time scales characterising each phenomenon described by the model and related to the paper degradation process. The parameters, functions and conditions that arise in the model are then dealt with. Finally we cover two additional models for comparison with the main model.

In Chapter 5, the experimentation carried out on our paper samples is reported. We analysed four different samples, to find information on the porous structure, diffusion coefficients and adsorption. This information is then fed into the model.

Chapter 6 presents the computational results of the model. Several scenarios are used and analysed showing the implications of the presence of a VOC and how degradation differs when the VOC's influence is not considered.

Finally, in Chapter 7 we draw conclusions as well as outline future work that would supplement and further our investigation.

Chapter 2

Understanding paper degradation

We wish to model the problem of mass transfer with chemical reaction of VOCs in regards to paper degradation. To do this, we need to understand in depth the complex degradation process, in particular the role that VOCs play in it.

2.1 Properties of paper

An initial step to understand how paper degrades is to know which types of paper exist and how they are manufactured.

Although paper is still a similar product today to what it has always been, there are and have been some variations to its manufacturing and to the composition of the pulps used. This affects to some degree how it degrades. We define paper as thin sheets made of fibre mixed with water. For the majority of paper-based materials, the fibre is made of cellulose.

2.1.1 Brief history of paper

Making paper is credited to have started in China in the 1$^{\text{st}}$ century BC [Hunter, 1978, Blumich et al., 2003], and paper is named after the papyrus plant (the Ancient Egyptians used papyrus as writing material). Early paper was made from bast fibres and this constituted the source of cellulose. After its invention in China, paper spread to the Islamic world. In the Islamic world they had machines for preparing the pulp from which the paper is made, leading to a more consistent quality of paper. By medieval times, paper was made using linen, hemp and cotton rags, which led to high quality paper, because the latter are highly pure in cellulose [Hunter, 1978].

In the 16$^{\text{th}}$ century there was an increase in demand for paper due to the invention of printing with moveable type, and also water powered mills for hammering pulp. The process was further industrialised, in particular in the second half of the 19$^{\text{th}}$ century, and wood pulp became the source of cellulose [Hunter, 1978]. This led to lower quality paper, as the wood source contains both lignin and
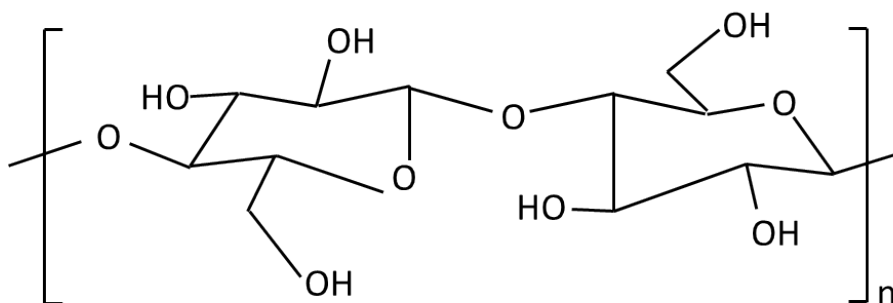
Figure 2.1: Structure of cellulose [Strlic and Kolar, 2005a]

hemi-cellulose impurities. An example of low quality (and therefore cheap) paper is newspaper; this contains a large amount of residual lignin from the wood source in its composition.

Finally, from the 1990s we are able to get "acid-free" paper, as more neutral substances are used in its treatment. The acidity of the paper is important as the more acidic it is, the more vulnerable it is to acid catalysed hydrolysis [Strlic and Kolar, 2005a, Carraher, 2007c]. This will be explored in more detail later on in this chapter.

2.1.2 Cellulose and its properties

Cellulose accounts for the majority of paper's composition and is therefore responsible for most of its behaviour. Cellulose was named by A. Payen in 1838, who successfully extracted the compound [Dumas, 1839, Payen, 1838].

It is a natural organic polymer, a polysaccharide, which is a polymeric carbohydrate structure of repeating saccharides joined by a glycosidic bond (shown in Figure 2.4). It is a relatively simple molecule, being a linear polymer with the same repeating unit (a homo-polymer). Its molecular formula is $(C_6H_{10}O_5)_n$. Its repeating unit (a glycose unit) is presented in Figure 2.1, which shows the monomer twice, one rotated 180° from the other (as reported by [Strlic and Kolar, 2005a, Emsley and Stevens, 1994]).

Cellulose is solid and fibrous, with chain lengths between the thousands and tens of thousands of monomers [Emsley and Stevens, 1994, Krassig, 1985, Carraher, 2007a]. The length of the chains varies widely and so cellulose is typically studied in terms of average molar mass. The width and shape of the molar mass distribution affects how the polymer behaves and the distribution is described by a probability density function [Nijenhuis and Krevelen, 2009a].

Cellulose is not soluble in water and there is no melting or softening due to the strong intermolecular hydrogen bonding. However it is hydrophilic and can have 70% loosely bound water present [Gnanou and Fontanille, 2008, Nicholson, 2006a].

Regions of high order in a polymer are described as (semi-)crystalline areas. Cellulose has a high tendency to organise in parallel arrangements and so it presents crystalline areas within an amorphous
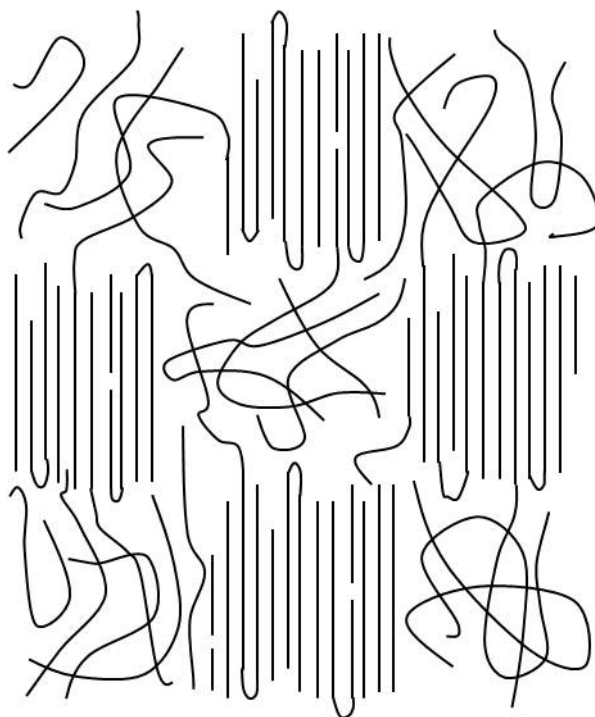
Figure 2.2: Polymer chains in crystalline and amorphous regions [Nijenhuis and Krevelen, 2009a]

matrix. This is shown in Figure 2.2. Because of this, its physical behaviour resembles that of crystalline polymers apart from melting, as the crystalline melting point is greater than the decomposition temperature (180ºC) [Nijenhuis and Krevelen, 2009a]. The crystallinity of a polymer impacts rigidity, as do intermolecular forces. The crystalline areas can prevent access of gases and liquids to cellulose chains and so prevents reactants for degradation reaching the chains [Lojewski et al., 2010, Nijenhuis and Krevelen, 2009a, Nicholson, 2006a, Krassig, 1985, Carraher, 2007a, Gnanou and Fontanille, 2008].

2.1.3 Other paper components

The history of paper shows that paper has had various sources for its fibres and has undergone different methods of manufacturing. It is possible to have paper made with pure cellulose [Dupont et al., 2007], however other components are present in most papers. Typically natural sources of cellulose contain also the natural polymers lignin and hemi-cellulose. These components are mostly washed away when the process generates the wood pulp for regular paper. A small percentage of them however remains after the wood pulp is generated, and therefore lignin and hemi-cellulose are the two main other components present in the pulp.

Hemi-cellulose is a branched polysaccharide. It has a random, amorphous structure with little strength, which is easily hydrolysed by dilute acids or bases and has shorter chains than cellulose [Gnanou and Fontanille, 2008].

Lignin is a more complex polymer with many cross links. It has phenolic groups as well as other
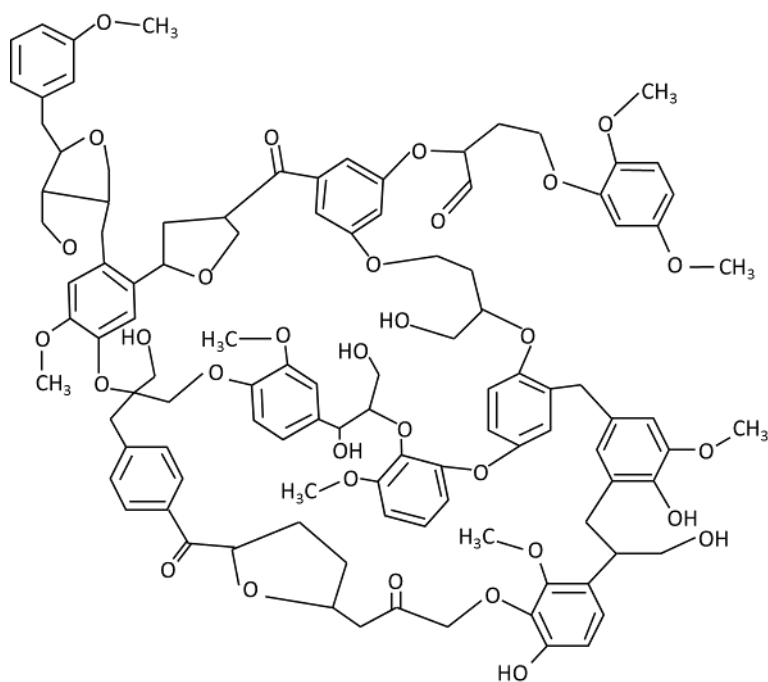
Figure 2.3: Example of possible lignin structure [Carraher, 2007b]

functional groups. These groups oxidise then hydrolyse and can give rise to a weak acidic solution [Carraher, 2007a]. Figure 2.3 shows an example of what lignin looks like and how complex it can be [Carraher, 2007b].

There are other components that can be introduced either during the pulping process or successively [Blumich et al., 2003, Dupont et al., 2007]. Iron gall ink is common in historic paper, it has a high acid and transition metal content and has been shown to release hydrogen peroxide [Strlic et al., 2010]. For sizing the paper, different substances have been used including gelatine, starch, alums and rosin. Alums are slightly acidic and rosin contains acids also.

Acid-free paper has had calcium or magnesium carbonate added to neutralise acids initially present in the paper. Typically the calcium or magnesium carbonate is added in excess, creating an alkaline reserve. Whilst the reserve is present, any new acid, either created by degradation or adsorbed from the environment, is neutralised.

Finally, other components are introduced when bleaching or colouring the paper.

2.2 Degradation reactions and their effects on paper

Paper degradation is a complex process with many mechanisms. There are two main types of reactions that contribute to the degradation process: hydrolysis and oxidation [Lojewski et al., 2010]. Hydrolysis occurs typically in the form of acid-catalysed hydrolysis and so is influenced by the paper's acidity.
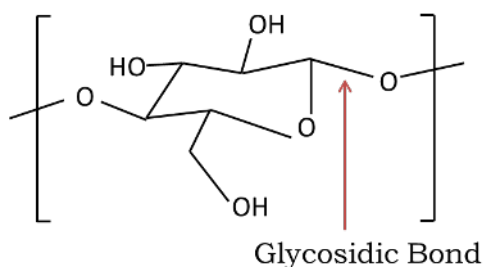
Figure 2.4: Glycosidic bond
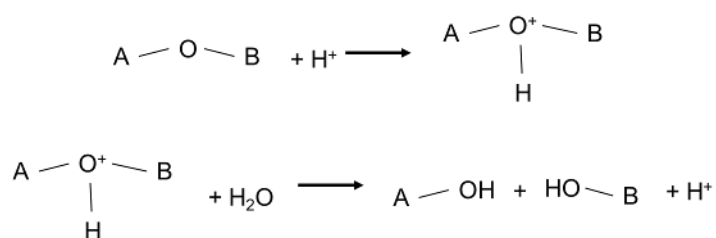
Figure 2.5: Acid-catalysed hydrolysis

We focus on the breaking down of cellulose in paper degradation, as cellulose is the main component of paper. These reactions also affect the lignin and hemi-cellulose, but are less predictable due to the complexity of the compounds.

The reactions contributing to the degradation affect paper in different ways, which we will examine below.

2.2.1 Bulk-chain reactions

These reactions reduce the molar mass of cellulose and are a scission (breaking) of the cellulose chain in the bulk of the chain, as opposed to a scission at the end of the chain. The reactions that do this have the most significant effect on paper. The cellulose chain splits into two sub-chains of comparable length, increasing the number of chains present in the system, but reducing the average chain's molar mass. As the chains split into sub-chains their entanglement changes. The bond that breaks in cellulose is the glycosidic bond, shown in Figure 2.4 [Zou et al., 1996].

The scission is achieved by acid-catalysed hydrolysis: the acid breaks a glycosidic bond in a cellulose molecule splitting the latter into two smaller molecules. This is a two-stage reaction and is shown in Figure 2.5. In this figure, A and B are two parts of the polymer chain of cellulose.

This mechanism reduces the chain length of the cellulose molecule, the scission occurring randomly along the cellulose chain. Areas of crystallinity may affect the hydrolysis as the reactants have less access to the chain for attack [Lojewski et al., 2010].
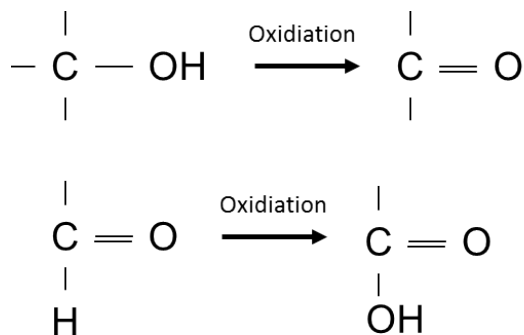
Figure 2.6: Oxidation examples

2.2.2 End-chain reactions

When a scission takes place near the end of the cellulose chain, the chain is split into a large macro-molecule and a considerably smaller molecule. The smaller molecule is a new compound that is either already a VOC, or can become one by later functional group changes described in Section 2.2.3. For the molecule to already be a VOC, functional group changes need to have already happened to the cellulose chain before splitting. The scission is from acid-catalysed hydrolysis as shown in Figure 2.5. The difference to the effect described in 2.2.1 is the position on the chain where the scission occurs. The cellulose chain is typically very long and if we assume the scissions take place randomly along the chain, the majority of the time the scission will occur in the bulk of the chain. End-chain reactions have a minimal effect on the properties of the cellulose due to the substantial length the cellulose chains have. The VOCs generated, however, could play a crucial role in paper degradation (refer to Section 2.3.3.1 for details); so there is an indirect effect that end-chain reactions have.

2.2.3 Functional group changes

Some reactions modify the functional groups on the chains affecting the properties of the latter. The variations possible help give rise to different VOCs when an end-chain scission takes place. An example of a functional group change would be a hydroxyl group (-OH) reacting to become a carbonyl group (C=O) [Lojewski et al., 2010].

The main two types of reactions causing changes to the functional groups on the chain are hydrolysis and oxidation. These reactions can happen on many of the carbon atoms within the molecule and so there are many possibilities.

Examples of oxidation changes to functional groups are shown in Figure 2.6. This shows a hydroxyl group being oxidised to become a carbonyl and a carbonyl then further oxidising to become a carboxyl group [Lojewski et al., 2010]. In cellulose, the carbonyl end groups are most likely to oxidise.

The first oxidation reaction can be reversed with reduction by gain of hydrogen and is shown in Figure 2.7 [Lojewski et al., 2010].
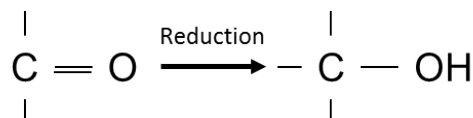
Figure 2.7: Reduction example
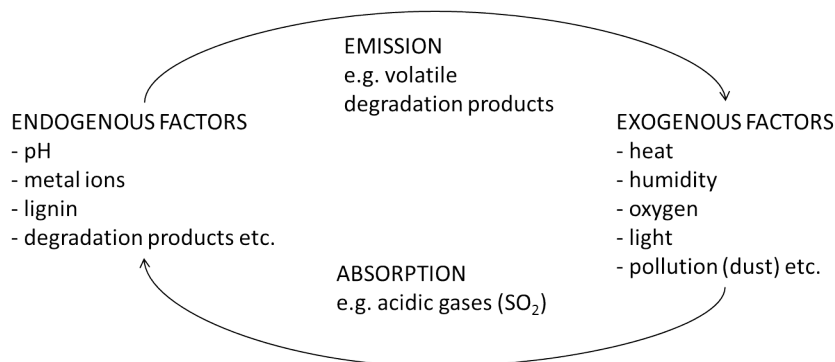
Figure 2.8: Factors affecting paper stability [Strlic and Kolar, 2005b]

This shows the wide range of possibilities for changes to the functional groups along the cellulose chain. As a consequence of this, when a scission occurs near the end of a chain, there can be a variety of VOCs produced with different functional groups present.

2.3 Causes of degradation

There are two categories of factors which cause degradation, external factors and internal factors. A summary of these factors is shown in Figure 2.8.

2.3.1 Internal factors

The internal factors are due to the manufacturing and the resulting composition of the paper.

The pH of paper is important as acid-catalysed hydrolysis in particular is influenced by whether the paper is acidic or alkali. The paper's initial pH is determined by its composition.

As cellulose is a semi-crystalline natural polymer, there being crystalline and amorphous areas within the paper, it is expected that the amorphous areas degrade faster than the crystalline areas as the amorphous areas are considered more reactive [Baranski, 2002].

Lignin content also plays a part as mentioned earlier, having different side groups in its complex structure, which adds to the acidity of the paper, thus helping acid-catalysed hydrolysis. It has also been shown that paper with lignin is more susceptible to oxidation [Lojewski et al., 2010].

Metal ions and other components introduced as part of the manufacturing of paper will also affect the acidity of the material.
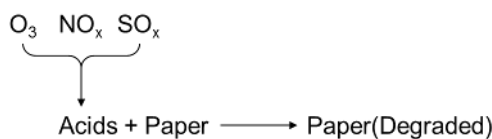
Figure 2.9: Example of some outside pollutants' effect

Finally, the products that the paper produces whilst degrading also contribute to the paper's acidity. These products are VOCs, and are produced from various reactions with the paper. This could be from end-chain reactions with cellulose or reactions with lignin or hemi-cellulose. Some of these compounds are acidic, decreasing the paper's pH and encouraging further the acid-catalysed hydrolysis.

2.3.2 External factors

The external factors are due to the environment in which the paper is kept in.

The humidity will have an effect on the water content within the cellulose: as the humidity increases, the water content in the paper will increase, encouraging hydrolysis [Menart et al., 2011].

Light is another factor that can affect the degradation of paper and polymers in general. The UV range of light is the most damaging. The mechanism by which light helps degrade paper is by a type of oxidation: photo-oxidation. The light causes radicals to form, these radicals then react with oxygen, leading to chain reactions. Pigments and fillers may also influence this process [Nicholson, 2006b].

Heat influences degradation as increasing the temperature of the paper encourages reactions. Therefore it will influence the rate of acid-catalysed hydrolysis and oxidation as well as other reactions. This can be minimised by keeping the paper in conditions where the temperature is kept low.

Pollutants like SO_x, NO_x and Ozone are a known issue as they react giving rise to acids which then participate in reactions with the paper, as shown in a simplified reaction in Figure 2.9 [Menart et al., 2011]. In addition to being produced by paper's degradation, VOCs can also be present due to external production and will be explored further in Section 2.3.3.

Pollutants produced externally are not a great concern as most archives and book repositories have air conditioning that eliminates most of them from the outside [Strlic and Kolar, 2005c].

Finally, biological degradation (micro and macro-organisms) is another external factor that affects paper, as these organisms can spread through from one material containing the paper to another. As will be discussed in section 2.6, these external factors are the easiest to protect against.

There are other factors that affect polymers like wind, erosion, and seasonal changes; however, it is not something to consider in our case as books are of course kept inside. There are also other factors that affect the quality of the paper quite suddenly, like fire, flood and poor handling and storage.

2.3.3 Volatile organic compounds

Volatile organic compounds are organic compounds that are typically present in the air as gas, but under normal temperature and pressure being liquid or solid. This is a general definition of VOCs, but there are others that slightly differ where the boiling point range of the compounds is specified. There are many hundreds of compounds that come under this definition (notable exceptions are carbon dioxide and carbon monoxide). Some compounds are ruled out by certain definitions. There are also similar terms for almost the same class of compounds, for example: hydrocarbons are also referred to as "reactive organic gases" [Hester and Harrison, 1995].

VOCs are air pollutants commonly found in the atmosphere at ground level in urban and industrial centres. VOCs are also indoor generated pollutants and so cannot be excluded in the way outdoor pollutants can [Hester and Harrison, 1995].

Sources of VOCs can be from human activity and pollution, or from biological sources like plants. Interest in VOCs has increased as understanding of their role in environmental problems improved. In particular their role in the following issues [Hester and Harrison, 1995]:

- Stratosphere ozone depletion.

- Ground level photo-chemical ozone formation.

- Toxic or carcinogenic human health effects (for example, benzene and 1,3-butadiene can be leukaemia inducing agents, and formaldehyde is a potential nasal carcinogen).

- Enhancing the global greenhouse effect.

- Accumulation and persistence in the environment.

Paints and coatings are a common indoor source of VOCs, and as such the industry are trying to reduce the effect by producing paints which have less VOC emissions (this does not necessarily mean the paint has less VOCs within it, but will have less emitted out) [ToolBase.org, 2011].

2.3.3.1 VOC generation

As mentioned in 2.3.1, a source of VOCs are degradation products that the paper produces. The VOCs are likely to be produced by oxidation and acid-catalysed hydrolysis reactions that break bonds near the end of the cellulose chains. Also they are created through reactions with the lignin and hemi-cellulose present in paper. Thus, we can write the following simplified reaction for the creation of VOCs:

$$Paper + Oxygen + Water \overset{(H^+)}{\rightarrow} (degraded)Paper + VOCs \tag{2.1}$$

Note that oxidation and acid-catalysed hydrolysis also degrade paper without creating VOCs.

It can be assumed that the creation of the VOCs has a negligible result on the immediate degradation of paper, as the creation reactions have a negligible contribution to the change in cellulose's properties. It is also probable that VOCs are generated with reactions with lignin and hemi-cellulose. VOCs may also react further to generate different VOCs within the paper.

The creation of VOCs has little effect on the state of paper, but their introduction into the system can then influence the rate of degradation. When VOCs are present, one would expect them to affect the local acidity of the paper. This can be seen, for example, if we look at acetic acid and formic acid's dissociation reactions and their equilibrium constants respectively:

$$CH_3COOH \rightleftharpoons CH_3COO^- + H^+; \, pKa = 4.75 \tag{2.2}$$

$$COOH_2 \rightleftharpoons CHOO^- + H^+; \, pKa = 3.75 \tag{2.3}$$
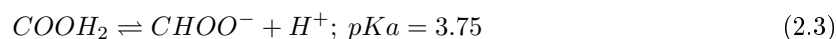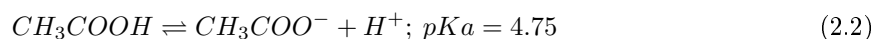
where pKa is the logarithm of the equilibrium constant. This constant shows how much the reaction favours the forward reaction when compared to the acidity of the system.

These are weak acids, but are strong enough to change the acidity of paper. This increase in acidity then affects the rate of acid-catalysed hydrolysis. With an increase in the rate of acid-catalysed hydrolysis the overall degradation rate increases creating more VOCs and increasing the acidity further. It has been shown that the presence of VOCs can cause the degradation of paper to increase and the removal of VOCs has a beneficial effect [Strlic et al., 2011, Menart et al., 2011].

2.3.3.2 VOC diffusion

After being generated, VOCs diffuse through the paper as gaseous compounds. As they diffuse, they can adsorb onto the surface of the paper or escape to the surrounding air. Their diffusion through the system will be driven by their concentration gradients in the gas phase. The VOCs adsorption will be governed by their thermodynamic equilibrium, which we express through adsorption isotherms. Generation, adsorption and diffusion of VOCs will all be explored further in Chapter 3. The concentration profile of the VOCs in the paper relates to the acidity profile in the paper through the VOCs dissociation. Therefore the local degradation rate of paper depends on the concentration profiles of the VOCs.

For a single sheet of paper, the VOCs have only the surrounding air to diffuse through; however, in a stack of paper the VOCs diffuse through the stack. In a book, it would be even more difficult for the VOCs to escape to the surrounding air as the cover would add extra resistance to their escaping. Thus, the single sheet of paper degrades more slowly than paper within a stack [Hanus et al., 1996]. It has been shown that paper in the middle of the stack is more degraded than that at the ends of the stack which are covered [Carter et al., 2000].
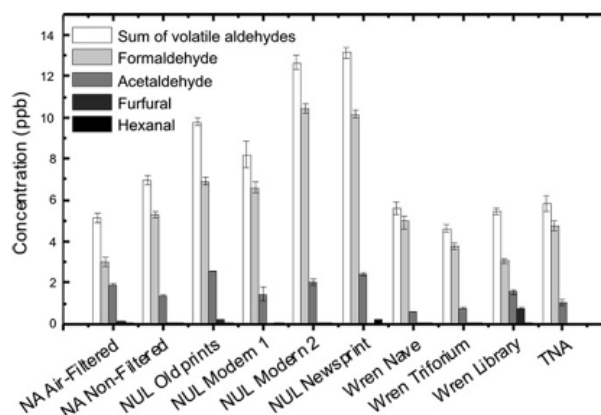
Figure 2.10: Concentrations of aldehydes in various repositories [Fenech et al., 2010]

2.3.3.3 Choosing a VOC to model

There are various VOCs that are produced during the degradation process, and studies have been carried out which identify acetic acid as a representative VOC in all paper types, as well as low molecular weight organic acids like formic acid and aldehydes. Acidic VOC are expected to affect the acidity of the paper. Figure 2.10 shows how VOCs are noticeable in the atmosphere surrounding the books [Fenech et al., 2010].

It has also been shown that in lignin containing papers, vanillic acid and arabinose are possible markers of degradation state, whilst in pure cellulose papers, glucose is a possibility [Fenech et al., 2010, Dupont et al., 2007]. A comprehensive list of VOCs found from naturally aged paper can be found in the article by A. Lattuati-Derieux et al. 2004.

As acetic acid is a representative VOC in all paper types and acidic, this VOC is chosen to be modelled. Resultingly, acetic acid is the VOC referred to throughout this body of work with regards to the model proposed and the resulting simulations.

2.4 Measuring degradation

As paper degrades, its colour changes and the pages feel more brittle to the touch. In Figure 2.11 there is an example of a book starting to degrade, this is a 1986 hardback copy of The Adventures of Tom Sawyer by Mark Twain. The writing is still clear, but the paper has started to show signs of of degradation in the margins, becoming more brittle and discoloured.

In Figure 2.12, we have a page from the Gutenberg Bible; a paper version kept in the British Library. The Gutenberg Bible was the first major printed book in Europe. The Bible was produced in the mid 1450s by Johann Gutenberg using movable type. Despite being over 500 years old, the paper is still in very good condition, although there are signs of ageing. This is in part due to the high quality
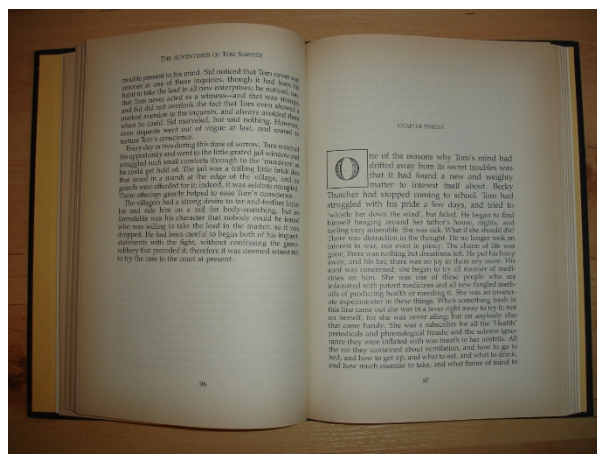
Figure 2.11: 1986 version of The Adventures of Tom Sawyer by Mark Twain

of paper used. The copy of The Adventures of Tom Sawyer is degrading at a different rate than the Gutenberg Bible because the composition of the paper is different.

The amount paper has changed from its original state needs to be measurable in order to quantify its degradation. Figure 2.13 shows the main ways in which the state of polymers in general are characterised in order for their degradation to be measured [Scott and Gilead, 1995].

The mechanical properties of paper are properties we desire from it as a user. These properties can be tested and are measurable. There are standardised tests for the strength, tearing resistance, folding endurance and colour change [Zou et al., 1994, ISO 1924-2:1994, ISO 1974:1990, ISO 5626:1993, McLaren, 1976]. In most tests on mechanical properties, the sample needed is large and the tests need many repetitions for reliable results. Moreover, the change in mechanical properties can only be noticed after there has been a substantial amount of degradation to the paper already. We consequently favour other methods of measuring degradation.

Viscometry is a destructive method that finds the average molecular weight (or degree of polymerisation, DP) of the paper; this is a simple and common measurement of polymer degradation. This requires a sample which is dissolved in a solvent, typically cupriethylenediamine hydroxide [Kacik et al., 2009, ISO 5351/1, 1981, SCAN-CM 15:88, 1988]. Once dissolved, the viscosity of the solution can be used to estimate the average molecular weight of the cellulose. It is an inexpensive and efficient method as it requires a much smaller sample than that required for measuring the mechanical properties and needs less repetition for reliable results. This method does not take cross-linking between cellulose chains into account and so if a large amount of cross linking occurs, the result will have errors. As the main polymer present in paper is cellulose, cross linking is not expected to be a major issue.

The DP is typically used to quantify the degradation of paper at a chemical level. We need to relate the DP to the mechanical properties as these are the desirable properties in which we are interested as a user. Figure 2.14 shows an example of such correlation [Zou et al., 1996]. It shows the relation between fold endurance and DP for a bleached bisulfite pulp. With relations like this, we can predict the mechanical properties from the DP. It has been proposed that when the DP goes below the range

Figure 2.12: Gutenberg Bible © The British Library Board
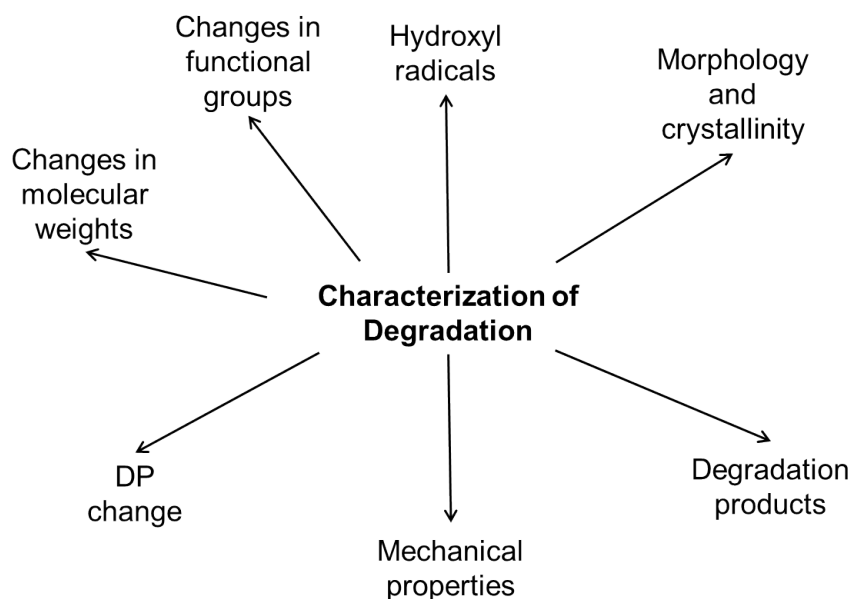
Figure 2.13: Characterisation of degradation in polymers [Scott and Gilead, 1995]

of 250-400, the paper is at the end of its usability [Menart et al., 2011]. Determining the DP for papers containing lignin can prove difficult as lignin is insoluble for the typical solvents used in viscometers [Strlic et al., 2009b].

Size Exclusion Chromatography is a more complex method of evaluating the molecular weight than viscometry; the column used needs calibration, and the preparation of the sample can take some time. However, more information can be gathered than through viscometry, as the distribution of molar mass is obtained as well as the molar-average molar mass and the mass-average molar mass [Sundholm and Tahvanainen, 2003].

Experimentation to find the paper's pH is commonly carried out. This is due to the importance the acidity of the paper has in the degradation process through acid-catalysed hydrolysis. There are several methods of testing the paper's pH. Some methods require a sample of the paper, for example Standard cold extraction, Micro-pH determination and Cold extraction with CO_2-equilibration [TAPPI T 509 Om-02, ASTM C778-97, 2002]. These are therefore destructive methods. There are also methods that require no sampling (surface pH determination and determination using pH pens); however, these are normally more error prone [Strlic et al., 2004].

Determining the alkaline reserve is another test as this shows how much the paper can adsorb and neutralise acidic gases, helping prevent the paper's acidification. The alkaline reserve is found by use of titrimetry. Titrimetry requires a sample that is typically put in a liquid reactant and then a reagent is slowly added so that a colour change can be noticed, this change indicating the alkalinity [TAPPI T 553 Om-00].

IR spectroscopy (or FTIR - Fourier Transform Infra Red) can be used to observe the changes in the functional groups on a polymer and to gain information on what happens to the polymer at
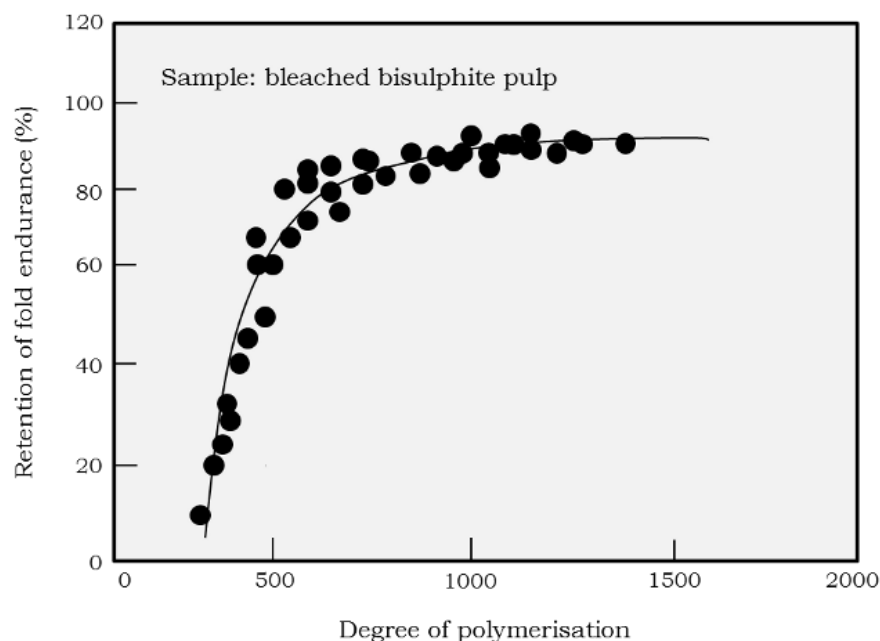
Figure 2.14: Dependence of fold endurance on mean degree of polymerisation [Zou et al., 1996]

a molecular level [Scott and Gilead, 1995]. Chemiluminescence analyses the hydroxyl radicals and monitors degradation at an early stage. It measures photons emitted and the intensity of the emission is dependent on the oxidation of the polymer [Scott and Gilead, 1995].

Nuclear Magnetic Resonance (NMR) methods have been used to characterise degradation and can now be non-destructive. This method can give insight into the water content as well as information on the crystallinity and amorphous regions [Blumich et al., 2003].

Gas Chromatography coupled with Mass Spectrometry is used to study the degradation products (VOCs), and, as mentioned above, is beneficial as the VOCs are expected to have low concentrations in air being therefore harder to detect [Fenech et al., 2010]. The samples for this are normally from emissions cells, like the Field and Laboratory Emission Cell (FLEC) [Ramalho et al., 2009], but can also be obtained elsewhere, for example in libraries and archives.

2.4.1 Accelerated ageing of paper

Natural ageing is a slow process and so to explore the degradation process, accelerated ageing methods are often employed. Essentially, this involves putting the material under certain atmospheric conditions (atmospheric composition and humidity) within an oven for a set time, and then taking measurements as if the material had aged naturally for a much longer period.

The main issue for accelerated ageing is to know its relation to natural ageing. How many days of artificial ageing are equivalent to how many days of natural ageing? To ensure that the accelerated ageing is a close approximation to natural ageing, comparisons are needed against naturally aged
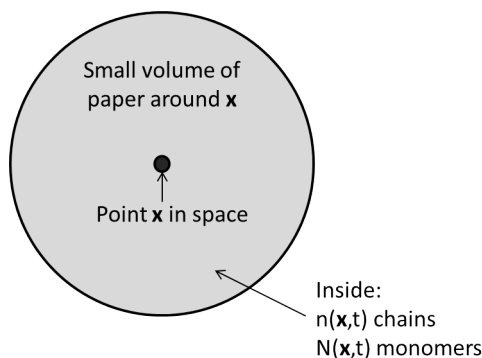
Figure 2.15: Small volume of paper

materials; so samples are needed from these, and it is preferable that these samples be taken from materials where there is no concern for their preservation [Baranski, 2002].

2.5   Degradation kinetics

It is not enough to be able to state the condition of the paper, or the amount the paper has degraded. We wish to describe the degradation rate, so that we can predict how degraded the paper will become. The most common way to describe the degradation rate is to relate it to the degree of polymerisation (DP) and the scission of the cellulose chains [Emsley and Stevens, 1994, Calvini and Gorassini, 2006, Zou et al., 1996].

2.5.1   Degree of polymerisation

The degree of polymerisation for a single chain of cellulose is defined as the number of monomers a chain contains. This is because cellulose is a linear polymer with one type of monomer. The average local DP for a system of cellulose chains is the local number of monomers divided by the local number of chains. To illustrate this, let us consider a small volume of paper around $\mathbf{x}$, as shown in Figure 2.15. Inside the volume we have the local number of chains $n(\mathbf{x}, t)$, and the local number of monomers $N(\mathbf{x}, t)$. The local DP is then given by:

$$DP(\mathbf{x}, t) = \frac{N(\mathbf{x}, t)}{n(\mathbf{x}, t)} \tag{2.4}$$

Typically in studies, the DP is not expressed as a function of the space coordinates, but is necessary here as it is the local profile of paper we are interested in. Let us remember that in general, paper degradation is not expected to be uniform across a page or a stack of pages.

2.5.2   Ekenstam's equation

With DP defined, we then wish to express the change in DP over time. At time t, it is:

$$DP(\mathbf{x}, t) = \frac{N(\mathbf{x})}{n(\mathbf{x}, t)} \tag{2.5}$$

The number of monomers is assumed to be constant, that is, no monomers are lost, but the number of chains will change with time as bonds break. After a differential time interval dt, the DP will become:

$$DP(\mathbf{x}, t + dt) = \frac{N(\mathbf{x})}{n(\mathbf{x}, t) + y(\mathbf{x}, t)dt} \tag{2.6}$$

where y is the mean number of bonds that break per unit time. The number of bonds that break is not assumed to be constant. We can now express the change in DP for the differential time interval as:

$$\frac{DP(\mathbf{x}, t + dt) - DP(\mathbf{x}, t)}{dt} = \left[\frac{N(\mathbf{x})}{n(\mathbf{x}, t) + y(\mathbf{x}, t)dt} - \frac{N(\mathbf{x})}{n(\mathbf{x}, t)} \right] \frac{1}{dt} = -\frac{N(\mathbf{x})y(\mathbf{x}, t)}{n(\mathbf{x}, t) \left[n(\mathbf{x}, t) + y(\mathbf{x}, t)dt \right]} \tag{2.7}$$

As dt is vanishing small $ydt \ll n$, which gives us the following differential equation:

$$\partial_t DP(\mathbf{x}, t) = -\frac{N(\mathbf{x})y(\mathbf{x}, t)}{\left[n(\mathbf{x}, t) \right]^2} = -\frac{y(\mathbf{x}, t)}{N(\mathbf{x})} \left[DP(\mathbf{x}, t) \right]^2 \tag{2.8}$$

We then define k_{DP} as the relative number of bonds that break per unit time, normalised with respect to the overall number of monomers:

$$k_{DP}(\mathbf{x}, t) \equiv \frac{y(\mathbf{x}, t)}{N(\mathbf{x})} \tag{2.9}$$

We then rearrange Equation 2.8 to get:

$$\partial_t DP(\mathbf{x}, t) = -k_{DP}(\mathbf{x}, t) \left[DP(\mathbf{x}, t) \right]^2 \tag{2.10}$$

This can then be integrated between time 0 and time t, giving us:

$$\frac{1}{DP(\mathbf{x}, t)} - \frac{1}{DP(\mathbf{x}, 0)} = \int_0^t k_{DP}(\mathbf{x}, \tau)d\tau \tag{2.11}$$

where $DP(t)$ is the average DP at time t, $DP(0)$ is the average DP at the start and t is the end limit of the integration.

If we assume that the amount of bonds breaking does not change with time, this can be reduced to the Ekenstam's equation, where k is no longer dependent on time [Zou et al., 1996, Ekenstam, 1936]:

$$\frac{1}{DP(\mathbf{x}, t)} - \frac{1}{DP(\mathbf{x}, 0)} = k_{DP}(\mathbf{x})t \tag{2.12}$$

2.5.2.1   Monomer loss due to VOC production

We said that the number of monomers, N, is constant and we assume no monomer loss. In section 2.2.2, however, we said that when a cellulose chain is broken near the end, the smaller of the resulting molecules is no longer considered to be a cellulose chain. We assume this smaller molecule has become a new compound which is either a VOC, or can become one with functional group changes and further reactions. Let us now consider what happens to the number of monomers when there is loss due to this VOC generation.

A cellulose chain with N_i monomers has $N_i - 1$ bonds. We assume that of these bonds, two are end of chain bonds. There are n chains, and so the total number of end chain bonds is $2n$. The total number of bonds for n chains is:

$$n(N_i - 1) = N - n \tag{2.13}$$

where N is the total number of monomers. The fraction of end bonds is:

$$\alpha(\mathbf{x}, t) = \frac{2n(\mathbf{x}, t)}{N(\mathbf{x}, t) - n(\mathbf{x}, t)} = \frac{2}{DP(\mathbf{x}, t) - 1} \tag{2.14}$$

This assumes that only the bonds connecting the very last monomers to the cellulose chain are end bonds. This fraction is 0.8% when $DP = 250$. This DP value is below what is considered for paper to be in a useable condition [Menart et al., 2011]. The fraction of inner chain bonds is then $1 - \alpha$. After a differential time interval dt, the number of monomers decreases by the number of bonds broken that are end chain bonds and the number of chains increases by the number of bonds broken that are mid chain bonds. Thus, the DP becomes:

$$DP(\mathbf{x}, t + dt) = \frac{N(\mathbf{x}, t) - \alpha(\mathbf{x}, t)y(\mathbf{x}, t)dt}{n(\mathbf{x}, t) + [1 - \alpha(\mathbf{x}, t)]\, y(\mathbf{x}, t)dt} \tag{2.15}$$

We can now express the change in DP for the differential time interval as:

$$\frac{DP(\mathbf{x}, t + dt) - DP(\mathbf{x}, t)}{dt} = \left[\frac{N(\mathbf{x}, t) - \alpha(\mathbf{x}, t)y(\mathbf{x}, t)dt}{n(\mathbf{x}, t) + [1 - \alpha(\mathbf{x}, t)]\, y(\mathbf{x}, t)dt} - \frac{N(\mathbf{x}, t)}{n(\mathbf{x}, t)} \right] \frac{1}{dt} \tag{2.16}$$

Which rearranges to:

$$\frac{DP(\mathbf{x}, t + dt) - DP(\mathbf{x}, t)}{dt} = -\frac{\alpha(\mathbf{x}, t)n(\mathbf{x}, t)y(\mathbf{x}, t) + [1 - \alpha(\mathbf{x}, t)]\, N(\mathbf{x}, t)y(\mathbf{x}, t)}{n(\mathbf{x}, t)\, \{n(\mathbf{x}, t) + [1 - \alpha(\mathbf{x}, t)]\, y(\mathbf{x}, t)dt\}} \tag{2.17}$$

Then as dt is vanishing small, $ydt \ll n$, and we have:

$$\partial_t DP(\mathbf{x}, t) = -y(\mathbf{x}, t) \left\{ \frac{\alpha(\mathbf{x}, t)n(\mathbf{x}, t) + [1 - \alpha(\mathbf{x}, t)]\, N(\mathbf{x}, t)}{[n(\mathbf{x}, t)]^2} \right\} \tag{2.18}$$

This then gives:

$$\partial_t DP(\mathbf{x},t) = -\frac{y(\mathbf{x},t)}{N(\mathbf{x},t)} \left\{ 1 - \alpha(\mathbf{x},t) \left[1 - \frac{1}{DP(\mathbf{x},t)} \right] \right\} [DP(\mathbf{x},t)]^2 \tag{2.19}$$

We can therefore once again write Equation 2.10, but in this case it is:

$$k_{DP}(\mathbf{x},t) \equiv \frac{y(\mathbf{x},t)}{N(\mathbf{x},t)} \left\{ 1 - \alpha(\mathbf{x},t) \left[1 - \frac{1}{DP(\mathbf{x},t)} \right] \right\} \tag{2.20}$$

On the right hand side of the equation, $(1 - 1/DP) \approx 1$, and $\alpha \ll 1$; therefore, with an excellent approximation, the equation above reduces to Equation 2.9. This illustrates that the small monomer loss due to end chain bonds breaking has little effect on the degradation rate directly. We have assumed that α and $1/DP$ are both much smaller than unity.

Equation 2.10 allows us to predict how paper degrades in every location in space as time goes by. However, to be able to use this equation, we need to know the degradation reaction constant k_{DP}.

2.5.3 Degradation reaction constant

The degradation rate is the rate of change in DP as expressed by Equation 2.10:

$$\text{degradation rate} = \partial_t DP(\mathbf{x},t) = -k_{DP}(\mathbf{x},t) [DP(\mathbf{x},t)]^2 \tag{2.21}$$

From this, it can be seen that the degradation rate is a function of k_{DP}. In the majority of work in literature [Zou et al., 1996], we usually find that this value is expressed as a function of temperature and the pre-exponential factor given by the Arrhenius equation:

$$k_{DP} = Ae^{-E/RT} \tag{2.22}$$

where A is the pre-exponential factor, E is the activation energy, R is the gas constant, and T is the absolute temperature.

The Arrhenius equation normally applies to a single reaction, but with paper we have multiple reactions. Due to this, the activation energy is therefore the sum of activation energies from multiple reactions, and the pre-exponential factor is a function of the factors which influence the degradation of paper. It has been suggested that the pre-exponential factor can be expressed as a function of acidity (shown as hydrogen ions), moisture content and oxygen content [Zou et al., 1996]:

$$A = ([H^+], [H_2O], [O_2]) \tag{2.23}$$

where $[H^+]$, $[H_2O]$ and $[O_2]$ are the concentrations of hydrogen ions, water and oxygen in the adsorbed phase in the paper, respectively. This follows as k_{DP} is proportional to the number of bonds broken per unit time; we expect that this number depends on temperature, acidity, water content and oxygen content as they affect the rates of reactions of oxidation and acid-catalysed hydrolysis.

It has been recently suggested that following equation relating k_{DP} to temperature, acidity and water content can be used [Collections Demography Part 4, 2013]:

$$\ln(k_{DP}) = a_0 + a_1[H_2O] + a_2\ln[H^+] - \frac{a_3}{T} \tag{2.24}$$

where a_1 and a_2 are constants, and a_0 is the constant which accounts for oxidation reactions. Here it has been assumed that the oxygen concentration is constant.

The acidity concentration is given by:

$$[H^+] = 10^{-pH} \tag{2.25}$$

The water concentration is expressed as [Paltakari and Karlsson, 1996]:

$$[H_2O] = \left(\frac{\ln(1-RH)}{1.67T - 285.655}\right)^{\frac{1}{2.491 - 0.012T}} \tag{2.26}$$

where the relative humidity (RH) is expressed as a ratio. Using Equation 2.24 and empirical information from 124 paper degradation experiments performed by different groups for different type of paper and at different temperatures, the following formula has been put forward:

$$\ln(k_{DP}) = 38.039 + 38.057\left(\frac{\ln(1-RH)}{1.67T - 285.655}\right)^{\frac{1}{2.491 - 0.012T}} + 0.24\left[\ln\left(10^{-pH}\right)\right] - \frac{14713}{T + 273.15} \tag{2.27}$$

where the units of k_{DP} are per year, and the temperature is in °C. The focus of our work is not deriving k_{DP}. We assume Equation 2.27 is correct and rely on this expression. We have shown that to find the local rate of degradation, we need to determine k_{DP}. To determine k_{DP} we currently use Equation 2.27 for which we need the RH and pH. To calculate the pH, we need the local concentrations of VOCs due to their effect on the acidity.

The degradation rate can then be expressed as:

$$\partial_t DP(\mathbf{x}, t) = -k_{DP}[T(\mathbf{x}, t), RH(\mathbf{x}, t), C_{v,1}(\mathbf{x}, t), ..., C_{v,n}(\mathbf{x}, t)][DP(\mathbf{x}, t)]^2 \tag{2.28}$$

This equation therefore implies that to find the local rate of degradation, we need to determine the local concentrations of VOCs, RH and temperature profile. Knowing the gas concentration profiles of VOCs, we can predict their solid phase concentration profiles. This in turn allows us calculate the acidity profile through the VOC dissociation and then predict k_{DP} for a known temperature and RH, and if we know the initial DP we can find the local rate of degradation. This relation will be explored in detail in Chapter 4.

2.6   Current conservation techniques

There are some practices for the conservation of materials that major archives and book collections carry out.

For example, the Vatican library has taken a keen interest in the preservation of its materials for a long time. Since 1475 they have been concerned with defending books against humidity, dust and insects. In 1555 they employed a restorer to mend the books and rewrite where there was damage, and then in 1591 they brought in preventive measures where they had periodical dust removal as well as storing the material in areas with favourable architectural features. More recently, in 1983, the Vatican library built underground stacks for manuscripts, and in 2000 they had a disinfestations project using anoxic systems and dust removal [Vatican Library, 2010].

Another example is the British Library. There they have on site the National Preservation Office. The British Library is not just concerned with the preserving of these materials, they are also concerned with being able to help that the knowledge within them be used now and in the future. The library keeps a copy (by law) of everything published in the UK. As they are open to the public, part of their conservation techniques starts with the requirements they have for the public in order to use their facilities. This includes having clean hands when handling books in order to not transfer dirt and grease. They also have advice to follow, like touching the items as little as possible:

"Follow the text with slips of paper rather than fingers to prevent making marks"

Moreover, the library's Collection Care department cares for items, ensuring that damaged or vulnerable items are looked after. They can physically repair the item, place it in a protective box, or make a copy to be used in its stead. The staff are provided advice on how the collections can be protected whilst in use and they have security in order to prevent vandalism and theft.

Furthermore the library has sections where the light is kept low as well as the temperature to slow the degradation of materials, and to help prevent the fading of inks and paints. Also the humidity is kept low to stave off mould and insect issues.

Until recently, British Standard 5454:2000 has been used as the standard for the storage of archival documents, suggesting the temperature of a collection should be between 14-16^{0}C, and humidity between 40-60% [British Library, 2010a]. This has since been replaced with PAS 198:2012 and PD 5454:2012, which suggests the temperature of the collection should be between 13-16^{0}C, and humidity between 35-60% [British Library, 2013].

When looking at polymers in general, there are also methods of stabilising the material in order to slow the degradation process. There are for example the options of including UV absorbers, anti-oxidants, quenchers (which dissipate the energy in photo excited materials) and hindered amine light stabilisers [Nijenhuis and Krevelen, 2009b].

Ideally, collections should be kept free of pollutants, but this is not always possible and recommendations have been made for safe exposure levels [Menart et al., 2011].

Chapter 3

Theory

This chapter will present the theory that is needed to develop the model outlined in the research objectives. The theory will be used to describe the concentration profile within books of our VOC, acetic acid, in the gas phase. It will cover how components move through the porous paper whilst they are in the gas phase, as well as how they adsorb into the paper, where the degradation reactions and acid dissociation occurs.

3.1 Mass transfer

As stated above, we intend to describe the concentration profile of a component in the gas phase within a stack of paper. The concentration profile will vary both in time and space. To determine it, we need to solve a mass transfer problem.

Paper is a solid porous material through which the VOCs move. This motion takes place in the pores of the material, with the VOCs as gases. The VOCs move through the material and escape into the air surrounding the paper.

As well as the multiple VOCs, there is air and water vapour moving through the material in the gas phase. This means that we are dealing with a multicomponent mass transfer problem.

Our main focus is the VOCs. We assume that they are generated in the solid phase. They then desorb into the gas phase where they diffuse through the medium, where they can then be adsorbed by paper or escape the system. This is explored further later in the chapter and can be seen illustratively in Figure 3.7.

3.1.1 Ordinary mass transfer

To investigate mass transfer, we start by first examining mass and molar fluxes. Denoted for a generic component A by $\mathbf{n}_A$ and $\mathbf{N_A}$, respectively, these are the rate of mass or moles that flows across a unit area normal to the component velocity. They are equal to:

$$\mathbf{n_A} = \rho_A \mathbf{v_A} \; ; \; \mathbf{N_A} = C_A \mathbf{v_A} \tag{3.1}$$

where ρ_A is the density of A in the mixture, $\mathbf{v_A}$ is the velocity of A and C_A is the concentration of A. These flux terms are vector quantities relative to fixed coordinates. For the rest of this body of work, we shall consider only molar fluxes for convenience.

The molar flux includes two types of mass transfer: convective and diffusive mass transfer. These represent respectively, the macroscopic and molecular processes of mass transfer. Convective mass transfer relates to the mean velocity of the fluid, which in general differs from the mean velocity of each single component of the mixture. Diffusive mass transfer, or ordinary molecular diffusion, is a molecular process and is caused by the random molecular motion.

The convective flux accounts for the mass transfer associated with the bulk fluid movement and is defined as:

$$(\text{Convective flux})_A \equiv C_A \mathbf{v}^* \tag{3.2}$$

where $\mathbf{v}^*$ is the average velocity of the mixture, defined as:

$$\mathbf{v}^* \equiv \sum_{i=1}^{n} y_i \mathbf{v_i} \; ; \; y_i \equiv \frac{C_i}{C} \tag{3.3}$$

where y_i is the mole fraction of component i, $\mathbf{v_i}$ is the velocity of component i, and C is the overall concentration of the mixture.

When the diffusive flux is negligible, the velocity of a component is the same as the mixture ($\mathbf{v_i} = \mathbf{v}^*$) and so the convective flux coincides with the overall molar flux.

To isolate diffusive mass transfer, we need to look at the mass transfer that occurs relative to the mean velocity of the mixture. We define the diffusion velocity as:

$$(\text{Diffusion velocity})_A \equiv \mathbf{v_A} - \mathbf{v}^* \tag{3.4}$$

and the diffusive flux $\mathbf{J_A}$ as:

$$\mathbf{J_A} \equiv C_A \left(\mathbf{v_A} - \mathbf{v}^* \right) \tag{3.5}$$

For a dilute binary solution, provided diffusive mass transfer is not fast and there is no forced convection, the velocity of the solvent tends to zero. The velocity of the mixture will then tend to $\mathbf{v}^* \approx y_A \mathbf{v_A}$ (where component A is the solute), and so we equation 3.5 becomes:

$$\mathbf{J_A} = y_A C \left(\mathbf{v_A} - \mathbf{v}^* \right) = y_A C \left(\mathbf{v_A} - y_A \mathbf{v_A} \right) = y_A C \left(1 - y_A \right) \mathbf{v_A} \tag{3.6}$$

If the solute is very diluted, $y_A \ll 1$ and therefore $1 - y_A \approx 1$; consequently, we have:

$$\mathbf{J_A} \approx y_A C \mathbf{v_A} = \mathbf{N_A} \tag{3.7}$$

As can be seen from Equation 3.7, the diffusive flux essentially equals the total flux, which implies that convective flux is zero.

This assumption for dilute mixtures renders mass transfer problems a lot simpler. In general, diffusion also causes convective mass transfer, and unless we make these assumptions, convective mass transfer must also be accounted for.

Combining the two molar flux terms, we can express the overall molar flux as:

$$\mathbf{N_A} = \mathbf{J_A} + C_A \mathbf{v}^* \tag{3.8}$$

When expanded, this gives us the original definition of the overall molar flux. These equations are all definitions of fluxes.

The definition of the diffusive flux, given by Equation 3.5, does not allow us to calculate $\mathbf{J_A}$, because we do not know the velocity $\mathbf{v_A}$. This is always true: we know, or can calculate through a suitable transport equation, the velocity $\mathbf{v}^*$ of the mixture, but we do not have any equations that allow us to calculate the velocities of the single constituents of the mixture. Consequently, Equation 3.5 is not useful for calculating $\mathbf{J_A}$. We need a constitutive equation that relates $\mathbf{J_A}$ to variables of the problem that, as opposed to $\mathbf{v_A}$, are either known or can be calculated using known transport equations [Cussler, 2009a, Taylor and Krishna, 1993a, Cussler, 2009b, Stewart et al., 2007a, Rorrer et al., 2001a].

3.1.1.1 Fick's law

Fick's law relates the diffusive flux to the concentration gradient in space. Fick's law states that a component can have a velocity relative to the average velocity of the mixture only if a concentration gradient exists. For the molar flux of component A moving through component B in a binary mixture, Fick's law reads:

$$\mathbf{J_A} = -C D_{AB} \partial_\mathbf{x} y_A \tag{3.9}$$

This equation introduces a diffusion coefficient D_{AB}. The diffusion coefficient depends on temperature, pressure and, to a far less extent, composition of the mixture.

If the mixture concentration is constant, then Fick's law can be written as follows:

$$\mathbf{J_A} = -D_{AB} \partial_\mathbf{x} C_A \tag{3.10}$$

In general, however, the gradient to be used in Fick's law is that of the mole fraction, not of the molar concentration.

We shall assume that the total concentration of the mixture is constant (with temperature and pressure constant).

This equation holds for binary systems; however, as stated before, we are dealing with a multi-component system. There are equations for these systems, but they are quite complex and cannot be easily solved. The complexity arises because in general all the components in the mixture interact, and diffusion reflects this complex interaction. The most common type of equations are the Maxwell-Stefan equations for multicomponent diffusion in gases [Taylor and Krishna, 1993b]. When used for dilute solutions, these equations reduce to the normal Fick's form.

In our situation, each component is dilute with respect to air. With this, we can make a simplification where we assume that each component only interacts with air, and does not "see" the other components. For example, we will have expressions for a particular VOC-air binary mixture. This simplification of a component-air mix is common and for examples of this please refer to the references included [Stewart et al., 2007a, Rorrer et al., 2001a, Cussler, 2009c, Taylor and Krishna, 1993c].

3.1.1.2 Chapman-Enskog theory

The binary diffusion coefficient D_{AB} for non polar gases can be predicted within 5% of its value by Chapman-Enskog theory which is based on kinetic theory. The resulting formula is given by [Stewart et al., 2007e]:

$$D_{AB} = 0.0018583 \sqrt{T^3 \left(\frac{1}{M_A} + \frac{1}{M_B} \right)} \frac{1}{p\sigma_{AB}^2 \Omega_{AB}} \qquad (3.11)$$

where T is the temperature, M_A is the molecular weight of gas A, M_B is the molecular weight of gas B, p is the pressure, σ_{AB} is a Lennard-Jones parameter, and Ω_{AB} is a collision integral for use with Lennard-Jones potential for the prediction of transport properties. Values for σ_{AB} and Ω_{AB} can be found from the relevant tables for common gas mixes or estimated for less common ones [Stewart et al., 2007d].

3.1.2 Mass transfer in porous materials

We are concerned with diffusion within a stack of paper. This is a porous medium, and so we need to investigate how diffusion occurs within the pores.

Within the paper the pores occupy a certain volume. This volume is where the components diffuse through the material in the gas phase. This volume, named void fraction or *porosity*, is denoted as ε and represents the fraction of the material which is not solid.

The pores in a sheet of paper are not expected to be of regular shape or connectivity. For pores that are not straight, the route the molecules go through in the pores is longer than if the pores were straight. This difference is accounted for by what is called pore *tortuosity*.
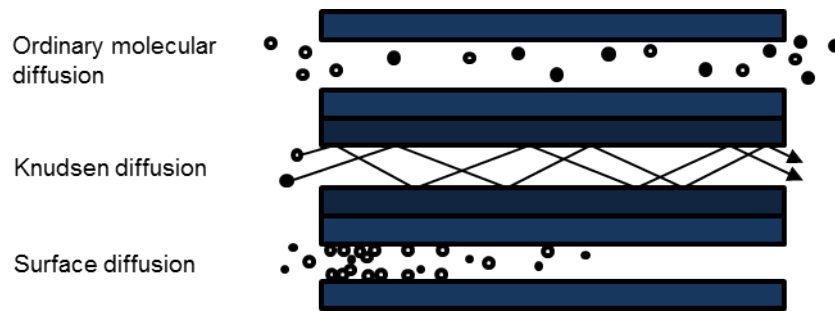
Figure 3.1: Pore diffusion mechanisms [Cussler, 2009d]

Both the paper's tortuosity and porosity are values that need to be found experimentally. This will be explored in the Experimentation chapter.

There are different mechanisms for how gas components diffuse through pores, and this is mostly based on the pore sizes. These mechanisms are shown in Figure 3.1.

When studying porous media and diffusion mechanisms, there are two main properties to consider: mean free path and pore diameter. The mean free path refers to the average distance covered by diffusing molecules between collisions with other molecules.

In ordinary molecular diffusion, the pore diameter is large compared to the mean free path and the diffusing molecules interact with each other more than with the pore walls. In Knudsen diffusion the pore diameter is small compared to the mean free path; the diffusing molecules then collide with the pore walls more than with each other. Finally, surface diffusion is where the molecules adsorb on the walls and then diffuse on the surface.

Pore sizes are classified as macropores, mesopores and micropores. Macropores have a diameter greater than 50nm. Micropores have a diameter less than 2nm. Mesopores are in between these two. The pores in paper are expected to be both in the mesopore and macropore range [Park et al., 2006]. In particular, we expect to find Knudsen diffusion to be the main mechanism for the gas molecules moving through the pores of the paper [Cussler, 2009e, Stewart et al., 2007b, Rorrer et al., 2001a].

3.1.2.1   Ordinary mass transfer in porous materials

For ordinary molecular diffusion, we have pore diameters that are large compared to the mean free path of the diffusing molecules. As such the gas molecules diffusing through will interact more with each other than with the pore walls [Cussler, 2009e]. We therefore describe this type of diffusion in the same way as equation 3.9, but taking the porosity and tortuosity into account:

$$\mathbf{J_A} = -\psi D_A \partial_\mathbf{x} C_A; \; \psi \equiv \frac{\varepsilon}{\tau} \tag{3.12}$$

where D_A is the diffusion coefficient, ε is the porosity, τ is the tortuosity and ψ is the ratio between them.

As mentioned, tortuosity needs to be taken into account because pores are not straight; so, the diffusion path through a pore whose distance in space is L has a length greater than L and equal to τL, with $\tau > 1$.

Porosity needs to be taken into account because for a given surface S of the porous medium, only a portion εS, where $\varepsilon < 1$, is crossed by pores and is therefore available to mass transfer.

One usually measures ψD_A. Then, since D_A and ε are typically known (the porosity can otherwise be easily measured), one can calculate τ.

3.1.2.2   Knudsen mass transfer in porous materials

Knudsen diffusion takes place when the pore diameter is smaller than the mean free path of the diffusing gas molecules, so that the gas molecules interact more with the pore walls than with each other. This happens when the density of the gas is very low or the pore diameter is very small. As a result of this the gas flux is reduced.

To measure whether Knudsen diffusion will play an important role in the system, one can calculate the Knudsen number [Rorrer et al., 2001a]:

$$\text{Kn} = \frac{\lambda}{d_{pore}} \tag{3.13}$$

where λ is the mean free path and d_{pore} is the pore diameter. The pore diameter is an approximation, as pores will not necessarily be circular in shape.

If Kn is greater than 1, then Knudsen diffusion can be important. The mean free path of any gas at standard temperature and pressure is of the order of 10^{-5}cm [Chapman and Cowling, 1970]. Using this value for the mean free path and a value for the pore diameter in the large mesopore range, we see that the Knudsen number is greater than unity:

$$\text{Kn} \approx \frac{10^{-7}m}{10^{-8}m} = 10 \tag{3.14}$$

With this we then have a Knudsen diffusivity term, D_{KA}, which relates to the pore diameter rather than to the path length. This can be expressed using the kinetic theory of gases [Rorrer et al., 2001a]:

$$D_{KA} = \frac{d_{pore}}{3} \left(\frac{8\kappa\eta T}{\pi M_A} \right)^{1/2} \tag{3.15}$$

where κ is the Boltzmann constant, η is the Avogadro constant, and M_A is the molecular weight of A.

The Knudsen diffusivity is not a function of pressure, and is not affected by the presence of the other components in the mixture. Also the temperature dependency is different to the molecular diffusion. This gives us the following flux equation, which does not have a bulk motion contribution:

$$\mathbf{N_A} = -\psi D_{KA}\partial_{\mathbf{x}}C_A \tag{3.16}$$

3.1.2.3 Overall mass transfer in porous materials

There are instances where both Knudsen diffusion and molecular diffusion will be important, and in these transition areas we express the resistance to mass transfer, the inverse of the diffusion coefficients, as resistances in series. Here we consider an overall diffusion coefficient, D_A, which takes both Knudsen diffusion and ordinary molecular diffusion into account:

$$\frac{1}{D_A} = \frac{1}{D_{AB}} + \frac{1}{D_{KA}} \tag{3.17}$$

This overall diffusion coefficient is applicable where the pore sizes vary between the range where both Knudsen and ordinary molecular diffusion occur [Rorrer et al., 2001a, Cussler, 2009e, Stewart et al., 2007b]. Using the porosity and tortuosity ratio, we then get an effective diffusion coefficient:

$$D_{Ae} = \psi D_A \tag{3.18}$$

3.1.3 Mass transfer in the fluid surrounding the porous material

We have outlined how to model mass transfer within the paper material, stating that diffusion will be the dominant type of mass transfer. The equations describing the process of mass transfer are second-order partial differential equations. To solve them, we need to assign the conditions at the boundaries of the material: the boundary conditions. There are different methods to prescribe these conditions; one instance requires the continuity of the fluxes at the boundaries. In order to assign the conditions, we need to investigate the mass transfer problem in the domain surrounding the paper volume. This is expected, as what happens inside the volume is affected by what happens outside of it.

The composition of the air outside the paper will influence the concentration profiles at the boundary of the paper, as gaseous compounds escape and enter the paper from outside. In most cases, where the paper is stored, the surrounding air will have forced convection due to air conditioning and other ventilation. In these scenarios, convective mass transfer will be the dominant type of mass transfer and diffusion will be negligible. There can of course be cases where the paper is stored in containers where the air is stagnant, and diffusion will again be the dominant type of mass transfer.

To express the flux in the surrounding air, the concentration profile and velocity profile across its volume are needed. In majority of the surrounding air, the velocity and concentration will have little variation. Between the surface of the stack of paper and the bulk of the surrounding air the velocity and concentration profiles will change more dramatically. This region is called boundary layer.

3.1.3.1 Boundary layer theory

As mentioned, between the surrounding air and the paper, a boundary layer will develop. This is because when there is flow over a solid, at the wall of the solid there is a "no-slip" boundary condition, as the fluid next to the surface does not move. As such, there is a velocity profile, where the velocity
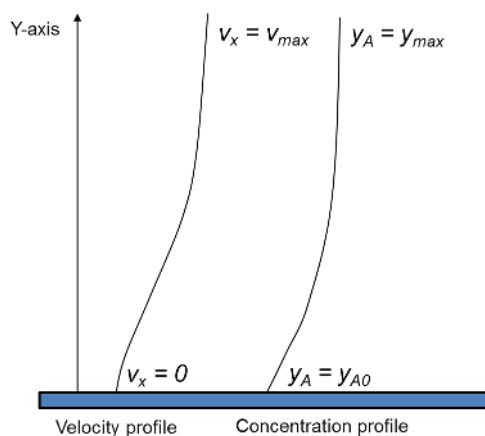
Figure 3.2: Concentration and velocity profiles [Stewart et al., 2007c]

at the surface of the paper will be zero and will increase as we move away from the surface until we reach the same velocity as the bulk mixture of the surrounding air.

Similarly, there will be a concentration profile. At the surface, the concentration will not be zero, and is called the surface concentration. This will then increase (or decrease depending on the direction of flux) to the same concentration as the bulk mixture. This is depicted in Figure 3.2 [Stewart et al., 2007c].

Calculating these profiles can be very complicated and unnecessary as we only are interested in the concentration or the flux at the surface; therefore more idealised, simpler models of the mass transfer phenomenon are available to use.

3.1.3.2   Mass transfer coefficient

The mass transfer coefficient is typically used in simplified mass transfer problems where the concentration's relation to time and space is not required. In flux equations with a mass transfer coefficient, the flux is assumed to be proportional to the concentration difference between the surface and the bulk.

For component A, we define the mass transfer coefficient, as follows:

$$N_{A,y} \equiv k_c \triangle C_A \tag{3.19}$$

where $N_{A,y}$ is the molar flux of A in the direction perpendicular to the surface of interest, $\triangle C_A$ is the concentration difference between the surface and the bulk concentrations of the fluid stream of A, and k_c is the mass transfer coefficient.

From this, the inverse of the mass transfer coefficient $1/k_c$ is described as the resistance to transfer through the moving fluid, and is generally a function of the system's geometry and of the fluid and flow properties [Taylor and Krishna, 1993d, Stewart et al., 2007c].

3.1.3.3 Empirical dimensionless correlations

It is suggested that the Sherwood number, Sh, is a function of the Reynolds number, Re, and of the Schmidt number, Sc [Rorrer et al., 2001b,c]. These numbers are defined as:

$$Sh \equiv \frac{k_c L}{D_{AB}} \; ; \; Re \equiv \frac{\rho v L}{\mu} \; ; \; Sc \equiv \frac{\mu}{\rho D_{AB}} \tag{3.20}$$

Where k_c is the mass transfer coefficient, L is a characteristic length, D_{AB} is the diffusivity coefficient, ρ is the density of the fluid, v is the characteristic speed of the fluid, and μ is the viscosity of the fluid.

This function depends on the problem at hand, for example for flat plates:

Laminar flow:

$$Sh = 0.664 Re^{1/2} Sc^{1/3} \tag{3.21}$$

Turbulent flow:

$$Sh = 0.036 Re^{1/2} Sc^{1/3} \tag{3.22}$$

In general, we have the following relation:

$$Sh = f(Re, Sc) \tag{3.23}$$

We assume laminar flow when the Reynolds number is smaller than 200000 and turbulent flow when the Reynolds number is greater than 200000 [Rorrer et al., 2001c].

This can help when studying mass transfer problems, as it relates the mass transfer coefficient to the bulk velocity. The flat plate correlation is the most relevant for our problem as the paper can be viewed as a flat plate. This relation can therefore be utilised when describing the continuity of the fluxes for the boundary conditions.

3.2 Adsorption

Adsorption is a particular type of sorption phenomenon. Other sorption phenomena are: desorption (which is the reverse of adsorption) and absorption. In adsorption, molecules from one state (liquid or gas) stick to the surface of a solid material. The material on which the molecules stick is called the adsorbent and the molecules that stick to it are called the adsorbate. Adsorption can then be split into two types: physical adsorption and chemical adsorption (chemisorption).

Physical adsorption is where the adsorbate is held to the surface of the adsorbent by weak inter-molecular Van der Waals forces. Chemical adsorption is where the adsorbate is held to the adsorbent

by strong chemical bonds. Adsorption differs from *absorption*, because in absorption molecules of one state are taken up by the *volume* of another substance in another state; for example, CO_2 gas molecules absorbed into a volume of liquid. Conversely, in adsorption molecules are adsorbed onto the *surface* of another solid substance.

As a general rule, the amount an adsorbate that adsorbs onto a surface is roughly proportional to the amount of surface [Cussler, 2009f].

3.2.1   Ordinary adsorption

At a set concentration of a substance in the gas phase (at a given temperature and pressure), there is a maximum concentration the substance can reach in the adsorbed phase on the solid surface.

The relation between the maximum concentration on the solid surface and the concentration in the gas phase at a given temperature and pressure is a thermodynamic (that is, an equilibrium) relation. Plots of this relation are called adsorption isotherms.

Isotherms relate the amount of adsorbate that is adsorbed against its concentration in the gas mixture. They depend on the temperature and pressure of the system, as well as on the adsorbent. For a particular temperature an isotherm can be generally described mathematically as [Cussler, 2009f]:

$$[A] = f(C_A) \tag{3.24}$$

where $[A]$ is the concentration of A in the adsorbed phase and C_A is the concentration of A in the gas phase. The adsorbed phase concentration is typically given in units of moles of solute per dry mass of adsorbent but can also be in terms of moles per area. Isotherms can also be expressed with the pressure of the adsorbate (p_A) in place of the gas phase concentration C_A.

In industry, the isotherm that is preferred is one where the adsorbent can adsorb a lot of the adsorbate when this is in low concentrations in solution. An unfavourable curve would be one in which the adsorbent only adsorbs well when the solute is very highly concentrated. This industrially unfavourable curve is conversely what we would prefer for our problem as the less acidic VOCs that are in the adsorbed phase, the smaller the increase in acidity. The simplest model for the isotherm would be a linear isotherm. A linear isotherm assumes:

$$[A] = K_A C_A \tag{3.25}$$

The linear isotherm is used for most simple theories, and is also called the Henry adsorption isotherm. Here, K_A is the Henry adsorption equilibrium constant for A. It is a useful approximation for cases where the concentrations in both the adsorbed phase and gas phase are low. This is because at low concentrations many isotherms display a linear correlation.

A more thorough theoretical model is the Langmuir isotherm. This model assumes that the adsorbent only has a certain number of "sites" where the adsorbate can attach to. We assume that the adsorbate cannot adsorb in multiple layers. This is expressed mathematically as:
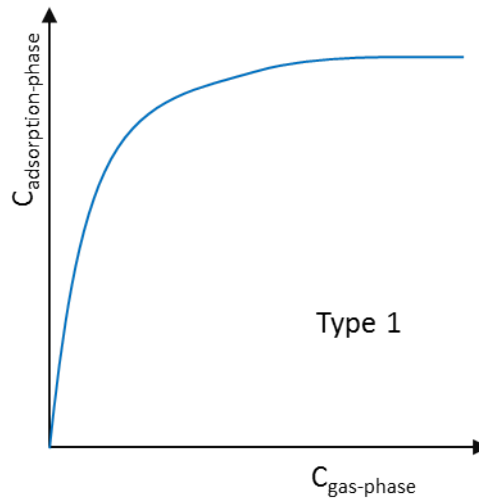
Figure 3.3: Type 1 Brunauer classification isotherm [Tiffonnet et al., 2002]
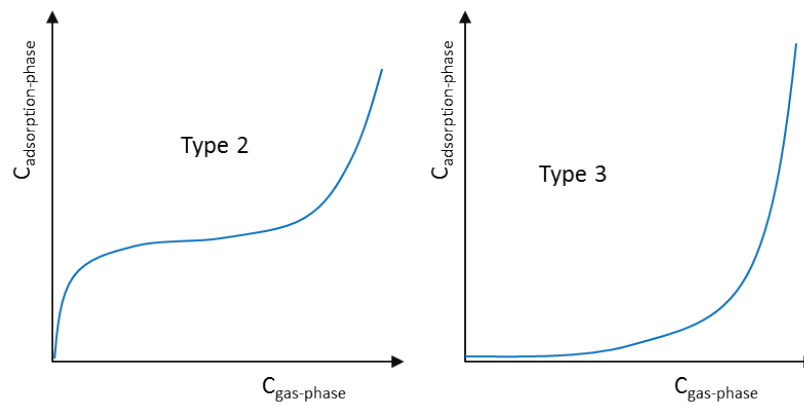
Figure 3.4: Type 2 & 3 Brunauer classification isotherms [Tiffonnet et al., 2002]

$$[A] = \frac{[A]^0 K_A C_A}{1 + K_A C_A} \tag{3.26}$$

where $[A]^0$ is the mono-layer sorbent concentration. In this model, as $C_A \to \infty$ it can be seen that $[A] \to [A]^0$. This implies that the adsorbent saturates, no longer being able to adsorb more, even if C_A increases further. This model when plotted follows the type 1 form of isotherm proposed by Brunauer and is shown in Figure 3.3. For more details please refer to the references [Cussler, 2009f, Tiffonnet et al., 2002].

The second and third types of isotherm proposed by Brunauer deal with multilayer adsorption. With this, an adsorbate can attach onto another adsorbate that is connected to a site on the material. Types 2 and 3 are shown in Figure 3.4.

Type 2 is initially the same as Type 1, but after levelling off, adsorption increases again as multilayer
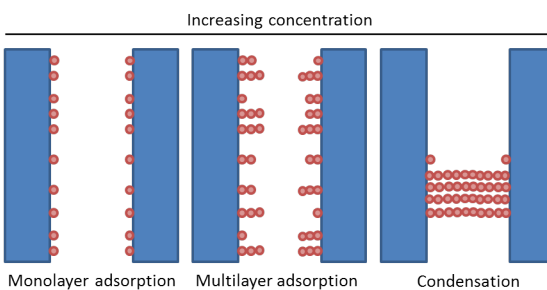
Figure 3.5: Adsorption in pores
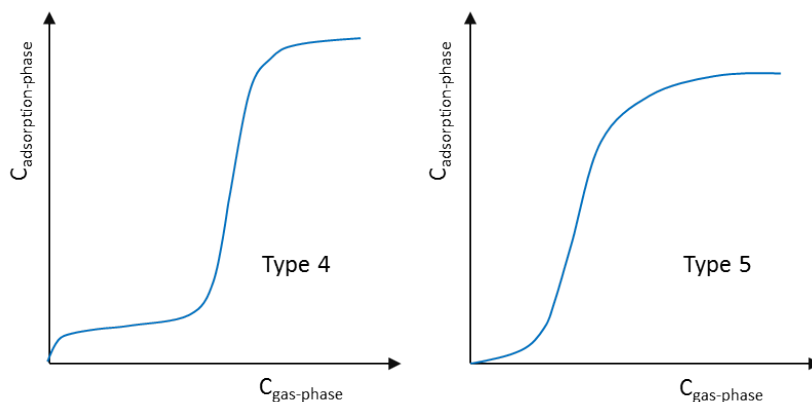
Figure 3.6: Type 4 & 5 Brunauer classification isotherms [Tiffonnet et al., 2002]

adsorption happens and adsorbate-adsorbate interactions become dominant. Type 3 is where there is little adsorption under low concentrations, but the adsorbed phase concentration increases rapidly once adsorption has started, due to adsorbate-adsorbate interactions.

We now explore how adsorption occurs within porous materials.

3.2.2   Adsorption in porous materials

Figure 3.5 shows how the adsorption process can work as the concentration of the adsorbate increases within pores. With monolayer adsorption, the interactions between the adsorbate and the adsorbent dominate. In multilayer adsorption, it is possible for the adsorbate-adsorbate interactions to dominate. This is because the majority of the adsorbing substance can now be interacting with other adsorbates which have already been adsorbed onto the material and formed at least one layer. In condensation, the pores have been completely filled; this happens when the gas pressure is greater than the saturation vapour pressure [Tiffonnet et al., 2002]. Condensation is not expected for the degradation compounds in paper as their concentrations will not be high enough.

Types 4 and 5 of the Brunauer classifications of isotherms are typical of porous materials and are shown in Figure 3.6.

They behave like Type 2 and 3 at first, but then both level off as the pores become filled with the adsorbate and are saturated, allowing no more of the adsorbate to be adsorbed [Tiffonnet et al., 2002].

With paper being a porous material, we expect the VOCs to follow Type 4 and 5. It is also expected that we are dealing with very low concentrations and therefore the isotherm can be viewed as linear, following the initial shapes of either Type 4 or 5. When the VOCs are in the adsorbed phase, they may participate in reactions. The gas phase concentration of VOCs is in thermodynamic equilibrium with the adsorbed phase, and so a change in the gas phase concentration is linked to a change in the adsorbed phase concentration.

3.3   Chemical reaction

In this chapter we have studied mass transfer in the gas phase and the relation between the gas phase and adsorbed phase through adsorption isotherms. We now explore the adsorbed phase, in particular the reactions that occur there.

In Chapter 2, we outlined the degradation reactions occurring within paper and the role VOCs played in the degradation process. These reactions need to be accounted for in the mathematical model as degradation compounds are both generated and destroyed within the system. To start, we explore how our work relates to a general reactive process in a porous medium.

3.3.1   Reactive process in a porous medium

A major type of reaction involving porous materials is that of a catalytic reaction. Ideally, a catalyst is a chemical species which affects the rate of reaction but emerges unchanged. In the catalytic process, the reaction occurs at or very near the interface. As time goes on, a catalyst can lose effectiveness through ageing, poisoning or fouling [Fogler, 2010d].

The general steps in a catalytic reaction are as follows [Fogler, 2010e]:

1. First the reactants diffuse from the bulk volume to the surface of the catalyst.

2. Then the reactants diffuse into the pores of the catalyst.

3. The reactants then diffuse from the pore bulk to the pore wall and adsorb onto the surface.

4. The reaction occurs.

5. The products produced in the reaction then desorb from the surface of the catalyst.

6. The products then diffuse out of the catalyst pores.

7. And finally diffuse into the bulk volume.
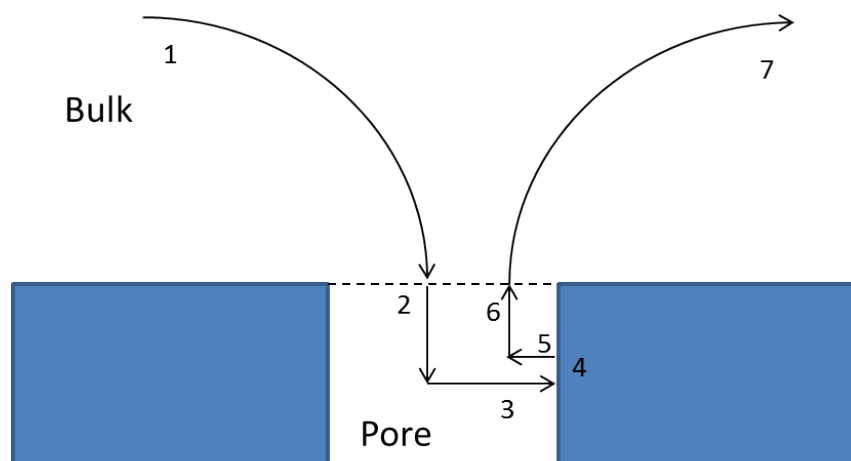
Figure 3.7: Catalyst reaction steps

This is similar to what we assume occurs in the scenario we are investigating and is displayed in Figure 3.7. In our scenario, the paper fibre is our solid catalyst, or more particularly, cellulose. In our case, however, cellulose does react and does not behave like a catalyst. We do not account for other components which make up the paper initially, as cellulose is the main component by a significant degree. The degradation compounds in paper diffuse through the pores, are adsorbed and desorbed as well as being involved in reactions in the adsorbed phase.

3.3.2 Rate of reaction and rate law

Usually, one defines r_A as the number of moles of A produced per unit time and volume. This quantity, consequently, is negative if A is a reactant and positive if A is a product. In this project, we require the rate of reaction for the VOCs we intend to study.

Reactions can be either homogeneous or heterogeneous. A homogeneous reaction is a reaction in which the reactants are in the same phase. A heterogeneous reaction is where the reactants are in two or more phases [Fogler, 2010a].

In a homogeneous reaction, the reaction rate is measured in the number of moles of the species reacting per unit volume, per unit time. In a heterogeneous reaction, the reaction rate is typically measured in the number of moles of the species reacting per unit time, per unit mass of the substance in the other phase (or per unit surface).

We will view our reactions as homogeneous, because we assume that the degradation reactions happen in the adsorbed phase with the cellulose fibres.

If we know the stoichiometry of the reactions, we can relate the reaction rates of each species to each other. For example, if we have a reaction of the following sort:

$$aA + bB \rightarrow cC + dD \tag{3.27}$$

We relate the reaction rates thus [Fogler, 2010b]:

$$\frac{-r_A}{a} = \frac{-r_B}{b} = \frac{r_C}{c} = \frac{r_D}{d} \tag{3.28}$$

Typically, the reaction rate is written as a product of a reaction rate constant k and concentrations of species involved in the reaction:

$$-r_A = k(T)f(C_A, ..., C_n) \tag{3.29}$$

where T is the absolute temperature and C_A to C_n are the concentrations of the species involved in the reaction.

When the reaction rate is expressed like this, it is referred to as rate law. The reaction rate constant relates to the particular species for which we have the reaction rate. The dependence of the reaction rate on concentrations is typically found through experimentation.

3.3.3 Arrhenius equation

When describing a reaction, the so-called reaction rate constant k is not actually constant, but is typically independent of the concentrations of the species involved in the reactions. Normally, the constant is dependent on temperature; in a gas phase reaction, it can be dependent on the pressure.

The Arrhenius equation gives the reaction constant as a function of temperature:

$$k = Ae^{-E/RT} \tag{3.30}$$

Where A is the pre-exponential factor, E is the activation energy, R is the gas constant, and T is the absolute temperature. The activation energy is found through experimentation with the reaction occurring at different temperatures.

The relation between reaction rate and temperature is needed, as experimentation for reaction rates will take place at different temperatures, even though in reality, paper is kept at room temperature which does not vary largely. We raise the temperature of paper in order to accelerate the ageing, which in turn gives a greater concentration change for analysis. Also changing the temperature can help explore how slight variations in temperature can affect the rate of reaction.

3.3.4 Rate of VOC generation

We now look at the reaction(s) that generate VOCs in the system.

Typically, the reaction rate for a reaction (or group of reactions) is unknown. To find the overall reaction rate with regards to a substance, the following algorithm is suggested [Fogler, 2010c]:

1. Postulate a rate law, using what knowledge is available about the system being studied and known rate laws for similar systems.

2. Choose the reactor type and design equations. Is the reactor running as continuous or as batch? This choice determines the design equations.

3. Process the data obtained from experiments in terms of the measured variable.

4. Make any further simplifications. For example, if a reactant is in excess we can simplify the model assuming that the concentration of the reactant is constant.

5. Calculate $-r_A$ as a function of the concentrations with the postulated equations and data.

6. Review and experiment further to confirm the data's fit for the rate law postulated. The work may need to be revised with some or all of the steps being revisited.

We will use this method for discerning the reaction rates and relevant rate laws for VOC generation.

3.3.4.1 Postulating a rate law for generating VOC

In Chapter 2, we outlined our assumption that the VOC generation is related to the degradation state through the cellulose monomer loss. This assumption is based on the evidence that the VOC we are considering, acetic acid, is produced as all paper types degrade. We know that the main component of any paper is cellulose and its degradation is considered the main indicator of the state of paper. We therefore assume that the cellulose degradation is responsible for the majority of the VOC production, although some may be due to other paper components.

Another simplification we have made, is that we have only one, dominant VOC. We choose acetic acid as our single VOC, as it is present in most paper types and strongly acidic by comparison to other VOCs found. This is a gross but necessary simplification, as the real system is much more complex, where it is possible many VOCs contribute differently to the acidity depending on their relative strengths. Also, some papers are alkaline, which means they have an alkali reserve. This would mean that as an acid is produced, it will not increase the acidity of the system as it is neutralised by the alkali compounds. When the reserve is exhausted, newly produced acid will then be able to increase the acidity. We now want to link the monomer loss rate to the generation of acetic acid.

At time t the local number of cellulose monomers is $N(\mathbf{x}, t)$. After a differential time dt, the number of monomers decreases by the local number of end chain bonds that break, as described in section 2.5.2.1:

$$N(\mathbf{x}, t + dt) = N(\mathbf{x}, t) - \frac{2y(\mathbf{x}, t)dt}{DP(\mathbf{x}, t) - 1} \tag{3.31}$$

where $y(\mathbf{x}, t)$ is the total number of bonds broken locally.

The change in monomers over time is then expressed as:

$$\partial_t N(\mathbf{x}, t) = -\frac{2y(\mathbf{x}, t)}{DP(\mathbf{x}, t) - 1} = -\frac{2k_{DP}(\mathbf{x}, t)N(\mathbf{x}, t)}{DP(\mathbf{x}, t) - 1} = -\alpha(\mathbf{x}, t)k_{DP}(\mathbf{x}, t)N(\mathbf{x}, t) \qquad (3.32)$$

where k_{DP} is the relative number of bonds that break per unit time, normalised with respect to the overall number of monomers and α is the fraction of end bonds given by:

$$\frac{2}{DP(\mathbf{x}, t) - 1} \qquad (3.33)$$

We cannot say that one monomer is equal to one molecule of acetic acid as a cellulose monomer is bigger than an acetic acid molecule and the monomer is capable of producing other VOCs. Also there will be an associated activation energy with the creation of acetic acid from the monomer.

We then have the following term for the generation of acetic acid:

$$r_{gen} = -\beta\partial_t N(\mathbf{x}, t) = \beta\alpha(\mathbf{x}, t)k_{DP}(\mathbf{x}, t)N(\mathbf{x}, t) \qquad (3.34)$$

where β is related to the amount of acetic acid produced by a monomer of cellulose leaving the chain. One further assumption we can make is that the number of monomers, although decreasing, would stay a vast large number that is nearly constant at least in terms of order of magnitude. We therefore define our reaction constant for VOC generation:

$$k_{vr} = \beta N \qquad (3.35)$$

Obtaining:

$$r_{gen} = k_{vr}\alpha(\mathbf{x}, t)k_{DP}(\mathbf{x}, t) \qquad (3.36)$$

The reaction constant k_{vr}, would then be found through experimentation continuing with steps 2 and onwards as described above.

3.3.5 Modelling the dissociation of acetic acid

We have an expression for the generation of acetic acid. We now need to express how the VOC's presence changes the local acidity when there is no alkaline reserve. The presence of the VOC affects the acidity of the system through acid dissociation, which in turn affects the degradation rate and VOC generation through the reaction constant k_{DP}. We assume there is enough water present for dissociation and that dissociation is infinitely fast in comparison to other reactions involved in our problem and deal with in terms of thermodynamics; therefore in this section we deal with equilibrium law.

The acid dissociation reaction for acetic acid is:

$$CH_3COOH \rightleftharpoons CH_3COO^- + H^+ \tag{3.37}$$
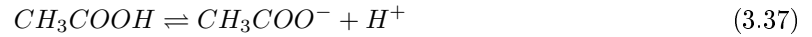
This follows the dissociation reaction for a monoprotic acid in aqueous solution. To lighten notation, we will use HA for acetic acid and A^- for the negative ion (the acid in its dissociated state). This definition ignores the hydrogen ions due to water's presence as its contribution is nearly zero. The definition also assumes that the water concentration is constant as it varies very little.

Initially, at time zero, we assume we have no acetic acid present. The paper has a set acidity which it will not decrease from, $[H_0^+]$.

At time t (at a general location $\mathbf{x}$) we have a total amount of the VOC $[HA]$ which we assume we know, that accounts for both the dissociated state $[A^-]$, and regular state of the VOC $[HA]_r$:

$$[HA](\mathbf{x}, t) = [HA]_r(\mathbf{x}, t) + [A^-](\mathbf{x}, t) \tag{3.38}$$

The acidity at time t is equal to the initial acidity, plus the amount of hydrogen ions produced due to acetic acid's dissociation which is equal to $[A^-]$:

$$[H^+](\mathbf{x}, t) = [H_0^+] + [A^-](\mathbf{x}, t) \tag{3.39}$$

Therefore, to know the local acidity at time t, we need to know $[A^-]$.

The acid dissociation constant for the equilibrium is defined as:

$$Ka = \frac{[A^-](\mathbf{x}, t)[H^+](\mathbf{x}, t)}{[HA]_r(\mathbf{x}, t)} = \frac{[A^-](\mathbf{x}, t)\left([H_0^+](\mathbf{x}, t) + [A^-](\mathbf{x}, t)\right)}{[HA](\mathbf{x}, t) - [A^-](\mathbf{x}, t)} \tag{3.40}$$

In the above equation, everything is known except $[A^-]$. To solve, we first rearrange Equation 3.40 to give the following quadratic:

$$0 = \left([A^-](\mathbf{x}, t)\right)^2 + ([H_0^+](\mathbf{x}, t) + Ka)\left([A^-](\mathbf{x}, t)\right) - Ka[HA](\mathbf{x}, t)$$

Which can be solved using the quadratic formula:

$$[A^-](\mathbf{x}, t) = \frac{\sqrt{([H_0^+](\mathbf{x}, t) + Ka)^2 + 4Ka[HA](\mathbf{x}, t)} - ([H_0^+](\mathbf{x}, t) + Ka)}{2}$$

When no VOC is present, this reduces to zero. We then can express the acidity at any time in terms of the initial acidity and the total VOC concentration in the adsorbed phase:

$$[H^+](\mathbf{x}, t) = [H_0^+](\mathbf{x}, t) + \frac{\sqrt{([H_0^+](\mathbf{x}, t) + Ka)^2 + 4Ka[HA](\mathbf{x}, t)} - ([H_0^+](\mathbf{x}, t) + Ka)}{2} \tag{3.41}$$
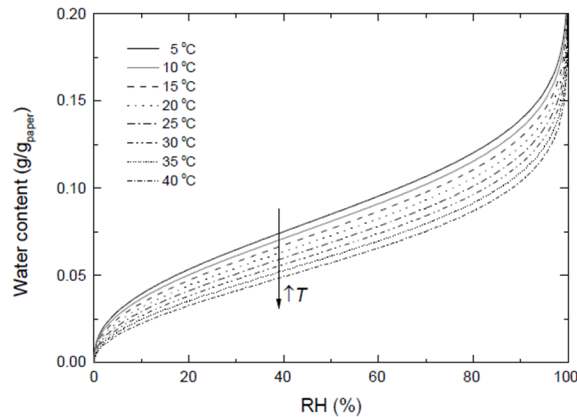
Figure 3.8: Water content of paper against relative humidity for different temperatures [Paltakari and Karlsson, 1996]

The acidity of the paper can increase above the initial acidity, or decrease back down to the initial acidity when the VOC is removed. We assume that the adsorbed phase concentration used in the adsorption isotherm is that of the total VOC concentration $[HA]$.

As we have assumed there is an excess of water, we cannot use these expressions for a dry environment. Figure 3.8 shows the water content of paper against relative humidity predicted by Equation 2.26 from Chapter 2 [Paltakari and Karlsson, 1996] and gives an indication of when relative humidity may be too low.

3.3.6 Alkaline reserve neutralisation

If we have an alkaline reserve, we assume it is in the form of calcium carbonate (sometimes it is magnesium carbonate). The calcium carbonate reacts with acetic acid giving the following neutralisation reaction:

$$2CH_3COOH + CaCO_3 \rightarrow CO_2 + H_2O + Ca\left(CH_3COO\right)_2 \tag{3.42}$$
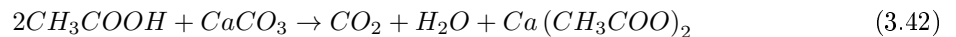
This reaction is made up from different steps. First we have the dissociation reactions of calcium carbonate and acetic acid:

$$CaCO_3 \rightleftharpoons Ca^{2+} + CO_3^{2-} \tag{3.43}$$

$$CH_3COOH \rightleftharpoons H^+ + CH_3COO^- \tag{3.44}$$
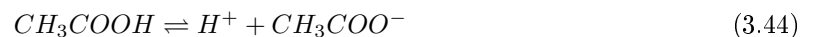
Then we have the reactions between the ions:

$$Ca^{2+} + 2CH_3COO^- \rightarrow Ca\left(CH_3COO\right)_2 \tag{3.45}$$

$$2H^+ + CO_3^{2-} \rightarrow CO_2 + H_2O \tag{3.46}$$

We assume that this neutralisation is instant. This would mean that any acetic acid produced in the adsorbed phase is instantly neutralised and the alkaline reserve decreased. In addition to this, any acetic acid in the gas phase would be adsorbed and neutralised. The alkaline reserve is fully depleted when all of the calcium carbonate has been used up in neutralising the acid. If we know the initial amount of calcium carbonate, we can calculate how much of the alkaline reserve remains at any time by knowing how much acid has been neutralised. This will be explored in more detail in Chapter 4.

Chapter 4

Model Development

In this chapter, we review work on other VOC mass transfer problems and see where they are applicable to this project. After this, we derive our model, using previous work as starting point. We will also derive alternative models for comparison.

4.1 Literature review on VOC mass transfer modelling

Here we review some previous work that has been carried out to model VOC concentration profiles in time and space. Articles that investigate VOC mass transfer typically focus on solving the problem in relation to indoor air quality (IAQ). This is because VOCs in the gas phase have been found to contribute to serious health problems and are emitted from a substantial amount of materials found indoors [Zhang and Niu, 2004]. In this section, we explore these articles because these will help us to develop a model suitable for our specific problem.

As these articles focus on IAQ, the important concentration profile they wish to predict is that in the air filling the room. This is an significant difference to the focus of this project, as we are interested in the concentration profile within the paper and not in the air surrounding it. The majority of articles does not consider the state of the materials emitting and adsorbing the VOCs, whilst we are concerned with linking the concentration profile within paper to the degradation state of the latter. Also, another major difference is that most articles consider an inert, non-reactive solid material, whereas in our case the material (paper) is reactive.

4.1.1 Different modelling approaches

There are two main approaches for modelling concentration profiles: the empirical and the theoretical approach.

4.1.1.1 Empirical approach

Empirical relations are based on results gained from experiments. When modelling IAQ problems, these results are typically obtained by using a test chamber with the material being studied placed within the chamber. The concentrations of VOCs are found through regular sampling of the air within the chamber over time, where the samples are then analysed, typically through gas chromatography. This information is then fitted to a curve, for example using non-linear regression curve fitting [Chang and Gui, 1992], or linear regression methods such as ordinary least squares [Dunn, 1987].

Empirical relations have the advantage of normally being simple and easy to use. As said, their parameters are determined by fitting the experimental data used to define the model [Dunn, 1987, Clausen, 1993, Guo et al., 2004]. Using non-linear regression curve fitting for the experimental data may lead to multiple solutions. Also the resulting parameters from an empirical relation may not be suitable for scale up for use in practical conditions, in real buildings [Sparks et al., 1996]. Finally, empirical relations do not provide any insight into the physics of the problem as typically they give information about bulk properties, not local properties and so the detail is much less.

As this project aims to understand better the process of degradation in paper, the empirical modelling approach is not suitable. Also, an empirical model would not be applicable for archives as they all have very different compositions in the collections they keep, which would be impossible to re-create in experiments.

4.1.1.2 Theoretical approach

Theoretical models are based on the fundamentals of mass transfer. Using a theoretical model, we can gain insight into what happens as the paper degrades; so these models are preferable to empirical relations. Some of these models can be solved analytically [Lee et al., 2005, Deng et al., 2008, Wang and Zhang, 2011] and therefore have a closed form solution. More complex models must be solved numerically [Yang et al., 2001], using numerical integration methods to solve the equations and obtain results. Experimental data either from the literature or by the researchers who created the models are used to validate the models.

There are different levels of complexity that these models attempt to tackle. The basic model has one single material within a room that emits VOCs. There are two ways to expand this. The first is to study multiple materials within a room and the second is to investigate materials with multiple layers. These two expansions can naturally be combined. These expansions are of interest to this work. A book can be considered as a multilayer material, where the covers are layers, as are the spine and the paper within. Then an archive or library has multiple books in a room, thus having multiple materials within a room.

These models typically consider the VOCs to be lumped together under one component [Murakami et al., 2003]. This is probably due to their concentrations being relatively low when summed together in comparison to the other components of air (water and oxygen in particular).

One problem some models have is that they only consider mass transfer in one dimension for simplicity [Lee et al., 2005, Wang and Zhang, 2011]. This is clearly not realistic for real cases. Other models are 2D, which is still not realistic [Murakami et al., 2003].

The focus of this project is to model the VOC concentration profiles within the paper, not the surrounding air. The surrounding air is important though, as the concentration profile is affected by what is around the book and so cannot be disregarded. Because of this, in principle we would have to model also the concentration profile in the surrounding air. This can be simple in cases where the surrounding air is stagnant and only diffusive mass transfer needs to be considered, but can be complicated in cases where convective mass transfer needs to be accounted for. We can use the mass transfer coefficient describing the mass transfer between the well mixed air through the boundary layer to the surface.

Some models that assume the surrounding air to be well mixed neglect to consider the boundary layer [Dunn, 1987, Little et al., 1994]. Other models have added complexity where they solve the velocity profiles in the surrounding air using Navier-Stokes equations [Deng and Kim, 2007]. These models can then analyse concentration profiles within a room in a more detailed fashion but are particular to the dimensions and properties of the room studied and hard to apply to other cases. Most models consider the boundary layer using the mass transfer coefficient and dimensionless empirical correlations [Lee et al., 2005, Zhang and Niu, 2004].

These simplifications to describing the surrounding air concentrations are necessary as real ventilation in rooms is complicated as are the geometries of some rooms. In addition, boundary layers are very thin, and solving the Navier-Stokes equations in the bulk and in the boundary layer is complicated and expensive computationally.

Some of these models use CFD for solving the mass transfer problems [Deng et al., 2008, Deng and Kim, 2007, 2004], but this can be time consuming and costly [Zhang and Niu, 2004]. Another complication encountered when using CFD is that there is a jump between the concentration of VOC in the gas-phase and the concentration in the solid-phase, which is described by an adsorption isotherm. This can cause the solution to diverge. To accommodate this, some models use the Air-Equivalent concentration in the solid phase [Yang et al., 2001, Deng and Kim, 2007, 2004]. This is partially because some of the materials they are observing are not porous materials. In porous materials jumps are not present as the concentration profile is always in the gas-phase.

4.1.1.3   Numerical VOC simulation by Yang et al.

The materials studied in VOC models are often assumed to be homogeneous and not to degrade over time. This is because the models do not take the state of the material into account as they focus on the air quality. The model put forward by Yang et al. for simulating VOC emissions from dry materials does consider that the materials will have different concentration profiles depending on its age. To accomplish this, the model has an "AGE" parameter [Yang et al., 2001].

The mass transfer in the material is described by diffusion:

$$\partial_t C_v = D_v \partial_{\mathbf{x}} \cdot \partial_{\mathbf{x}} C_v \tag{4.1}$$

where C_v is the concentration of the VOC and D_v is the diffusion coefficient through the material.

If the material is new, the initial conditions are:

$$C_v(\mathbf{x}, t = 0) = C_{v,0} \tag{4.2}$$

where $C_{v,o}$ is the initial concentration of the compound in the solid slab. For an aged material, the initial condition is:

$$C_v(\mathbf{x}, t = 0) = C_{v,0}F(\mathbf{x}, AGE) \tag{4.3}$$

where AGE is the age of the material in days, $F(\mathbf{x}, AGE)$ is the function used to describe the initial profile in the solid. When the age of a material is zero, it is assumed that there is a uniform concentration distribution. When age is non-zero, a non-uniform concentration is assumed. To simulate different ages, a numerical simulation was carried out for the AGE period assuming the material is in a small scale chamber. The concentration distributions in the material are then used as the initial concentration in the material for new simulations for materials of that age.

The simulation results showed emission rates for smaller AGE are higher at the beginning and that the effect of AGE diminishes after a period.

Although this model allows a non-uniform concentration distribution, it assumes no VOCs are produced through degradation reactions as the material ages, and the only way for the material to contain more VOCs through time is via diffusion from the air surrounding the material where the surrounding air has a higher VOC concentration. If the surrounding air is ventilated so that the VOCs are evacuated constantly, the material would eventually have a negligible amount of VOCs so as to be no longer considered as a source (or sink) of VOC emissions.

4.1.1.4   Analytical VOC model by Lee et al.

The analytical model by Lee et al. considers materials where VOCs are generated or eliminated by chemical reactions [Lee et al., 2005]. This generation or elimination is part of what is referred to as secondary source/sink behaviour of VOCs with respect to materials [Wolkoff, 1995].

Most models do not consider secondary source/sink behaviour. Source behaviour is where the material generates VOCs in the surrounding air, while sink behaviour is where the material removes VOCs from the surrounding air. Materials can be both a source and sink of pollutants. Primary and secondary source/sink behaviour are described as follows:

- Primary source behaviour is the emission of VOCs into the gas phase which were originally physically adsorbed within the porous material.

- Primary sink behaviour is the transfer of VOCs into the material from the gas phase into the physically adsorbed phase.

- Secondary source behaviour is the emission of VOCs by means other than the primary source behaviour, including VOCs generated from chemical reactions.

- Secondary sink behaviour is sink behaviour by means other than the primary sink behaviour, which includes chemical reactions and chemical adsorption.

The analytical model proposed by Lee et al. has the following governing equation, encompassing diffusion through the gas phase, surface diffusion and generation or elimination of VOCs due to secondary source/sink behaviour:

$$\varepsilon \partial_t C_v + \partial_t[v] = D_{e,g} \partial_{\mathbf{x}} \cdot \partial_{\mathbf{x}} C_v + D_{e,ad} \partial_{\mathbf{x}} \cdot \partial_{\mathbf{x}}[v] \pm g(\mathbf{x}, t) \tag{4.4}$$

where ε is the porosity, C_v is the gas phase concentration, $[v]$ is the adsorbed phase concentration, $D_{e,g}$ is the effective gas-phase diffusion coefficient of the porous material, $D_{e,ad}$ is the effective surface diffusion coefficient of the porous material, $g(\mathbf{x}, t)$ is the VOC generation/elimination due to secondary source/sink behaviour.

Different hypothetical generation functions were considered. The first set they considered was a constant rate of VOC at 3 different locations: throughout the whole solid material, only at the material-air interface, and only at the bottom of the surface. The second set used a sinusoidal function to represent secondary source behaviour that has a periodic nature.

One problem the model has is that there are few models or experiments to compare results with due to the small number of models considering secondary behaviour. Another problem is that *the model assumes that the VOC generation rate is a known function of time and space* [Lee et al., 2005, Wang and Zhang, 2011]. Let us consider a reactant A whose generation rate is given by the known function:

$$r_A = r_A(C_A) \tag{4.5}$$

We then can express the reaction rate as:

$$r_A = r_A[C_A(\mathbf{x}, t)] = g(\mathbf{x}, t) \tag{4.6}$$

Here we are combining two functions, that of the reaction rate r_A and that of the concentration C_A. The first is the function given by Equation 4.5, which we know, while the second is $C_A(\mathbf{x}, t)$, which we do not know and want to determine. This model combines the two functions giving $g(\mathbf{x}, t)$. This function is unknown and therefore cannot be used in this form. Assuming to know the function $g(\mathbf{x}, t)$ allows to integrate the differential equations analytically; however this does not make any sense in a real problem.

4.1.1.5   Analytical VOC model by Wang et al.

The analytical model by Wang et al. [Wang and Zhang, 2011] is a mass transfer model for VOC emissions from dry multi-layer building materials. The model considers chemical reactions within the
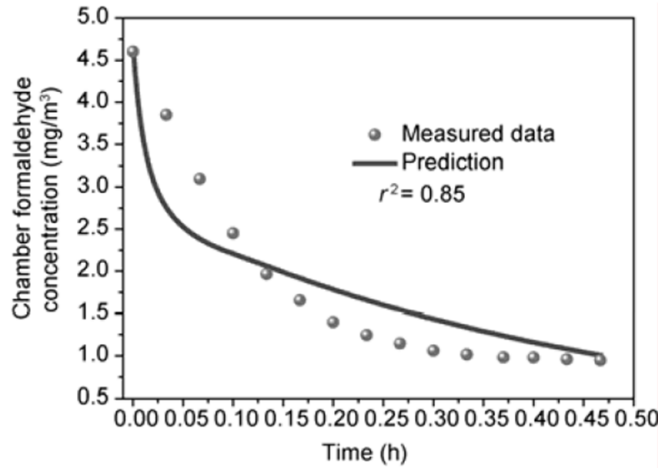
Figure 4.1: Formaldehyde degradation prediction and measured [Wang and Zhang, 2011]

materials and the concentration profile through the material is described by the following equation:

$$\partial_t C_v = D_v \partial_{\mathbf{x}} \cdot \partial_{\mathbf{x}} C_v \pm g(\mathbf{x}, t) \tag{4.7}$$

where C_v is the concentration of the VOC, D_v is the diffusion coefficient through the material and $g(\mathbf{x}, t)$ is the chemical reaction rate. The model assumes mass transfer through the material is one-dimensional.

To validate the model, they used a clean porous honeycomb ceramic material in an airtight stainless steel chamber. A known quantity of formaldehyde was injected into the chamber and the concentration measured in real time. They then used these results to get the adsorption and material diffusion coefficients for formaldehyde.

The material was then coated in a thermal catalyst and placed in the chamber again. Formaldehyde was again injected with the concentration in the chamber measured. The concentration decreased quickly due to the degradation effect of the catalyst. The degradation was assumed to be a first order reaction expressed as:

$$g(\mathbf{x}, t) = -kC_v(\mathbf{x}, t) \tag{4.8}$$

where k is the reaction constant and is calculated from the concentration measured in the chamber.

The material was then removed from the chamber to dilute the residual formaldehyde left in it. The material was placed back in the chamber and another (smaller) volume of formaldehyde was injected into the chamber. The concentration predicted by the model was compared with the measured results and is shown in Figure 4.1. The results agreed reasonably well. Deviation between the measured and predicted values could be due to a non uniform distribution of the catalyst or that the degradation rate given in Equation 4.8 is not adequate.

With this model, Wang et al. were able to show how primary sink/source behaviour is expected to dominate initially and secondary sink/source dominates later. The model shows the benefit that information on the reactions of VOCs in materials has on the predictive ability of the model. Although the model considers mass transfer as one-dimensional through the material, it provides insight into how both primary and secondary sink/source behaviour can influence VOC emission and concentrations.

4.2 Model's relation to degradation

In this section we consolidate the knowledge established in Chapter 2 to show the necessity of our model and how it relates to the paper degradation rate.

4.2.1 Recap of previous work

We start by revisiting how degradation is measured. We stated in Section 2.5 that the most common way of describing the degradation rate was through the degree of polymerisation (DP) and that the change in DP is caused predominantly by acid-catalysed hydrolysis. We then reported the change in DP based on the work of Ekenstam in Equation 2.8 as:

$$\partial_t DP(\mathbf{x}, t) = -k_{DP}(\mathbf{x}, t)DP(\mathbf{x}, t)^2 \tag{4.9}$$

where k_{DP} is the relative number of bonds that break per unit time and equivalent to a reaction rate constant. This "constant" is related to temperature, acidity and relative humidity and must be obtained from literature; in our case, we employed the following equation:

$$\ln(k_{DP}) = 38.039 + 38.057 \left(\frac{\ln(1 - RH)}{1.67T - 285.655} \right)^{\frac{1}{2.491 - 0.012T}} + 0.24 \left[\ln \left(10^{-pH} \right) \right] - \frac{14713}{T + 273.15} \tag{4.10}$$

where RH is the relative humidity ratio, and T is the temperature in °C. We can see that as the degradation constant is a function of relative humidity and acidity, so must the degradation rate be.

The acidity concentration is given by:

$$[H^+] = 10^{-pH} \tag{4.11}$$

The relative humidity relates to the water concentration as follows:

$$[H_2O] = \left(\frac{\ln(1 - RH)}{1.67T - 285.655} \right)^{\frac{1}{2.491 - 0.012T}} \tag{4.12}$$
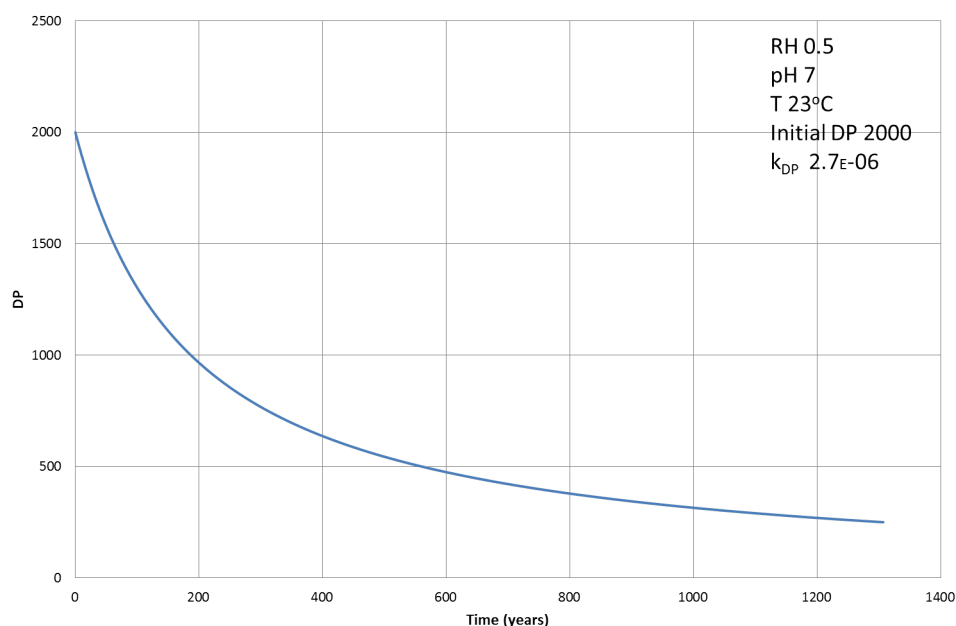
Figure 4.2: DP change in time with a constant k_{DP}

4.2.2 Exploring the degradation rate constant

If the water and acidity concentrations are constant, then k_{DP} must also be constant (for a given temperature and pressure). We would then expect the degradation to follow the curve shown in Figure 4.2.

When paper is created, there is a nearly uniform composition across a page and with each page in a book. Due to this, we would expect a uniform degradation across a page and for all pages in a book. As this is not the case, we conclude that k_{DP} is not constant and so either the acidity or water concentration (or both) are not constant. Controlled environments for paper materials keep the humidity constant and so water concentrations are expected to be nearly constant, despite being consumed in hydrolysis reactions. We know that VOCs are produced by degradation reactions and that many are acidic. These acidic VOCs can therefore be expected to influence the acidity of the system. For the VOCs to cause the system to not have uniform degradation, the VOCs must be able to move through the system and have a non-uniform concentration throughout the latter. As these VOCs are detected in the gas phase, it is reasonable to assume that these compounds are able to diffuse through the pores of paper. As a result, we wish to model the concentration profile of a VOC for its role in the non-uniform degradation rate found in a volume of paper. With this, we now define our quantitative goals.

4.2.2.1 Goals

Paper degrades over time. The degradation rate is expected to change both over time and space within the paper. Knowing how the paper degrades, methods of prevention can be explored. The degradation

rate is expected to be negatively affected with time, as the acidity increases due to the presence of VOCs being generated as paper degrades.

We want to predict how the spatial concentration profile a of VOC evolves in the gas phase *within* a book. We then aim to link this concentration profile to the local paper rate of degradation. This is quantified by the rate of change of the degree of polymerisation of the paper, which is linked to the state of the mechanical properties of the paper.

4.3 Deriving the mathematical model

In this section we develop a mathematical model to describe the reactive mass transfer phenomena taking place in books. To do so, we shall use the knowledge built in the previous chapters as well as the literature described earlier in this chapter. This includes our understanding of how the degradation compounds are involved in the process, as well as the constitutive equations describing the mass transfer and the role that adsorption plays.

We start by defining the system which we intend to model. We have a three dimensional stack of paper with a set height, length and width. The volume is porous, with solid paper fibres and voids; it therefore has an associated porosity, specific surface area and tortuosity.

We assume the temperature and pressure are constant, i.e. that the system is isothermal and isobaric. We will also initially assume that there is no alkaline reserve present.

We view the paper as a reactive material. Species diffuse as gases through the voids in the volume. The species adsorb and desorb from the gas phase to the adsorbed phase on the paper fibres. When the species is in the adsorbed phase it can dissociate and is then involved in degradation reactions with the paper. This is shown in Figure 4.3.
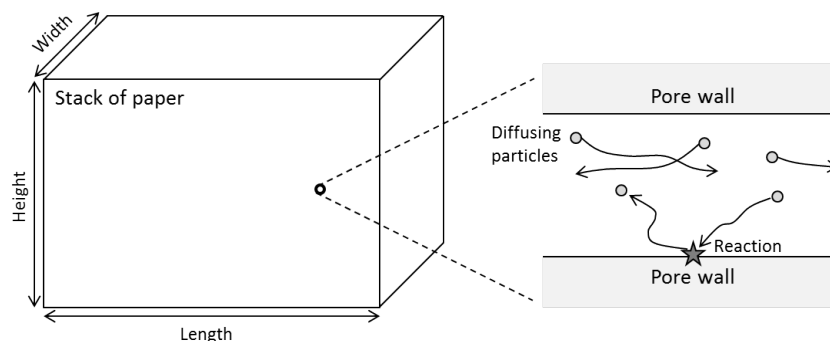
Figure 4.3: Diagram of system

We intend to model the VOC acetic acid's concentration profile across the volume. Let us look at a mass balance for the VOC across the volume following the balance of mass equation:

$$Accumulation = In - Out + Generation \tag{4.13}$$

Accumulation occurs in the pore voids and on the pore walls. We need to account for the surfaces of the pores bounding the control volume as they accumulate VOCs through adsorption. Combining this with the accumulation in pore voids gives us two accumulation terms:

$$Accumulation = Acc_{pore} + Acc_{surface} = \varepsilon\partial_t C_v + \sigma\partial_t[v] \tag{4.14}$$

where Acc_{pore} is the accumulation in the gas phase in the pore, $Acc_{surface}$ is the accumulation in the adsorbed phase on the pore walls, ε is the porosity, σ is the surface area per unit volume, C_v is the molar concentration in the pore voids in the gas phase and $[v]$ is the molar concentration at the pore surface from the solid side in the adsorbed phase.

We now look at the *In* and *Out* terms of the mass balance. We assume there is no diffusion or convective mass flow in the adsorbed phase. We also assume there is no convective flow in the gas phase as it will be negligible in comparison to diffusive flow due to the VOC being in low concentration.

The overall molar flux in the volume is then described as follows:

$$\mathbf{N}_v = \mathbf{J}_v = -D_{ve}\partial_{\mathbf{x}}C_v \tag{4.15}$$

where $\mathbf{N}_v$ is the total molar flux, $\mathbf{J}_v$ is the diffusive molar flux and D_{ve} is the overall effective diffusion coefficient. The net input is then equal to:

$$In - Out = -\partial_{\mathbf{x}} \cdot \mathbf{N}_v = D_{ve}\partial_{\mathbf{x}} \cdot \partial_{\mathbf{x}}C_v \tag{4.16}$$

The only term left in the mass balance is the generation term. We assume there is no reaction involving VOCs in the gas phase. In the adsorbed phase we do have reactions, and so the generation term per unit volume is as follows:

$$Generation = \sigma r_v \tag{4.17}$$

where r_v is the reaction rate per unit volume of paper in the adsorbed phase for the VOC. This reaction rate is the overall reaction rate, taking the generation due to paper degradation into account.

We combine equations 4.13, 4.14, 4.16 and 4.17 to give:

$$\varepsilon\partial_t C_v + \sigma\partial_t[v] = D_{ve}\partial_{\mathbf{x}} \cdot \partial_{\mathbf{x}}C_v + \sigma r_v \tag{4.18}$$

This gives us a general equation for the concentration profile of the VOC which we can now investigate further.

4.3.1   Solving the mass balance

In equation 4.18, we have two concentration variables, C_v and $[v]$. We therefore need a second balance equation to solve the problem.

The second mass balance is written for the VOC referring to a control "volume" that coincides with the pore surface. The concentrations around the pore surface are shown in Figure 4.4. We have assumed there is no surface diffusion. The net input can be described using a mass transfer coefficient equation between the pore bulk and the pore surface:

$$IN - OUT = k_m[C_v - \hat{C}_v] \tag{4.19}$$

where k_m is the mass transfer coefficient relating to mass transfer from the pore bulk volume to the surface of the pore, and $\hat{C}_v$ is the concentration of the VOC at the pore surface in the gas phase.

Pore bulk volume

c_v

$\hat{c}_v$

Pore surface

Pore wall $[v]$
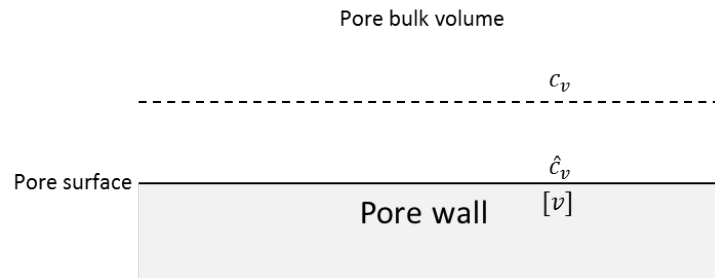
Figure 4.4: Concentration variables from the pore bulk to surface

Accumulation is the same as the surface accumulation term in equation 4.14. Generation is still the same as stated in equation 4.17. Combining this information gives:

$$\partial_t[v] = k_m[C_v - \hat{C}_v] + r_v \tag{4.20}$$

Finally we relate the surface concentration in the gas phase with the surface concentration in the adsorbed phase. These are related through the adsorption equilibrium relation:

$$[v] = f_v(\hat{C}_v) \tag{4.21}$$

where f_v is the adsorption isotherm for the VOC. We now have the balance equations needed for the model. With accompanying initial condition, boundary conditions and constitutive equations, the model can be solved. These conditions and equations will be explored later in this chapter.

4.3.2   Exploring timescales

Our model equations take diffusion, reaction and adsorption into account. Each phenomenon will have its own time scale associated with it. We assume that adsorption is significantly fast when compared to diffusion and reaction processes. With this assumption, we now explore the balance equations further.

We start by assuming for simplicity, a linear adsorption isotherm:

$$[v] = K_v \hat{C}_v \tag{4.22}$$

where K_v is the adsorption equilibrium constant for the VOC. This assumption is reasonable as we expect that the concentrations in the gas and adsorbed phases to be low.

Combining Equations 4.18 and 4.20 gives:

$$\partial_t C_v = \frac{D_{ve}}{\varepsilon}[\partial_{\mathbf{x}} \cdot \partial_{\mathbf{x}} C_v] - \frac{\sigma k_m}{\varepsilon}[C_v - \hat{C}_v] \tag{4.23}$$

and:

$$\partial_t \hat{C}_v = \frac{k_m}{K_v}[C_v - \hat{C}_v] + \frac{r_v}{K_v} \tag{4.24}$$

We now non-dimensionalise both equations 4.23 and 4.24, we define the following non-dimensional variables:

$$\varphi_v = \frac{C_v}{C_r} \tag{4.25}$$

$$\tilde{t} = \frac{t}{t_r} \tag{4.26}$$

$$\tilde{\mathbf{x}} = \frac{\mathbf{x}}{x_r} \tag{4.27}$$

$$\tilde{r_v} = \frac{r_v}{r_{v,r}} \tag{4.28}$$

where φ is the dimensionless concentration, C_r is the concentration scale, $\tilde{t}$ is the dimensionless time, t_r is the time scale, $\tilde{\mathbf{x}}$ is the dimensionless length, x_r is the length scale, $\tilde{r_v}$ is the dimensionless reaction rate and $r_{v,r}$ is the reaction rate scale.

Substituting these into equation 4.23 yields:

$$\partial_{\tilde{t}} \varphi_v = \frac{D_{ve} t_r}{\varepsilon x_r^2} \partial_{\tilde{\mathbf{x}}} \cdot \partial_{\tilde{\mathbf{x}}} \varphi_v - \frac{\sigma k_m t_r}{\varepsilon}[\varphi_v - \hat{\varphi}_v] \tag{4.29}$$

Doing the same for equation 4.24:

$$\partial_{\tilde{t}} \hat{\varphi}_v = \frac{k_m t_r}{K_v}[\varphi_v - \hat{\varphi}_v] + \frac{r_{v,r} t_r}{K_v} \tilde{r_v} \tag{4.30}$$

From equations 4.29 and 4.30, the following characteristic times appear:

$$\tilde{t}_1 = \frac{\varepsilon x_r^2}{D_{ve}} \tag{4.31}$$

$$\tilde{t}_2 = \frac{\varepsilon}{\sigma k_m} \tag{4.32}$$

$$\tilde{t}_3 = \frac{K_v}{k_m} \tag{4.33}$$

$$\tilde{t}_4 = \frac{K_v}{r_{v,r}} \tag{4.34}$$

where $\tilde{t}_1$ represents the characteristic time for the diffusion process, $\tilde{t}_2$ and $\tilde{t}_3$ represents the characteristic time for the adsorption process, and $\tilde{t}_4$ represent the characteristic times for the reaction process. Substituting these characteristic times into equations 4.29 and 4.30 we get:

$$\partial_{\tilde{t}}\varphi_v = \frac{t_r}{\tilde{t}_1} \partial_{\tilde{\mathbf{x}}} \cdot \partial_{\tilde{\mathbf{x}}}\varphi_v - \frac{t_r}{\tilde{t}_2}[\varphi_v - \hat{\varphi}_v] \tag{4.35}$$

And:

$$\partial_{\tilde{t}}\hat{\varphi}_v = \frac{t_r}{\tilde{t}_3}[\varphi_v - \hat{\varphi}_v] + \frac{t_r}{\tilde{t}_4}\tilde{r}_v \tag{4.36}$$

If we have non-dimensionlised correctly (properly scaled), then the following terms will have unit order of magnitude:

$$M\{\partial_{\tilde{t}}\varphi_v\} = M\{\partial_{\tilde{t}}\hat{\varphi}_v\} = M\{\partial_{\tilde{\mathbf{x}}} \cdot \partial_{\tilde{\mathbf{x}}}\varphi_v\} = M\{\varphi_v\} = M\{\hat{\varphi}_v\} = M\{\tilde{r}_v\} = 1 \tag{4.37}$$

where M indicates the magnitude of the term.

The difference between φ_v and $\hat{\varphi}_v$ can be of unit order of magnitude or smaller. It is reasonable to assume that initially the difference has unit order of magnitude:

$$M\{\varphi_v - \hat{\varphi}_v\} = 1 \tag{4.38}$$

We have assumed that adsorption is significantly fast compared to the diffusion and reaction characteristic times, giving us the following relations:

$$\frac{\tilde{t}_2}{\tilde{t}_1} \ll 1 \tag{4.39}$$

$$\frac{\tilde{t}_3}{\tilde{t}_4} \ll 1 \tag{4.40}$$

Initially, for short times, the adsorption process will be the cause of changes in φ_v and the characteristic time will be $\tilde{t}_2$ for equation 4.35:

$$\partial_{\tilde{t}}\varphi_v = \frac{\tilde{t}_2}{\tilde{t}_1}\partial_{\tilde{\mathbf{x}}}\cdot\partial_{\tilde{\mathbf{x}}}\varphi_v - [\varphi_v - \hat{\varphi}_v] \tag{4.41}$$

The first term on the left hand side is negligible and so the equation reduces to:

$$\partial_{\tilde{t}}\varphi_v = -[\varphi_v - \hat{\varphi}_v] \tag{4.42}$$

Similarly, the characteristic time will be $\tilde{t}_3$ for equation 4.36:

$$\partial_{\tilde{t}}\hat{\varphi}_v = [\varphi_v - \hat{\varphi}_v] + \frac{\tilde{t}_3}{\tilde{t}_4}\tilde{r}_v \tag{4.43}$$

The second term on the left hand side is negligible and so the equation reduces to:

$$\partial_{\tilde{t}}\hat{\varphi}_v = [\varphi_v - \hat{\varphi}_v] \tag{4.44}$$

We now convert these terms back into their dimensional forms. Equation 4.42 becomes:

$$\partial_t C_v = -\frac{\sigma k_m}{\varepsilon}[C_v - \hat{C}_v] \tag{4.45}$$

Equation 4.44 becomes:

$$\partial_t \hat{C}_v = \frac{k_m}{K_v}[C_v - \hat{C}_v] \tag{4.46}$$

We now combine equations 4.45 and 4.46 to give the relation between C_v and $\hat{C}_v$:

$$\partial_t C_v = -\frac{\sigma K_v}{\varepsilon}\partial_t \hat{C}_v \tag{4.47}$$

This shows that as C_v increases, $\hat{C}_v$ decreases and vice versa. This is because the VOCs are reaching the pore surface from the pore voids or the other way round depending on which has the higher initial concentration.

During this temporal boundary layer, the difference between C_v and $\hat{C}_v$ becomes smaller, as do their dimensionless counterparts φ_v and $\hat{\varphi}_v$. As the difference approaches zero we can no longer neglect terms in equations 4.41 and 4.43. This is because the terms now have an equal order of magnitude. Let us consider Equation 4.35:

$$M\{\partial_{\tilde{t}}\varphi_v\} = M\left\{\frac{t_r}{\tilde{t}_1}\partial_{\tilde{\mathbf{x}}}\cdot\partial_{\tilde{\mathbf{x}}}\varphi_v\right\} = M\left\{\frac{t_r}{\tilde{t}_2}[\varphi_v - \hat{\varphi}_v]\right\} = 1 \tag{4.48}$$

From this we get:

$$M\left\{\frac{t_r}{\tilde{t}_1}\right\} = 1 \tag{4.49}$$

We then do the same for equation 4.36:

$$M\{\partial_{\tilde{t}}\hat{\varphi}_v\} = M\left\{\frac{t_r}{\tilde{t}_3}[\varphi_v - \hat{\varphi}_v]\right\} = M\left\{\frac{t_r}{\tilde{t}_4}\tilde{r}_v\right\} = 1 \tag{4.50}$$

From which we get:

$$M\left\{\frac{t_r}{\tilde{t}_4}\right\} = 1 \tag{4.51}$$

As a result of equations 4.49 and 4.51, we see that the timescales chosen before are no longer appropriate. Outside the temporal boundary layer, the timescales are $\tilde{t}_1$ and $\tilde{t}_4$. We therefore write equation 4.35 as:

$$\partial_{\tilde{t}}\varphi_v = \partial_{\tilde{\mathbf{x}}} \cdot \partial_{\tilde{\mathbf{x}}}\varphi_v - \frac{\tilde{t}_1}{\tilde{t}_2}[\varphi_v - \hat{\varphi}_v] \tag{4.52}$$

And equation 4.36 as:

$$\partial_{\tilde{t}}\hat{\varphi}_v = \frac{\tilde{t}_4}{\tilde{t}_3}[\varphi_v - \hat{\varphi}_v] + \tilde{r}_v \tag{4.53}$$

4.3.3 Outside the temporal boundary layer

To explore outside the temporal boundary layer, we use the methods of perturbation theory [Deen, 1998]. We will use these methods to achieve an approximate asymptotic solution. The asymptotic behaviour we are dealing with is described in equations 4.39and 4.40. To start, we define the small parameter α:

$$\alpha \equiv \frac{\tilde{t}_2}{\tilde{t}_1} \tag{4.54}$$

We also define the ratio given by equation 4.40 in terms of the same small parameter:

$$\alpha\eta \equiv \frac{\tilde{t}_3}{\tilde{t}_4} \tag{4.55}$$

where:

$$\eta \equiv \frac{\sigma K_v}{\varepsilon} \cdot \frac{\tilde{t}_1}{\tilde{t}_4} \tag{4.56}$$

We are interested in deriving an asymptotic solution for $\alpha \ll 1$, where η is a fixed number. Using these definitions we rewrite equations 4.52 and 4.53 as follows:

$$\partial_{\tilde{t}}\varphi_v = \partial_{\tilde{\mathbf{x}}} \cdot \partial_{\tilde{\mathbf{x}}}\varphi_v - \frac{1}{\alpha}[\varphi_v - \hat{\varphi}_v] \tag{4.57}$$

and:

$$\partial_{\tilde{t}}\hat{\varphi}_v = \frac{1}{\alpha\eta}[\varphi_v - \hat{\varphi}_v] + \tilde{r}_v \tag{4.58}$$

Next we expand our dimensionless concentration variables as power series with respect to α:

$$\varphi_v = \sum \alpha^n \varphi_{v,n} = \varphi_{v,0} + \alpha\varphi_{v,1} + O(\alpha^2) \tag{4.59}$$

$$\hat{\varphi}_v = \sum \alpha^n \hat{\varphi}_{v,n} = \hat{\varphi}_{v,0} + \alpha\hat{\varphi}_{v,1} + O(\alpha^2) \tag{4.60}$$

In these power series we are only considering the first two terms. This is normally enough to give a good approximation. Including these series in equation 4.57 we get:

$$\partial_{\tilde{t}}\varphi_{v,0} + \alpha\partial_{\tilde{t}}\varphi_{v,1} = \partial_{\tilde{\mathbf{x}}} \cdot \partial_{\tilde{\mathbf{x}}}\varphi_{v,0} - \frac{1}{\alpha}[\varphi_{v,0} - \hat{\varphi}_{v,0}] + \alpha\partial_{\tilde{\mathbf{x}}} \cdot \partial_{\tilde{\mathbf{x}}}\varphi_{v,1} - [\varphi_{v,1} - \varphi_{v,1}] + O(\alpha^2) \tag{4.61}$$

This then is rearranged to:

$$\alpha\partial_{\tilde{t}}\varphi_{v,0} = \alpha\partial_{\tilde{\mathbf{x}}} \cdot \partial_{\tilde{\mathbf{x}}}\varphi_{v,0} - [\varphi_{v,0} - \hat{\varphi}_{v,0}] - \alpha[\varphi_{v,1} - \varphi_{v,1}] + O(\alpha^2) \tag{4.62}$$

Including the series in equation 4.58 we get:

$$\partial_{\tilde{t}}\hat{\varphi}_{v,0} + \alpha\partial_{\tilde{t}}\hat{\varphi}_{v,1} = \frac{1}{\alpha\eta}[\varphi_{v,0} - \hat{\varphi}_{v,0}] + \frac{1}{\eta}[\varphi_{v,1} - \hat{\varphi}_{v,1}] + \tilde{r}_v + O(\alpha^2) \tag{4.63}$$

Which is then rearranged to:

$$\alpha\eta\partial_{\tilde{t}}\hat{\varphi}_{v,0} = [\varphi_{v,0} - \hat{\varphi}_{v,0}] + \alpha[\varphi_{v,1} - \hat{\varphi}_{v,1}] + \alpha\eta\tilde{r}_v + O(\alpha^2) \tag{4.64}$$

The first approximation terms yields the following:

$$O(1): \ \varphi_{v,0} - \hat{\varphi}_{v,0} = 0 \tag{4.65}$$

The $O(\alpha)$ terms give:

$$O(\alpha): \ \partial_{\tilde{t}}\varphi_{v,0} = \partial_{\tilde{\mathbf{x}}} \cdot \partial_{\tilde{\mathbf{x}}}\varphi_{v,0} - \varphi_{v,1} - \varphi_{v,1} \tag{4.66}$$

$$O(\alpha): \ \eta\partial_{\tilde{t}}\hat{\varphi}_{v,0} = \eta\tilde{r_v} + [\varphi_{v,1} - \hat{\varphi}_{v,1}] \tag{4.67}$$

We now put these equations back into their dimensional forms. Equation 4.66 becomes:

$$\varepsilon\partial_t C_{v,0} = D_{ve}\partial_{\mathbf{x}} \cdot \partial_{\mathbf{x}}C_{v,0} - \frac{\varepsilon}{\tilde{t}_1}[C_{v,1} - \hat{C}_{v,1}] \tag{4.68}$$

Similarly, equation 4.67 becomes:

$$\sigma K_v\partial_t\hat{C}_{v,0} = \sigma r_v + \frac{\varepsilon}{\tilde{t}_1}[C_{v,1} - \hat{C}_{v,1}] \tag{4.69}$$

We now combine equations 4.68 and 4.69:

$$\varepsilon\partial_t C_{v,0} + \sigma K_v\partial_t\hat{C}_{v,0} = D_{ve}\partial_{\mathbf{x}} \cdot \partial_{\mathbf{x}}C_{v,0} + \sigma r_v \tag{4.70}$$

From the first approximation terms in equation 4.65 we have:

$$\varphi_{v,0} = \hat{\varphi}_{v,0} \tag{4.71}$$

Which can be expressed in the dimensional form as:

$$C_{v,0} = \hat{C}_{v,0} \tag{4.72}$$

Substituting into equation 4.70 gives:

$$\varepsilon\partial_t C_{v,0} + \sigma K_v\partial_t C_{v,0} = D_{ve}\partial_{\mathbf{x}} \cdot \partial_{\mathbf{x}}C_{v,0} + \sigma r_v \tag{4.73}$$

Which can finally be arranged to:

$$[\varepsilon + \sigma K_v]\partial_t C_{v,0} = D_{ve}\partial_{\mathbf{x}} \cdot \partial_{\mathbf{x}}C_{v,0} + \sigma r_v \tag{4.74}$$

We now have an approximation of the problem, expressed in terms of $C_{v,0}$. This approximation is valid outside the temporal boundary layer and the initial conditions can be provided by the asymptotic solution within this boundary layer.

4.4 Model summary

Here in the interest of clarity we will report the entire model. Rearranging Equation 4.74, our concentration profile is expressed as:

$$\partial_t C_v(\mathbf{x}, t) = \frac{D_{ve}}{\varepsilon + \sigma K_v} \partial_\mathbf{x} \cdot \partial_\mathbf{x} C_v(\mathbf{x}, t) + \frac{\sigma}{\varepsilon + \sigma K_v} r_v(\mathbf{x}, t) \tag{4.75}$$

From this equation, it can be seen that we need to provide information on how the diffusion coefficient D_{ve}, the adsorption coefficient K_v and reaction rate r_v are expressed. We shall explore these in the following sections. The reaction rate will reflect how the concentration profile is linked to the degradation profile. We shall also discuss the porosity term ε and the unit surface area σ. Then we will report the initial and boundary conditions that we will use in-conjunction with the model. Finally, we will discuss how the alkaline reserve is accounted for.

4.4.1 Diffusion Coefficient

We expect both ordinary molecular diffusion and Knudsen diffusion to be important, and we need to account for the porosity and irregular pore shape. As such we utilise Equations 3.18 and 3.17 described in section 3.1.2.3 giving:

$$\frac{1}{D_{ve}} = \psi(\frac{1}{D_{v,air}} + \frac{1}{D_K}) \tag{4.76}$$

where D_{ve} is the overall effective diffusion coefficient, $D_{v,air}$ is the ordinary molecular diffusion coefficient, D_K is the Knudsen diffusion coefficient, while ψ is the ratio between the porosity and tortuosity.

The Knudsen diffusion coefficient can be found theoretically and values for the ordinary molecular diffusion coefficient are readily available for common air-compound mixtures. Experimentation is required to find the coefficient ψ that accounts for the tortuosity and porosity; this will be covered in the next chapter.

4.4.2 Adsorption function

In reporting our model, we have assumed a linear adsorption isotherm and as a result had the adsorption coefficient K_v for our VOC. The actual isotherm shape is unknown. To find the relation between the adsorbed phase concentration and gas phase concentration, experimentation is needed and will be included in the next chapter.

It is reasonable to assume a linear adsorption function as we are dealing with very low concentrations and a small concentration range. As discussed in Chapter 3, Section 3.2.2, we expect the isotherm to follow the initial shapes of either Type 4 or 5 of the Brunauer classifications of isotherms shown in Figure 3.6.

4.4.3 Reaction kinetics

The reaction kinetics that will be used are outlined in Chapter 3, section 3.3.4. The reaction rate for the generation of acetic acid is:

$$r_v(\mathbf{x}, t) = k_{vr}\alpha(\mathbf{x}, t)k_{DP}(\mathbf{x}, t) \tag{4.77}$$

where α is the fraction of end bonds:

$$\alpha(\mathbf{x}, t) = \frac{2}{DP(\mathbf{x}, t) - 1} \approx \frac{2}{DP(\mathbf{x}, t)} \tag{4.78}$$

The second reaction rate constant k_{DP}, for the relative number of bonds that break per unit time, is given by Equation 4.10.

We assume that the relative humidity and temperature are constant. These equations show how the reaction rate relies both on the degradation rate (through the DP) and the acidity. The degradation rate was re-iterated in this chapter in Equation 4.9. The acidity is given in Chapter 3 by Equation 3.41:

$$[H^+](\mathbf{x}, t) = [H_0^+](\mathbf{x}, t) + \frac{\sqrt{([H_0^+](\mathbf{x}, t) + Ka)^2 + 4Ka[HA](\mathbf{x}, t)} - ([H_0^+](\mathbf{x}, t) + Ka)}{2} \tag{4.79}$$

where $[H^+]$ is the acidity, $[H_0^+]$ is the initial acidity of the paper and Ka is the acid dissociation constant.

4.4.4 Other parameters

The porosity term ε and the unit surface area σ are particular to the paper. In our model we have assumed that these values are constant. These values may change as paper degrades, but it is most likely that they do not change significantly until paper has degraded substantially and is already beyond practical use. Both the porosity and unit surface area will be found through experimentation.

4.4.5 Initial conditions

For the initial condition, we assume that paper has a uniform concentration of the VOC:

$$C_v(\mathbf{x}, t = 0) = C_v^0 \tag{4.80}$$

where C_v^0 is the initial concentration of the VOC. Some VOCs are created when paper is made and so their concentrations are not necessarily zero initially. We assume that our VOC, acetic acid, does have an initial zero concentration.

We would also assume a uniform concentration for the DP and acidity. The initial DP and acidity will depend on the paper being modelled.

4.4.6   Boundary conditions

There are numerous options for possible boundary conditions. One that is applicable to nearly all cases is that at the surface at the base of the volume, the molar flux of the VOC normal to the surface is zero.

$$\mathbf{N}_{v,surface}.\mathbf{n} = 0 \tag{4.81}$$

where $\mathbf{N}_{v,surface}.\mathbf{n}$ is the flux normal to the bottom surface. The molar flux is zero as the surface on which the volume is placed is considered non porous so no mass can flow through it. This condition depends on the material the paper is placed on. We also apply this boundary condition to any other surfaces of the paper that are against a non porous surface through which no mass transfer can occur, for instance, when the paper is kept in a tightly sealed container.

If we assume that a surface of paper is surrounded by air, then at the boundary, the flux normal to the surface in the surrounding air is the same as the flux normal to the surface in the paper:

$$\mathbf{N}_{v,surface}^{air}.\mathbf{n} = \mathbf{N}_{v,surface}^{paper}.\mathbf{n} \tag{4.82}$$

where the flux in the paper is given by:

$$\mathbf{N}_{v,surface}^{paper}.\mathbf{n} = -D_{Ae}\partial_{\mathbf{x}}C_v^{paper}.\mathbf{n} \tag{4.83}$$

where $\mathbf{n}$ is the unit vector in the direction normal to the surface and C_v^{paper} is the concentration at the boundary on the paper side.

At the surface of the paper, the tangential velocity of the air relative to the boundary is zero due to the "no-slip" boundary condition. The mass transfer at the surface on the air side is by diffusive means:

$$\mathbf{N}_{v,surface}^{air}.\mathbf{n} = -D_{air}\partial_{\mathbf{x}}C_v^{air}.\mathbf{n} \tag{4.84}$$

where D_{air} is the diffusivity coefficient for the VOC in the surrounding air, and $\partial_{\mathbf{x}}C_v^{air}$ is the concentration gradient in the surrounding air. Both equations 4.83 and 4.84 require concentration profiles, where concentration profile in the paper volume is described by our model.

To simplify calculating the flux normal to the surface we can use the mass transfer coefficient defined in Chapter 3, Equation 3.19:

$$\mathbf{N}_{v,surface}^{air}.\mathbf{n} = k_c\Delta C_v \tag{4.85}$$

where k_c is the mass transfer coefficient and $\triangle C_v$ is the concentration difference between the boundary surface and the surrounding air bulk concentration. The concentration of the VOC in the gas phase at the the paper-air interface will be the same, as shown in Figure 4.5.

Surrounding air

$$C_v^{air} = C_v^{paper}$$

Paper with pores
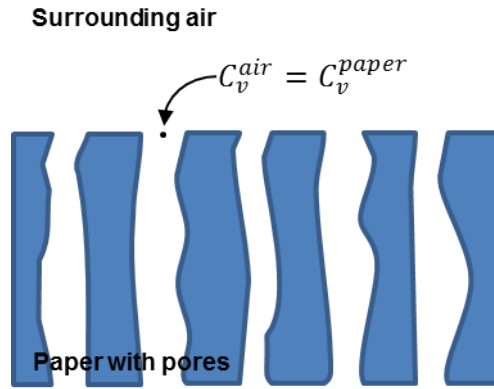
Figure 4.5: Paper-air concentration equivalence

Therefore, if we solve the mass flux equation for the concentration in the air at the paper-air interface, we can use this concentration for the same equations in the paper at the interface. Figure 4.6 shows the mass transfer coefficient's role in the mass transfer problem.

y-direction

Air

$C_{v,bulk}^{air}$ $N_{v,surface}^{air}.\boldsymbol{n} = -D_{air}\partial_{\boldsymbol{x}}C_v^{air}.\boldsymbol{n} = k_c\left(C_{v,bulk}^{air} - C_{v,surface}^{air}\right) = N_{v,surface}^{paper}.\boldsymbol{n}$

$C_{v,surface}^{air}$ $N_{v,surface}^{air}.\boldsymbol{n} = -D_{air}\partial_{\boldsymbol{x}}C_v^{air}.\boldsymbol{n}$

Paper

$C_{v,surface}^{paper}$ $N_{v,surface}^{paper}.\boldsymbol{n} = -D_{paper}\partial_{\boldsymbol{x}}C_v^{paper}.\boldsymbol{n}$
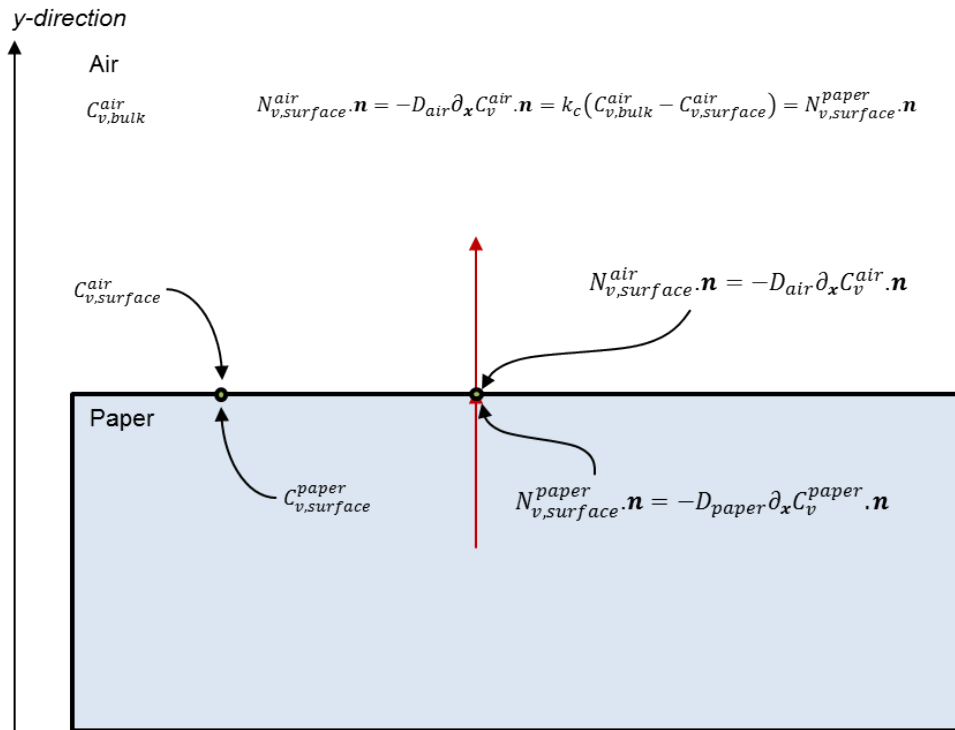
Figure 4.6: Paper-air boundary

Here we assume the resistance to mass transfer occurs between the well mixed bulk of the surrounding air and the surface of the paper. The flux in the y direction is as follows:

$$\mathbf{N}_{v,surface}^{air}.\mathbf{n} = k_c(C_{v,bulk}^{air} - C_{v,surface}^{air}) \tag{4.86}$$

where $C^{air}_{v,bulk}$ is the concentration of the VOC in the air in the bulk of the surrounding air and $C^{air}_{v,surface}$ is the concentration at the surface. This boundary condition assumes the bulk to be well mixed, which is likely in rooms well air conditioned or ventilated.

The mass transfer coefficient can be calculated using the empirical relations outlined in Chapter 3, Section 3.1.3.3, where the mass transfer coefficient is related to the bulk velocity.

4.4.7 Including the alkaline reserve

When we have an alkaline reserve, we assume there is a non-zero concentration of calcium carbonate in the paper. When we do not have an alkaline reserve, the general equation for the concentration profile of the VOC is described by Equation 4.18. If there is an alkaline reserve, then we have an additional term S for the consumption of the VOC:

$$\varepsilon\partial_t C_v + \sigma\partial_t[v] = D_{ve}\partial_{\mathbf{x}}\cdot\partial_{\mathbf{x}}C_v + \sigma r_v - S \qquad \text{for } [CaCO_3] > 0 \tag{4.87}$$

If the VOC is generated by reaction in the adsorbed phase, it is instantaneously consumed by the alkaline reserve. Therefore, there is no VOC accumulation. If the VOC is not generated, but arrives through diffusion in the gas phase, then it is instantaneously adsorbed and instantaneously consumed by the alkaline reserve. Again, there is no VOC accumulation. As a result, we get:

$$\varepsilon\partial_t C_v + \sigma\partial_t[v] = 0 \tag{4.88}$$

and therefore:

$$S = D_{ve}\partial_{\mathbf{x}}\cdot\partial_{\mathbf{x}}C_v + \sigma r_v \tag{4.89}$$

Thus, whilst an alkaline reserve is present, we cannot have any accumulation of acetic acid.

We need to be able to express how the calcium carbonate is consumed.We remind ourselves of the neutralisation reaction:

$$2CH_3COOH + CaCO_3 \rightarrow CO_2 + H_2O + Ca\left(CH_3COO\right)_2 \tag{4.90}$$
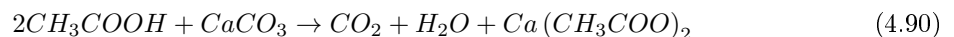
From the stoichiometry, we can see that the consumption is half that of the consumption of acetic acid:

$$Accumulation = Generation = -\frac{1}{2}\left(D_{ve}\partial_{\mathbf{x}}\cdot\partial_{\mathbf{x}}C_v + \sigma r_v\right) = \partial_t\left[CaCO_3\right] \qquad \text{for } [CaCO_3] > 0 \tag{4.91}$$

where $[CaCO_3]$ is the concentration of calcium carbonate in the solid phase per unit volume of paper.

We now have expressions for both acetic acid and calcium carbonate whilst an alkaline reserve is present.

4.5   Additional models for comparison

Here we will define two other models which can be used to help evaluate our main model.

One model will assume that the VOC is generated by the degradation process but does not then affect the degradation rate. This model is nearly the same as the model we derived, except there is now no longer a change in acidity. As a result, the VOC concentration profile has no effect on the degradation rate, so we would expect a uniform degradation rate across the volume. The VOC profile will still be an indicator of degradation as the generation of the VOC still depends on the degradation state. However, the difficulty in linking the VOC profile to the degradation will be due to the environment the paper has been kept in.

The second model is a specific case of our main model, where we assume that the VOC is not generated by the degradation process, but does affect the acidity when present. The mass balance therefore is:

$$\varepsilon \partial_t C_v + \sigma \partial_t [v] = D_{ve} \partial_{\mathbf{x}} \cdot \partial_{\mathbf{x}} C_v \tag{4.92}$$

Using a similar exploration of timescales like that in the main model, we get:

$$\partial_t C_v [\varepsilon + \sigma K_v] = D_{ve} \partial_{\mathbf{x}} \cdot \partial_{\mathbf{x}} C_v \tag{4.93}$$

Where the degradation rate and change in acidity are the same as defined in the main model. This model will show the concept of how a VOC that isn't produced by paper but diffuses into the paper can still influence the degradation rate through the acidity change.

These models will be explored further in Chapter 6.

Chapter 5

Experimentation

In the previous chapter, we derived our model of the VOC concentration profile. We now describe the experimentation that needs to support the model. This includes experiments performed for finding information concerning the physical properties of paper, diffusion coefficients and adsorption isotherms.

5.1 Samples used

For these experiments, the same paper samples are used to provide a consistent picture. The provided sample information is summarised in Table 5.1 and samples A, B and C are shown in Figure 5.1. The samples were chosen as they display a range of different pHs and different ages. For all experiments, the papers are conditioned to room temperature and humidity. The samples were characterised and provided by the UCL Centre for Sustainable Heritage, except for the density which was measured by averaging the results of 3 known volumes for each sample. The pH was measured by the UCL Centre for Sustainable Heritage using standard cold extraction.

Sample	Age	Description	Approximate pH	Density (kg/m^3)
A	1937	bleached cellulose, yellowish appearance, rosin sized	6.1	780
B	1922	Lignin containing, made from ground wood, rosin sized	4.9	809
C	1997	bleached cellulose, white appearance, CaCO3 alkaline reserve	8.1	798
D	near new	Whatman Filter paper, non coated, near pure cellulose	7.0	634

Table 5.1: Paper samples for experiments

Whatman filter paper is typically used in filtration experiments [Analytics Shop, 2013]. It is a near pure cellulose paper with a high initial DP (2300). This paper was chosen as it would be a good

standard to compare against, even though printed books do not use it. The other three samples are from books and so are useful as examples of materials that would be expected in libraries and archives.
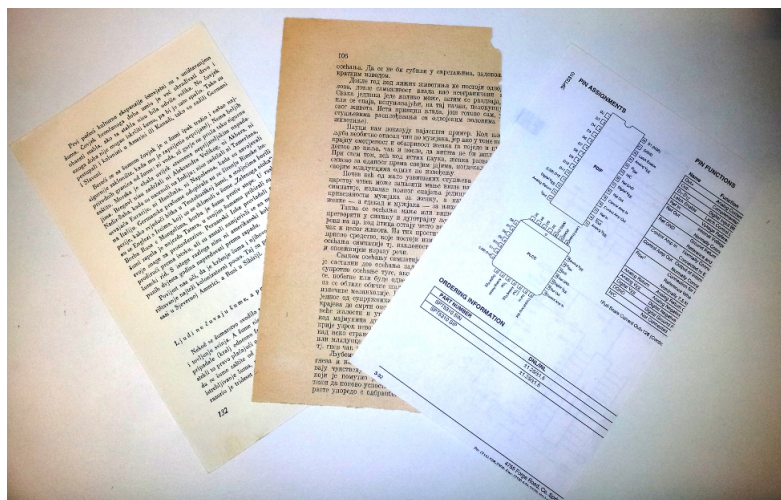
Figure 5.1: Photograph of "real" paper samples A, B and C in sequence

5.2 Porosity, surface area and mean pore diameter

The porosity, surface area and pore diameter of a sheet of paper will vary with each paper type. The porosity influences gas diffusion as it describes the volume available for the gases to diffuse through. The surface area relates to adsorption and reaction as it is a measure of the area available in the volume for adsorption and reactions to occur. The pore diameter indicates whether Knudsen diffusion should be taken into account as well as being part of the calculation for the Knudsen diffusion coefficient, as described in Chapter 3, Section 3.1.2.2.

Using a BET instrument, we can measure the porosity, specific surface area and pore diameter of our paper samples; however, let us first review other methods for finding these properties.

5.2.1 Pore structure experimental methods

There are various experimental methods to investigate porous structures. To understand the morphological characterisation of a material, image analysis like scanning electron microscopy (SEM) is used. With SEM, micrographs of the material at 400x magnification can show where voids in the material are and their shape [Wistara and Young, 1999].

One method for finding the porosity of a material relies on gas expansion. This involves using two connected containers under different pressures, with one containing the material. One container initially has a near vacuum pressure (V_1) and the other (V_2) is at a set pressure and contains a known volume of paper. This set up is shown below in Figure 5.2.
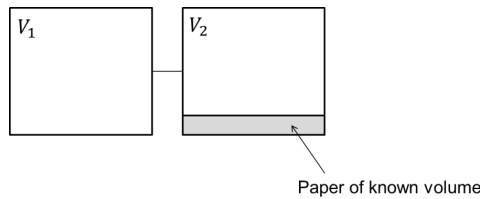
Figure 5.2: Gas expansion diagram

The valve is then opened connecting the two compartments and the pressure read when it has reached equilibrium. The volume of the pores can then be calculated:

$$V_{pores} = V_{paper} + \frac{P_{final}}{P_2 - P_{final}} V_1 - V_2 \tag{5.1}$$

where V_{paper} is the volume of the paper, V_{pores} is the volume of the pores in the paper, P_{final} is the final pressure of the system, P_2 is the initial pressure of the second container. The porosity can then be calculated by:

$$\varepsilon = \frac{V_{pores}}{V_{paper}} \tag{5.2}$$

An approximate technique for porosity testing is to use imbibition. Here the sample is typically immersed in water or another liquid and the liquid fills the pores. The sample is weighed before and after immersion and with the density of the liquid, the porosity is calculated.

Another, more comprehensive method is Mercury Intrusion Porosimetry (MIP) which provides pore size distribution, mean pore diameter, pore volume and surface area. MIP involves forcing mercury into the pores of the material with increasing pressure. Mercury is used as a non wetting liquid as it is assumed that a non wetting liquid only intrudes the capillaries under pressure. The method is based on the Washburn equation which describes the relationship between pressure and pore radius:

$$P = \frac{-2\gamma \cos \theta}{r} \tag{5.3}$$

where P is the pressure, γ is the surface tension of mercury, θ is the contact angle and r is the intrusion radius for cylindrical pores. The contact angle and surface tension of mercury are known. The pore size distribution is determined from the volume of mercury intruded at each pressure increment and the total porosity is determined from the total volume intruded.

The pressure is increased to have mercury fill all the pores and MIP instrumentation can achieve very high pressure values. MIP is widely used and has commercial instruments available. It can identify pores in the macropore range and the large mesopore range. One problem associated with MIP is the "Ink Bottle" problem where the diameter of the throat of a pore is calculated rather than the rest of the pore [Abell et al., 1999].

The method we will be using is a gas adsorption method based on BET theory. We use this method as the BET machine produces reliable results that give a range of information on the sample tested and is

readily available in our department. All these methods except the micrograph method are destructive as the paper needs to be cut to the correct sample sizes.

5.2.1.1 BET theory

The BET instrument uses a gas adsorption method, specifically, the BET nitrogen adsorption method. This method gives information on the porous structure by measuring the adsorption isotherm of the sample. The specific surface area is calculated from knowing the concentration needed to cover the material with a single layer of adsorbate; this is called the monolayer sorbent concentration.

BET theory is based on Langmuir Theory for monolayer adsorption, whose resulting equation is reported in Chapter 3, Section 3.2.1, Equation 3.26. Proposed by Brunauer, Emmett and Teller, BET theory extends Langmuir theory to multilayer adsorption [Brunauer et al., 1938]. This is expressed mathematically as:

$$[A] = \frac{[A]^0 K_{BET} p_A}{\left(1 - \frac{p_A}{P_A^{sat}}\right)\left(1 - \frac{p_A}{P_A^{sat}} + K_{BET} p_A\right)} \tag{5.4}$$

where $[A]$ is the concentration of the adsorbate A adsorbed (typically in mol/kg$_{adsorbent}$), $[A]^0$ is the monolayer sorbent concentration (mol/kg$_{adsorbent}$), K_{BET} is the BET constant, p_A is the partial pressure of A, P_A^{sat} is the saturation pressure of A. BET theory assumes that each first layer molecule attached to the material is a site for the adsorption of a molecule in the next layer.

Equation 5.4 can be rearranged into its linear form and plotted:

$$\frac{p_A}{[A]\left(P_A^{sat} - p_A\right)} = \frac{1}{[A]^0 K_{BET}} + \frac{K_{BET} - 1}{[A]^0 K_{BET}}\left(\frac{p_A}{P_A^{sat}}\right) \tag{5.5}$$

where:

$$\text{Dependent variable} = \frac{p_A}{[A]\left(P_A^{sat} - p_A\right)} \quad ; \quad \text{Independent variable} = \frac{p_A}{P_A^{sat}} \tag{5.6}$$

This plot is obtained experimentally by measuring the amount adsorbed at set relative pressures. The more linear the plot, the more accurate the results. The linearity is restricted to a limited part of the plot, typically between $\frac{p_A}{P_A^{sat}}$ values of 0.05 and 0.30 [Sing et al., 1985]. Extrapolating from the linear section the slope and intercept are determined:

$$\text{Slope} = \frac{K_{BET} - 1}{[A]^0 K_{BET}} \quad ; \quad \text{Intercept} = \frac{1}{[A]^0 K_{BET}} \tag{5.7}$$

This can be rearranged for the monolayer sorbent concentration:

$$[A]^0 = \frac{1}{\text{Slope} + \text{Intercept}} \tag{5.8}$$

Knowing the monolayer sorbent concentration, we can then calculate the specific surface area, A_s:

$$A_s = \frac{[A]^0 \theta \eta}{m}$$

(5.9)

where θ is the surface area occupied by one molecule at the analysis temperature given by literature, η is the Avogadro constant and m is the mass of the sample. It has been suggested that the BET method is best for Types 2 and 4, but not 1 and 3 of the Brunauer classification of isotherms as shown in Chapter 3, Figures 3.4 and 3.6 [Sing et al., 1985].

The units of the specific surface area are m^2/kg. For our model, we want σ, the surface area per unit volume. To convert the specific surface area, we multiply it by the sample's density.

5.2.1.2 Porosity

For the surface area, we needed conditions where a complete monolayer of adsorbed molecules was achieved. By extending these conditions and therefore the isotherm we can evaluate more about the pore structure.

The pressure is increased, the gas condenses in the smallest pores first continuing until saturation is reached. The pore volume can be calculated from the amount of gas adsorbed at a relative pressure close to unity:

$$V_{pore} = \frac{P V_{ads} V_m}{RT}$$

(5.10)

where V_{pore} is the pore volume, V_{ads} is the volume of gas adsorbed, V_m is the molar volume of liquid adsorbed, T is the temperature, R is the universal gas constant and P is the pressure. This assumes that the pores are then filled with condensed adsorbate in normal liquid state. The volume of liquid is assumed to be the pore volume and by dividing by the total volume we can calculate the porosity.

5.2.1.3 Pore diameter

The average pore radius is based on the Kelvin equation and is given by:

$$\frac{2}{r_k} = -\frac{RT}{\gamma^{lg} V_m} \ln \left(\frac{p_A}{P_A^{sat}} \right)$$

(5.11)

where r_k is the Kelvin radius, $\frac{p_A}{P_A^{sat}}$ is the relative pressure at which condensation occurs and γ^{lg} is the surface tension of the liquid condensate [Sing et al., 1985]. This assumes that the pores are cylindrical. The pore diameter is then double the Kelvin radius.

5.2.2 Experimental preparation and procedure

The BET setup consists of two pieces of equipment. The degas instrument and the BET instrument. The degas instrument is shown in Figure 5.3. This instrument is used to prepare the samples for the

BET instrument. The degas instrument provides a flow of nitrogen to the samples and dries them. If the water content in the samples is too high, the BET instrument cannot operate.
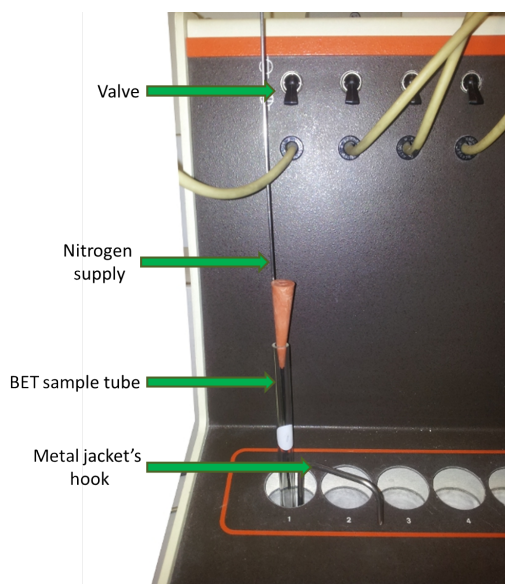
Figure 5.3: Degas instrument

The BET instrument is shown in Figure 5.4. The instrument we are using is a Micromeritics TriStar surface area and porosity analyzer [Micromeritics, 2012]. The process flow diagram for the instrument is shown in Figure 5.8. This instrument carries out the adsorption and desorption on the samples, from which various properties are calculated. The instrument is connected to the computer through which the parameters are controlled and input for the experimental runs.
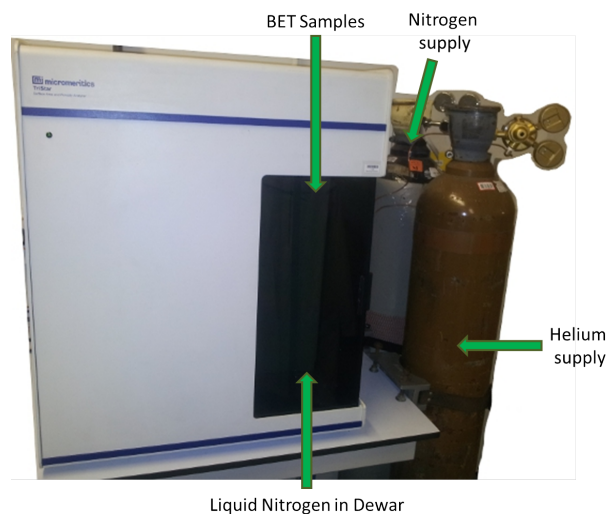
Figure 5.4: BET instrument

The paper samples need to be prepared for use. This involves using a punch to cut the paper to a size so that it can be placed in the tubes. This is shown in Figures 5.5 and 5.6. The sample is weighed before being put in the tube.
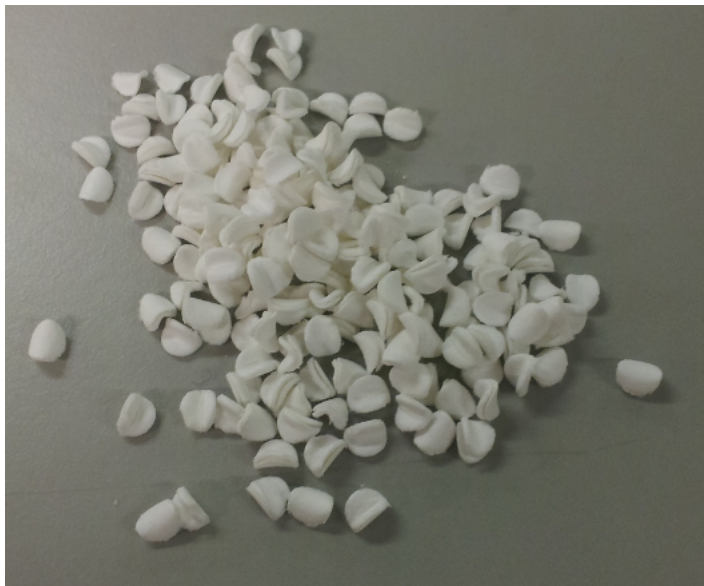
Figure 5.5: Paper samples prepared for BET instrument

Figure 5.6: Paper samples in tubes for use in BET instrument

The more paper is packed in the tube, the more accurate the results will be.

The sample is then degassed to prepare it for use in the BET instrument. Degassing cleans the sample by using an inert gas, in this case nitrogen, at increased temperature to get rid of adsorbed molecules like water.

To explore whether the process of degassing had an effect on the results, the samples were degassed for three different time periods: 3 hours, 6 hours and overnight (approximately 15 hours). Each sample had three measurements taken for each degas time. The tubes containing the samples are placed in metal jackets, shown in Figure 5.7, and then put in the degas instrument. A rod that delivers the nitrogen is then placed in the tube as close to the paper as possible and a rubber bung is placed on the top to secure the rod (see Figure 5.3). The temperature is then set to 90ºC, and the nitrogen turned on.
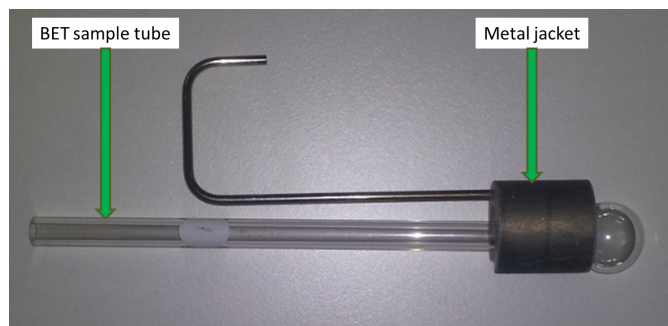
Figure 5.7: Tube with metal jacket

After the sample has been in for the set time period, the nitrogen and temperature controls are turned off and the rods delivering the nitrogen are taken out with care. The tubes are then taken out of the degas instrument using the metal jackets. The samples are then weighed again to compare the change in mass due to degassing. This is so we use the correct mass for our calculations.

The samples are then ready for the BET instrument. A thermal jacket is placed over the tube and a stopper placed in the top. The tubes are inserted into the instrument, with a maximum of three at a time. A dewar of liquid nitrogen is placed below them, the nitrogen and helium gas supplies are turned on, as is the BET instrument.

The BET instrument can run three samples simultaneously. The sample mass values are entered into the computational software on the PC connected to the machine, then the instrument settings are checked and finally the sample runs are started.
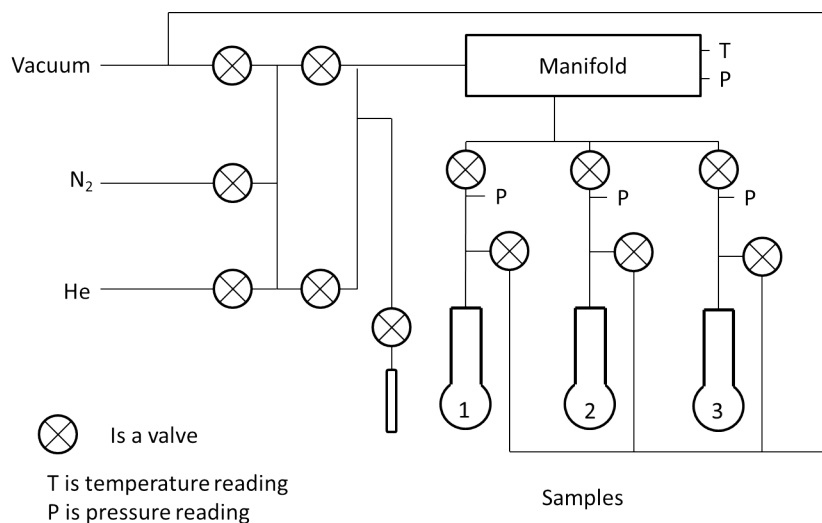
Figure 5.8: BET instrument flow diagram

When the sample runs are complete, the instrument sends the data to the connected PC, and the data can be reviewed through its computational software.

5.2.3 BET instrument results

Here we present the average results for each sample, for each degas time. For the individual results with standard deviations, please refer to Section A.1 in the appendices.

5.2.3.1 Surface area

The surface area results are summarised in Table 5.2. A large surface area would provide lots of space for molecules to be adsorbed and desorbed from. In the case of paper degradation, it means there is more of the material exposed to harmful compounds like VOCs. Inversely it could also mean that in a well conditioned environment, harmful compounds the paper produces can be removed from the paper more easily.

It can be seen that Samples A changes the most with different degas times. This may be due to the initial water content of the samples and how much is removed when degassing. If the majority of free water is removed quickly, we expect little change between the different degas times. Sample A increases slightly after 6 hours and more dramatically for the overnight degas, implying that a more significant amount of water may have been removed or that the pore dimensions have changed with water removal. This could suggest that some papers are more susceptible to change of water content than others, which would in turn affect the degradation reactions occurring in the papers.

In libraries and archives, paper would not undergo degassing. As such we expect results at small degas times to be closer to the values we would achieve in typical conditions. All of the "real" paper samples (A,B and C) are within a very small range for the 3 hour and 6 hour degas times. This could imply that paper in archives and libraries will all have a similar surface are to each other.

Comparing the surface areas to other materials, samples A, B and C are larger than gypsum and chipboard which have a surface area of approximately 970000 and 930000 m^2/m^3 respectively [Tiffonnet et al., 2002].

Sample	3h	6h	Overnight
A	1402500	1476200	3299200
B	1452600	1428700	1193500
C	1422200	1337400	1342700
D	950400	855500	988200

Table 5.2: Surface areas results summary (m^2/m^3)

5.2.3.2 Porosity

The porosity results are shown in Table 5.3. A large porosity means that there is more space for the molecules to move in the gas phase within the paper volume. In order to know how freely the molecules move through a material, we also need to consider the pore diameter and tortuosity. Sample A again has the most dramatic change as degas time increases. It shows the opposite trend to the other papers with the pore volume increasing with degas time. The "real" papers are closest to each other in value

with the lowest degas time again suggesting that under typical conditions, papers may be within a small range. Sample C appears to be the most resilient to degas time, changing very little as this increases.

Compared to catalysts [Soukup et al., 2008], the porosity values are quite small. This is understandable as catalysts are made in order to have a large porosity to aid reactions. The smaller porosity suggests that VOC movement will be hindered and therefore more likely to have a dramatic concentration gradient.

Sample	3h	6h	Overnight
A	0.0042	0.0049	0.0114
B	0.0041	0.0040	0.0031
C	0.0036	0.0037	0.0037
D	0.0029	0.0026	0.0025

Table 5.3: Porosity results summary

5.2.3.3 Mean pore diameter

The mean pore diameter results are shown in Table 5.4. In Chapter 3, Section 3.1.2.2 we stated that Knudsen diffusion is important if the Knudsen number shown in Equation 3.13 is greater than 1. With our results here, the Knudsen number is between 7 and 11; this confirms that Knudsen diffusion should be considered. For Sample A, the pore diameter is less affected by the degas time than the other previous parameters, suggesting that as water was removed, more pores were emptied giving rise to higher porosity and surface area.

Like the porosity, the pore diameters are smaller than those found in catalysts [Soukup et al., 2008], as a larger pore diameter allows molecules more freedom for diffusion. Due to this, we expect diffusion to be more hindered by paper than in porous catalysts. Larger molecules would be hindered more, so large VOCs could have very different local concentrations across a paper volume.

Pore diameter values for paper found through MIP have been in the range of 1.5-22μm and so our values are at least 10 times lower [Moura et al., 2005]. This could be due to the high pressure used in MIP (up to 207 MPa) increasing the sizes of the pores.

Sample D has the lowest density, surface area, porosity and the highest pore diameter for the 3 hour degas time. As the density is low and the surface area is low, we therefore expect a higher pore diameter as a smaller pore diameter would mean more pores and consequently a larger surface area.

Sample	3h	6h	Overnight
A	11.92	13.20	13.81
B	11.32	11.25	10.46
C	10.12	10.87	10.79
D	12.09	12.04	10.10

Table 5.4: Pore diameter results summary (nm)

5.3 Effective diffusion coefficient

In this section, we will outline the experimental procedure used for the measurement of the diffusion coefficients and tortuosity in our four paper samples. The diffusion coefficient used in the model is an effective one that includes contributions from the Knudsen and binary diffusion coefficients. As well as this, it also accounts for the shape, size and interconnectivity of the pores, which is represented by the ratio between the porosity and tortuosity. We experimentally find the effective diffusion coefficient for a test gas, and from the latter the tortuosity of our paper samples. With the tortuosity calculated we can predict the effective diffusion coefficient for other gases and in our case, acetic acid. We will explore the method used and the alternatives, as well as the apparatus.

We have previously outlined diffusion's role as the method of mass transfer of VOCs in the gas phase through our porous medium, paper. The diffusion coefficient arises through the use of Fick's law as outlined in Section 3.1.1.1.

5.3.1 Diffusion coefficient measurement methods

The many different techniques for measuring diffusion coefficients usually fall into two categories: steady state and unsteady state methods. Diffusion experiments are important in industry as there are many porous materials, typically catalysts, through which mass transfer occurs where diffusion is the limiting step. Difficulties arise with diffusion experiments as it is hard to separate the diffusive flux from other mass transfer mechanisms. Other transport mechanisms include viscous flow caused by non zero pressure gradients, convective flow and surface diffusion.

An unsteady state method example is the Stokes diaphragm cell shown in Figure 5.9.
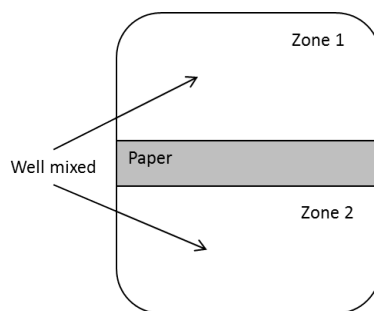
Figure 5.9: Unsteady diffusion set-up

With this type of cell, known initial concentrations are in the zones above and below the paper. After a set time, the concentrations are measured in the zones and from this the diffusion coefficient can be calculated.

Another dynamic method is the pulse technique, which injects a pulse of a trace compound to one side of the material membrane and monitors the compound out of the membrane [Suzuki and Smith]. This technique requires more advanced equipment. The pulse technique, Stokes diaphragm and other

unsteady state methods need more complex maths to solve compared to steady state methods as they have to account for adsorption within the membrane.

A standard steady state example is a Wicke-Kallenbach cell, shown in Figure 5.10 [Soukup et al., 2008]. In this method, gas streams flow parallel on either side to a membrane, with a species of one gas stream diffusing over the membrane into the other stream. A steady state is achieved by having the flow rates constant and allowing the system time to have a constant concentration gradient. This method is widely used for porous pellets and is the method we we will be utilising. To use the Wicke-Kallenbach cell, the pressure difference over the membrane needs to be maintained at zero. Another disadvantage with the cell is that only major pores are accounted for as small or dead end pores aren't involved in the diffusion across the membrane [Valus and Schneider, 1981]. The cell typically is used with a binary gas mixture, but has been used with ternary systems [Capek and Seidel-Morgenstern, 2001].
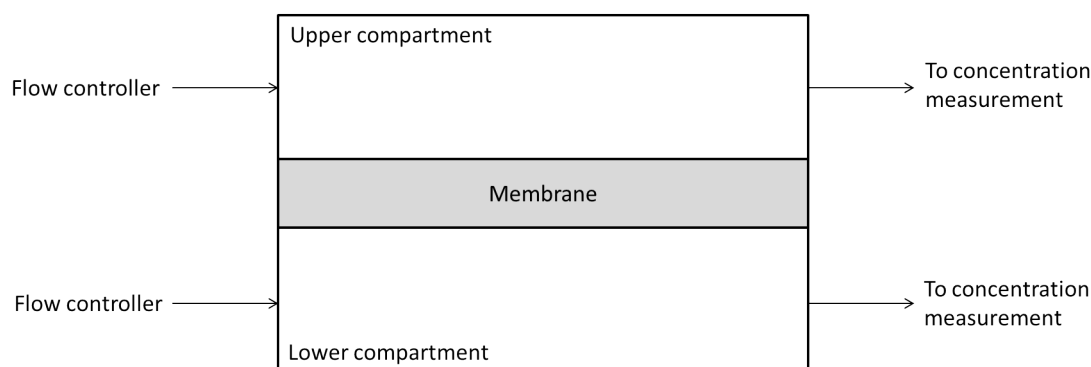
Figure 5.10: Example diagram of Wicke-Kallenbach cell [Soukup et al., 2008]

A steady state alternative to the Wicke-Kallenbach cell is to use a Graham's diffusion cell, which is based on the Wicke-Kallenbach cell but modified using Graham's law, given here for a binary gas system [Soukup et al., 2008, Graham, 1833]:

$$\frac{N_A}{N_B} = -\sqrt{\frac{M_B}{M_A}} \tag{5.12}$$

where N_A and N_B are the fluxes or components A and B respectively and M_A and M_B are their molecular weights. The law states that at a constant pressure, the ratio of fluxes of two diffusing gases in a porous medium if proportional to the inverse square root of their molecular weights. This law is valid for the Knudsen region and isobaric diffusion in a porous medium, and has also been shown to be valid outside of these regions.

With these methods, an issue is knowing when steady state has been achieved. In terms of the experimental results, the Wicke-Kallenbach and Graham cell very similar [Soukup et al., 2008].

5.3.2 Calculating the tortuosity and effective diffusion coefficients

We are using a Wicke-Kallenbach cell with a binary gas mixture. The gases used are nitrogen and hydrogen. The nitrogen is the carrier gas through which we will measure hydrogen diffusing through. The concentration of hydrogen needs to be low so that only diffusion through nitrogen is considered and not self diffusion. With this cell, the compositions and flowrates of the inlet streams are set and the outlet compositions are measured.

We set or measure the volumetric flowrates of the cell and from these calculate the flowrates through the membrane. We are then able to convert the flowrates to molar fluxes which are then used to calculate the effective diffusion coefficients and tortuosities. As the measurements are made in terms of volume and the pressure and temperature are assumed constant, we start by writing a balance for the system in terms of volumetric flowrates. The information used in the balance is shown in Figure 5.11.
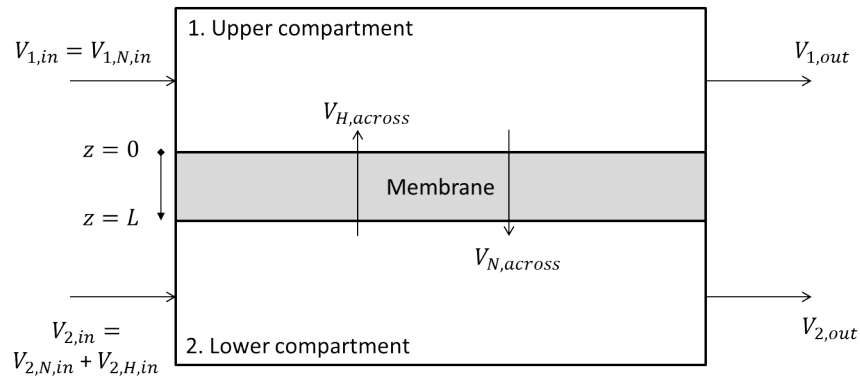
Figure 5.11: Balance diagram over cell

We assume both the upper and lower compartments are well mixed. We start with the first compartment, which has pure nitrogen fed in, with hydrogen transferring into the compartment through the membrane. The total volumetric flowrate out of the compartment is described mathematically as follows:

$$\dot{V}_{1,out} = \dot{V}_{1,N,in} + \dot{V}_{H,across} - \dot{V}_{N,across} \tag{5.13}$$

where $\dot{V}_{1,out}$ is the total volumetric flowrate in the outlet stream, $\dot{V}_{1,N,in}$ is the volumetric flowrate of nitrogen in the inlet stream, and $\dot{V}_{H,across}$ and $\dot{V}_{N,across}$ are the volumetric flowrates of hydrogen and nitrogen across the paper membrane respectively.

By definition, the total volumetric outlet flowrate is be expressed as:

$$\dot{V}_{1,out} \equiv \frac{\dot{V}_{H,across}}{\omega_H} \tag{5.14}$$

where ω_H is the volumetric fraction of hydrogen in the out stream for the first compartment. We then rearrange for $\dot{V}_{H,across}$:

$$\dot{V}_{H,across} = \frac{\dot{V}_{1,N,in} - \dot{V}_{N,across}}{\frac{1}{\omega_H} - 1} \tag{5.15}$$

Now we proceed with the second compartment where we have both nitrogen and hydrogen in the inlet stream:

$$\dot{V}_{2,out} = \dot{V}_{2,N,in} + \dot{V}_{2,H,in} + \dot{V}_{N,across} - \dot{V}_{H,across} \tag{5.16}$$

The total outlet flowrate is defined as:

$$\dot{V}_{2,out} \equiv \frac{\dot{V}_{2,N,in} + \dot{V}_{N,across}}{\omega_N} \tag{5.17}$$

Using Equation 5.17 in Equation 5.16 and rearranging:

$$\dot{V}_{N,across} = \frac{\dot{V}_{2,H,in} - \dot{V}_{H,across}}{\frac{1}{\omega_N} - 1} - \dot{V}_{2,N,in} \tag{5.18}$$

For simplification we define two new variables:

$$\alpha_N = \frac{1}{\omega_N} - 1; \quad \alpha_H = \frac{1}{\omega_H} - 1 \tag{5.19}$$

With these and our expression for the volumetric flowrates of hydrogen across the membrane in Equation 5.15, we rearrange Equation 5.18:

$$\dot{V}_{N,across} = \frac{\alpha_H \dot{V}_{2,H,in} - \dot{V}_{1,N,in} - \alpha_N \alpha_H \dot{V}_{2,N,in}}{\alpha_N \alpha_H - 1} \tag{5.20}$$

We now rearrange Equation 5.15:

$$\dot{V}_{H,across} = \frac{\alpha_N \dot{V}_{1,N,in} - \dot{V}_{2,H,in} + \alpha_N \dot{V}_{2,N,in}}{\alpha_N \alpha_H - 1} \tag{5.21}$$

With Equations 5.20 and 5.21 we can now work out the mean fluxes:

$$N = \frac{\dot{V}_{across}}{A} C \quad N_N = \frac{\dot{V}_{N,across}}{A} y_N C \quad N_H = \frac{\dot{V}_{H,across}}{A} y_H C \tag{5.22}$$

where N, N_N, and N_H are the total, nitrogen and hydrogen fluxes respectively, C is the overall concentration calculated using ideal gas law, y_N and y_H are the molar fractions of nitrogen and hydrogen and A is the cross-section area.

In Chapter 3 we gave the overall molar flux as the diffusive flux and the convective flux combined as shown in Equation 3.8. We expressed the diffusive flux through the constitutive equation given by

Fick's law. With the cell, we cannot disregard the convective flux as the velocity of the mixture is not near zero. Using Fick's law, the molar flux of hydrogen is:

$$N_H = -CD_{eH}d_{\mathbf{z}}y_H + C_H\mathbf{v_z^*} \tag{5.23}$$

where D_{eH} is the effective diffusion coefficient of hydrogen, C_H is the concentration and $\mathbf{v_z^*}$ is the average velocity of the mixture in the z direction. The effective diffusion coefficient of hydrogen is found using Equations 3.18 and 3.17 described in section 3.1.2.3:

$$D_{eH} = \psi D_H \quad \text{with} \quad \frac{1}{D_H} = \frac{1}{D_{H,N}} + \frac{1}{D_{K,H}} \tag{5.24}$$

where D_H, $D_{H,N}$ and $D_{K,H}$ are the overall diffusion coefficient, the ordinary molecular diffusion coefficient and Knudsen diffusion coefficient of hydrogen respectively, ψ is the ratio between the porosity and tortuosity.

Equation 5.23 can be rearranged for a binary mixture to [Youngquist, 1970]:

$$N_H = -CD_{eH}d_{\mathbf{z}}y_H + y_H N \tag{5.25}$$

The Maxwell-Stefan equation for a binary mixture yields the same result as Equation 5.25 showing that the diffusion coefficient for Fick's law and Maxwell-Stefan equations are equivalent. The diffusion coefficient is given by Equation 4.76 in Chapter 4 and accounts for porosity and tortuosity.

We now rearrange Equation 5.25 to a more convenient form for integration:

$$N_H = -\frac{CD_{eH}}{1 - \alpha y_H}d_{\mathbf{z}}y_H \tag{5.26}$$

where:

$$N = N_H + N_N = N_H(1 + \frac{N_N}{N_H}) \quad \text{with} \quad \alpha = 1 + \frac{N_N}{N_H} \tag{5.27}$$

This equation can be further changed using Graham's law given in Equation 5.12.
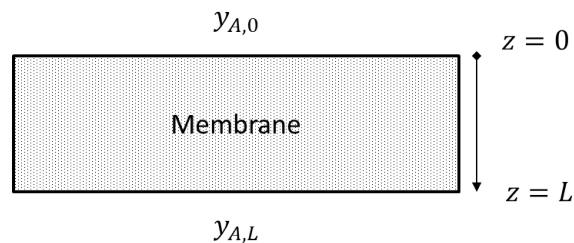
Figure 5.12: Mass fractions shown over paper membrane

We now integrate over the thickness of the membrane, using the notation shown in Figure 5.12:

$$N_H = \frac{-CD_{eH}}{L\alpha} \ln \left[\frac{1 - \alpha y_{H,L}}{1 - \alpha y_{H,0}} \right] \tag{5.28}$$

where L is the length or thickness of the membrane.

We now rearrange these equations. We rearrange for the porosity and tortuosity ratio, ψ:

$$\psi = \frac{N_H L\alpha}{CD_H} \frac{1}{\ln \left[\dfrac{1 - \alpha y_{H,L}}{1 - \alpha y_{H,0}} \right]} \tag{5.29}$$

The diffusion coefficients $D_{H,N}$, $D_{K,H}$ and D_H are worked out theoretically as outlined in Equations 3.11, 3.15 and 3.17 respectively in Chapter 3.

The porosity is known from Section 5.2 and so the tortuosity can be worked out using the value for ψ. The effective diffusion coefficient is calculated using Equation 3.18 from Chapter 3.

5.3.3 Wicke-Kallenbach cell apparatus and procedure

5.3.3.1 Apparatus

The cell we are using is an example of a Wicke-Kallenbach cell. The set-up used is outlined in Figure 5.13. The main component of the set-up is the diffusion cell, which has two inlet gas feeds controlled by mass flow controllers (MFCs), two outlet gas streams and our porous material inside acting as the membrane. The set-up has a pressure reader and flow controls for the gas streams. Finally, the set-up has a gas chromatograph (GC) which is used for determining the concentrations of the gas species in the inlet and outlet gas streams. The cell is operated at room temperature.
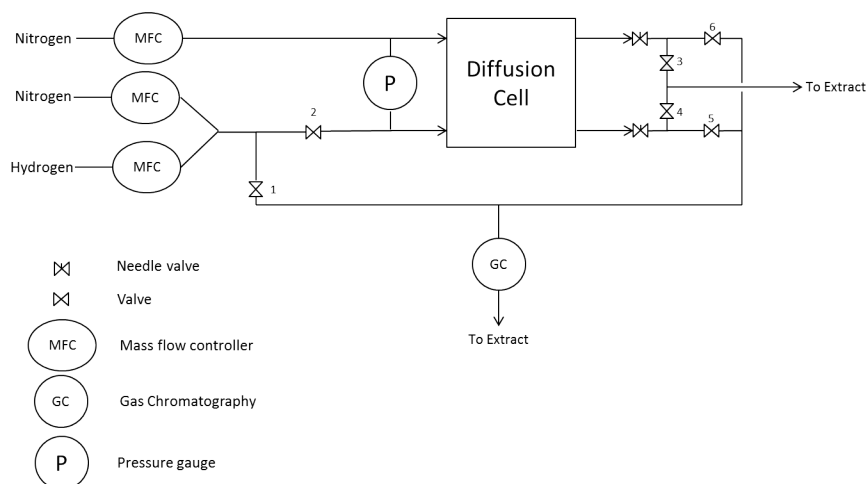
Figure 5.13: Diffusion cell set-up

The diffusion cell is shown in Figures 5.14 and 5.15. It has two inlets and two outlets. The membrane

is placed at the bottom of a cylindrical chamber, between the two gas streams at 45° angle from the streams.
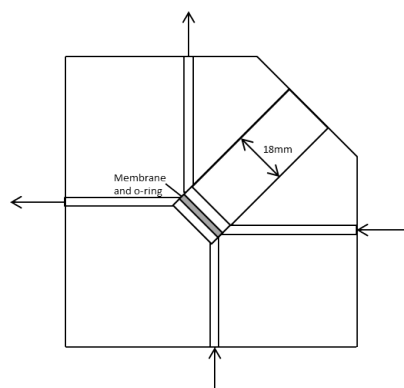
Figure 5.14: Diagram of diffusion cell
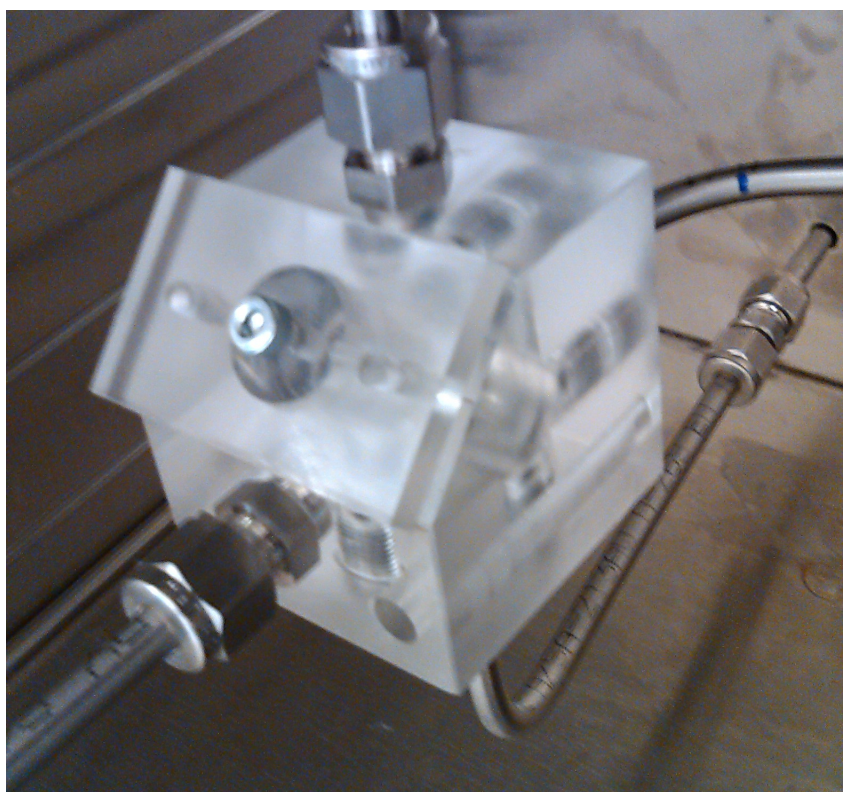
Figure 5.15: Photo of diffusion cell

The membrane is secured by rubber O-rings either side. The O-rings have an outer diameter of 18mm. The paper samples have a diameter of 16mm and the active area due to the shape of the cell has a diameter of 11mm. After the membrane and O-rings are fitted, they are secured by a cylindrical plug

fitting the chamber. Five sheets of paper were used for each sample, as too few caused the sample to break and too many causes the air flow to be altered.

The gases we are using are hydrogen and nitrogen. The nitrogen is the carrier gas, and the hydrogen is the gas we measure diffusing across the membrane. One side of the diffusion cell has pure nitrogen at the inlet and the other side has a nitrogen-hydrogen mix.

The flow rates are controlled with mass flow controllers and the pressure across the cell is read using a pressure meter. The pressure can be adjusted with needle valves.

All the streams are connected to the GC and when a stream is being sampled to measure the concentrations, the relevant valves are opened so that the stream flows to the GC instead of the extract as shown in Figure 5.16.

	1	2	3	4	5	6
Mix inlet		■			■	■
Mix outlet	■			■		■
Outlet from pure Nitrogen side	■		■		■	

Figure 5.16: Valve setup

5.3.3.2 Procedure

Before calibration of the mass flow controllers and of the GC, a leak test is carried out. The leak test is to ensure that all connections are properly fitted. To perform the leak test, we have gas run through the system and Snoop Liquid Leak Detector [Swagelok, 2012] is used on all connections which produces large bubbles if leaks are found.

With leaks eliminated, calibration can begin. We start by calibrating the mass flow controllers for the gases. The input and output streams are disconnected from the GC and connected to a gilibrator to measure the flow rates. Each controller was tested separately. The controllers are set to specific flow rates in standard cubic centimetres per minute (*sccm*) via the computer they are connected to and, after the flow has reached a steady state, are measured by the gilibrator. From these results, a calibration curve is achieved. All three calibration curves gave straight lines and can be seen in Figures 5.17, 5.18 and 5.19. To ensure that there was no diffusion across the membrane, a metal disc was used in place of a paper sample.
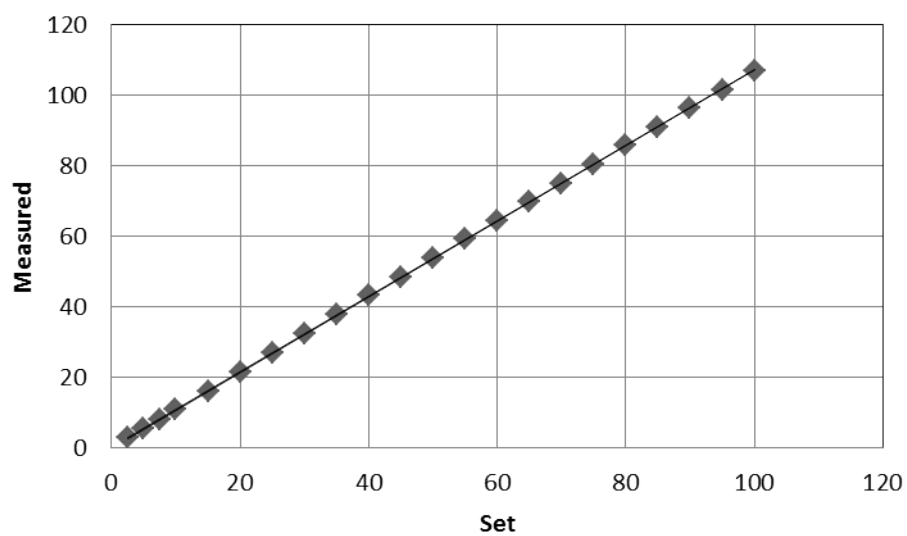
Figure 5.17: Calibration curve for pure nitrogen mass flow controller (in SCCM)
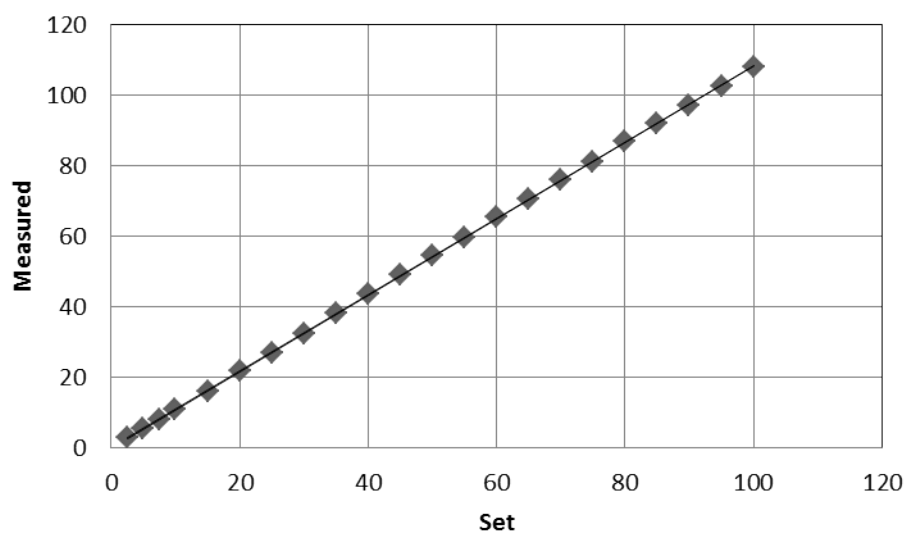
Figure 5.18: Calibration curve for mix nitrogen mass flow controller (in SCCM)
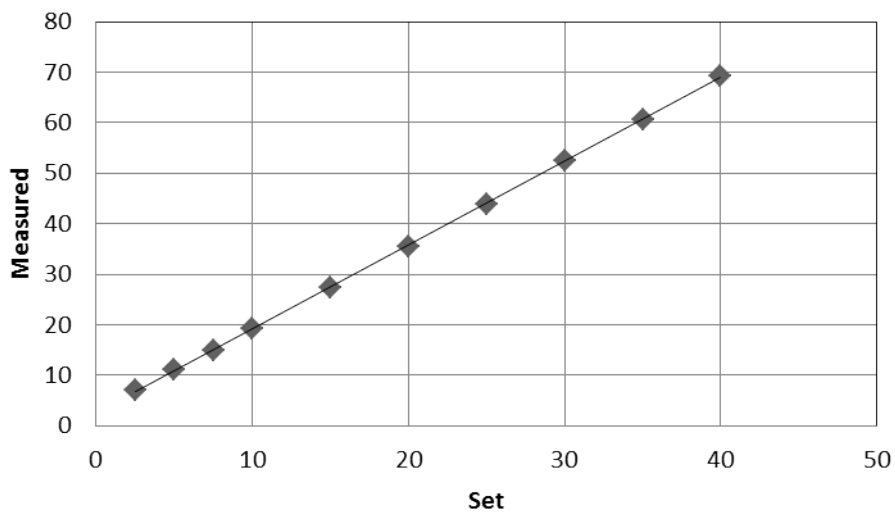
Figure 5.19: Calibration curve for mix hydrogen mass flow controller (in SCCM)

The final calibration is for the GC. For this, the GC is reconnected to the system. Using the mass flow controllers and their calibration curves, known mixtures are set and sampled by the GC. The GC sends the results to the computer, and from the resulting peak areas a calibration curve is achieved as seen in Figure 5.20. The GC calibration should be checked frequently as it is more likely to change with time than the mass flow controllers.
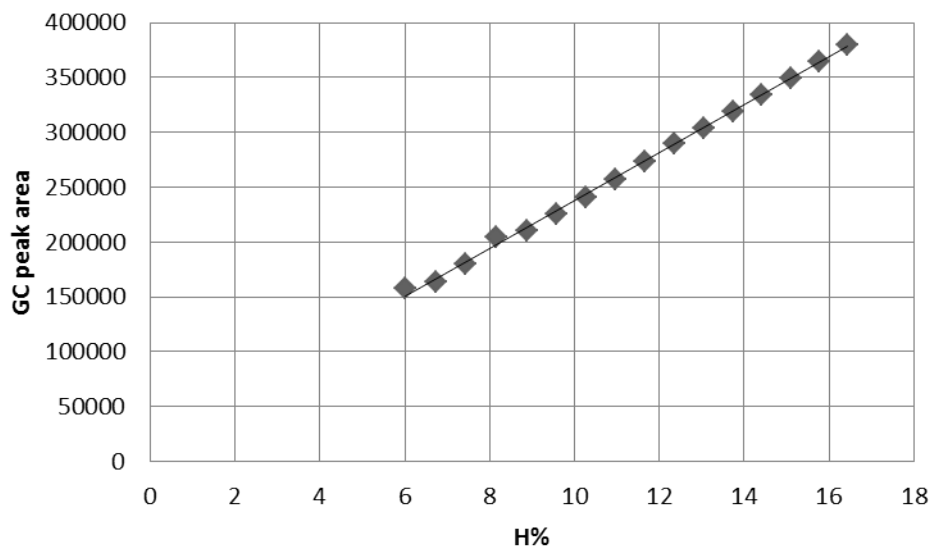
Figure 5.20: GC calibration curve

With the calibration complete, experimentation on the paper samples can start. The paper is cut

to 15mm diameter circles, and 5 sheets are used. The sample is placed in the diffusion cell with the O-rings and then sealed. The nitrogen and hydrogen gas feeds are opened and the mass flow controllers are set to particular mixture values. The mixes tested are shown in Table 5.5. The hydrogen content cannot be too high as then self diffusion cannot be neglected.

Pure nitrogen MFC (sccm)	Mix nitrogen MFC (sccm)	Mix hydrogen MFC (sccm)
50	97.5	2.5
50	95.0	5.0
50	92.5	7.5
50	90.0	10.0

Table 5.5: Mass flow controller compositions tested for samples

The valves are then opened first to the mix inlet orientation as shown in Figure 5.16. The needle valves are adjusted until the pressure reading on the pressure gauge is as close to zero as possible (typically within 10 Pa). Once the system has reached steady state, the GC can take samples. 5 samples are taken for each stream, after this, the valve orientation is changed for the next stream. Again, the needle valves are adjusted, we wait for steady state and then GC samples are taken. Once this has been done for the three streams the next mixture for the mass flow controllers can be set and the procedure repeated.

After all mixtures have been completed, the mass flow controllers are set to zero and the system is degassed with nitrogen. Then the gas is all turned off and the next sample can be put in.

For the calibration data used for the calibration graphs and the raw data for the tortuosity and acetic acid diffusion results, please refer to Section A.2 in the appendices.

5.3.4 Tortuosity results

Figure 5.21 shows the tortuosity values. Sample D, the Whatman filter paper, shows the lowest values. The "real" paper samples fall within a close range to each other compared to the Whatman paper. The oldest paper, Sample B, varies the most having the highest values for most of the hydrogen-nitrogen mixes. Both Sample A and Sample B have similar values for their porosity, surface area and pore diameter, the main difference may be due to Sample B having a higher density than A. However, Sample C has a slightly higher density than B but lower porosity and pore diameter, and has the lowest tortuosity value.

The porosity and pore diameter values used in calculations were that of the 3 hour degas times given in Section 5.2.3 as it was considered that these values would be closest to real condition values with water content.
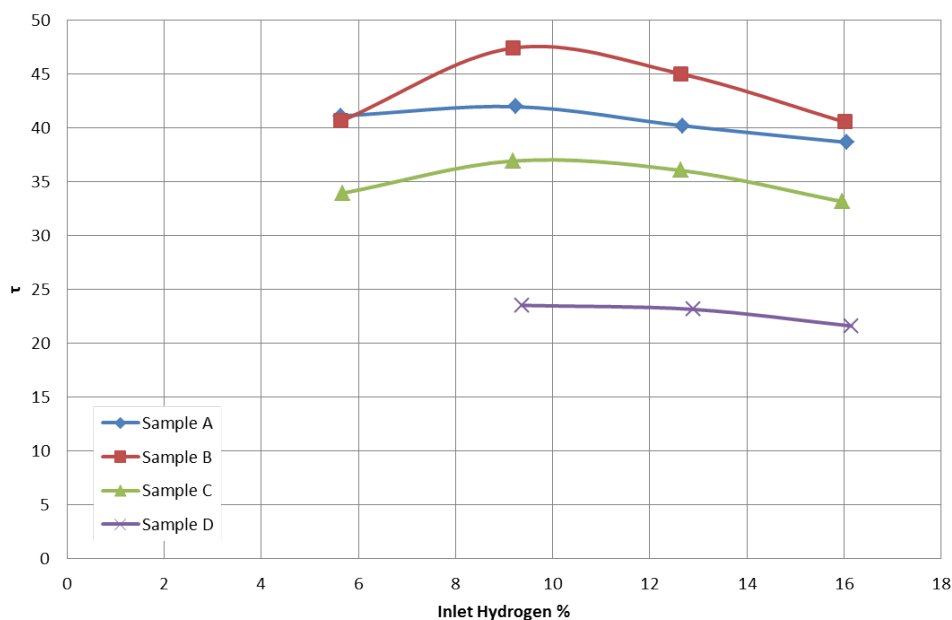
Figure 5.21: Comparison of tortuosity values

The tortuosity values vary slightly depending on the hydrogen percentage even though we would expect it to remain constant. A tabulated summary of the results can be found in the appendices, section A.2.3.

To extend the results, different thicknesses of each paper sample could be tested. This would help establish an average tortuosity value for each sample and show whether the thickness has an effect on the result. Samples of different ages would give information on how the tortuosity of samples change through time as the material degrades. More samples would show if the tortuosity of papers varies largely or stays within a small range.

5.3.4.1 Acetic acid diffusion coefficient prediction

Using the tortuosities calculated, we can now estimate the effective diffusion coefficient for our VOC, acetic acid, that we wish to model. To do this, we use Equations 3.17 and 3.18. We use Equation 3.15 to work out the Knudsen diffusion coefficient for acetic acid and for the ordinary molecular diffusion coefficient, we use 0.1235 cm^2/s from literature [Lugg, 1968]. The results are shown below in Figure 5.22.

Sample D has the greater diffusion coefficient, most likely due to the sample having the larger pore diameter. Sample A has the second largest pore diameter and also has the second largest diffusion coefficient values. However Sample B has a large pore diameter than C but both have a similar range for their diffusion coefficients. The effective diffusion coefficient for all samples is, as expected, smaller than for other wood based materials; the effective diffusion coefficient for acetone through chipboard being 1.5E-06 m^2/s [Lee et al., 2005].

The results can be found in table form in the appendices, Section A.2.4.
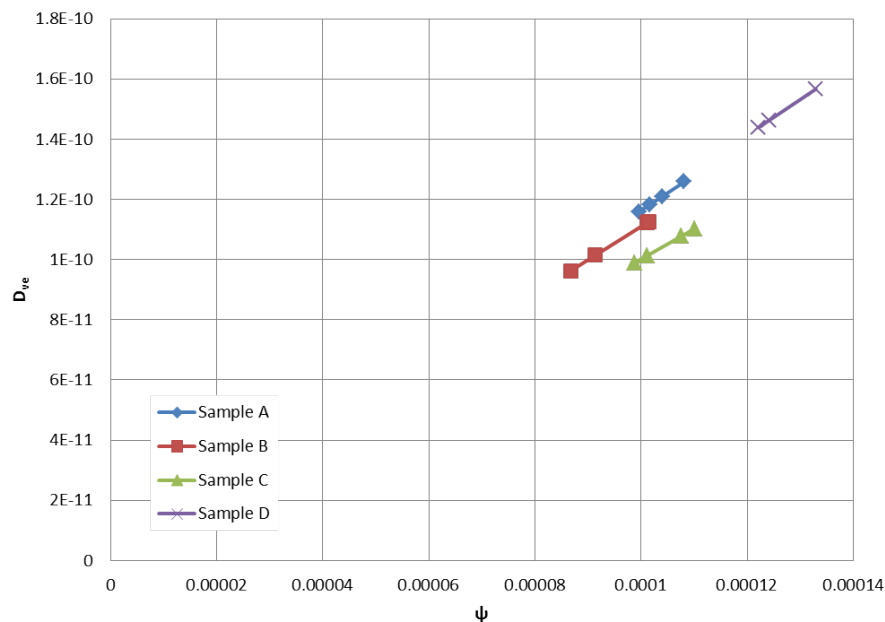
Figure 5.22: Fick's model values for D_{ve} (m^2/s)

5.4   Adsorption isotherm

Here we explain how we get our adsorption function in the form described in Chapter 3, Section 3.2.1, Equation 3.24. We will discuss the methods of finding adsorption functions as well as our work using propionic acid and how it relates to our VOC model.

5.4.1   Adsorption function measurement methods

One method used for finding the adsorption isotherm experimentally is that used by Tiffonet et al. 2002. Isotherms were found for both porous and non porous materials. The isotherms were found using a temperature controlled, 46 litres stainless steel chamber containing the adsorbing material. The chamber is stainless steel so as to minimise the interactions with the adsorbate and the surfaces of the chamber. The chamber initially contains a nitrogen-oxygen mix to avoid the influence of other components in the air in the experiment. A known concentration of the adsorbate is then injected into the chamber and mixed into the air by an internal fan. The air is then sampled at regular intervals to find the concentration of the adsorbate in the air in order to establish when the gas phase concentration is in equilibrium with the adsorbed phase. After this, other known concentrations of the adsorbate are injected, to establish more equilibrium points of the isotherm. This is shown in Figure 5.23 for the material chipboard and the adsorbate acetone [Tiffonnet et al., 2002].
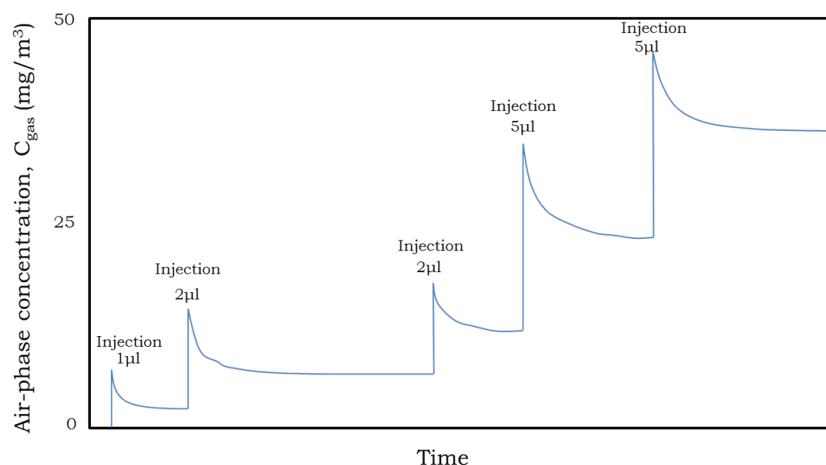
Figure 5.23: Acetone/chipboard air phase concentration [Tiffonnet et al., 2002]

Another method for finding information about adsorption isotherms is head space analysis. There is static or dynamic head space analysis [Sparkman et al., 2011].

In static head space analysis, the concentration is measured from the gas phase above the adsorbing material. The adsorbing material can be a solid but is typically a liquid as shown in Figure5.24. The concentration in the gas phase is measured through a GC (and then typically through a mass spectrometer). This method needs to be calibrated in order to quantify the VOC being measured. To do this, known liquid sample concentrations must be tested first.
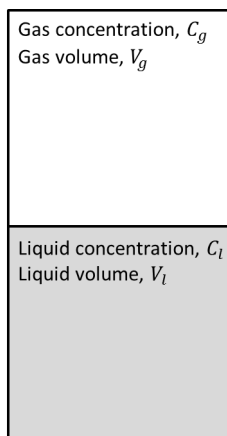
Figure 5.24: Static head space sample [Sparkman et al., 2011]

In dynamic Head Space analysis, gas is bubbled through the sample and the species of interest is trapped as the gas is purged. This is shown in Figure 5.25. The trap is then heated, the species desorbed and injected into the GC. Typically dynamic head space analysis has a lower detection threshold than the static method. However solid phase micro extraction (SPME) method of sampling for a GC can also get very low detection rates. With SPME, a fibre is inserted into the sample's

head space, where it adsorbs compounds for a set period of time (and temperature). The fibre is then withdrawn and placed in the GC where the compounds are thermally desorbed. Using SPME takes a lot of calibration as the adsorption and desorption times and temperatures are optimised as well as the GC cycle and which fibre is used [Sparkman et al., 2011].
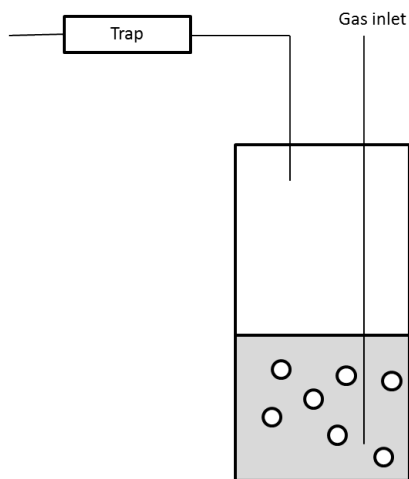
Figure 5.25: Dynamic head space set up [Sparkman et al., 2011]

The method we will be using is based on that of Tiffonet et al. with a relatively simple set up, which can be easily calibrated and can measure VOC concentration in real-time.

5.4.2 Adsorption apparatus and procedure

For our method, we have two 5 litre glass jars in which our paper samples are placed, which have a VOC sensor inside and a point for injection of known VOC amounts. A photograph and diagram of the equipment is shown in Figure 5.26. The VOC sensors are Alphasense PID-AH PhotoIonisation Detectors [Alphasense, 2011]. The glass jars are kept at room temperature and relative humidity.
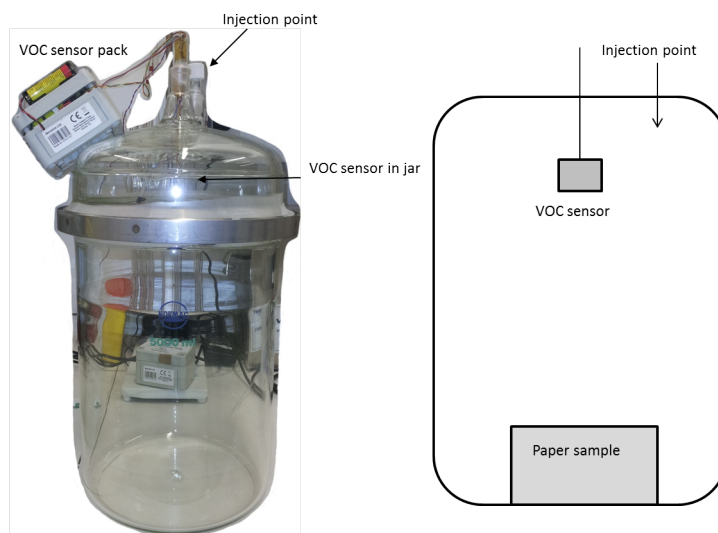
Figure 5.26: Photo and diagram of equipment

In order to inject a small enough concentration, we first prepare a known concentration of our VOC, in this case propionic acid, in a 5 litre bag. The bag is prepared by first filling with nitrogen and then injecting $40\mu L$ of propionic acid (giving a concentration of 2600 ppm in the bag). The bag is ready to use when the acid has vapourised. Propionic acid is used as the sensors used are able to detect it where they cannot detect acetic acid and it is hoped their adsorption isotherms are similar as they are similar compounds; both are simple carboxylic acids, propionic acid having an extra carbon and two hydrogen atoms, the pKa of acetic acid is 4.76, propionic acid is 4.88. It is assumed that the acid does not adsorb on the glass walls.

The VOC sensors need to be calibrated before using with paper present. To do this, we inject known quantities of the acid from the bag into the jar to get a calibration curve. After each injection, we need to wait until the system has reached equilibrium. This can be confirmed when the readings remain consistent and a time interval of 10 minutes was used as shown in Figure 5.27.
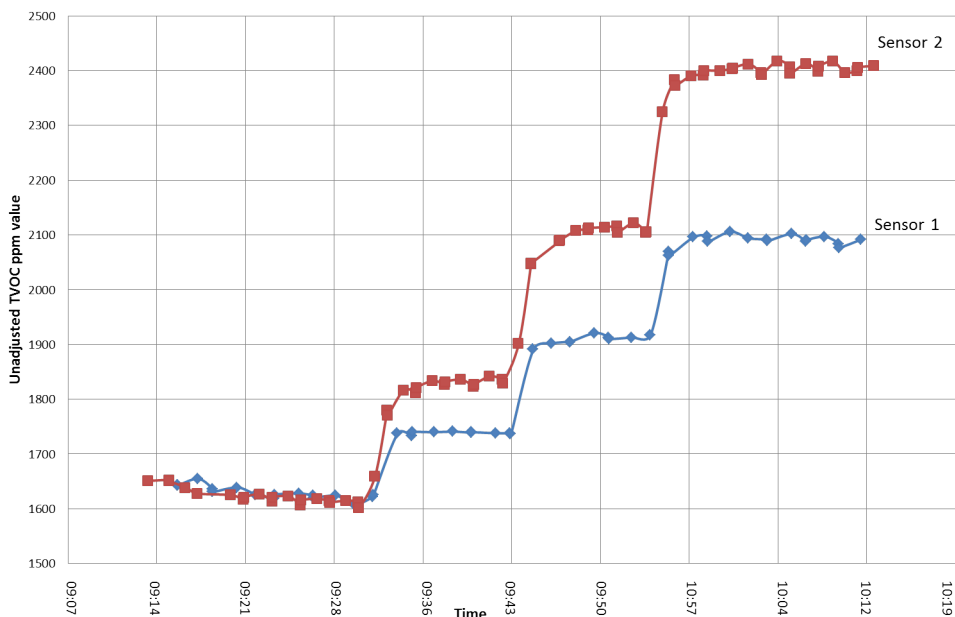
Figure 5.27: Calibration equilibrium time of sensors

With the sensors calibrated, we can now test paper samples. A sample of about A5 size is put into the jar in such a way that virtually all of the surface area is available for the acid to be adsorbed into. We then inject known volumes into the jar, and measuring the gas phase concentration, we can calculate the adsorbed phase concentration. With paper present, the time required for the concentration to reach steady state was longer and so was monitored to see when it was suitable for the next injection (typically being 1-2 hours).

This assumes no loss of acid through leaks, and to minimise this possibility, all seals were wrapped in parafilm.

Knowing the quantity of acid injected, we can calculate the total number of moles of acid in the jar. From our reading, we know the moles of acid in the gas phase, taking this away from the total number of moles of acid, we get the amount adsorbed. This is then divided by the surface area of the sample available to get the concentration (in mol/m^2):

$$[v] = \frac{mol_{v,ads}}{A_s} \tag{5.30}$$

where $mol_{v,ads}$ is the moles of propionic acid adsorbed, A_s is the total area of the sample.

After each test, the jars are cleaned by removing the paper, extracting the air in a fume cupboard and having dry air flow through the jars.

5.4.3 Adsorption isotherm results

The results of each paper's isotherm are shown in Figure 5.28 and Table 5.6. Ideally more experimentation would be carried out to improve the adsorption coefficients. For the raw data of the adsorption experimentation, please refer to Section A.3 in the appendices.

Sample D has the lowest adsorption coefficient value and is the least adsorbent of the samples which could be explained by the sample's low surface area. We would then expect the other samples to all be more adsorbent and have similar values to each other. Sample A however has an adsorption coefficient value closer to Sample D. This could be due to the composition of the sample.

These adsorption values are comparable to formaldehyde on wood fibreboard, another cellulose based material, where the values are 0.0054m and 0.0050m for different medium density fibreboards [Xiong et al., 2012].

Although each sample has been fitted to a straight line, Sample C follows a slight curve. This may imply that it follows Type 4 isotherm as shown in Section 3.2.2 Figure 3.6. Another issue for Sample C is the alkaline reserve. All samples took between one and two hours to reach to reach a steady state with the gas phase and adsorbed phase concentrations in equilibrium. Whilst Sample C is reaching equilibrium, the acid in the adsorbed phase can undergo neutralisation. If the neutralisation was instant in comparison to adsorption, the gas concentration would constantly decrease until zero or the alkaline reserve is consumed. As this is not the case, we can assume that the neutralisation is either on a similar timescale to adsorption, or slower. For the purpose of the model, we assume that neutralisation is on a similar timescale to adsorption, which we assumed is significantly fast compared to diffusion and the degradation rate in Chapter 4, Section 4.3.2. To explore this assumption, further experimentation would be needed where the concentration in the glass jar is measured for a significant time after the steady state is reached to see when a decrease in gas phase concentration happens. A possible problem is concentration drop due to leakage starting to affect the results.

To find more information on the shapes of the isotherms, more concentrations can be explored, within the range already explored and beyond it. Another extension would be to investigate the desorption isotherm as it is possible for the desorption isotherm to be different to the adsorption isotherm [Tiffonnet et al., 2002].
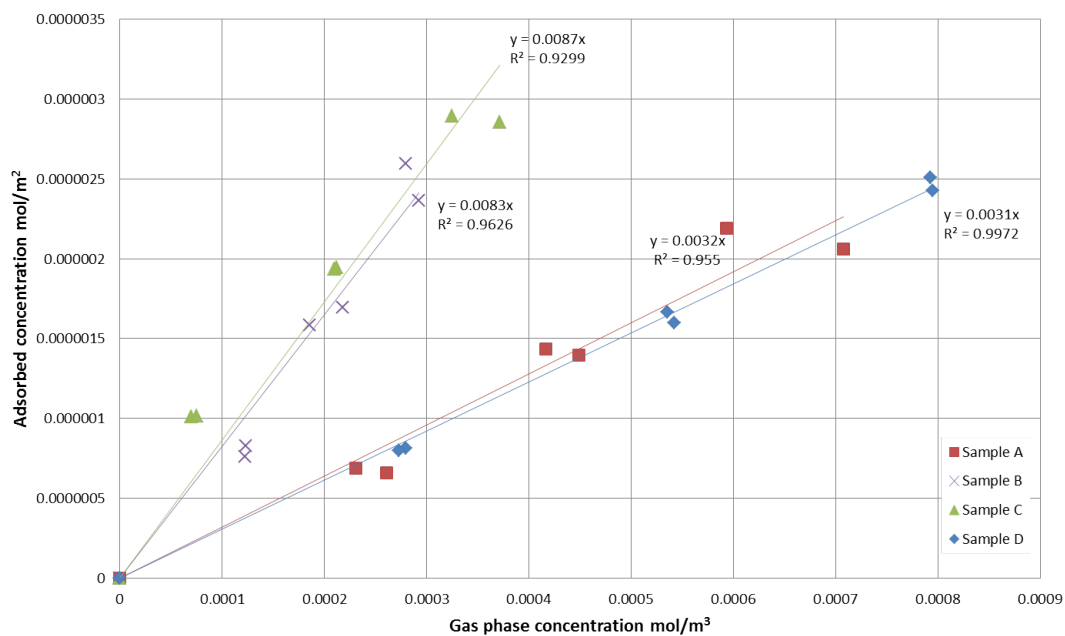
Figure 5.28: All isotherms

Sample	Linear constant K_v (m)
A	0.0032
B	0.0083
C	0.0087
D	0.0031

Table 5.6: Sample adsorption coefficients

Chapter 6

Computational modelling

From the work in Chapter 4, we have a mathematical model describing our VOC's concentration profile through a paper volume. In Chapter 5, we found, through experimentation, values for the variables and parameters for four different paper samples that cannot be calculated or found in the literature.

These experiments do not include the values for the constants for the VOC generation reaction, which will be explored further here.

In this chapter we will review the computational tools available; we will reiterate the equations governing the main model and additional models outlined in Chapter 4, and show how the experimental work is included in the equations. Then, we will go over the scenarios we will explore computationally, and the boundary and initial conditions that are used to describe them mathematically. Finally we will go through the results gained from the computational simulations.

6.1 Modelling tools

Here we explore the different computational tools. For some mass transfer problems like those discussed in Chapter 4 involving VOCs, Computational Fluid Dynamics software is often used. This software allows the user to define the geometry of the problem, then create a mesh for the solver to consider, and then specify their model and which phenomena to account for. The boundary and initial conditions are then set, as is the solving method, and the simulation is run. The advantage is that complex problems can be solved and different phenomena and parameters explored relatively quickly as the model is changed to suit the user's needs. The software requires reasonably powerful computers and, depending on the simulation, can run for some time. In our case, CFD is unnecessary as our problem is not a fluid dynamics problem, but a diffusion problem as the fluid dynamics do not play a significant role. Due to this, we shall use other options [ANSYS, 2013].

A familiar computational tool in engineering is MATLAB, a numerical computation environment. With MATLAB, one writes the equations that define the model rather than select the equations describing the phenomena of interest. However, unless the additional Simulink toolbox is available, one cannot

solve three dimensional second order partial differential equations [Mathworks, 2013]. As the Simulink toolbox is unavailable, we therefore need another computational tool.

In order to solve three dimensional second order partial differential equations, we can use gPROMS. This is a process modelling tool that can have custom modelling and can also have one model defined with different parameters and boundary conditions explored in different simulations [PSEnterprise, 2013]. An example of the code used for the simulations is given in Appendix B.

6.2 Model algorithm

Here we present the algorithm for our model which we will use for our computational simulations. The algorithm is for paper with or without an alkaline reserve.

Locally within the paper volume, we first need to know if there is an alkaline reserve. An alkaline reserve is present when the calcium carbonate concentration is above zero.

If an alkaline reserve is present, acetic acid is neutralised by the calcium carbonate and so the local VOC concentration is given by:

$$\varepsilon \partial_t C_v + \sigma \partial_t [v] = 0 \tag{6.1}$$

where C_v is the gas phase concentration of the VOC (acetic acid).

The local calcium carbonate concentration profile is given by Equation 4.91 from Chapter 4:

$$\partial_t \left[CaCO_3 \right] (\mathbf{x}, t) = -\frac{1}{2} \left(D_{ve} \partial_{\mathbf{x}} \cdot \partial_{\mathbf{x}} C_v(\mathbf{x}, t) + \sigma r_v(\mathbf{x}, t) \right) \tag{6.2}$$

where $[CaCO_3]$ is the concentration of calcium carbonate in the solid phase per unit volume of paper, σ is the unit surface area, r_v is the reaction rate for the generation of acetic acid and D_{ve} is the effective diffusion coefficient. Whilst the alkaline reserve is present, the local acidity remains the same as the initial acidity. The alkaline reserve is consumed when the calcium carbonate concentration equals zero.

If an alkaline reserve is not locally present, either because it was never present or because it has been consumed, the local VOC concentration is described by Equation 4.75 in Chapter 4:

$$\partial_t C_v(\mathbf{x}, t) = \frac{D_{ve}}{\varepsilon + \sigma K_v} \partial_{\mathbf{x}} \cdot \partial_{\mathbf{x}} C_v(\mathbf{x}, t) + \frac{\sigma}{\varepsilon + \sigma K_v} r_v(\mathbf{x}, t) \tag{6.3}$$

where ε is the porosity and K_v is the adsorption coefficient.

The local calcium carbonate concentration is zero, and since it does not change, we have:

$$\partial_t \left[CaCO_3 \right] (\mathbf{x}, t) = 0 \tag{6.4}$$

The local acidity is now given by Equation 3.41 in Chapter 3:

$$H^+(\mathbf{x}, t) = H_0^+ + \frac{\sqrt{([H_0^+](\mathbf{x}, t) + Ka)^2 + 4KaK_vC_v(\mathbf{x}, t)} - ([H_0^+](\mathbf{x}, t) + Ka)}{2} \tag{6.5}$$

where H^+ is the hydrogen ion concentration, Ka is the acid dissociation equilibrium constant and H_0^+ is the initial acidity of the paper.

Whether an alkaline reserve is present or not, the VOC reaction rate is given by Equation 4.77 in Chapter 4:

$$r_v(\mathbf{x}, t) = k_{vr}\alpha(\mathbf{x}, t)k_{DP}(\mathbf{x}, t) \tag{6.6}$$

where k_{vr} is a reaction constant for the generation of the VOC, k_{DP} is the degradation rate reaction "constant" and α is given by:

$$\alpha(\mathbf{x}, t) = \frac{2}{DP(\mathbf{x}, t) - 1} \tag{6.7}$$

where DP is the local degree of polymerisation.

The degradation reaction rate constant is a function of temperature, relative humidity and acidity based on Equation 4.10 from Chapter 4. This equation is rearranged to give:

$$k_{DP}(\mathbf{x}, t) = \exp(a)\left\{[H^+](\mathbf{x}, t)\right\}^b \tag{6.8}$$

where b is 0.24 and:

$$a = 38.039 + 38.057\left(\frac{\ln(1 - RH)}{1.67T - 285.655}\right)^{\frac{1}{2.491 - 0.012T}} - \frac{14713}{T + 273.15} \tag{6.9}$$

where RH is the relative humidity and T is the temperature in °C. For each simulation, we assume the relative humidity and temperature are constant and known.

Finally, the degradation rate is given by Equation 2.10 in Chapter 2:

$$\partial_t DP(\mathbf{x}, t) = -k_{DP}(\mathbf{x}, t)\left[DP(\mathbf{x}, t)\right]^2 \tag{6.10}$$

When we consider the additional model where the acidity is not affected by the VOC concentration (No Acidity Change, NAC), we remove Equation 6.5 from the model as the acidity of the paper remains constant. When we consider the additional model where there is no VOC generation by paper, but the VOC concentration profile still affects the acidity and the degradation rate (No Reaction, NR), the model remains the same, but k_{vr} is zero. For the NR model, for the VOC concentration profile to not be zero, VOCs must diffuse into the paper from outside the volume.

For all simulations we assume the initial VOC concentration in the paper is zero. When considering a particular VOC, it is possible that the initial concentration in paper is zero. This depends on the VOC

	A	**B**	**C**	**D**
$D_{ve}(\text{m}^2/\text{year})$	0.00379	0.00333	0.00330	0.00470
$\sigma(\text{m}^2/\text{m}^3)$	1402500	1452600	1422200	950400
$K_v(\text{m})$	0.0032	0.0083	0.0087	0.0031
$\varepsilon(\text{m}^3/\text{m}^3)$	0.0042	0.0041	0.0036	0.0029

Table 6.1: Paper properties used for model

Sample	**Acidity (hydrogen ion concentration)**	**pH**	**DP**
A	7.58578E-07	6.12	1037
B	1.1749E-05	4.93	1330
C	8.51138E-09	8.07	1916
D	0.0000001	7.00	2300

Table 6.2: Initial acidities and DP

and the paper, as each paper will have different VOCs present from its composition. To find initial concentrations of VOCs, methods like head space analysis in conjunction with GC-MS could be used. The initial alkaline reserve, DP and acidity are specific to the paper being simulated. The boundary conditions for the model are specific to the scenario being simulated and will be explored in Section 6.4. The effective diffusion coefficient, unit surface area, adsorption constant and porosity are specific to the paper or papers being simulated.

For our main model and the NAC model we need values for the reaction constant k_{vr} for the generation of the VOC. An initial value of 1 is used as this falls within the expected range shown later in Section 6.5.6, where the constant is explored.

Our initial simulations are run until all samples reach a DP of 250, as it is suggested that this value marks the end of paper's usability [Menart et al., 2011].

6.3   Sample paper properties

In Chapter 5, we found values for the effective diffusion coefficient, unit surface area, adsorption constant and porosity variables for four paper types which are summarised in Table 6.1.

The diffusion values used are from the results given in Chapter 5, Section 5.3.4.1. The porosity and surface area values used are from Chapter 5, Sections 5.2.3.2 and 5.2.3.1 respectively. The values used are from the three hour degas time, as longer degas times remove more water from the samples, and realistically water would normally be present.

The acidities used are based on Table 5.1 from Chapter 5 and shown here in Table 6.2 with the initial DP values. Sample C also has an alkaline reserve of 20% by mass, which gives a concentration of 1618 mol/m^3. The intial DP of the samples and Sample C's alkaline reserve were provided by the UCL Centre for Sustainable Heritage.
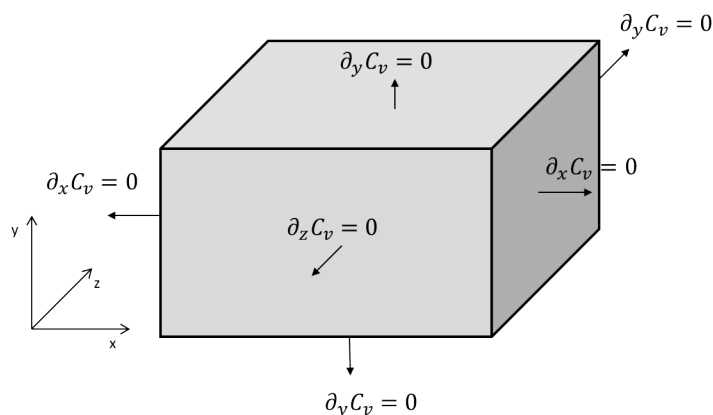
Figure 6.1: Sealed fitted container

6.4 Modelling scenarios

For our simulations, we will consider different scenarios. These scenarios will decide the boundary and initial conditions. The scenarios are chosen to try and represent as best as possible different ways in which paper is stored.

We shall investigate paper volumes contained within three different environments: in a sealed container with the same dimensions as the paper volume; a container with the paper volume and surrounding air; and a shelf in a large room.

6.4.1 Sealed fitted container

The sealed fitted container assumes that the paper volume is surrounded by a material through which mass transfer does not occur. It could be that the paper is kept in a tight fitting plastic wallet or pressed in glass, like a picture frame. As such, we get the following boundary condition for the mass flux normal to all paper surfaces:

$$\partial_n C_v = 0, \quad n = x, y, z \tag{6.11}$$

This is shown in Figure 6.1.

6.4.2 Sealed container with air

The sealed container with air assumes that the top surface of the paper volume is in contact with surrounding air. The container is considered small enough that we can neglect convective mass transfer of VOCs and assume only diffusive mass transfer in the surrounding air. The mass transfer in the surrounding air is therefore given by:
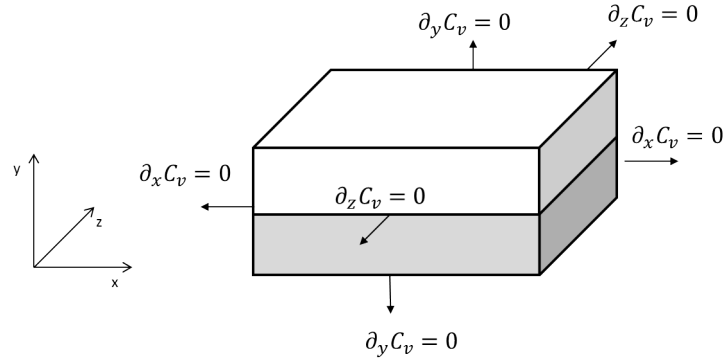
Figure 6.2: Sealed container with air

$$\partial_t C_v^{air} = -D_{air}\partial_{\mathbf{x}}.\partial_{\mathbf{x}}C_v^{air} \tag{6.12}$$

where D_{air} is the VOC ordinary molecular diffusion coefficient and C_v^{air} is the VOC concentration in the surrounding air.

Between the paper domain and the air domain we set the following conditions based on Figure 4.6 from Chapter 4, Section 4.4.6:

$$-D_{air}\partial_y C_{v,surface}^{air} = -D_{ve}\partial_y C_{v,surface}^{paper} \tag{6.13}$$

and:

$$C_{v,surface}^{air} = C_{v,surface}^{paper} \tag{6.14}$$

where $C_{v,surface}^{air}$ and $C_{v,surface}^{paper}$ are the VOC concentrations at the paper-air interface on the air side and paper side respectively.

The container, like the sealed fitted container, is assumed to be made of a material through which mass transfer does not occur and so at the borders Equation 6.11 applies. This is shown in Figure 6.2.

For this scenario, we assume that the initial concentration of VOC in the surrounding air is zero.

6.4.3 Paper volume on shelf

For the paper volume on a shelf, we assume that the shelf is the size of the base of the paper volume. The top and front plane are exposed to the surrounding air. At the boundaries, we describe the flux normal to the surfaces exposed to the surrounding air as:

$$\mathbf{N}_{v,surface}^{air}.\mathbf{n} = k_c\Delta C_v \tag{6.15}$$

where k_c is the mass transfer coefficient and ΔC_v is the concentration difference between the surface and the bulk concentration.

$$N_{A,y,surface}^{air} = k_c\left(C_{A,bulk}^{air} - C_{A,surface}^{air}\right) = N_{A,y,surface}^{paper}$$

$$\partial_y C_v = 0$$

$$\begin{aligned} N_{A,z,surface}^{air} \\ = k_c\left(C_{A,bulk}^{air} - C_{A,surface}^{air}\right) \\ = N_{A,z,surface}^{paper} \end{aligned}$$

$$\partial_x C_v = 0$$

$$\partial_x C_v = 0$$

$$\partial_y C_v = 0$$
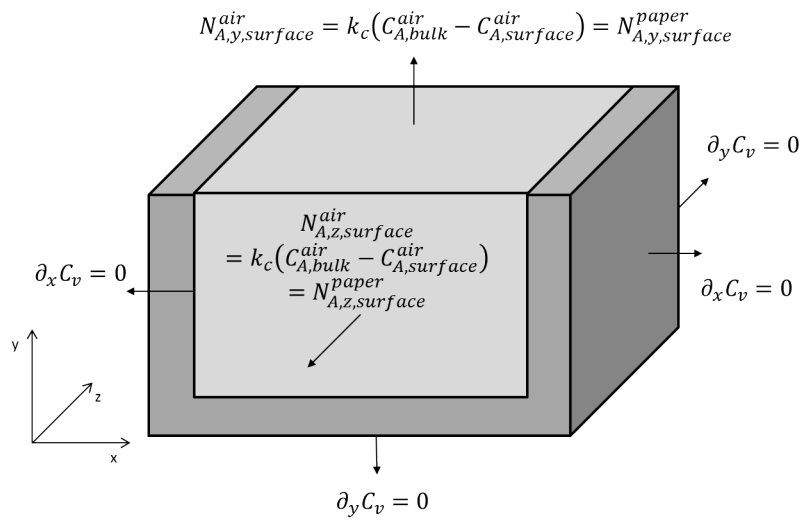
Figure 6.3: Paper volume on shelf
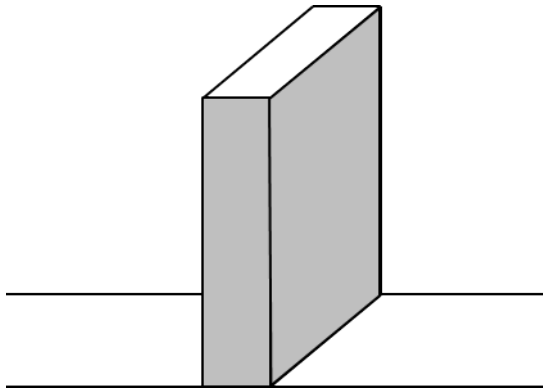
Figure 6.4: Book on a shelf

We make a further assumption that the room is large enough and conditioned so that the bulk VOC concentration is always zero.

It is also assumed that the base is a material through which mass transfer does not occur and so Equation 6.11 applies. This is shown in Figure 6.3.

6.4.3.1   Book on a shelf

An extension of the paper volume on a shelf is the book on a shelf, shown in Figure 6.4. To simulate a book, we assume that the front and back covers and the spine are made of a material through which mass transfer does not occur. Due to this, the difference between the book on a shelf and the paper volume on a shelf is that the front plane is no longer exposed to the surrounding air and Equation 6.11 applies again.
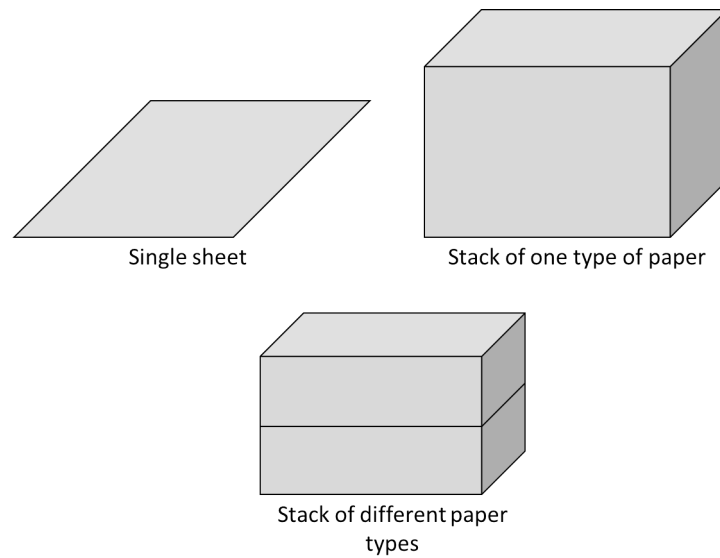
Figure 6.5: Different paper volumes for modelling

Sample	Sheet thickness (m)
A	0.000142
B	0.000098
C	0.000108
D	0.000168

Table 6.3: Sheet thickness

6.4.4 Paper volume configurations

In addition to the four paper types, there are different configurations of paper volumes we will invest-igate: a single sheet of paper, a stack of paper, two stacks of different paper types next to each other and a book. The book configuration was shown in Section 6.4.3.1 and in Figure 6.4. The others are shown in Figure 6.5. By investigating a stack of paper and a single sheet, we can see if the benefit of storing a single sheet is significant, even when tightly sealed. Having the different paper types next to one another in stack, we are able to explore how one paper will affect the other.

The dimensions for the paper volumes are based on an example soft-back book. The width of the paper is 0.198m and the length is 0.13m. The stack height is 0.044m and the single sheet heights are shown in Table 6.3. For the book, the height becomes 0.198m, and the width is 0.044m.

6.5 Simulation results

We now go through the results of the various computational simulations. We will go through the different scenarios to check the validity of the model predictions from a qualitative standpoint. As such, for our initial simulations, we are interested in the trends shown and whether they are reasonable.

The first simulations we run are at normal room conditions (23°C and 50% relative humidity). Then we will run the simulations for the sealed fitted container under lower temperature and relative humidity conditions (14°C and 40% relative humidity). After this, we will explore the sensitivity of the other parameters found in the model as well as the mass transfer coefficients between the paper and bulk air. We then have simulations to investigate what happens when the VOC is removed periodically from the sealed container. These are followed by simulations where we look at the consequences of storing paper samples next to one another. Finally, we will run simulations based on applicable literature.

As the paper volume degrades, the value of DP decreases. In general, however, the degradation rate is not uniform in space: the volume degrades faster in some regions and slower in others. Consequently, as pointed out before, DP is a function of both time and space coordinates:

$$DP = DP(\mathbf{x}, t) \tag{6.16}$$

Most of the figures below refer to the time at which $DP(\mathbf{x}, t)$ reaches for the first time the value of 250 within the volume. Because the degradation rate is non uniform, the DP will not be, in general, equal to 250 everywhere within a volume, but just in one point or region in the volume.

For briefness, in what follows, we will just say that these figures refer to the moment in which the paper has degraded to a DP of 250, even though this expression is not very accurate.

6.5.1 Sealed fitted container

In the sealed fitted container, the spatial profiles are uniform. This is because the initial spatial profiles are uniform, and when VOCs are produced, they are unable to escape the paper volume through diffusion due to the no flux boundary conditions and so no concentration gradient occurs. As the profiles are uniform, it does not matter whether we consider a single sheet or a stack.

For Sample C, the VOC concentration is zero throughout the paper volume through time as the alkaline reserve is never fully consumed over the lifetime of the paper. The alkaline reserve concentration is shown in Figure 6.6. The figure shows how over the lifetime of the paper, the alkaline reserve is barely depleted, going down to 1606.8 mol/m^3 and so the VOC (acetic acid) generation has no effect on the degradation rate as it is all neutralised.

The other three samples all have upward curves for VOC gas phase concentration change with time shown in Figure 6.7. In Table 6.4, we have the initial VOC generation rates for each sample based on their initial DP and pH, with normal room conditions for calculating k_{DP}. As we can see it goes in order of acidity with Sample B generating VOCs the fastest and Sample D the slowest.

Sample A has the fastest VOC gas phase concentration increase, reaching 0.0047 mol/m^3 in 470 years. Sample A has a faster increase than Sample B due to the adsorption coefficient K_v; this means that more of the VOCs produced by Sample B stay in the adsorbed phase. Sample D has the slowest VOC gas phase concentration increase and the largest initial DP, but reaches a higher VOC concentration value by the end of its lifetime (0.0051 mol/m^3 in 618 years).
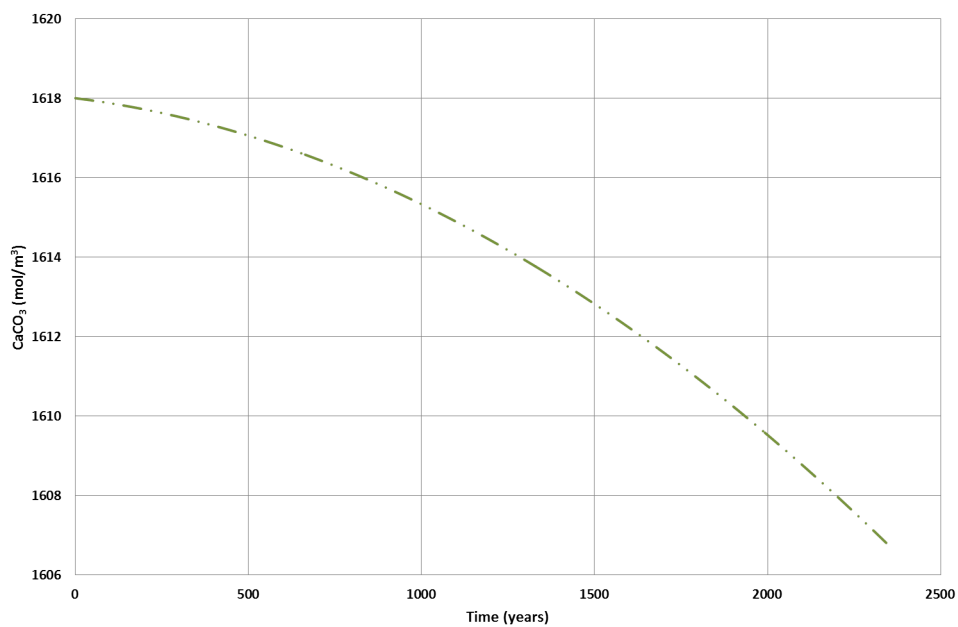
Figure 6.6: Alkaline reserve concentration change with time for Sample C in a sealed container

Sample	Initial r_v (mol/m^2.year)
A	8.4E-09
B	1.3E-08
C	1.5E-09
D	2.3E-09

Table 6.4: Initial VOC generation rates
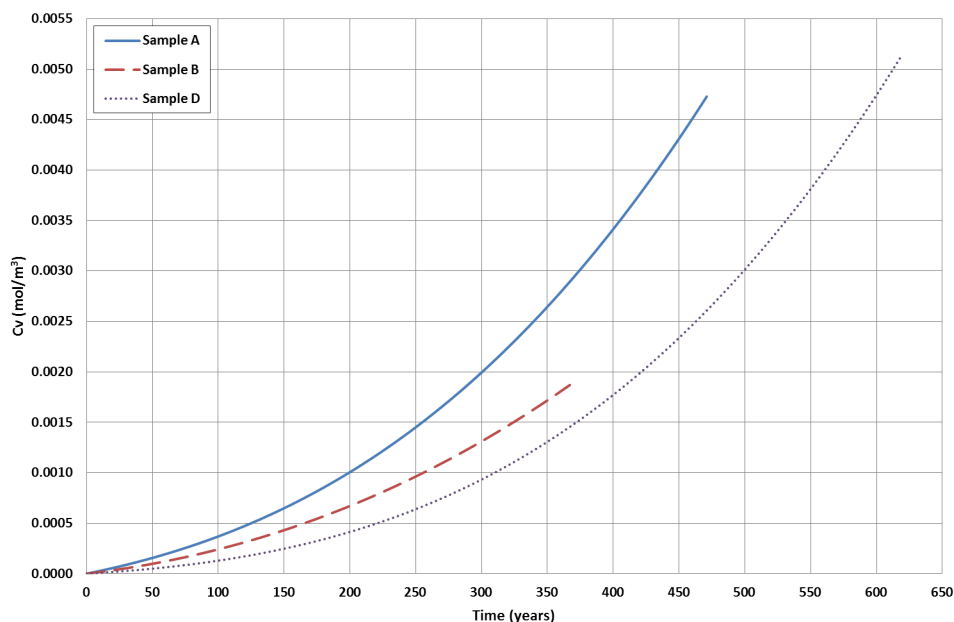
Figure 6.7: VOC gas phase concentrations change with time in a sealed container

The acidity changes with time for samples A, B and D are shown in Figure 6.8. Sample B reaches the highest hydrogen ion concentration as it starts with a significantly higher initial concentration. This sample's higher adsorption coefficient K_v compared to samples A and D also means a larger portion of the VOC present in the paper is in the adsorbed phase. Sample D has the greatest change in acidity. This is because when the hydrogen ion concentration is low, a greater portion of the VOC in the adsorbed phase will dissociate than if the hydrogen ion concentration was higher.

Figure 6.9 shows the acidity change for samples A, B and D on a pH scale. Both Sample A and D end at approximately pH 5. The general trend of increasing acidity with time agrees with accelerated ageing experiments from the literature [Shahani et al., 1989, Carter et al., 2000, Bulow et al., 2000].

The DP change with time for the four samples is shown in Figure 6.10 with the DP's y-axis minimum set at 250. The samples degrade in order of acidity. Sample C takes the longest to degrade, 2345 years, as it is the least acidic and the alkaline reserve neutralises the VOCs. As the VOC concentration for Sample C is always zero, the acidity is constant and so is k_{DP}. The degradation rate for Sample C can therefore be expressed by Equation 2.12 from Chapter 2:

$$\frac{1}{DP(\mathbf{x}, t)} - \frac{1}{DP(\mathbf{x}, 0)} = k_{DP}(\mathbf{x})t \qquad (6.17)$$

Sample B is the fastest to degrade, 367 years, as it is the most acidic sample. Sample A degrades in 471 years and Sample D degrades in 618 years.

We now compare the main model simulation results with the NAC model results. Figure 6.11 shows the VOC gas phase concentrations change with time. For samples A, B and D, the VOC gas phase concentration reaches the same as the main model, but in a longer time.
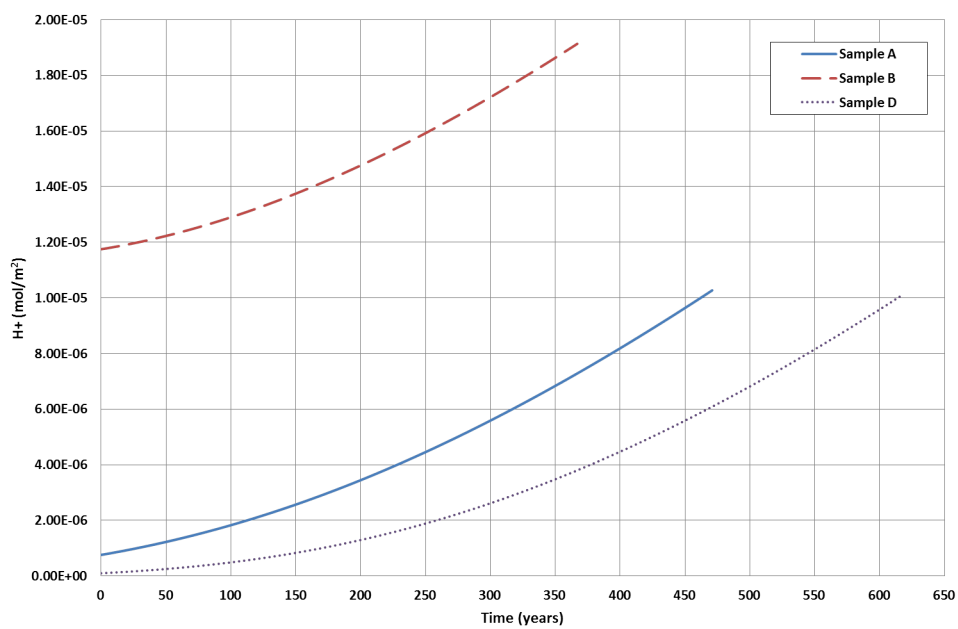
Figure 6.8: Acidity change with time in a sealed container
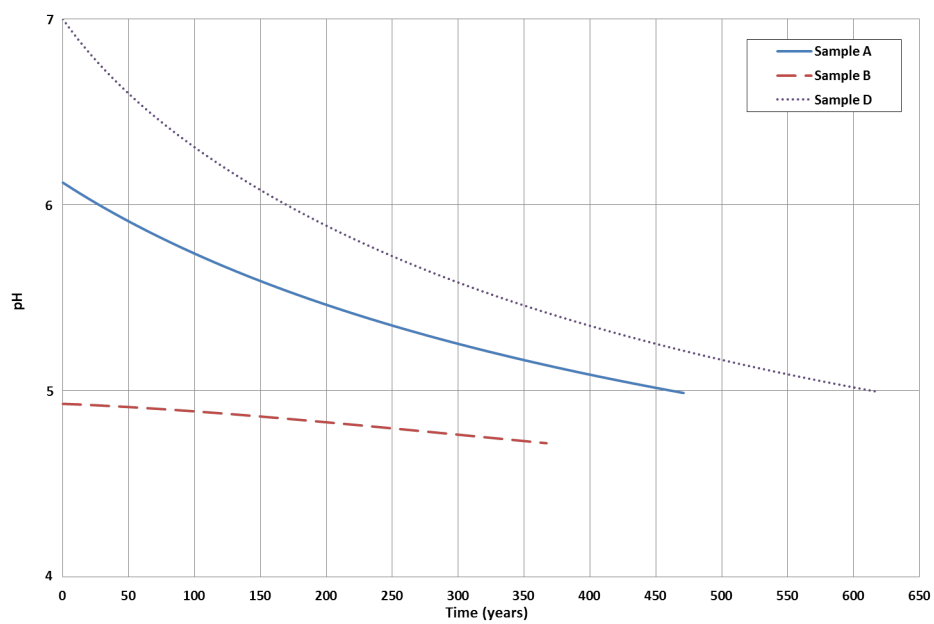
Figure 6.9: pH change with time in a sealed container
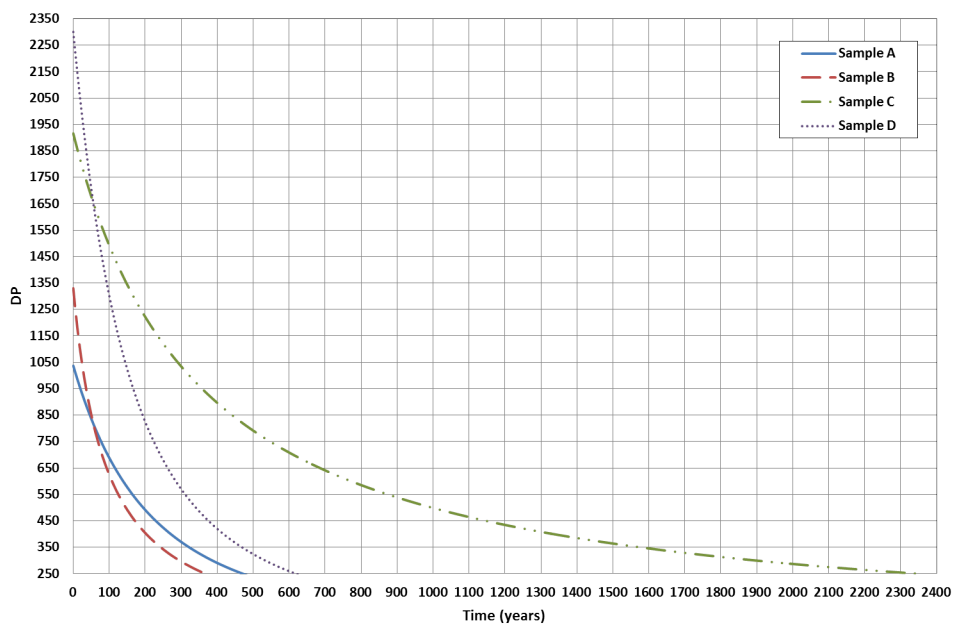
Figure 6.10: DP change with time in a sealed container
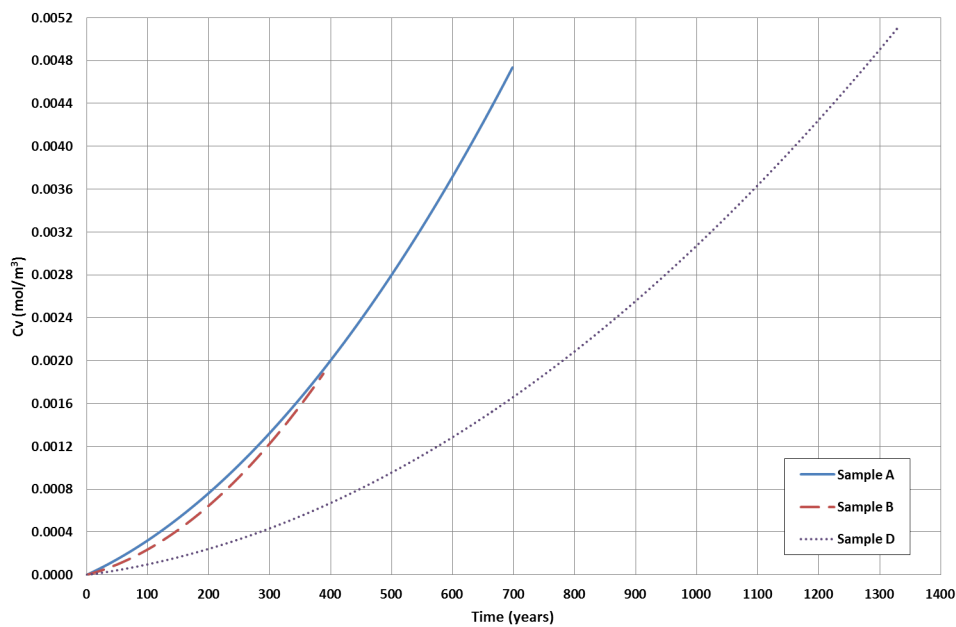
Figure 6.11: NAC model VOC gas phase concentrations change with time
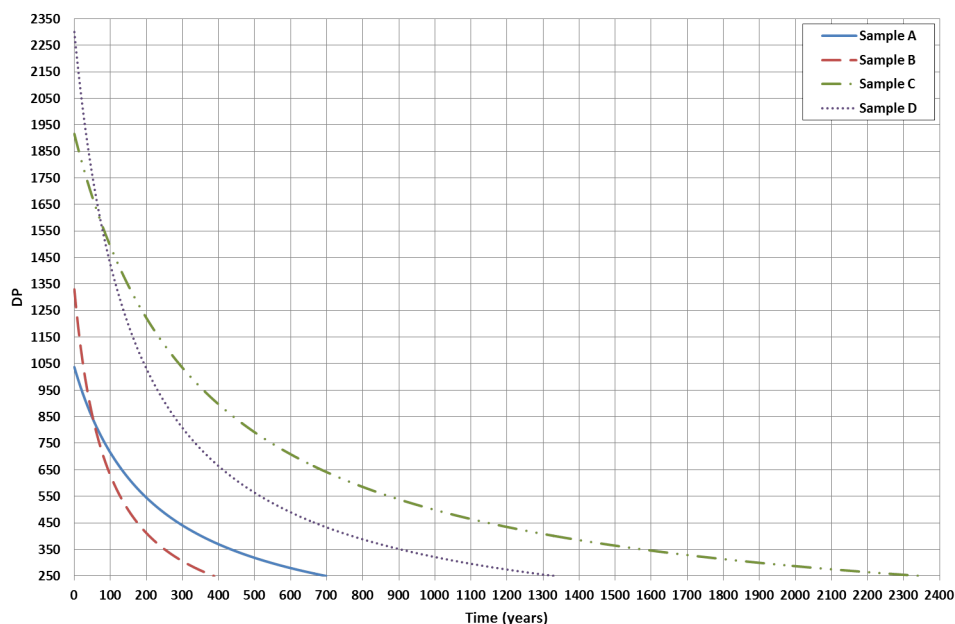
Figure 6.12: NAC model DP change with time

Figure 6.12 shows the DP change with time. Sample C takes the same time to degrade as for both models the acidity does not change. The samples still degrade in order of acidity but all take longer to degrade. This is because k_{DP} is a constant for the NAC model, whereas k_{DP} increases in the main model (except for Sample C).

Comparing the two models shows the potential problem of not considering the effect of VOCs. Sample A shows a 32% decrease in degradation time compared to the NAC model, Sample B shows a 5.2% decrease and Sample D shows a 54% decrease. The most acidic sample, Sample B, is the least affected by VOC's presence as the change in acidity has less effect on k_{DP}. The less acidic samples with no alkaline reserve are worst affected.

6.5.2 Sealed container with air

Before we ran the simulations for the sealed container with air, we had to decide the dimensions of the container. The width and length are the same as the paper's volume. The height of the container is set at 30 cm as it is a reasonable height for a small storage container. The diffusion coefficient D_{air} from Equation 6.12 is approximately 390 m^2/year, which is converted from the literature value of 0.1235 cm^2/s [Lugg, 1968]. With this example, the concentration profiles will be uniform across the length and width, but expected to differ across the height of the paper sample.
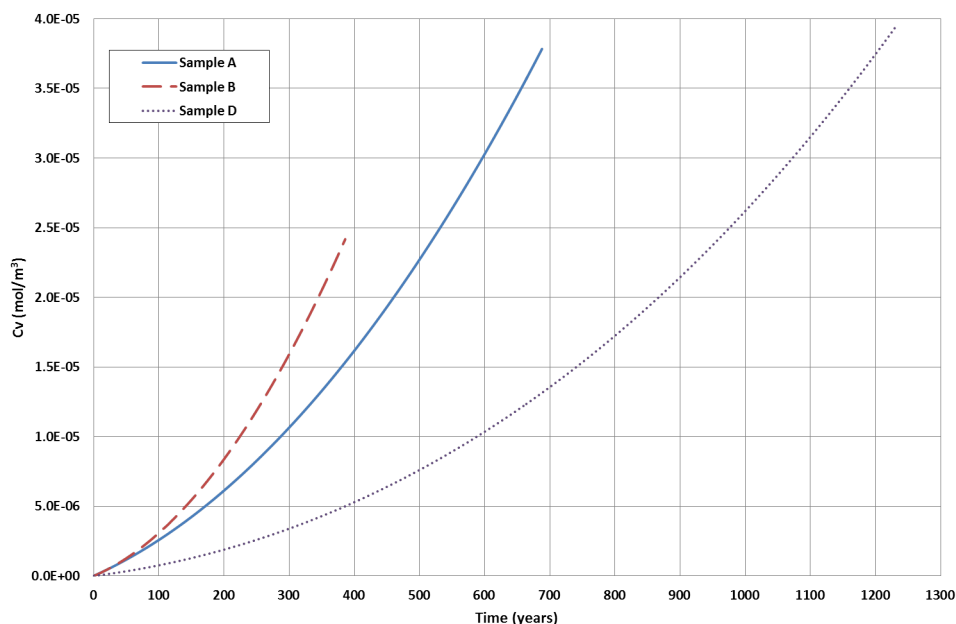
Figure 6.13: VOC gas phase concentrations change with time in a single sheet of paper in a sealed container with air

6.5.2.1 Single sheet

The single sheet is too thin for any noticeable differences in the concentrations spatially. For Sample C, any VOC generated in the adsorbed phase is instantaneously neutralised by the alkaline reserve as it was for the sealed fitted container. As a result, the alkaline reserve concentration with time for Sample C is the same as for the sealed fitted container and its degradation is also the same as before.

The VOC gas phase concentration change with time for samples A, B and D are shown in Figure 6.13. The VOC gas phase concentrations are all dramatically lower than for the sealed fitted container. Sample A reaches 3.8E-05 mol/m^3, Sample B reaches the lowest with 2.4E-05 mol/m^3 and Sample D reaches the highest with 3.9E-05 mol/m^3. This is expected as now there is a volume of air for the VOC to diffuse into and only a sheet of paper in the volume producing VOCs.

Figure 6.14 shows the pH change with time. With lower VOC concentrations, we have smaller pH changes. Using the pH scale, we can see that Sample D has the most significant change from its initial pH.

Sample A degrades in 688 years, a 1.3% decrease in degradation time compared to the NAC model results. Sample B, which has the smallest change in pH, degrades in 386 years, a 0.3% decrease. Sample D degrades in 1230 years, a 7.6% decrease. The smaller pH changes mean the degradation times are longer than the sealed container. We therefore can see that the more significant the change in pH a sample has, the greater the percentage change it has on the degradation time.
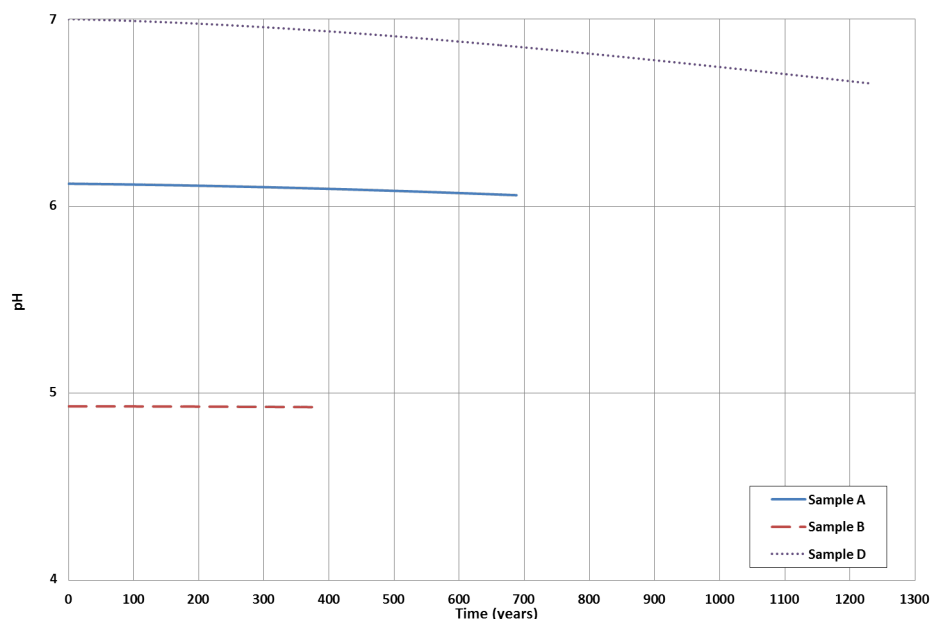
Figure 6.14: pH change with time in a single sheet of paper in a sealed container with air

6.5.2.2 Stack

Like the single sheet, the stack has no noticeable difference in the concentrations spatially. This is as the container volume is small and limited, and diffusion fast, resulting in the VOC concentration across the whole container volume being virtually uniform. Sample C degrades as before. Figure 6.15 shows the VOC gas phase concentration change with time. The concentrations are higher than the single sheet as there is now more paper in the container of the same volume, but lower than the sealed fitted container. Sample A reaches 0.0035 mol/m^3, Sample B reaches the lowest with 0.0016 mol/m^3 and Sample D reaches the highest with 0.0036 mol/m^3

The pH change with time is shown in Figure 6.16. The pH change is close to the sealed fitted container, but slightly lower. As a result, the degradation times are closer to the sealed fitted container than the single sheet in the container with air. Sample A degrades in 491 years, a 30% decrease from the NAC model, Sample B degrades in 268 years, a 4.7% decrease, and Sample D degrades in 659 years, a 50% decrease.

Having paper stored in a container with air can therefore extend the life of paper, with virtually no difference in the concentrations spatially. The more air in the container, the more the life of the paper is extended. Having paper stored in containers with air would result in a larger amount of space being needed to store the paper. If the container was large it is unlikely that we could only consider diffusion for mass transfer and would need to take convective mass transfer into account.

Accelerated ageing experiments by Shahani et al. [Shahani et al., 1989] compares the degradation of sheets to stacks in an oven. The VOCs can escape the paper volume to the rest of the oven and so is like our sealed container with air. The experiments show that the stack degrades faster than the
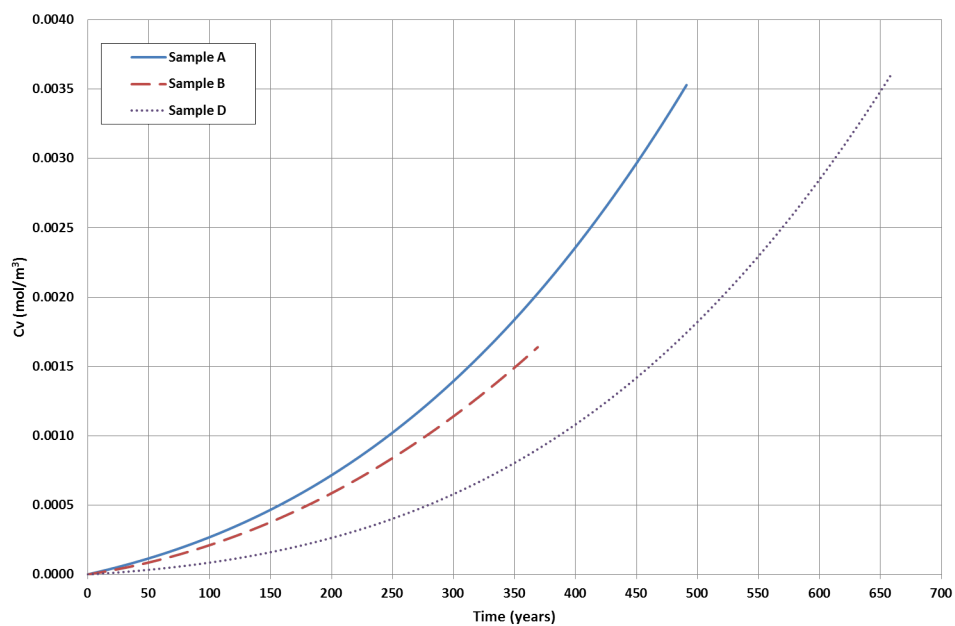
Figure 6.15: VOC gas phase concentrations change with time in a stack of paper in a sealed container with air
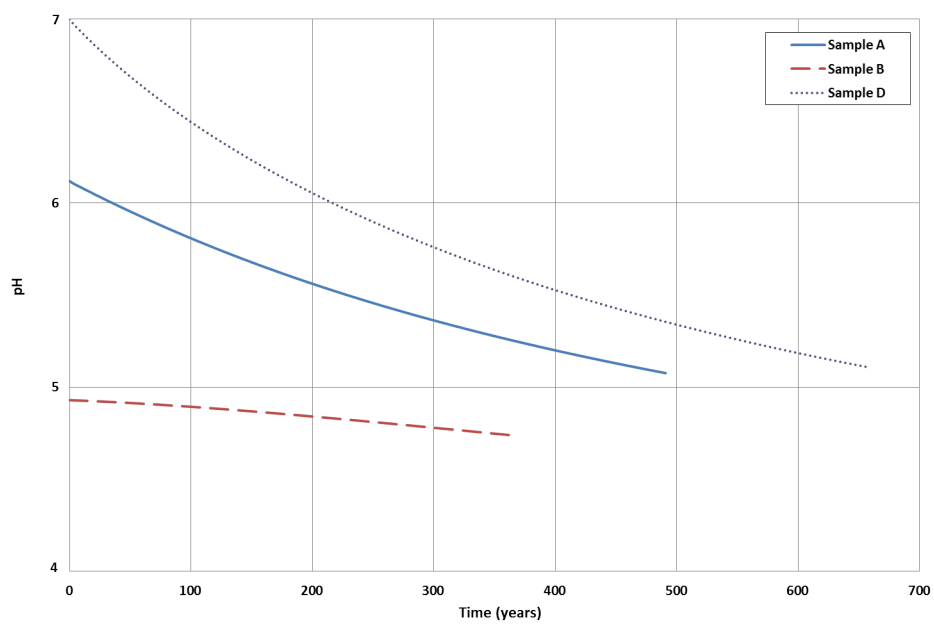
Figure 6.16: pH change with time in a stack of paper in a sealed container with air

sheet, which our model shows as well.

6.5.3   Paper volume on shelf

For modelling paper volume on a shelf, we first need a value for the mass transfer coefficient k_c used in the boundary conditions. The mass transfer coefficient was found from the Sherwood number, which was calculated using the empirical correlation given in Chapter 3, Equations 3.21 and 3.22. Rearranging the Sherwood number, the mass transfer coefficient is given by:

$$k_c = \frac{D_{air} Sh}{L} \tag{6.18}$$

where D_{air} is the diffusivity coefficient of the VOC in air, L is the characteristic length of the paper volume and Sh is the Sherwood number. For the sheet and stack of paper, L is 0.198 m, and for the book L is 0.044 m.

A velocity of 0.1 m/s was assumed as a reasonable velocity within the range expected in standard rooms [Uhde et al., 1998]. Using this velocity, the Reynolds number is below 200000 and so we assume laminar flow. This gave a k_c of approximately 50500 m/s for the sheet and stack and 107000 m/s for the book. This value shall be explored further later in the chapter.

For all volumes considered on a shelf, Sample C degrades as before with no change in degradation time or differences spatially due to the alkaline reserve and so we discuss samples A, B and D.

6.5.3.1   Single sheet

We first examine a single sheet on a shelf. The single sheet again shows no noticeable differences in the concentrations spatially. As the sheet is so thin, the VOCs generated by the paper easily escape to the surrounding air and so VOC concentration during the degradation is always negligible. Resultingly, the acidity of the samples does not change from the initial values and the degradation times are the same as the NAC model.

6.5.3.2   Stack

For the stack, the concentration profiles are not uniform spatially at the end of the degradation time. The VOC gas phase concentration is largest away from the exposed surfaces. Figure 6.17 shows how the VOC gas phase concentration changes with height, from the middle of the top sheet to the middle of the bottom sheet when each sample has reached a DP of 250 at a point within the volume. The top sheet VOC gas phase concentration is virtually zero as the VOCs escape to the surrounding air. The concentration difference between the top and bottom sheet becomes more pronounced as time goes on as more VOCs are produced. The concentrations are significantly lower than those reached for the sealed fitted container. Sample A reaches 4.9E-05 mol/m^3, Sample B reaches 9.4E-05 mol/m^3, and Sample D reaches 2.17E-05 mol/m^3.
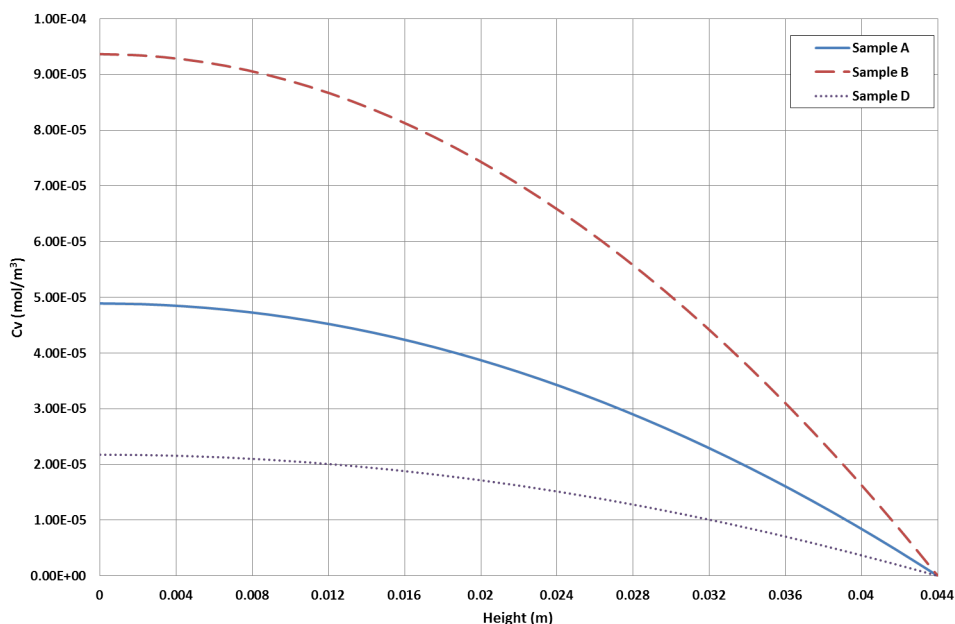
Figure 6.17: VOC gas phase concentrations change with height for a stack on a shelf for samples when degraded

Sample B has a higher VOC gas phase concentration at the bottom of the volume than Sample A as the majority of the VOCs leave the system and so Sample B's higher VOC generation means the sample has more VOC in both the adsorbed and gas phase. Figure 6.18 shows the VOC gas phase concentration change with time at the bottom of the stack in the middle of the sheet. Within 10 years, Sample B's VOC gas phase concentration overtakes that of Sample A.

Figure 6.19 shows how the pH changes with height. At the exposed surfaces of the paper volume, the pH remains the same as the initial pH as the VOC concentrations there are virtually zero. As we go away from the exposed surfaces, the pH decreases as the VOC concentration increases. The pH change through the stack (and through time) is very small as the VOC concentration building up in the stack is low because the majority of the VOC escapes into the surrounding air.

Accelerated ageing experiments by Carter et al. and Bulow et al. [Carter et al., 2000, Bulow et al., 2000] show a similar, though more pronounced, trend where the acidity through the stack at the end of the experiment is highest away from the exposed planes, and also show how the acidity increases within the stack through time.

Figure 6.20 shows the DP changes with height at the end of the each sample's degradation time. The DP is lowest away from the exposed planes as the VOC concentration is higher and the pH is lower, increasing the degradation rate. As such, the DP is lowest at the bottom of the stack. Sample D shows the largest difference between the top and bottom, with top having a DP of 266.3 and the bottom having a DP of 250. The difference is largest for Sample D as the sample takes longer to degrade, allowing more time for the building VOC concentration gradient to effect the local degradation rate. Table 6.5 shows the k_{DP} values for the top and bottom of each sample when they have reached a DP
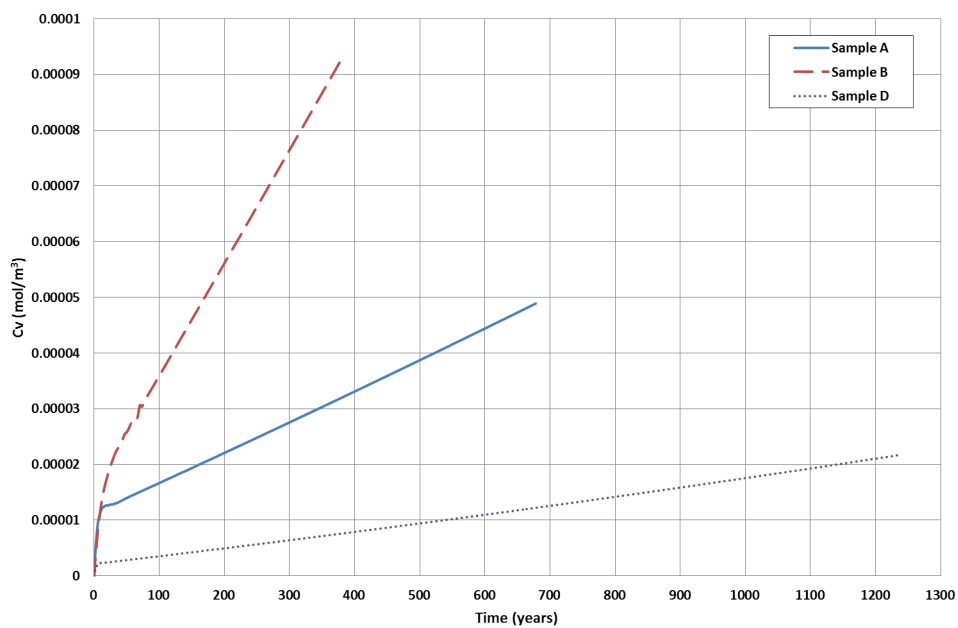
Figure 6.18: VOC gas phase concentrations change with time at the bottom of each sample for a stack on a shelf
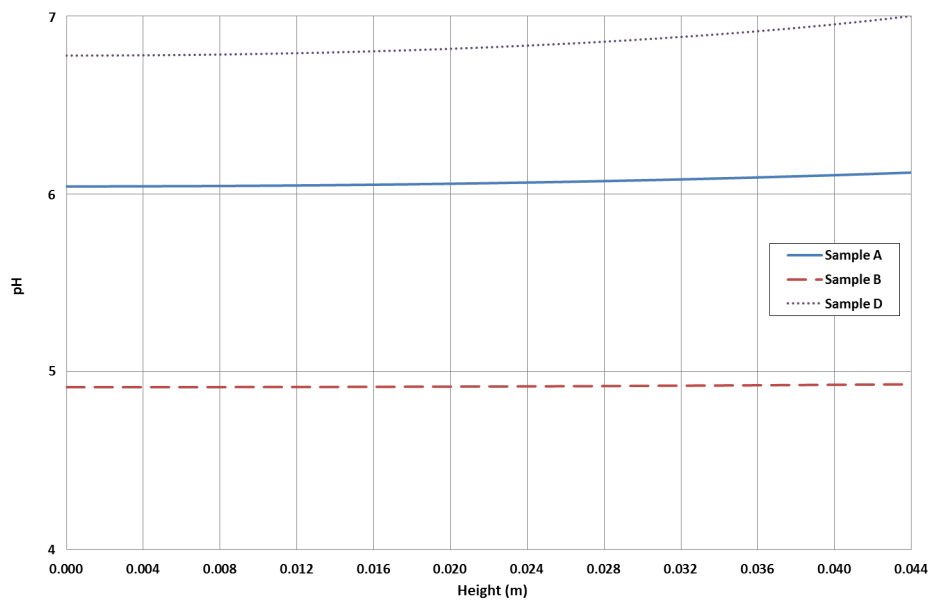
Figure 6.19: pH change with height for a stack on a shelf for samples when degraded

Sample	Top	Bottom
A	4.36E-06	4.55E-06
B	8.41E-06	8.49E-06
D	2.68E-06	3.03E-06

Table 6.5: Final k_{DP} values for samples at the top and bottom of the stack
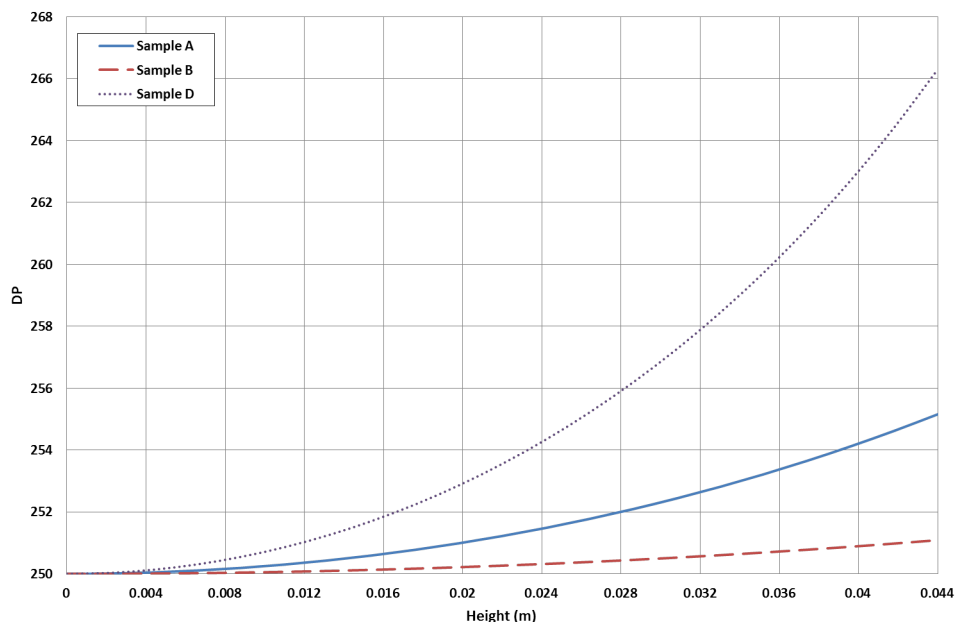
Figure 6.20: DP change with height for a stack on a shelf for samples when degraded

of 250. From this table we can see that Sample D has the largest difference in k_{DP} between the top and bottom of the stack.

Figure 6.21 shows the DP profile for the front of the bottom page of Sample D. From this we can see that the majority of the page has the same DP and the variation all happens close to the exposed plane.

The samples' worst degraded parts of the paper volume reach a DP of 250 quicker than the sheet or NAC model. Sample A degrades in 679 years, a 2.6% decrease from the NAC model, Sample B degrades in 385 years, a 0.5% decrease, and Sample D degrades in 1240 years, a 6.8% decrease.

6.5.3.3 Book

Like the stack, the book concentration profiles are not uniform spatially at the end of the degradation time. VOCs can only escape the book through the top plane, and so the VOC profile is not uniform in height, but is with length and width. The exposed top plane is smaller than the stack top plane and the VOC build up at the bottom of the book is larger than the stack. Figure 6.22 shows the VOC gas phase concentration change with height when each sample has reached a DP of 250 at a point
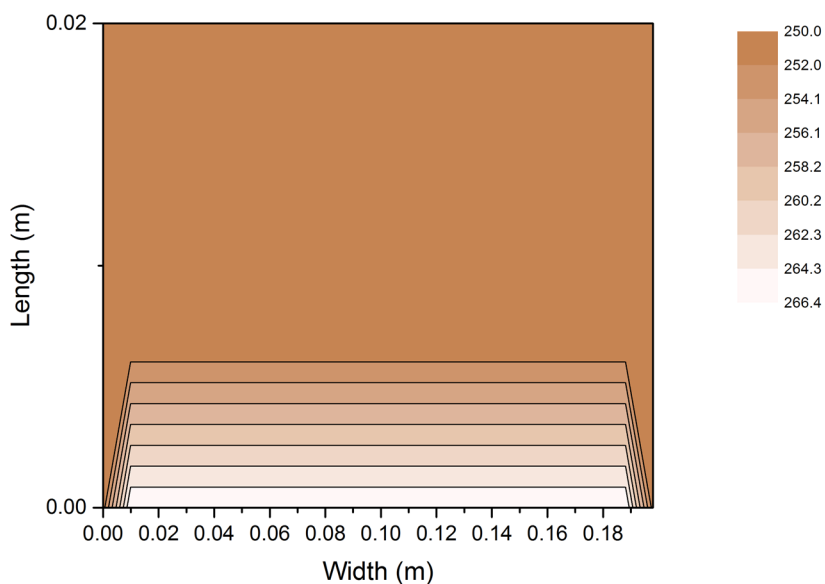
Figure 6.21: DP profile for the front of the bottom sheet of Sample D

within the volume. At the top, the VOC gas phase concentration is virtually zero as the VOCs escape to the surrounding air. Sample B has the largest VOC gas phase concentration at the bottom with 0.00121 mol/m^3 although Sample A is much closer to Sample B than for the stack on a shelf with a concentration of 0.00116 mol/m^3. Sample D has the smallest VOC gas phase concentration with 0.00070 mol/m^3.

As the VOC concentrations at the bottom are larger than at the top, the paper is more acidic at the bottom than at the top also. Figure 6.23 shows the pH change with height for each sample. The change is greater than that we see with the stack on a shelf, with both Sample A and D going lower than a pH of 6.

Figure 6.24 shows the DP change with height at the end of the each sample's degradation time. Sample D again shows the largest variation in DP with the top of the book having a DP of 387 and the bottom a DP of 250. Sample B still shows only a small variation in DP. This is as the degradation time is much smaller that Sample D, and so the VOC concentration difference has less time to influence the degradation rate. Also the pH change is smaller for Sample B due to the sample's higher initial acidity.

The VOC gas phase concentration change with time at the bottom of the book is shown in Figure 6.25. As we can see, Sample A initially has a higher concentration than B as it acts like the sealed container, until 125 years when Sample B overtakes and they follow the trend of the stack on a shelf.

Figure 6.26 shows the pH change with time at the bottom of the book. The most significant change is by Sample D, which approaches the same pH of Sample A by the end of its life time. The book samples all degrade faster than the other shelf simulations but slower than the sealed fitted container and the stack in the sealed container with air. Sample A degrades in 538 years, a 23% decrease on the NAC model, Sample B degrades in 371 years, a 4.1% decrease and Sample D degrades in 802 years,
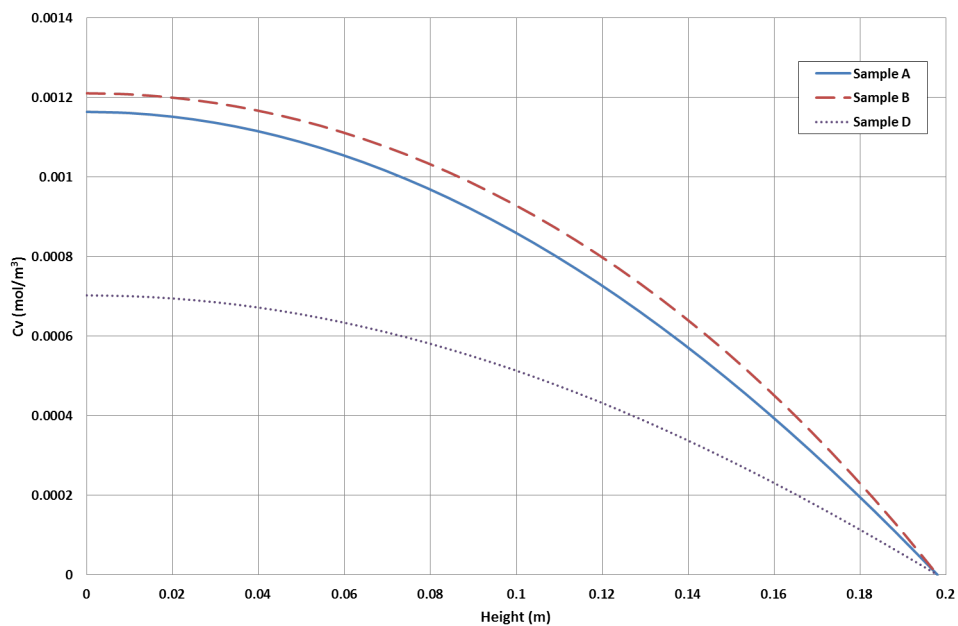
Figure 6.22: VOC gas phase concentrations change with height for a book on a shelf for samples when degraded
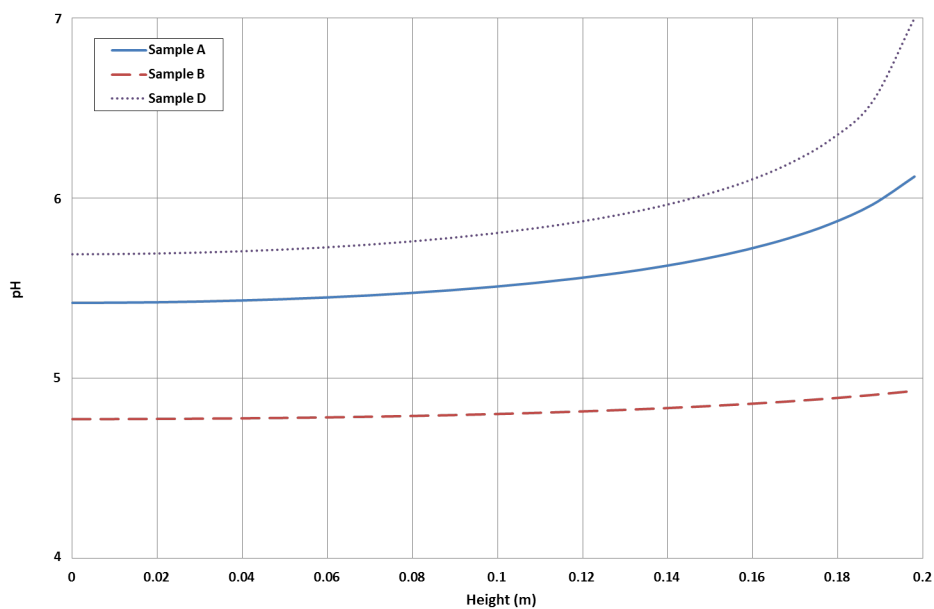
Figure 6.23: pH change with height for a book on a shelf for samples when degraded
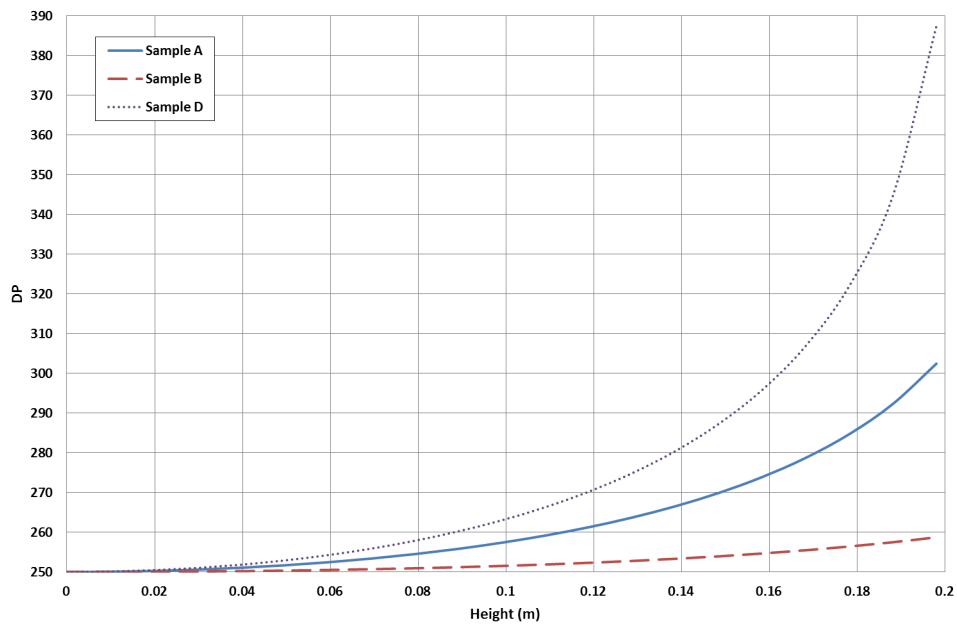
Figure 6.24: DP change with height for a book on a shelf for samples when degraded
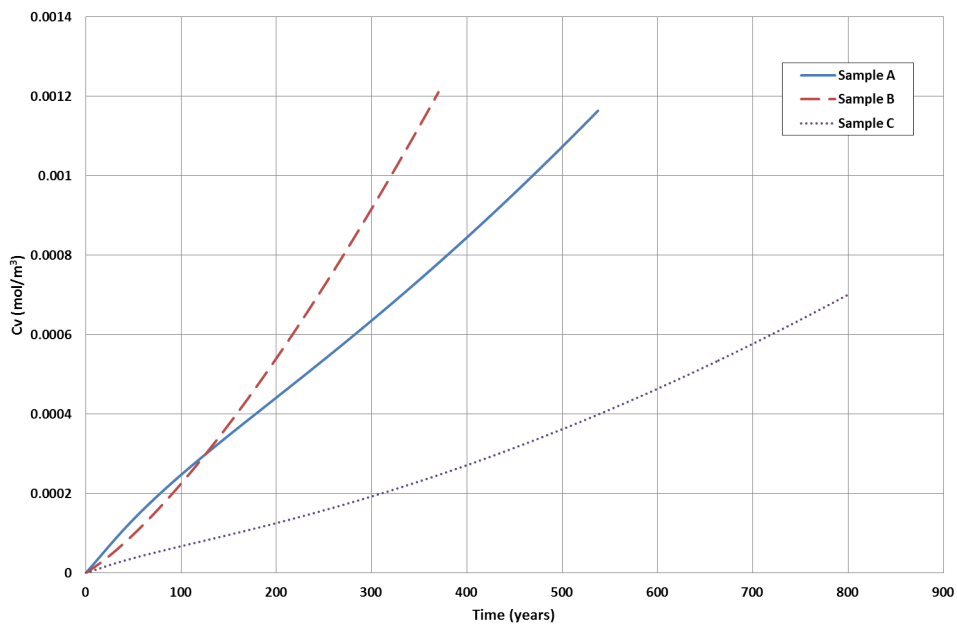
Figure 6.25: VOC gas phase concentrations change with time for a book on a shelf
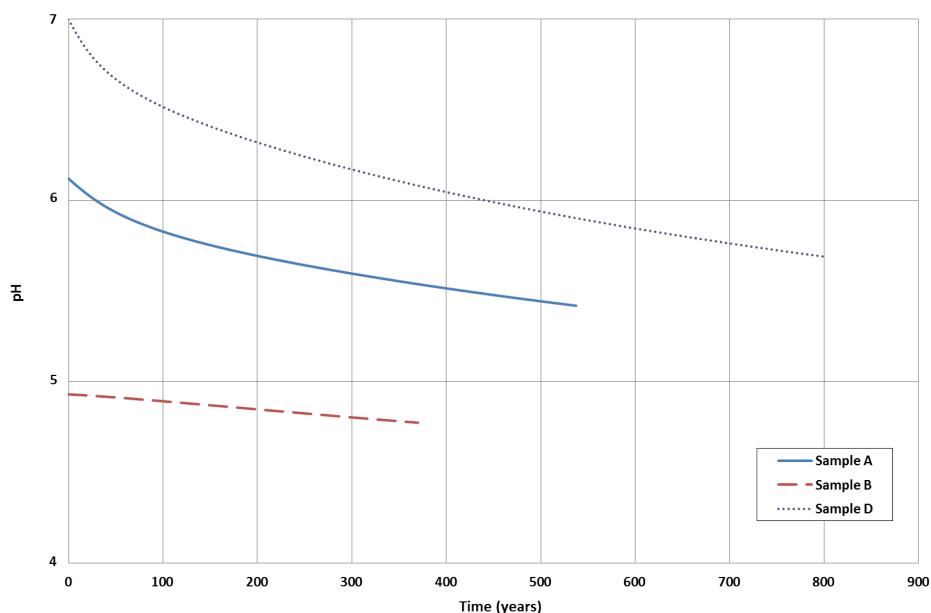
Figure 6.26: pH change with time for a book on a shelf

a 40% decrease. Although the book on a shelf does not degrade as fast as the sealed fitted container, it can have a noticeable degradation gradient across a page. Papers with low acidity and no alkaline reserve would be most at risk of this gradient appearing.

6.5.3.4 NR model comparison to Main model

The NR model is used for the book on the shelf scenario. For VOCs to be present in the book, they must come from the surrounding air. When the concentration in the surrounding air is very low, there is no noticeable effect on the degradation of the book as the VOCs do not significantly change the acidity.

When the VOC gas phase concentration is high enough, for example 0.001 mol/m^3, then the degradation of the book is affected. However, this concentration value is significantly higher than that found typically for acetic acid in archives, where concentrations can be approximately 1E-09 mol/m^3 [Menart et al., 2011].

Figure 6.27 shows the VOC gas phase concentration change with height when Sample A has degraded to a DP of 250 using the NR model and the main model when the surrounding air has a bulk concentration of 0.001 mol/m^3. By the time the sample has fully degraded using the NR model, the VOC gas phase concentration is virtually uniform, but this uniform concentration is not reached instantly. Figure 6.28 shows how it changes with time at the bottom of the book. By the time the sample has fully degraded using the main model, the bottom of the page has a higher VOC gas phase concentration as VOCs have diffused in from outside the book and are produced in the book.
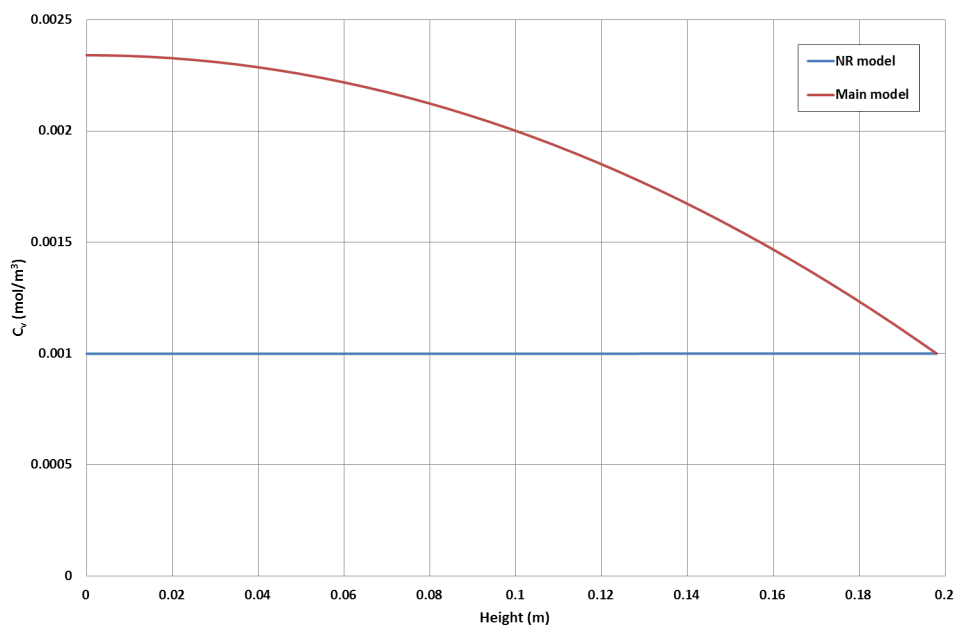
Figure 6.27: VOC gas phase concentration change with height for a book on a shelf when the sample has degraded to a DP of 250 for NR model comparison to main model
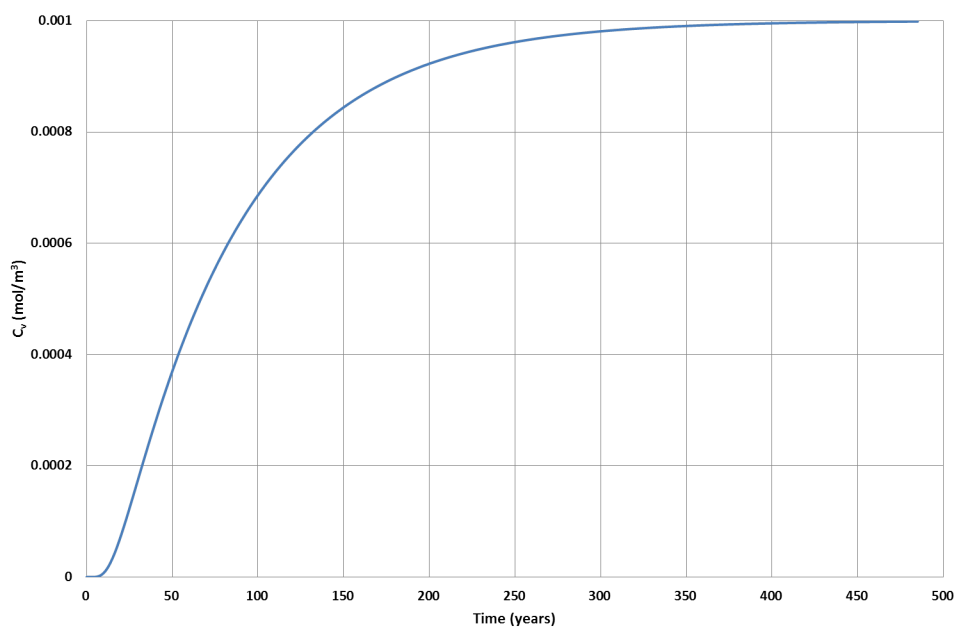
Figure 6.28: VOC gas phase concentration change with time at the bottom of a book for Sample A using the NR model
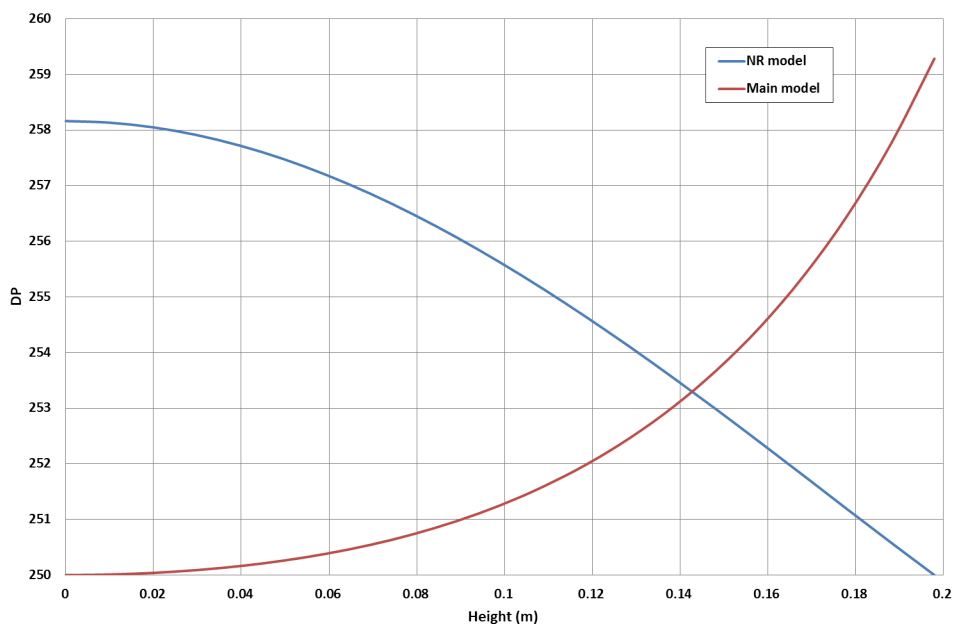
Figure 6.29: DP change with height for a book on a shelf for the NR model at 485 years and the main model at 463 years

Figure 6.29 shows the DP change with height when Sample A has degraded using the NR model and the main model. The NR model is more degraded at the top of the book because the VOC concentration is higher at the top until the concentration is virtually uniform. For the main model, the bottom is more degraded. The difference between the top and bottom in DP for the main model is less pronounced than when a surrounding air bulk concentration of zero is used. Figure 6.30 shows the DP change with time at the top and bottom of the book for the main model simulation. We can see that initially the top degrades faster as the VOCs diffusing in from outside the book are more significant than those produced by the book. After 288 years, the bottom degrades faster as the VOCs produced by the book are more significant than those diffusing in from outside the book. This, of course, assumes that the book is left on the shelf for over 450 years, which is very unlikely. However, in these simulations we aim to see if the trends predicted by the model are qualitatively reasonable. We are carrying out a qualitative validation of the model, and the trends do appear to be reasonable.

With the NR model, we can see how degradation can be affected by outside pollutants if they are the only significant factor. Using the main model we are able to include the effects of outside pollutants as well as those of the VOCs produced internally. By only considering the outside pollutants, the NR model predicts that Sample A degrades in 485 years, but considering the VOCs produced internally, the main model predicts that Sample A will degrade in 463 years.
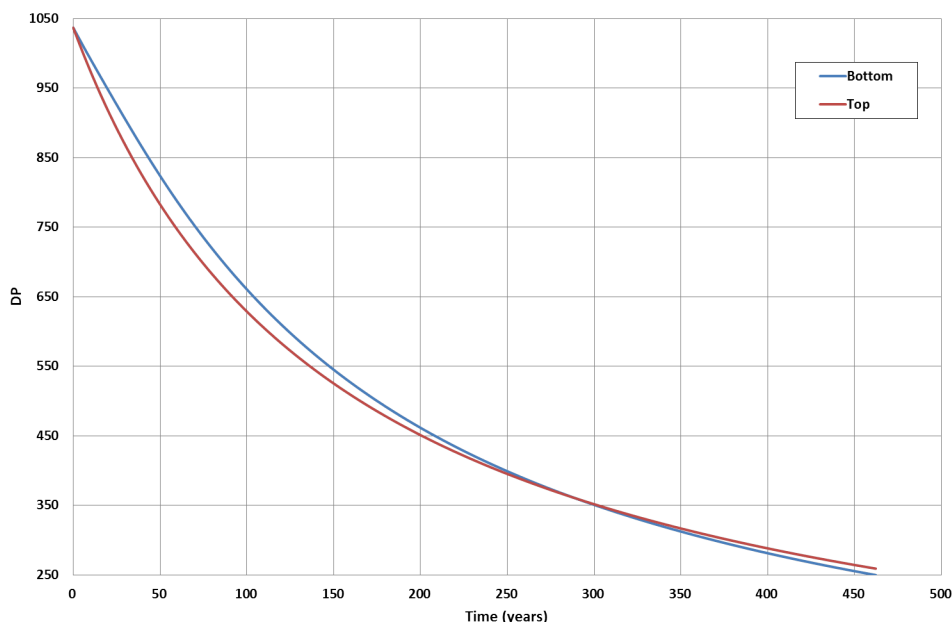
Figure 6.30: DP change with time for a book on a shelf for main model where bulk concentration is non zero

	Sample A	Sample B	Sample C	Sample D
NAC	697	387	2345	1331
Sealed fitted container	471 *(-32%)*	367 *(-5.2%)*	2345 *(0%)*	618 *(-54%)*
Sheet in container with air	688 *(-1.3%)*	386 *(-0.3%)*	2345 *(0%)*	1230 *(-7.6%)*
Stack in container with air	491 *(-30%)*	369 *(-4.7%)*	2345 *(0%)*	659 *(-50%)*
Sheet on shelf	697 *(0%)*	387 *(0%)*	2345 *(0%)*	1331 *(0%)*
Stack on shelf	679 *(-2.6%)*	385 *(-32%)*	2345 *(0%)*	1240 *(-32%)*
Book on shelf	538 *(-23%)*	371 *(-4.1%)*	2345 *(0%)*	802 *(-40%)*

Table 6.6: Summary of degradation time in years for each sample

6.5.4 Summary of normal room condition simulations

Table 6.6 gives a summary of the different scenarios for the normal room condition simulations. The table shows that the alkaline reserve protects Sample C in all the simulations; thus, Sample C always degrades in the same time. We can see that the sealed container is worse for samples without an alkaline reserve as the VOCs do no escape the paper and affect the acidity. The sheet on a shelf is the best system configuration as long as the surrounding air is free of any pollutants as the VOCs escape the whole paper volume, although this arrangement is not very practical.

Figure 6.31 shows the VOC gas phase concentration plotted against DP for a point in the volume of Sample A. For the scenarios where the degradation is uniform, it does not matter which point we have chosen. For the non uniform scenarios, we chose the point where DP reaches 250 first within the volume, and so the change in DP reflects a change in time. This shows that one could not predict DP based only on VOC gas phase concentration, as the different scenarios give very different results.
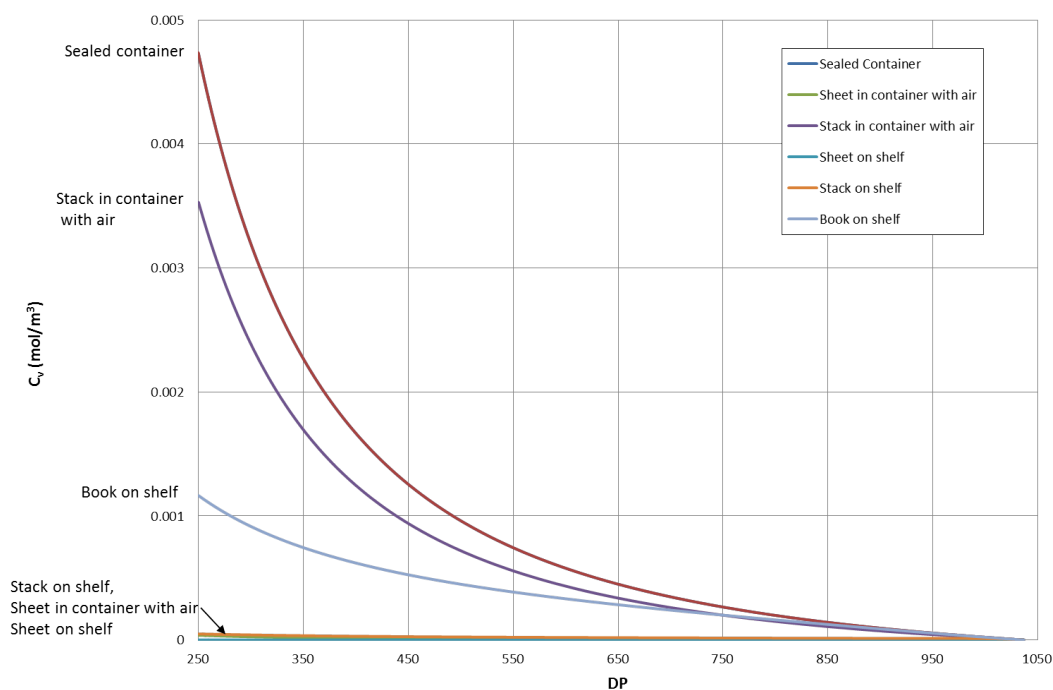
Figure 6.31: VOC gas phase concentration plotted against DP for Sample A

Figure 6.32 shows the VOC generation rate plotted against DP for Sample A. Like Figure 6.31, for the non uniform scenarios, we chose the point where DP reaches 250 first within the volume. The lower the DP, the more the generation rates for the scenarios differ from each other as the acidity difference between each scenario grows. The generation rate increases most during the sample's lifetime for the sealed fitted container as the VOCs increase the acidity in the sample most in this scenario. The rate increases least for the sheet on a shelf scenario as the acidity change is negligible during the sample's lifetime.

If we rearrange the VOC generation formula given in Equation 6.6, we get:

$$DP(\mathbf{x}, t) = 1 + \frac{2k_{DP}k_{vr}}{r_v(\mathbf{x}, t)} \tag{6.19}$$

This shows that, to predict the DP, we would need to measure or know the VOC generation rate, k_{vr} and k_{DP}. We can calculate k_{DP} using Equations 6.8 and 6.9. We do not currently know k_{vr}. For our simulations so far, we have assumed a k_{vr} of 1 as this falls within the expected range shown later in Section 6.5.6. For an accurate value of k_{vr}, experimentation is needed and we explore this in Chapter 7, Section 7.1.
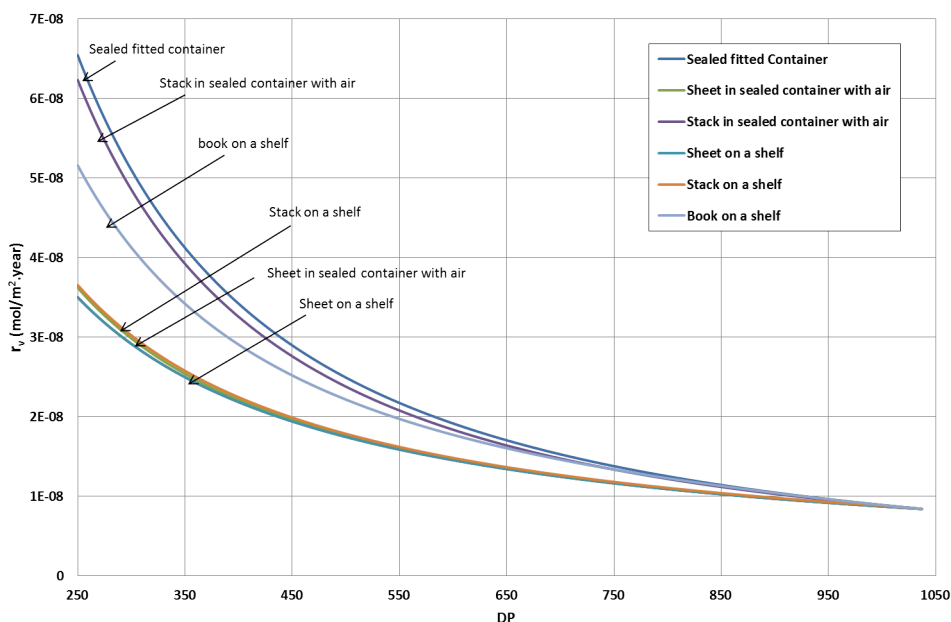
Figure 6.32: VOC generation rate plotted against DP for Sample A

6.5.5 Lower temperature and relative humidity conditions

The previous simulations assumed a normal room temperature and relative humidity. In Chapter 2, Section 2.6 we stated that, until recently, BS 5454:2000 was used as standard for the storage of archival documents.

For this simulation, we have the sealed fitted container scenario with a temperature of 14°C and relative humidity of 40%, the lowest values in the ranges given by BS 5454:2000. As we are using the sealed fitted container scenario, the concentration and degradation profiles are uniform across the volumes. The VOC gas phase concentration and acidity reaches the same values for the sealed fitted container at normal room conditions, but now all samples degrade in a much longer time. The longer degradation time is due to the constant a in Equation 6.8 for expressing k_{DP} now being smaller, meaning k_{DP} is lower. The same VOC gas phase concentration is reached as the VOC generation and degradation rate, which are linked to each other, have a linear relationship with k_{DP}.

The DP change with time is shown in Figure 6.33. Sample A degrades in 2240 years, a 376% increase on the normal room conditions for a sealed container, Sample B degrades in 1900 years, a 418% increase, Sample C degrades in 12153 years, a 418% increase and Sample D degrades in 3203 years, also a 418% increase. From this, the advantages of using the lower temperature and relative humidity are clear.

6.5.6 VOC reaction rate constant exploration

The reaction constant k_{vr} from Equation 6.6 was initially set to unity in the simulations; however, we now explore this value in more detail, including how a change in this value affects the degradation
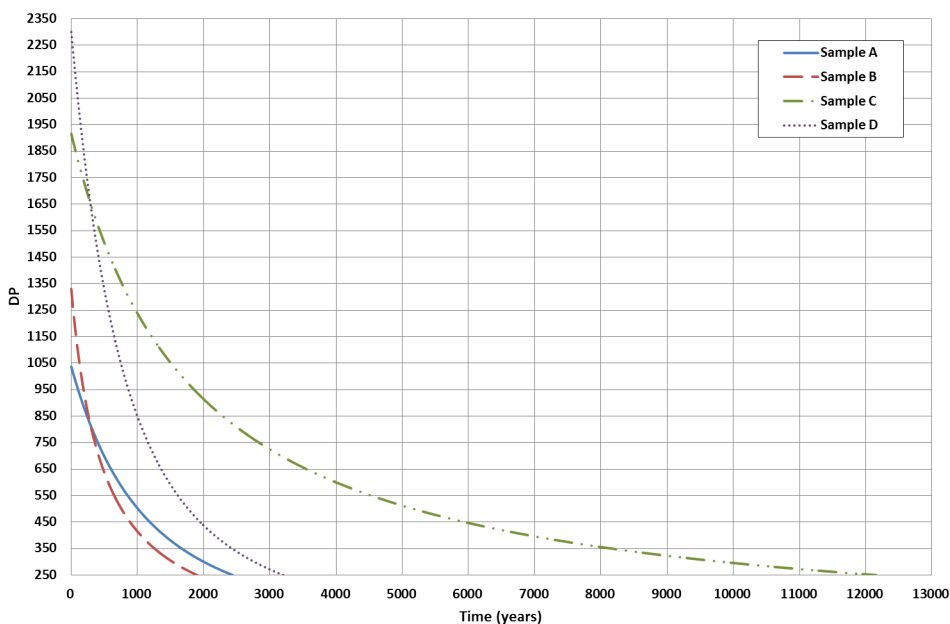
Figure 6.33: DP change with time for a sealed fitted container using BS 5454:2000 conditions

time for the sealed fitted container at room temperature. The sealed fitted container is chosen as this system is uniform.

6.5.6.1 Comparison to Ramalho et al. emission rates

Work by Ramalho et al. (2009) quantified emissions of VOCs from two model papers, Step2 and Step3, after sheets were aged in closed tubes for different periods of time. The Step2 sample had an approximate pH of 6.2 and Step3's pH was 5.1. The samples were conditioned at 23°C and 50% relative humidity before being placed in glass tubes in a dry oven at 100°C. After being degraded for a set period of time, the samples were removed from the oven and were reconditioned for 24 hours to 23°C and 50% relative humidity.

The VOC emissions were characterised using a Field Laboratory Emission Cell (FLEC) connected to tenax tubes for VOC capture, where experiments were performed in a climate controlled room set at 23°C and 50% relative humidity. A sampling time of 24 hours was used. The results for acetic acid are shown in Figure 6.34.

If we assume that the emission rate is directly related to the generation rate, we can estimate our reaction constant k_{vr}. We make this assumption as the FLEC set up can be compared to our single sheet on a shelf scenario. Clean air is continuously provided into the FLEC, providing a surrounding air VOC concentration of zero. Like our single sheet on a shelf, we assume all the acetic acid generated by the paper all escapes to the surrounding air and is captured by tenax tubes at the air outlets. Therefore, with this assumption, the emission rate is equivalent to the generation rate.

To use the emission rate to estimate k_{vr}, we need to convert it to the same units as the generation
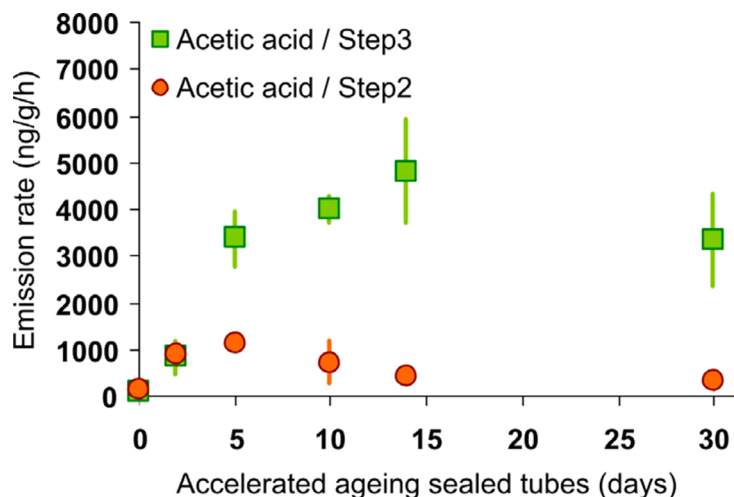
Figure 6.34: Emission rate of acetic acid [Ramalho et al., 2009]

Emission rate (ng/g/h)	Step2 k_{vr}	Step3 k_{vr}
1	15	8
10	150	81
100	1500	810
1000	15000	8100
5000	-	40500

Table 6.7: Estimate k_{vr} values

rate, $\dfrac{mol}{m^2 year}$. The mass of acid is converted to mols by dividing by the molar mass of acetic acid. The mass of paper is converted to surface area (m^2) by multiplying the mass and the average surface area by mass (m^2/g) of our samples (see Appendix, Section A.1). Finally, we convert the time scale, hours, to years.

We can now convert the emission rate to the generation rate r_v. To calculate k_{vr} from the generation rate, we rearrange Equation 6.6:

$$k_{vr} = \frac{r_v}{\alpha k_{DP}}; \quad \text{where} \quad \alpha = \frac{2}{DP - 1} \tag{6.20}$$

We estimate α by assuming a DP of 1430 (the average of our real paper samples) and k_{DP} is calculated using the sample's given pH, temperature and relative humidity values.

As the emission rates in Figure 6.34 cover a large range of values, k_{vr} was estimated for different magnitudes and are shown in Table 6.7.

The k_{vr} values predicted in Table 6.7 could be too high as the work by Ramalho et al. predicts emission rates which are not necessarily equivalent to production rates. The acetic acid (or another VOC) released could have been present in the adsorbed phase of the paper before the accelerated ageing, or produced during the accelerated ageing. As such, the emission rate is not due solely to the amount produced during the 24 hour sampling period, but also due to VOCs produced prior to the

sampling that were still in the adsorbed phase of the paper. To avoid this issue, paper would need to be placed under vacuum for a period of time before sampling, in an attempt to remove any VOCs already present in the paper. Another issue is that whilst the samples are being aged in glass tubes, the oxygen in the tube is depleted leading to a different degradation rate than if oxygen is present [Baranski, 2002].

With the predicted k_{vr} values, we now have an approximation for the range of variation, with values of the order of 1 to 10,000. We therefore use the lower value of 1 for k_{vr}, for the majority of our simulations, as a reasonable starting point. For more accurate evaluation of k_{vr}, we would need experimentation that can measure VOC generation for a known temperature, relative humidity, acidity of sample and DP. This will be explored further in Chapter 7, Section 7.1.

6.5.6.2 Small k_{vr}

We now examine having smaller values for k_{vr} than 1. First, we reduce k_{vr} to 0.1. For Sample C, the alkaline reserve is less depleted compared to when k_{vr} is 1, going down to 1616.9 mol/m^{2}and the sample degrades in the same time. The reserve is less depleted as less VOC is generated, meaning less of the reserve is needed to neutralise the VOC.

Samples A, B and D have much lower VOC concentrations compared to when k_{vr} is 1 and the values are of an order of magnitude lower. As a result, the acidity change is less and all samples degrade in a longer time. Sample A reaches a VOC gas phase concentration of 0.00021 mol/m^{3}and degrades in 620 years, a 32% increase. Sample B reaches a VOC gas phase concentration of 0.00044 mol/m^{3}and degrades in 384 years, a 4.6% increase. Sample D reaches a VOC gas phase concentration of 0.00051 mol/m^{3}and degrades in 926 years, a 50% increase.

Sample B shows the smallest increase to its degradation time as it is the most acidic and when additional acid is produced it has the least effect on the pH. Sample D conversely shows the largest increase in degradation time as it is the least acidic sample.

Reducing k_{vr} to 0.01 increases the degradation times even further. Sample C's alkaline reserve only goes down to 1617.9 mol/m^2.

The VOC concentrations are even smaller and so there is even less of an acidity change. Sample A reaches a VOC gas phase concentration of 4.7E-05 mol/m^{3}and degrades in 685 years, a 45% increase. Sample B reaches a VOC gas phase concentration of 1.9E-05 mol/m^{3}and degrades in 386 years, a 5.2% increase. Sample D reaches a VOC gas phase concentration of 5.1E-05 mol/m^{3}and degrades in 1209 years, a 96% increase.

Sample B again shows the smallest increase and emphasises how acidic paper gains the least from a small VOC generation rate.

6.5.6.3 Large k_{vr}

Now we explore what happens with k_{vr} values larger than 1. Increasing the k_{vr} to 10 causes Sample C's alkaline reserve to deplete more than before, down to 1505.9 mol/m^2 and so the sample still retains
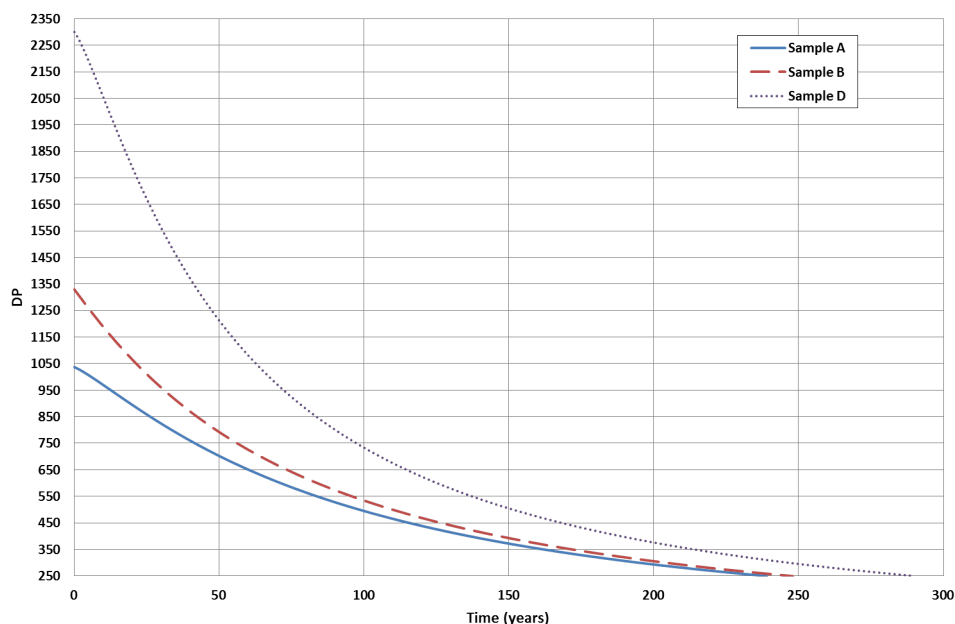
Figure 6.35: DP change with time with k_{vr} set to 100

the vast majority of its reserve.

The VOC gas phase concentration for samples A, B and D all increase and they are in a range an order of magnitude higher compared to when k_{vr} is 1. The samples all degrade faster as the VOC concentration causes an increase in acidity and degradation rate. Sample A reaches a VOC gas phase concentration of 0.047 mol/m^{3}and degrades in 332 years, a 30% decrease. Sample B reaches a VOC gas phase concentration of 0.019 mol/m^{3}and degrades in 315 years, a 14% decrease. Sample D reaches a VOC gas phase concentration of 0.051 mol/m^{3}and degrades in 412 years, a 33% decrease.

Sample B now shows the smallest decrease as the increase in VOC production does not increase the pH as dramatically as it does for the less acidic samples.

A k_{vr} of 100 depletes Sample C's alkaline reserve more, to 496.5 mol/m^2. Although the sample's alkaline reserve has been depleted significantly more, a large amount of the reserve is still present and so the sample degrades in the same time as before. For samples A, B and D, the VOC gas phase concentrations increase further and are in a range an order of magnitude higher than when the k_{vr} is 10. The samples all degrade in under 300 years and the DP change with time is shown in Figure 6.35.

Sample A reaches a VOC gas phase concentration of 0.47 mol/m^{3}and degrades in 239 years, a 49% decrease. Sample B reaches a VOC gas phase concentration of 0.19 mol/m^{3}and degrades in 248 years, a 32% decrease. Sample D reaches a VOC gas phase concentration of 0.51 mol/m^{3}and degrades in 290 years, a 53% decrease.

Sample A's degradation rate is now faster than Sample B as it quickly reaches a similar pH and so the initial DP becomes the deciding factor in which sample degrades first. The pH change with time is shown in Figure 6.36. Sample D has the largest percentage decrease as the acidity has increased the
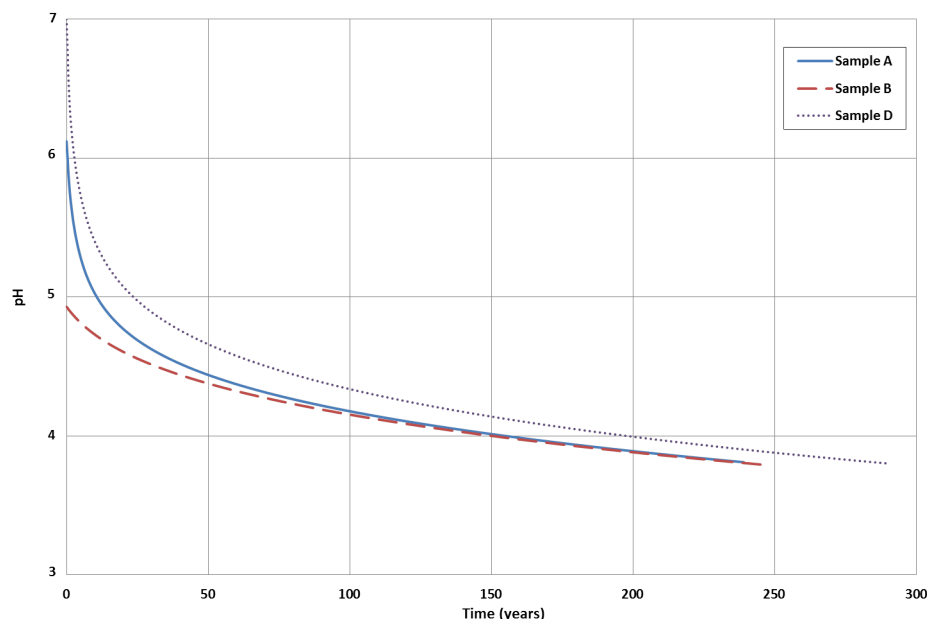
Figure 6.36: pH change with time with k_{vr} set to 100

most.

This sensitivity analysis shows the importance and worth for further investigation of k_{vr}. The simulations showed that generally, a sample with a high acidity is less affected than a sample with a low acidity and no alkaline reserve.

6.5.7 Diffusion and mass transfer coefficient sensitivity

To explore how the diffusion constant D_{ve} affects the degradation we increase and decrease its value by one order of magnitude.

The different mass transfer coefficients are calculated using different velocities for the Reynolds number. Velocities in the range 0.01-0.3 m/s are suggested as expected in standard rooms [Uhde et al., 1998]. We have used values from 3-0.001 m/s. As such, the Reynolds number was always laminar, and Equation 3.21 was used. In addition, mass transfer coefficients up to two orders of magnitude higher and lower were explored.

All the simulations for different effective diffusion coefficients and mass transfer coefficients used the book on a shelf scenario, although the stack on the shelf could also have been used. The results did not give any noticeable variation spatially or with time compared to the original values used for the effective diffusion coefficients or the mass transfer coefficient. This is as mass transfer through the gas phase of the paper volume is significantly faster than the generation in the adsorbed phase.

Experimentation where temperature was cycled supports our assumption of fast mass transfer [Strlic et al., 2009a]. In the experimentation carried out by Strlic et al., different paper samples were sealed

in containers with sensors. The containers were then put in temperature controlled ovens and the temperature was cycled between room temperature and 35°C. The response in the VOC gas phase concentration recorded by the sensors was almost instantaneous. The VOC concentration increased when the temperature was increased as a new equilibrium was found between the gas phase and adsorbed phase in the paper. The VOC concentration then decreased when the temperature was returned down to room temperature. If mass transfer was not fast, then the gas phase concentration change recorded by the sensors would not have been almost instantaneous.

6.5.8 Adsorption coefficient sensitivity

With a high adsorption coefficient K_v, we expect more of the VOC present to be in the adsorbed phase and so increase the paper's acidity more. In Figure 6.37, we show the DP change with height in a book for Sample A when it has reached a DP of 250 for the normal K_v, and when we increase and decrease its value by one order of magnitude. The simulations used the book on a shelf scenario.

When K_v is high, the DP change with height has a larger variation than normal. This is because when one reaches the top of the book, the VOC gas phase concentration drops rapidly towards zero at all times and so near the top of the page the adsorbed phase concentration rapidly drops towards zero. At the bottom of the page, the VOC gas phase concentration is at its highest, and a larger portion of the total VOC concentration is in the adsorbed phase concentration due to the high K_v. With more VOC in the adsorbed phase, the acidity change is more and the sample degrades quicker than the 538 years with the normal K_v, now degrading in 474 years.

Conversely, when K_v is low, the DP change with height has a smaller variation. As less VOC is in the adsorbed phase, the acidity change is less in the paper and the sample degrades in a longer time, 662 years.

6.5.9 Sensitivity analysis on the porosity, surface area, initial pH, initial DP and alkaline reserve

To see if the porosity and unit surface area values have a significant effect on the degradation, we use values one order of magnitude higher and lower than that used for the earlier simulations. The simulations used the book on a shelf scenario. The porosity and surface area changes had no noticeable effect.

Our previous simulations have shown how the pH of the sample is important. We now run simulations with Sample A having a range of pH to help illustrate further the effect of acidity. Figure 6.38 shows the DP change with time for Sample A using a pH of 3, 4, 5 and 7. The simulations used the sealed fitted container scenario and so the profiles are uniform spatially.

With a pH of 3, Sample A degrades in 125 years, a 73% decrease on the degradation time with the sample's pH of 6.12. With a pH of 4, it degrades in 216 years, a 54% decrease; with a pH of 5, it degrades in 353, a 25% decrease, and with a pH of 7 it degrades in 508 years, a 7.9% increase. As we
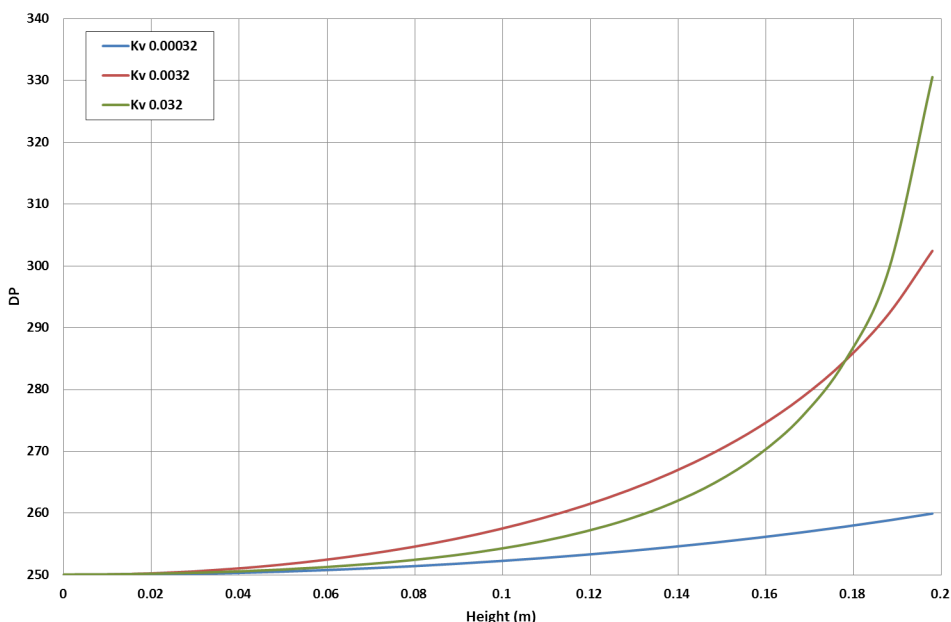
Figure 6.37: DP change with height for Sample A using different adsorption coefficients

can see, Sample A with a pH of 3 reduces the degradation time the most. The increase in degradation time when the pH is 7 is not a large percentage as the hydrogen concentration difference between pH 7 and 6.12 is smaller than a pH of 6.12 and pH of 5.

To show how the initial DP affects the degradation rate, we run simulations with Sample A having an initial DP of 2500, 2000 and 1500. The simulations used the sealed fitted container scenario. Figure 6.39 shows the DP change with time. For all three initial DPs the degradation time is longer than with the sample's initial DP of 1037. With an initial DP of 2500, the degradation time is 571 years, a 21% increase, with a DP of 2000 the degradation time is 552 years, a 18% increase and with a DP of 1500 the degradation time is 522 years, an 11% increase. As expected, the higher the DP, the longer the degradation time.

For all the previous simulations involving Sample C, the alkaline reserve was never fully depleted. We now explore how Sample C degrades with different starting alkaline reserves. Figure 6.40 shows the DP change with time for different initial alkaline reserve percentages, where we have used the sealed fitted container scenario. With an initial reserve of 1%, the sample still degrades in 2345 years as the reserve is not fully consumed during the life time of the sample. If we reduce the initial reserve to 0.1%, the reserve is consumed (in 1947 years) and so the sample degrades in 2067 years as the VOC concentration is then allowed to build up and affect the paper's acidity. If the reserve is 0.01%, the reserve is consumed in 449 years and the sample degrades in 927 years. The discontinuities seen in the figure for 0.01% and 0.1% are expected as they are when alkaline reserve is consumed and the degradation rate after is negatively affected by the VOC concentration increase. Finally, if no reserve was present, the sample would degrade in 618 years. This shows that with even a small reserve of 1%, the effect of increased acidity on a sample can be stopped and so prolong the life of paper.
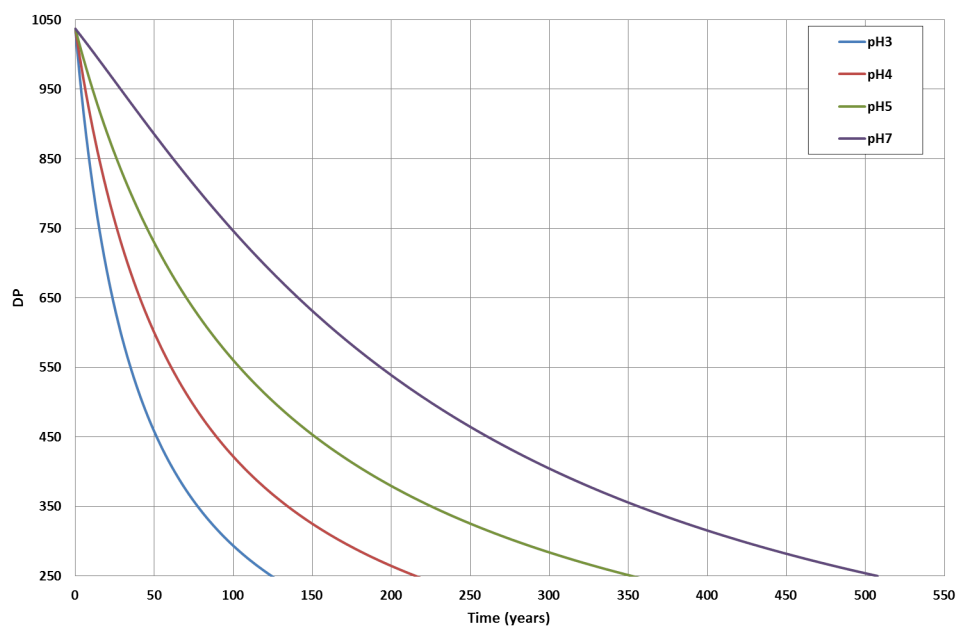
Figure 6.38: DP change with time for Sample A using different starting pH values
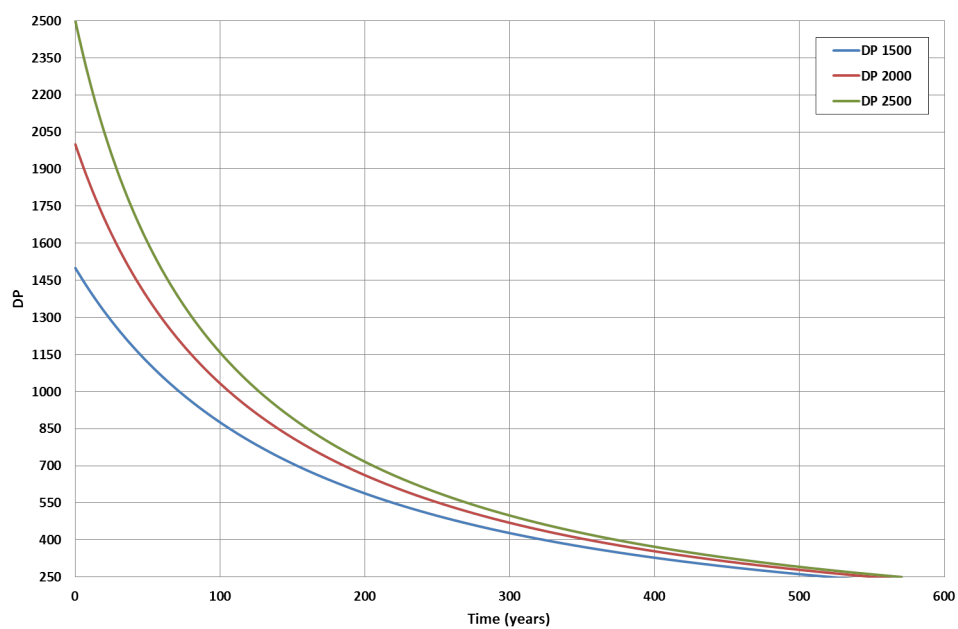
Figure 6.39: DP change with time for Sample A with different initial DP values
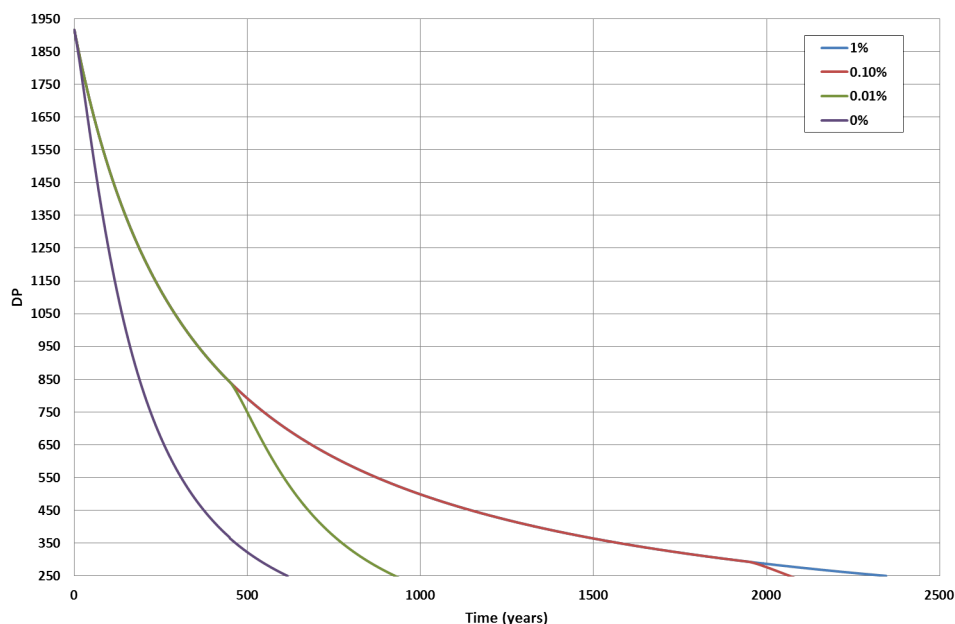
Figure 6.40: DP change with time for different alkaline reserve amounts

6.5.10 Periodic VOC removal

In the following simulation, the VOC is entirely removed every 5 years and therefore, its concentration drops to zero every 5 years. The scenario used for the simulation is the sealed fitted container. This could represent the container being opened and used every 5 years, or a deliberate act of flushing the VOCs from the container as part of a conservation routine. Figure 6.41 shows the VOC gas phase concentration change with time for Sample A. The concentration reaches much smaller values than for the normal sealed fitted container with no VOC removal as it only has 5 years to build up at a time. The general increase is due to the DP decreasing with time, which makes the VOC production rate increase.

The DP change with time for Sample A is shown in Figure 6.42. The sample takes 685 years to degrade, a 45% increase compared to no periodic removal. This shows the potential for extending the life of paper without frequent conservation intervention.

6.5.11 Paper samples stored together

To test what happens when two different samples are stored together, a simulation was run with Sample A next to Sample C in a sealed fitted container. The samples were arranged as shown in Figure 6.43.

Sample C degrades as before due to its alkaline reserve. Sample A degrades uniformly with width and length, but not with height. This is because the VOC diffuses across to Sample C, where it is neutralised due to the alkaline reserve, and so a concentration gradient appears. The bottom of Sample
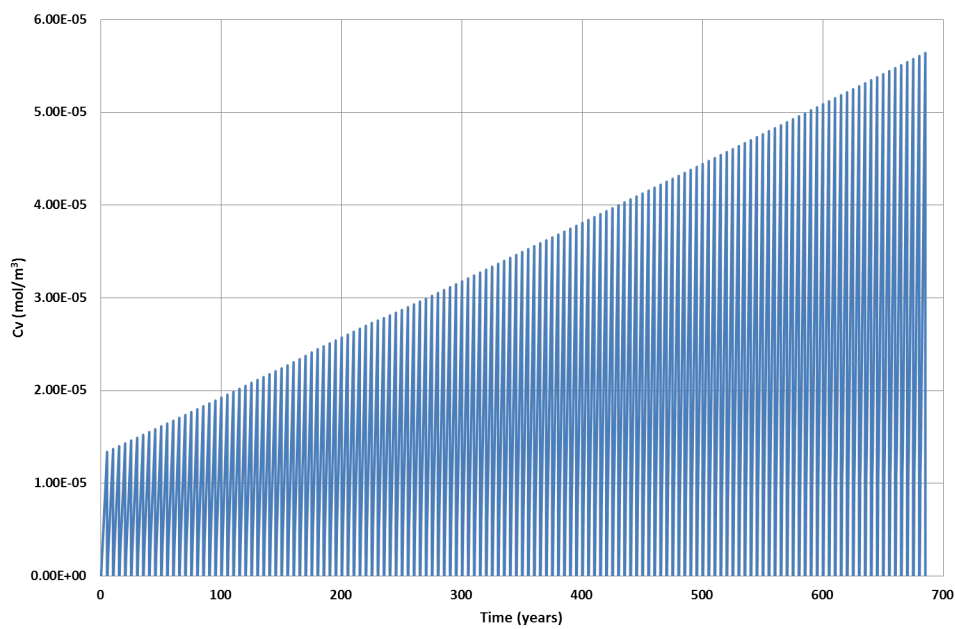
Figure 6.41: VOC gas phase concentration change with time for Sample A with VOC gas phase concentration set to zero every 5 years
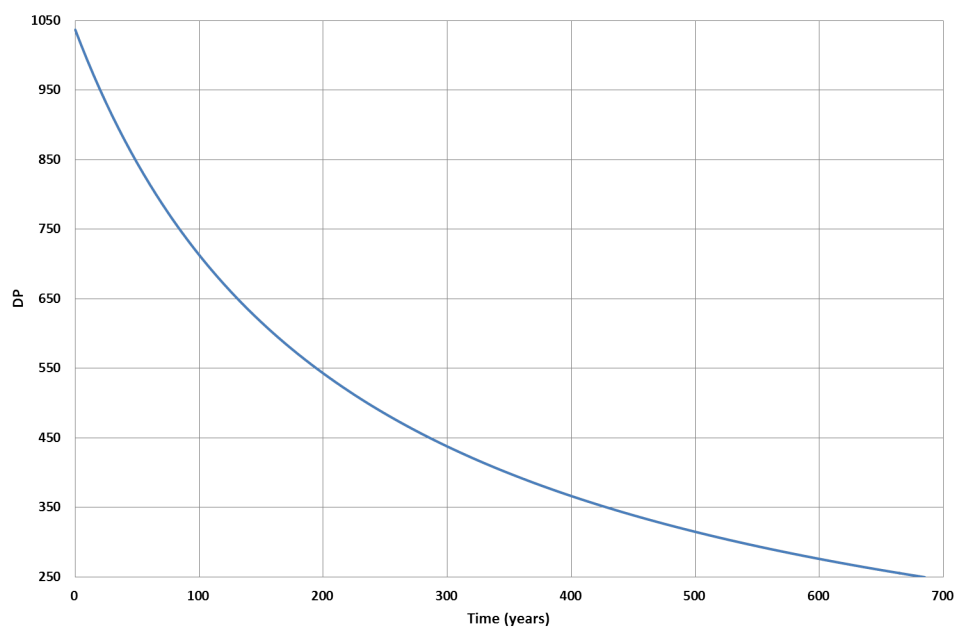
Figure 6.42: DP change with time for Sample A with VOC gas phase concentration set to zero every 5 years
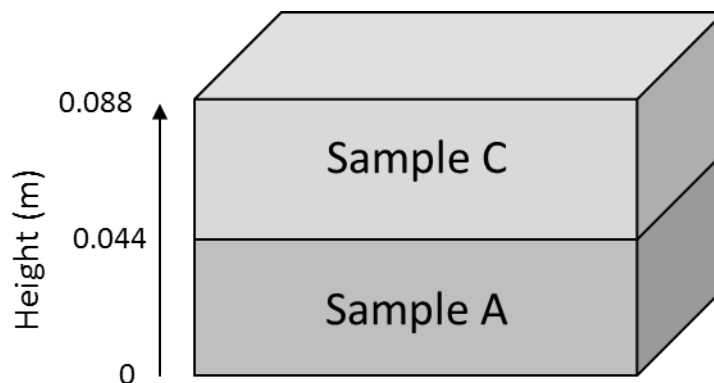
Figure 6.43: Samples A and C stored next to each other

A has the highest VOC gas phase concentration as it is the furthest away from Sample C. Resultingly, the bottom of Sample A is more acidic and degrades at a faster rate.

Figure 6.44 shows the VOC gas phase concentration change with height for Sample A when it has degraded to a DP of 250. The largest concentration seen is much smaller than when Sample A is in the fitted container alone as the majority diffuses across to Sample C.

Figure 6.45 shows the DP change with height for Sample A. As the VOC concentrations seen across the height are small, the variation in DP is not very large being under 5 units in difference. Sample A takes longer to degrade compared to when in the sealed fitted container alone, now taking 677 years, a 44% increase. If we had one sample that produced nearly no VOC (but had no alkaline reserve) next to one that produced large amounts of VOC, we would see that the sample producing nearly no VOC would degrade faster than alone as VOCs now diffuse across from the other sample, which would degrade slower as seen in Sample A. We therefore see the potential problems and benefits of storing different papers next to each other. If a high VOC producing paper is wanted to be preserved for longer, it could be placed next to a sacrificial paper that produces a low amount of VOCs or has a large alkaline reserve in order for the VOCs to diffuse away. It should also be noted that it is not necessarily the sample that degrades fastest that will produce the most VOCs and we cannot just consider paper materials by their degradation state.

This simulation result agrees with the experimental work by Strlic et al. (2010), where different paper samples were stored with a reference paper in vials. The results showed that the reference papers degraded faster when stored with groundwood containing paper with pHs of 4.9 and 5.1, and either at the same rate or slower with rag papers with pHs of 5.1, 5.7 and 7.8. The alkali reserve in the rag papers was assumed to be a good absorber for the VOCs emitted from the reference paper, negating the effect of VOCs on the reference paper.
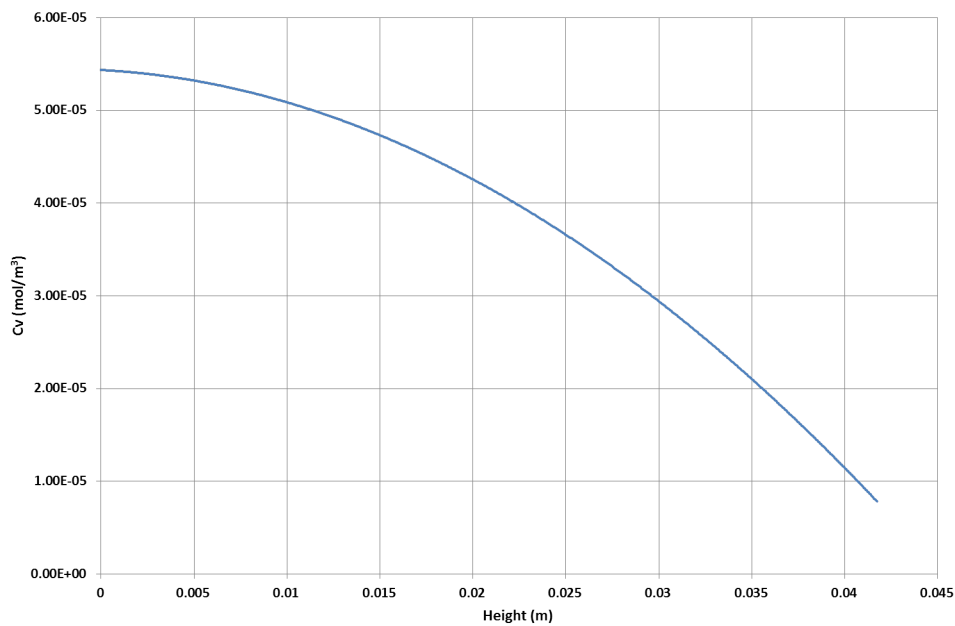
Figure 6.44: VOC gas phase concentration change with height for Sample A when stored with Sample C
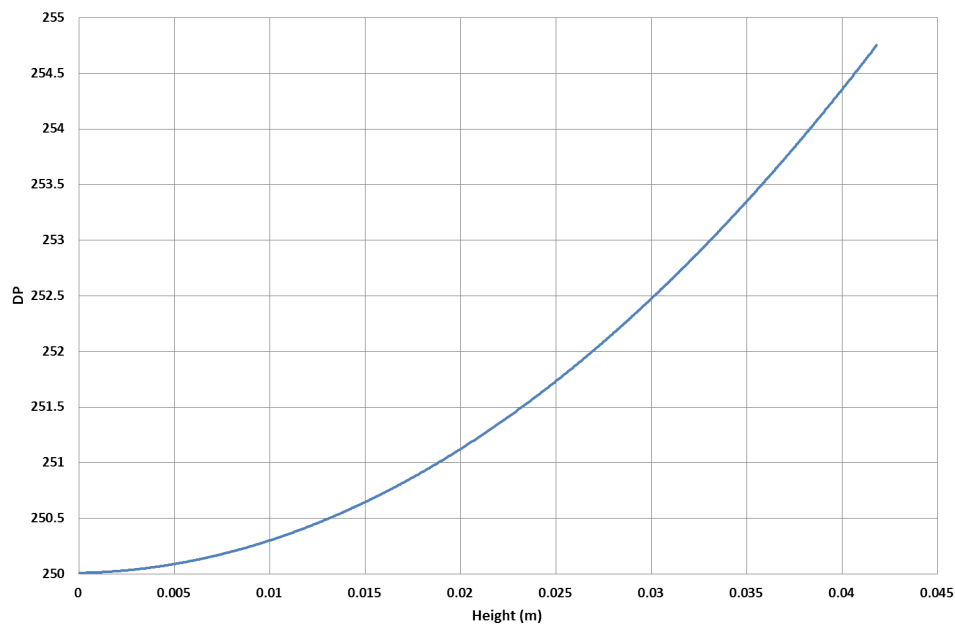
Figure 6.45: DP change with height for Sample A when stored with Sample C
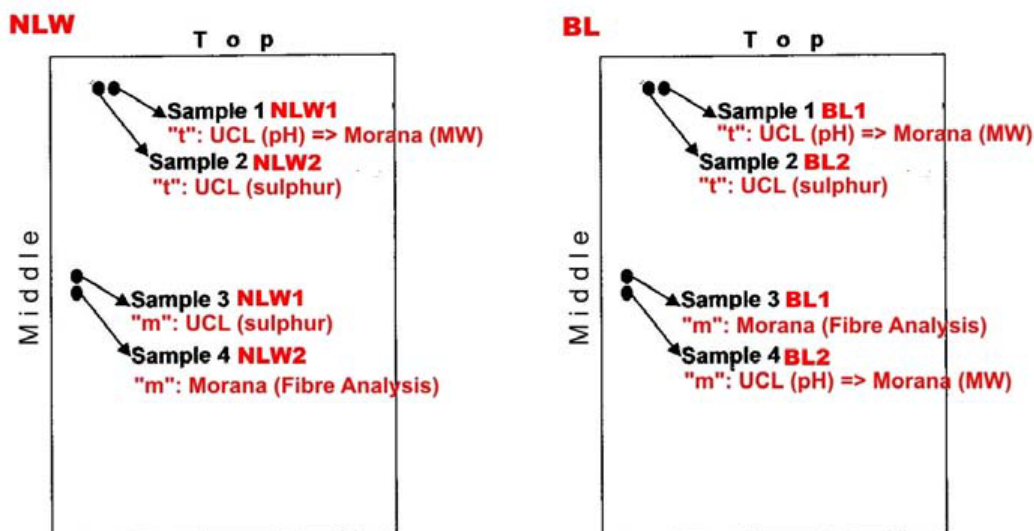
Figure 6.46: Sampling positions[British Library Identical Books Project, 2009]

6.6 Comparison to experimental results in the literature

To help evaluate the simulations and model, we will investigate degradation experimentation results from the literature. We will run simulations based on the data from the literature, seeing if our model can replicate the results.

6.6.1 The British Library Identical Books Project

The Identical Books Project was carried out using books from British Library (BL) and the National Library of Wales (NLW) [British Library Identical Books Project, 2009]. The project had multiple aims including comparing identical books from the BL and the NLW. The BL now has an extremely stable environment which is mechanically climatised, whilst the NLW environment is variable. Historically, however, the BL has had more pollution due to being in central London. Four samples were taken for each identical book, two near the top of the page and two in the middle of the page, all towards the spine as shown in Figure 6.46. The books used for the project were all kept on shelves in the libraries.

The results of the project suggested that the margins generally were less acidic than the centres of the pages, with the trend being more pronounced in the NLW books. This trend agrees with what is predicted by our simulations with the samples on shelves, which was more noticeable for the stack and book samples. For books made of groundwood paper, the NLW books were significantly more acidic than the BL books in the margin, and this trend was more noticeable in the more acidic examples.

The DP results showed that the margins were less degraded, but the difference was very small and statistically insignificant (although the difference was more pronounced in the NLW books). This difference is again what is predicted with the simulations for samples on shelves, and the very small

difference may be due to the the samples not being stored for long enough, or that the VOCs generated are in very small concentrations.

A similar study described in the project report compared books in New York and the Hague. This study found that the New York books were more acidic than those in the Hague, and that the margins were more acidic than the centres of the book pages [J.B.G.A., 1997]. A possible explanation of these results could be that there are pollutants present in the bulk air surrounding the books, diffusing into them having a stronger effect than VOCs produced internally by the books.

6.6.1.1 Simulating NLW books

All the books simulated were from the NLW as they are less likely to have outside pollutants affecting the degradation rate and profile compared to the BL books. Books between 1890 and 1970 are selected as they all have a similar composition and samples with pH lower than 7 were used to avoid unknown alkaline reserves. Books where the DP was highest in the margin compared to the centre were chosen so that VOCs produced internally have a stronger effect on the degradation as opposed to VOCs diffusing in externally. Finally we use books where the lowest DP seen is above 250 as this is the limit used in our previous simulations.

Table 6.8 summarises the books used for simulation. We simulate the books as a book on a shelf, where the surrounding air concentration of VOC is zero. The recorded temperature and relative humidity during the project's undertaking was 15-23ºC and 30-65% respectively. As a result, we use the normal room conditions (23ºC and 50% relative humidity) used for the majority of our previous simulations. Without any information on each book's storage history, we assume each book was stored on a shelf for its entire life. DP and pH top are the DP and pH measured at the top of the page, whilst DP and pH middle are the values measured in the middle of the page. For each sample we also know the height and length of the book, but not the width, and so a value of 0.03m is used. This value does not affect the simulation results because the book on a shelf scenario results in a uniform profile across the length and width.

We assume that each book's DP and pH was initially uniform spatially. To estimate the initial DP for the sample, we assume that at the top of the page, the acidity remains constant and so k_{DP} at the top of the page is constant. This means the measured pH at the top of the page is equivalent to the initial pH for the book. Knowing the age of the book, we can then rearrange Equation 6.17 as follows:

$$DP(\mathbf{x},0) = \frac{1}{\dfrac{1}{DP(\mathbf{x},0)} - k_{DP}(\mathbf{x})t_a} \tag{6.21}$$

where t_a is the age of the book, and k_{DP} is calculated using Equation 6.8.

We make this assumption because in our previous simulations, where the book is in contact with the surrounding air, the VOC concentration is negligible and the acidity change is negligible. For the porosity, unit surface area, adsorption coefficient and effective diffusion coefficient, we use the average of our four samples. The values of the parameters for the four samples do not have a wide range of variation, so it is reasonable to assume an average.

Book ID	Age	DP top	DP middle	pH top	pH middle
BL051	92	600	400	5.52	5.21
BL073	82	500	400	4.97	4.80
BL099	72	400	200	5.16	5.00
BL130	62	600	500	4.88	4.81
BL131	62	1200	700	5.78	5.76
BL132	62	1000	400	5.24	5.91
BL134	62	1200	1100	5.00	4.90
BL135	62	1100	600	4.91	4.85
BL143	62	1700	1200	5.75	5.67
BL146	62	1300	800	6.20	5.96
BL157	52	1000	300	5.17	4.83
BL160	52	500	400	5.09	4.90
BL161	52	1000	500	4.84	4.77
BL162	52	900	800	5.04	4.94
BL163	52	800	400	4.90	4.70
BL164	52	500	300	4.91	4.71
BL166	52	700	300	5.34	5.30
BL171	52	1000	900	5.11	4.80
BL172	42	1400	900	5.56	5.47
BL176	42	1000	600	5.95	5.12
BL177	42	1400	800	6.20	5.39
BL183	42	1100	1000	5.18	5.04
BL187	42	1500	1100	5.31	5.02
BL188	42	800	600	5.16	4.91
BL190	42	1100	600	5.67	5.40
BL222	92	600	300	4.89	4.70
BL223	82	600	300	5.14	5.00
BL232	92	800	400	4.97	4.88
BL287	87	900	700	6.99	5.73
BL294	56	1000	600	4.97	4.59
BL327	62	1100	900	5.20	5.14
BL369	87	900	500	5.95	5.26
BL413	69	900	500	4.69	4.54
BL415	60	800	400	5.11	4.74
BL416	55	800	600	5.04	4.80
BL432	87	800	600	5.13	5.04

Table 6.8: Identical book project sample data

To run our simulations, we have two options with respect to k_{vr}. The first is to assume a set k_{vr} to predict everything else, in particular the pH and DP in the middle of the page. This option, however, may lead to poor results, with the pH and DP in the middle of the page being over and under estimated for the books.

The second option, which we will use, is to find the k_{vr} for each book that achieves the measured DP in the middle of the page. With this option, we would expect the pH in the middle of the page to either be the same as the measured pH, or more acidic; this is as we do not know the complete history of the books and our simulations assume the books have never been opened and that the front, back and spine of the book are non porous.

Table 6.9 shows the k_{vr} found for the books from our simulations. Earlier, in Section 6.5.6.1, we had a maximum k_{vr} of approximately 40,000 and so we do not go beyond this value for our simulations. The table also includes the highest VOC gas phase concentration seen in each book. The highest concentration appears at the end of the degradation time away from the top of the book. At room temperature and pressure, the total gas concentration of all species is 42 mol/m^3. Nine of the thirty five samples exceed this value and are in bold in the table.

The table also lists the pH at the end of the degradation time at the top of the book and in the middle. The pH in the middle from the simulations is more acidic than the pH measured. The acidity increase in the simulations is due to the VOC accumulation in the adsorbed phase. This VOC accumulation is not permanent and if the book has been opened, some of the VOCs escape similarly to how we described in Section 6.5.10, and so the pH would return towards the initial pH.

For the measured values, the pH difference between the middle and the top of the book could be due to acidic compounds accumulating in the adsorbed phase in the centre that cannot escape to the gas phase and are trapped between the fibres [Baranski, 2002].

A possible cause for the simulations over-estimating the k_{vr} value in some cases is that there are other causes of degradation acting on the books. If the centre of the page has a higher relative humidity than the top margin, the degradation constant k_{DP} would be higher, causing a faster degradation rate in the centre of the page. Other compounds important to degradation could also have a gradient present in the book, like oxygen, or a non acidic compound. These gradients could affect the degradation profile, but not the acidity. It has been suggested that the degradation constant k_{DP} could be composed of two rate constants: k_h and k_{ox}, for acid hydrolysis and oxidation respectively [Strlic and Kolar, 2005d].

Book ID	k_{vr}	pH top	pH middle	C_v middle
BL051	800	5.52	3.60	0.38
BL073	500	4.97	3.72	0.22
BL130	700	4.88	3.75	0.19
BL131	2500	5.78	3.57	0.44
BL132	*300000*	*5.16*	*2.23*	*203.47*
BL134	65	5.00	4.56	0.0045
BL135	25000	4.91	2.97	6.52
BL143	200	5.75	4.41	0.012
BL146	600	6.20	3.97	0.076
BL157	*>400000*	*5.11*	*2.25*	*182.00*
BL160	3000	5.09	3.37	1.09
BL161	*200000*	*4.83*	*2.45*	*72.80*
BL162	150	5.04	4.31	0.016
BL163	*400000*	*4.87*	*2.21*	*215.85*
BL164	*400000*	*4.86*	*2.11*	*347.06*
BL166	*>400000*	*5.21*	*2.17*	*263.60*
BL171	100	5.11	4.45	0.0086
BL172	5000	5.56	3.54	0.51
BL176	25000	5.93	3.02	5.31
BL177	8500	6.19	3.37	1.07
BL183	120	5.18	4.48	0.0076
BL187	1500	5.31	3.89	0.10
BL188	6000	5.16	3.36	1.13
BL190	60000	5.75	2.82	13.55
BL222	*50000*	*4.88*	*2.54*	*48.09*
BL223	*60000*	*5.12*	*2.51*	*54.89*
BL232	15000	4.97	2.91	8.60
BL287	11	6.99	5.05	0.0013
BL294	16000	4.97	3.09	3.76
BL327	200	5.20	4.26	0.020
BL369	1300	5.95	3.57	0.44
BL413	35000	4.69	2.82	13.16
BL415	*160000*	*5.08*	*2.40*	*89.41*
BL416	2000	5.04	3.58	0.41
BL432	300	5.13	3.97	0.070

Table 6.9: Identical book project simulation data

Chapter 7

Future work and conclusions

In this chapter, we anticipate the additions and improvements that can be carried out to further the work presented in this thesis.

In Chapter 2 we investigated paper degradation and the role VOCs played in it. In particular we identified acetic acid as a VOC that could be considered as a general representative and thus used it as our VOC in the mass transfer model developed in Chapter 4. Chapter 5 covered the experimentation to support the model. There were experiments for the effective diffusion coefficient, porosity, surface area, pore diameter and adsorption coefficient of four different samples. A noticeable absentee was experimentation for the reaction constant k_{vr} for the production of VOC which we will cover here.

In Chapter 6 we carried out computational simulations of the main model and of additional ones exploring the effects of different scenarios. Here, we will anticipate how these simulations can be extended and improved.

We will also review the experimentation and model to see how these areas could be expanded.

7.1 VOC generation reaction rate constant

First, we remind ourselves of where the reaction constant k_{vr} features within the model. The reaction constant is originally introduced in Chapter 3, Section 3.3.4.1 in Equation 3.36 as part of the VOC generation term:

$$r_v(\mathbf{x}, t) = k_{vr}\alpha(\mathbf{x}, t)k_{DP}(\mathbf{x}, t) \tag{7.1}$$

where r_v is the rate of VOC generation, k_{DP} is the reaction constant associated with the degradation rate and α is the fraction of end bonds:

$$\alpha(\mathbf{x}, t) = \frac{2}{DP(\mathbf{x}, t) - 1} \tag{7.2}$$

In Chapter 3, Section 3.3.4, we reported the sequences of steps for finding a reaction rate. The first step was to postulate a rate law, as we did. The successive steps require a suitable experimentation set up, with the relevant design equations in order to obtain data by which we can calculate the reaction rate constant. We now investigate the options for this experimentation.

In Chapter 6, Section 6.5.6.1, we used the experimentation work of Ramalho et al. to see if we could estimate k_{vr} from an emission rate. This was only an estimation though and to get better information, further experimentation would be ideal.

It can be seen from Equation 7.1 that if we know k_{DP} and α, and can measure the rate of VOC generation, we can consequently calculate k_{vr}. We then need methods for measuring the rate of VOC generation where k_{DP} and α are known.

The variable α is known when the DP is known. If the time scale for measuring the rate of VOC generation is small compared to the time scale of DP change, we can assume DP is constant. If the DP is assumed to be constant, then we can measure this using a method such as viscometry before carrying out the experiment for measuring the rate of VOC generation.

The reaction constant associated with the degradation rate, k_{DP}, is not a constant, but a function of temperature, relative humidity and acidity of the sample. If the experiment is performed in a controlled environment, the temperature and relative humidity will be constant. The acidity however is expected to change as VOCs are generated. Similarly to how we approach the DP, if the time scale for measuring the rate of VOC generation is small compared to the time scale of the acidity change, we can assume the acidity to be constant. With these assumptions, we can then assume k_{DP} to be a constant which can be calculated using Equation 4.10 from Chapter 4, Section 4.2.1, for a known temperature, relative humidity and acidity of the sample.

We will first review the emission rate experimentation carried out by Ramahlo et al. (2009) and then present different methods for measuring the generation rate: two through measuring the VOC concentration in a liquid phase and another through the gas phase.

For measuring in either phase, we would need to know the initial concentration of the VOC. The simplest solution is to have the initial concentration to be zero. A method to help ensure the concentration is zero would be to place the sample in a vacuum to draw out any VOC present. One major issue for experimentation is the difficulty of detecting acetic acid or many other VOCs due to their low concentrations. A method to increase the concentrations to make them more detectable is to increase the temperature; we will consider this in Section 7.1.4.

7.1.1   Emission rates of VOCs experimentation by Ramahlo et al.

In the article by Ramalho et al. (2009), two types of paper were used. The paper samples underwent accelerated ageing, where one sheet is placed in a sealed tube for 2, 5, 10, 14 and 30 days in a dry oven at 100ºC. Before going into the oven, the paper samples were preconditioned to 23ºC and 50% relative humidity. After coming out of the oven, the paper samples were then reconditioned to these values over a period of 24 hours.
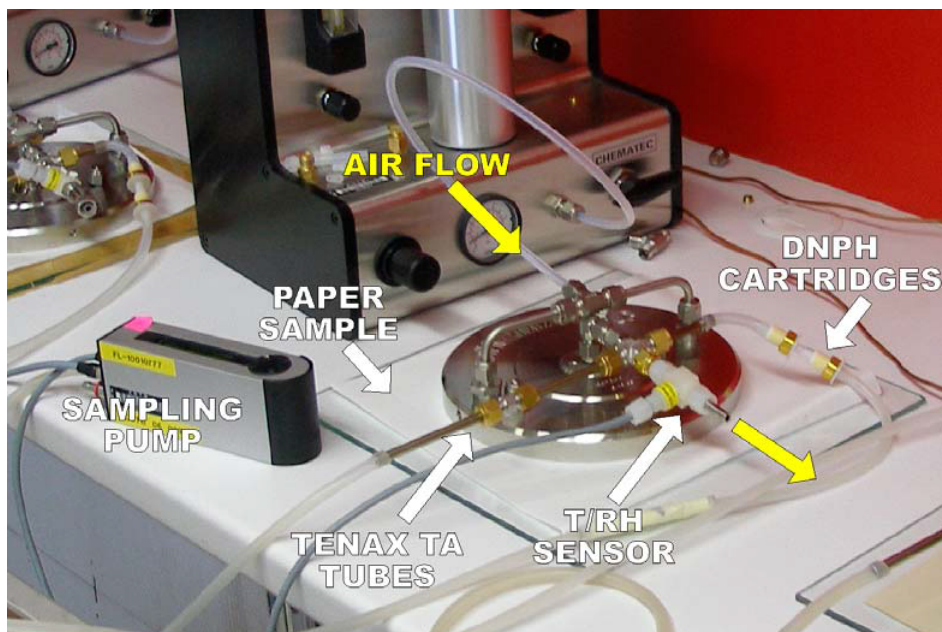
Figure 7.1: FLEC set-up with paper sample

The aged sample is then placed in the FLEC in a climate controlled room (23ºC and 50% relative humidity), and clean air at 50% relative humidity is continuously provided into the FLEC. The VOCs are sampled at the air outlet of the cell over 24 hours. The VOCs are captured using Tenax sorbent tubes that have an adsorbent material coating that adsorbs the VOCs. The collected VOCs are then desorbed by heating the tubes and passed through the GC-MS so the VOCs can be quantified. The set-up is shown in Figure 7.1.

The method of using the FLEC and Tenax sorbent tubes is possible for finding k_{vr}. One issue is that acetic acid capture via Tenax sorbent tubes is not at its optimum at room temperature and is better for the tubes at lower temperatures [Tenax TA information, 2013]. Another issue is ensuring that the measured VOC values are relatable to the generation rate. This can be solved if VOCs are removed from the paper samples before experimentation begins. A way of doing this is to place the paper under vacuum. Another option is to measure the VOC concentrations at the start of the experiment.

The VOC mass balance for the FLEC can be written as:

$$V d_t C_v = A r_v - \dot{Q} C_v \tag{7.3}$$

where V is the volume of the cell, C_v is the concentration in the gas phase, A is the area of the paper sample, r_v is the rate of VOC generation and $\dot{Q}$ is the volumetric flow rate. The term on the left hand side is the rate of accumulation, whereas the first and second terms on the right hand side are the VOC generation by the paper in the cell, and the flow rate of VOC leaving the cell respectively.

If we assume there is no accumulation of VOC in the cell, the balance reduces to:

$$Ar_v = \dot{Q}C_v \tag{7.4}$$

We assume a constant rate of VOC generation during the sampling time, Δt. The amount of VOC captured over the sampling time is $\dot{Q}C_v\Delta t$. Dividing by the sampling time, we get $\dot{Q}C_v$, from which we can calculate the VOC generation rate. The larger the sampling time, the larger the amount of VOC captured, leading to better measurements of C_v.

7.1.2 Liquid phase acetic acid measurements

Here we shall explore two methods for measuring acetic acid in the liquid phase. Both will explore how the acetic acid is captured in the liquid phase before measuring in a GC-MS.

7.1.2.1 Batch concentration method

For the first method of measuring acetic acid in the liquid phase, we first seal a known mass of our paper sample in a container. The sample is then left for a set period of time. This allows acetic acid to generate and build up in the container. The time period should be long enough that there is sufficient build up of acetic acid, but not overly long so that there would be a noticeable change in DP and acidity. The total amount of acetic acid produced would be:

$$A[v] + VC_v \tag{7.5}$$

where A is the area of the paper sample, V is the volume of the container, $[v]$ is the concentration in the adsorbed phase of the paper, and C_v is the concentration in the gas phase. Dividing by the time sealed, t_f, we get an average generation rate:

$$\langle r_v \rangle = \frac{A[v] + VC_v}{t_f} \tag{7.6}$$

We assume over the time sealed that the acidity and DP of the sample are constant. The gas phase can be expressed through the adsorption isotherm (assumed linear here):

$$[v] = K_v C_v \tag{7.7}$$

This gives:

$$\langle r_v \rangle = \frac{\left(A + \dfrac{V}{K_v}\right)[v]}{t_f} \tag{7.8}$$

We then inject a known quantity of a solvent into the container which will draw out the acetic acid from the adsorbed phase. How much of the acetic acid can be drawn out will depend on the solvent and so
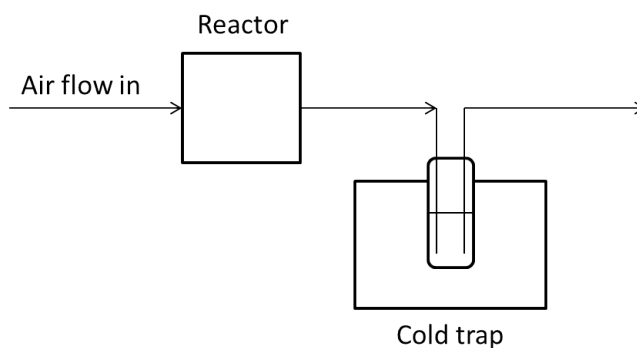
Figure 7.2: VOC capture set up

calibration for the solvent used would be needed. The solvent is then extracted from the container and can be analysed in a GC-MS system. With a calibrated GC-MS, the concentration of acetic acid in the solvent can be measured, from which the adsorbed phase acetic acid concentration can be calculated using the volume of solvent injected.

For optimum results the following variables should be considered: the volume of the solvent and mass of paper sample, the choice of solvent, and the time the paper is left in the sealed container.

When the volume of solvent is low and the mass of the paper sample is high, we will have a much higher (and consequently easier to measure) concentration of acetic acid in the solvent compared to when the volume is high and mass is low. A problem with a high mass of paper sample is the potential of consuming all the oxygen and changing the degradation path. The solvent should be chosen for its ability to absorb acetic acid and examples are acetonitrile or DMF.

A GC-MS is ideally used as opposed to simply a GC, as the MS is used to identify the peaks, which allows us to identify a potentially large number of different VOCs present.

7.1.2.2 Cold trap method

The Ramalho set-up is a "trapping" method for VOC measuring. An alternative trapping method is a cold trap. Figure 7.2 shows a basic example set-up of a cold trap experiment.

The reactor could simply be a vial with the paper sample inside as shown in Figure 7.3, although the FLEC could be used in place of the vial, which would offer more control and options.

The air at a set temperature and relative humidity flows through the reactor containing the paper sample and then flows out of the reactor carrying any VOCs produced which have entered the gas phase. The cold trap consists of bubbling the air through a solvent contained in a vial which is in an ice bath. After a sampling period, the vial can then be placed in the GC and analysed. Knowing the air flow rate, surface area of paper and concentration, a mean emission rate can be calculated over the sampling period. The humidity may cause issues with the sample as it would add water to the solvent.

Depending on the solvent used, an ice bath may not be necessary. The benefit to this method is that the VOCs are not building up around the sample and so the acidity of the sample will not change.

Set
RH In
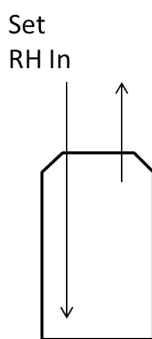
Figure 7.3: Sample vial

7.1.3 Gas phase acetic acid measurement

Solid-Phase Mirco Extration (SPME) with GC-MS is a highly sensitive detection method usable for both information on the adsorption of VOCs as mentioned in Chapter 5, Section 5.4.1, and generation rate of VOCs in paper.

SPME uses a fibre, which is a short thin rod of fused silica coated with an adsorbent polymer. The fibre can be used in the headspace over aqueous or solid samples or placed directly in aqueous samples. The fibre can have different polymers to target different compounds. After exposing the fibre to the sample for a set period of time, it is injected into the the GC, where the compounds are thermally desorbed for a set period of time and transferred into the GC column. The GC and MS then separate and identify the different compounds in the mixture [Sparkman et al., 2011].

For our experiment, we would have a paper sample in a sealed container like the batch concentration method had, but instead of injecting a solvent, the SPME fibre would be inserted without touching the paper. The fibre is left in for a set period of time to allow it to adsorb the VOCs before being withdrawn and inserted into the GC-MS. Once in the GC-MS, the VOCs are thermally desorbed from the fibre. The advantage of SPME is that it can achieve low detection rates. There are different fibres available depending on which compounds one wishes to study. The length of time the fibre is inserted in the container needs to be optimised, as well as the time and temperature used for thermal desorption in the GC-MS. This can be very time intensive. SPME can be used as an additional step in the other methods also, where the fibre is either inserted into the solvent and adsorbed the VOCs, or used in the headspace of the solvents.

7.1.4 The dependence of k_{vr} on temperature

One common issue with all the methods is that the time needed for a measurable amount of VOCs to be produced depends on the sensitivity of the VOC detection method. If the sensitivity is low, the time needed will be high. Increasing the temperature of the samples is a frequently used way of reducing the time needed and is referred to as accelerated ageing. We assume that k_{vr} is a function of temperature. To find how k_{vr} changes with temperature, we would need to experiment at different

elevated temperatures. With experiments completed at different temperatures, we would then be able to extrapolate the results to predict the value of k_{vr} at room temperature and lower. The extrapolation procedure, however, always leads to uncertainty and one cannot be sure that the extrapolated results are really valid.

7.2   Accelerated ageing simulations

In Chapter 2, Section 2.4.1, we talked about the importance of accelerated ageing experiments in the field of heritage science. Accelerated ageing experiments can be carried out in many different ways. Different temperatures and relative humidities can be used, different sample volumes can be explored and the sample can be in sealed conditions or in ovens where the air is constantly pumped through.

To successfully run simulations for accelerated ageing experiments, we need to know how our variables change with temperature and relative humidity. To get accurate information on how the variables change with temperature and relative humidity, more experimentation would be required.

We expect the adsorption rate, reaction rate and diffusion rate to all change with temperature. In addition, the acid equilibrium constant for our VOC also would change with temperature. Equation 2.8 from Chapter 2 describes how the degradation reaction constant k_{DP} is affected by temperature and relative humidity.

If we were able to successfully run simulations using accelerated ageing conditions, we would be able to describe more accurately the correlation between accelerated ageing and natural ageing rather than relying on empirical evidence.

One problem for accelerated ageing is that, at elevated temperatures, the degradation path can change. It has been suggested that oxidation reactions increase at elevated temperatures. Therefore, there is a limit to how high a temperature is used, as the higher the temperature, the less relevant the results. Another problem is the relative humidity: in a sealed container, the relative humidity will change for different temperatures and this change must be accounted for.

7.3   Experimentation expansion

We have already mentioned how more experimentation at different temperatures and relative humidities would be beneficial for our simulations, in particular for simulations based on artificial ageing.

If we want to simulate more paper samples, the experimentation carried out would need to be repeated for the new samples. Increasing the sample set size could help establish trends between samples across acidity or DP. With a large number of different samples experimented on, we would be able to more accurately predict the behaviour of paper materials we wish to preserve. If values can be assumed to be within a certain range then we can eliminate the need for experiments and still get accurate results from simulations.
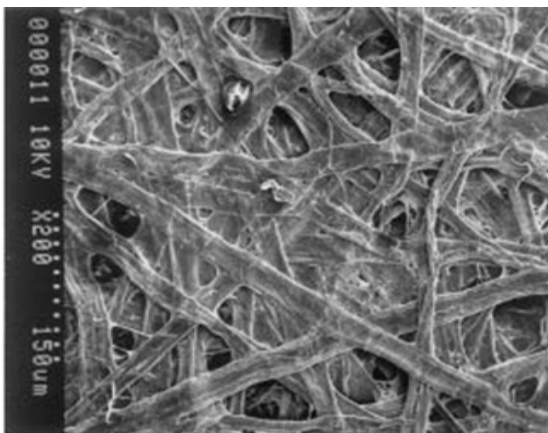
Figure 7.4: SEM image (x200) of handsheet from never dried pulps [Wistara and Young, 1999]

To explore how the adsorption coefficient K_v changes with higher temperatures we can perform the experiment with the glass jar (as described in Chapter 5, Section 5.4.2) on a heated plate at different set temperatures. The heated plate would not work for values below room temperature. One way to do the experiment at lower temperatures (and would also work for higher temperatures) is to perform the experiments in a climate controlled room. We would also ideally have experimentation for the binary diffusion coefficient D_{air} for acetic acid in air at different temperatures.

To expand the experiments relating to the effective diffusion coefficient, the thickness of the sample used in the experiment can be explored. It may be the case that a thin sample is more easily distorted by the air flows and so gives less accurate results for the tortuosity.

Additional experimentation such as microscopy techniques on our samples would help give more understanding of the pore structure of paper. A particular type of Microscopy, Scanning Electron Microscopy (SEM) would be useful as it provides good information on the 3D view of the structure. An example is shown below in Figure 7.4 [Wistara and Young, 1999].

Finally, our experiments can be expanded to include other materials associated with paper. In our simulations where the paper was in a sealed container, we assumed the container could have no mass flow through it and it was non-reactive. Cardboard containers are not uncommon, and are paper based materials which may produce more VOCs than the paper being stored; also they are porous and so mass can flow through them. Similarly, when simulating a book, we assumed the covers and spine were non-porous and mass could not flow through. Experimentation on the covers and spine of book would allow us to asses this assumption.

7.4 Model expansion

The model assumes the relative humidity is constant. Libraries and archives without climate control may not have constant relative humidity. When the relative humidity changes, it is possible that the paper volume develops a non uniform profile of relative humidity. To account for this, we would need

to model the relative humidity for the paper volume. We would expect that the paper volume furthest away from an exposed surface would change the least when the relative humidity changes. As such, that part of the volume would degrade closer to the rate before the change, whilst the exposed surface would now degrade at a different rate.

The temperature may also not remain constant. When modelling fluctuating temperature, we would initially assume that a temperature change is felt instantly across the paper volume. However, it may later be necessary to model a temperature profile if this assumption is not sufficient.

The VOC our model considers is acetic acid, an acidic VOC which affects the acidity of the system (or the alkaline reserve if present). By considering a different acidic VOC, for example formic acid, we could compare how each compound affects the acidity and degradation rate. Using this model for a non acidic VOC, we expect there to be no change in acidity and if an alkaline reserve is present, it will not be depleted. As such, the rate of VOC generation would be an indicator of degradation state, but not influence the degradation rate. Although the model considers acid-catalysed hydrolysis of cellulose to be the main degradation reaction, these non-acidic VOCs, could influence degradation rate through other degradation reactions and so if known could be included in a model expansion.

A complicated expansion would be to include more than one VOC. The complication would arise as we would need to consider how each VOC would interact with each other and their effect on the acidity. With more VOCs included, one could see if the additional VOCs bring a significant change in the accuracy of results.

Our model describes the concentration profile of a VOC for a volume of paper. Our degradation rate was based on Ekenstam's equation given in Chapter 2, Section 2.5, where the DP degradation constant was given by Equation 2.27. A further exploration of the VOC concentration profile is to include different degradation models, such as the Levelling-off degree of polymerisation (LODP) method [Calvini and Gorassini, 2006], for comparative purposes.

7.5   Conclusions

We have shown in this chapter the need for more experimentation on paper's production of VOC, and how this information would be used in our simulations. Also we have shown the potential for the model to compare natural ageing with artificial ageing.

Having identified VOCs' role in the degradation of paper, we derived a mass transfer model that describes a VOC's profile in a paper volume. The model encompassed diffusion and reaction phenomena and adsorption. We report again the model describing the VOC profile in a paper volume:

$$\partial_t C_v(\mathbf{x}, t) = \frac{D_{ve}}{\varepsilon + \sigma K_v} \partial_{\mathbf{x}} \cdot \partial_{\mathbf{x}} C_v(\mathbf{x}, t) + \frac{\sigma}{\varepsilon + \sigma K_v} r_v(\mathbf{x}, t) \tag{7.9}$$

where C_v is the VOC gas phase concentration, D_{ve} is the overall effective diffusion coefficient, ε is the porosity, σ is the surface area per unit volume, K_v is the adsorption coefficient and r_v is the generation rate of the VOC in the adsorbed phase.

	A	**B**	**C**	**D**
$D_{ve}(\mathrm{m^2/year})$	0.00379	0.00333	0.00330	0.00470
$\sigma(\mathrm{m^2/m^3})$	1402500	1452600	1422200	950400
$K_v(\mathrm{m})$	0.0032	0.0083	0.0087	0.0031
$\varepsilon(\mathrm{m^3/m^3})$	0.0042	0.0041	0.0036	0.0029
$d_{pore}(\mathrm{nm})$	11.92	11.32	10.12	12.09

Table 7.1: Paper properties found through experimentation

The model is linked to the degradation rate (reported again below in Equation 7.10) through the generation rate of the VOC which is a function of the DP of paper and the degradation rate constant k_{DP}. The model is also linked to the degradation rate as the VOC generation affects the acidity of the system, and k_{DP} is a function of the acidity.

$$\partial_t DP(\mathbf{x}, t) = -k_{DP}(\mathbf{x}, t) \left[DP(\mathbf{x}, t) \right]^2 \tag{7.10}$$

The model also accounts for when an alkaline reserve is present and the depletion of the reserve due to acetic acid is given by:

$$\partial_t \left[CaCO_3 \right] = -\frac{1}{2} \left(D_{ve} \partial_{\mathbf{x}} \cdot \partial_{\mathbf{x}} C_v(\mathbf{x}, t) + \sigma r_v(\mathbf{x}, t) \right) \tag{7.11}$$

where $[CaCO_3]$ is the concentration of calcium carbonate, the compound typically responsible for the reserve.

To use the model, experimentation was required and the results are summarised in Table 7.1. The simulations showed the negative effect of VOCs in different scenarios. In a sealed fitted container at room conditions, where VOCs cannot escape, a decrease in lifespan up to 54% was seen and a book on a shelf showed up to a 40% decrease in comparison to a degradation model where the acidity of paper does not change with time. Lowering the temperature to 14ºC and relative humidity to 40% was shown to have a beneficial effect, increasing the lifespan by over 375% for all samples.

Using the model, we simulated the degradation for books from the British Library Identical Books Project [British Library Identical Books Project, 2009]. If the degradation of the books was only described using Equation 7.10 with a constant k_{DP}, the non uniform degradation across the volume could not be explained, and the degradation in the middle of the page would be underestimated as the increase in k_{DP} over time is not accounted for.

The simulations were able to explain the difference in DP across a book's page for most of the books selected; however, for a few of the books the k_{vr} value and VOC gas phase concentrations were too high. A likely explanation for this is that other factors in addition to VOCs that also affect the degradation rate were occurring which are not covered by our model.

The simulations explored different VOC related paper properties that affect the degradation rate. As such, an archivist can ask themselves the following questions about the paper they are storing:

1. Is the paper acidic?

An acidic paper is at risk of degrading faster than alkali papers. Mathematically, the acidity features in the degradation constant k_{DP} given in Chapter 2, Equation 2.27. The more acidic the sample, the higher the value of k_{DP} and so the larger the degradation rate. Paper with a significant alkaline reserve last longer and degrade uniformly in space. Neutralising and buffering solution [GMW equipment, 2014] is available for non-aqueous de-acidification and buffering of bound books. The solution neutralizes acids as it deposits non-toxic alkaline buffer into the structure of the paper.

2. Does the paper have high adsorption of VOCs?

   A paper that adsorbs a lot of VOCs has the danger of adsorbing VOCs that are produced by the materials it is stored with. In addition to this, when it produces VOCs, a larger quantity will stay in the adsorbed phase. A paper that adsorbs a lot of VOCs and does not have an alkaline reserve will have a larger change in its acidity if VOCs are allowed to build up, which in turn leads to faster degradation.

3. Does the paper produce a large amount of VOCs?

   A simple test for this is the smell of the paper! A paper that produces a large amount of VOCs influences the acidity of the paper, and of the paper it is stored with. It is also expected that paper will produce VOCs in larger quantities as it ages.

Knowing the answer to these questions allows a collection manager to assess their storage options.

A sealed container will ensure the degradation profile across a material is uniform. Another benefit of keeping paper in a sealed container is that it prevents outside pollutants from harming the paper. The material of the container should be carefully considered and should not produce any compounds that could be damaging to the material. For a material in a container, the lifespan can be further extended by periodic removal of VOCs to prevent their build up. One cause of VOC removal for a book is being read and opened up allowing VOCs to escape to the surrounding air. Other options for the removal if the books are not available to read could be using equipment similar to a fume cupboard or small scale equipment like that shown in Figure 7.5 [GMW equipment, 2014]. The mobile vacuum panel can be used for both single sheets and bound books.

If a paper sample producing large VOC concentrations is kept isolated, the VOC build up will still negatively affect their own degradation time. As such, these types of materials in particular should be frequently treated if kept in a container. Caution must be taken when storing more than one paper material in the same container as well, guarding against one paper negatively affecting another.

Storing a sample on a shelf means that VOCs are allowed to escape to the surrounding air. However, the degradation is no longer uniform across the volume. A simple action to prevent this could be to change the orientation of the material on the shelf frequently. If the room with the shelves is well ventilated, then the VOC concentration in the air surrounding the paper material will always be negligible.

Figure 7.5: Mobile Vacuum Panel [GMW equipment, 2014]

Bibliography

A.B. Abell, K.L. Willis, and D.A. Lange. Mercury intrusion porosimetry and image analysis of cement-based materials. *Journal of Colloid and Interface Science*, 211:39–44, 1999.

Alphasense. http://www.alphasense.com, January 2011.

Analytics Shop. http://www.analytics-shop.com/gb/sample-preparation/filters/filters-by-manufacturer/whatman-filter.html, June 2013.

ANSYS. http://www.ansys.com/Products/Simulation+Technology/Fluid+Dynamics, January 2013.

ASTM C778-97. Standard Test Methods for Hydrogen Ion Concentration (pH) of Paper Extracts (Hot-Extraction and Cold-Extraction Procedures). 2002.

A. Baranski. Ageing kinetics of cellulose and paper. *Restaurat*, 23:77–88, 2002.

B. Blumich, S. Anferova, S. Sharma, A.L. Segre, and C. Federici. Degradation of historical paper: nondestructive analysis by NMR-MOUSE. *Journal of Magnetic Resonance*, 161:204–209, 2003.

British Library. Taking care of our collections. British Library leaflet, 2010a.

British Library. Psalter World Map c.1265. http://www.bl.uk/magnificentmaps/map1.html, November 2010b.

British Library. Preservation Advisory Centre. http://www.bl.uk/aboutus/stratpolprog/collectioncare/publications/booklets, January 2013.

British Library Identical Books Project. Final report. Centre for Sustainable Heritage, University College London, 26th May 2009.

Stephen Brunauer, P.H. Emmett, and Edward Teller. Generalization of Langmuir's theory to multimolecular adsorption. *Journal of the American Chemical Society*, 60:309–319, 1938.

A. Bulow, P. Begin, H. Carter, and T. Burns. Migration of volatile compounds through stacked sheets of paper during accelerated ageing. *Restaurator*, pages 187–203, 2000.

Calvini and Gorassini. On the rate of paper degradation: lessons from the past. *Restaurator*, 27: 275–290, 2006.

Pavel Capek and Andreas Seidel-Morgenstern. Multicomponent mass transport in porous solids and estimation of transport parameters. *Applied Catalysis A: General*, 211:227–237, 2001.

Charles E. Carraher. *Polymer Chemistry - Naturally Occurring Polymers: Plants, 9.2 Cellulose*, pages 261–265. Seymour/Carraher's, 7th edition, 2007a.

Charles E. Carraher. *Polymer Chemistry - Figure 9.6 Representitive structure of lignin*, page 294. Seymour/Carraher's, 7th edition, 2007b.

Charles E. Carraher. *Polymer Chemistry - 9.2.1 Paper*, pages 263–265. Seymour/Carraher's, 7th edition, 2007c.

Henry Carter, Paul Begin, and David Grattan. Migration of volatile compounds through stacked sheets of paper during accelerated ageing. *Restaurator*, pages 77–84, 2000.

John C.S. Chang and Zhishi Gui. Characterization of organic emissions from a wood finishing product - wood stain. *Indoor Air*, 2:146–153, 1992.

Sydney Chapman and T.G. Cowling. *The mathematical theory of non-uniform gases: an account of the kinetic theory of viscosity, thermal conduction and diffusion in gases - Chapter 5*, pages 88–89. Cambridge U.P, 3rd edition, 1970.

Per Axel Clausen. Emissions of volatile and semivolatile organic compounds from waterborne paints - the effect of film thickness. *Indoor Air*, 3:269–275, 1993.

Collections Demography Part 4. Modelling Change and Damage in Collections. https://www.youtube.com/watch?v=dCvbZTQljQE, Febuary 2013.

E.L. Cussler. *Diffusion - Mass Transfer in Fluid Systems - Models for Diffusion*, pages 1–12. Cambridge University Press, 3rd edition, 2009a.

E.L. Cussler. *Diffusion - Mass Transfer in Fluid Systems - Diffusion in Concentrated Solution*, pages 56–94. Cambridge University Press, 3rd edition, 2009b.

E.L. Cussler. *Diffusion - Mass Transfer in Fluid Systems - Diffusion in Dilute Solutions*, pages 13–55. Cambridge University Press, 3rd edition, 2009c.

E.L. Cussler. *Diffusion - Mass Transfer in Fluid Systems- Fig 6.4-1 Pore diffusion effects*, page 190. Cambridge University Press, 3rd edition, 2009d.

E.L. Cussler. *Diffusion - Mass Transfer in Fluid Systems - Diffusion of Interacting Species*, pages 161–210. Cambridge University Press, 3rd edition, 2009e.

E.L. Cussler. *Diffusion - Mass Transfer in Fluid Systems - Adsorption*, pages 425–452. Cambridge University Press, 3rd edition, 2009f.

William M. Deen. *Analysis of Trasport Phenomena - 3. Scaling and approximation techniques*, pages 73–112. Oxford, 1998.

Baoqing Deng and Chang Nyung Kim. A new CFD model for VOC emission based on the general adsorption isotherm. *JME International Journal*, 47:396–402, 2004.

Baoqing Deng and Chang Nyung Kim. CFD simulation of VOCs concentrations in a resident building with new carpets under different ventilation strategies. *Building and Environment*, 42:523–531, 2007.

BaoQing Deng, Bo Yu, and Chang Nyung Kim. An analytical solution for VOCs emission from multiple sources/sinks in buildings. *Chinese Science Bulletin*, 53:1100–1106, 2008.

J-B Dumas. Report on a memoir of Mr Payen, regarding the composition of woody matter. *CR*, 8: 51–53, 1839.

James E Dunn. Models and statistical methods for gaseius emission testing of finite sources in well-mixed chambers. *Atmospheric Environment*, 21:425–430, 1987.

Anne-Laurence Dupont, Celine Egasse, Aude Morin, and Frederique Vasseur. Comprehensive characterisation of cellulose and lignocellulose degradation products in aged papers: Capillary zone electrophoresis of low-molar mass organic, carbohydrates, and aromatic lignin derivatices. *Carbohydrate Polymers*, 68:1–16, 2007.

A. Ekenstam. The behaviour of cellulose in mineral acid solutions: kinetic study of the decomposition of cellulose in acid solution. *Ber. Deutschen Chem. Gesellschaft*, 69:553, 1936.

A M Emsley and G C Stevens. Kinetics and mechanisms of the low-temperature degradation of cellulose. *Cellulose*, 1:26–56, 1994.

Ann Fenech, Matija Strlic, Irena Kralj Cigic, Alenka Levart, Lorraine T. Gibson, Gerrit de Bruin, Konstantinos Ntanos, Jana Kolar, and May Cassar. Volatile aldehydes in libraries and archives. *Atmospheric Environment*, 44:2067–2073, 2010.

H. Scott Fogler. *Elements of Chemical Reaction Engineering - 1.1 The Rate of Reaction, -rA*, pages 4–8. Pearson, 4th edition, 2010a.

H. Scott Fogler. *Elements of Chemical Reaction Engineering - 3.1 Basic Definitions*, pages 80–82. Pearson, 4th edition, 2010b.

H. Scott Fogler. *Elements of Chemical Reaction Engineering - 5.1 The Algorithm for Data Analysis*, pages 254–255. Pearson, 4th edition, 2010c.

H. Scott Fogler. *Elements of Chemical Reaction Engineering - 10.1 Catalyst*, pages 645–655. Pearson, 4th edition, 2010d.

H. Scott Fogler. *Elements of Chemical Reaction Engineering - 10.2 Steps in a Catalytic Reaction*, pages 655–671. Pearson, 4th edition, 2010e.

Fujitsu Europe. scanners' section. http://www.fujitsu.com/emea/products/scanners/, January 2014.

GMW equipment. http://www.gmw-shop.de/shop-uk/index.html, January 2014.

Yves Gnanou and Michel Fontanille. *Organic and Physical Chemistry of Polymers - 14.2.1 Cellulose*, pages 496–499. Wiley, 2008.

T. Graham. On the law of the diffusion of gases. *Phil. Mag*, pages 175–190, 269–276, 351–358, 1833.

H. Guo, F. Murray, S.C. Lee, and S. Wilkinson. Evaluation of emissions of total volatile organic compounds from carpets in an environmental chamber. *Building and Environment*, 39:179–187, 2004.

J. Hanus, M. Komornikova, and J.J. Minarikova. Changes in some mechanical properties of paper during the ageing in an archival box. *Edinburgh ICOM-CC 11th Triennial Meeting*, 2:510–516, September 1996.

Hester and Harrison. *Volatile Organic Compounds in the Atmosphere*, pages 1–15. The Royal Society of Chemistry, 1995.

Dard Hunter. *Papermaking: The History and Technique of an Ancient Craft*. Courier Corporation, 1978.

ISO 1924-2:1994. Paper and Board - Determination of Tensile Properties - Part 2: Constant Rate Elongation Method.

ISO 1974:1990. Paper- Determination of Tearing Resistance (Elmendorf Method).

ISO 5351/1. Cellullose in Dilute Solutions - Determination of Limiting Viscosity Number - Part 1: Method in Cupri-Ethylene-Diamine (CED) Solution. 1981.

ISO 5626:1993. Paper - Determination of Folding Endurance.

Havermans J.B.G.A. A study of the cause of damage in pairs of books. *TNO Institute of Industrial Technology*, 1997.

JPEG committee. http://jpeg.org/jpeg/index.html, November 2010.

Frantisek Kacik, Danica Kacikova, Michal Jablonsky, and Svetozar Katuscak. Cellulose degradation in newsprint paper ageing. *Polymer Degradation and Stability*, 94:1509–1514, 2009.

Hans Krassig. *Cellulose and its Derivatives - Chemistry, Biochemistry and Applications - Structure of Cellulose and its Relation to Properties of Cellulose Fibers*, pages 3–25. Ellis Horwood, 1985.

C.-S. Lee, F. Haghighat, and W.S. Ghaly. A study on VOC source and sink behaviour in porous building materials - analytical model development and assessment. *Indoor Air*, 15:183–196, 2005.

JC Little, AT Hodgson, and AJ Gadgil. Modeling emission of volatile organic compounds from new carpets. *Atmospheric Environment*, 28:227–234, 1994.

Tomasz Lojewski, Katarzyna Zieba, Arkaduisz Knapik, Jacek Bagniuk, Anna Lubanska, and Joanna Lojewska. Evaluating paper degradation progress. cross-linking between chromatographic, spectroscopic and chemical results. *Applied Physics At*, 100:809–821, 2010.

G A Lugg. Diffusion coefficients of some organic and other vapors in air. *Analytical Chemistry*, 40: 1072–1077, 1968.

Mathworks. http://www.mathworks.co.uk/, January 2013.

K. McLaren. The development of the CIE 1976 (L*a*b*) uniform colour-space and colour-difference formula. *JSDC*, pages 338–341, 1976.

Eva Menart, Gerrit de Bruin, and Matija Strlic. Dose-response functions for historic paper. *Polymer Degradation and Stability*, 96:2029–2039, 2011.

Micromeritics. http://www.micromeritics.com/Product-Showcase/TriStar-II-Series.aspx, February 2012.

M J Moura, P J Ferreira, and M M Figueiredo. Mercury intrusion porosimetry in pulp and paper technology. *Powder Technology*, 160:61–66, 2005.

S. Murakami, S. Kato, K. Ito, and Q. Zhu. Modeling and CFD prediction for diffusion and adsorption within room with various adsorption isotherms. *Indoor Air*, 13:20–27, 2003.

John W. Nicholson. *The Chemistry of Polymers - 1.4.15 Cellulose*, pages 18–19. RSC Publishing, 3rd edition, 2006a.

John W. Nicholson. *Chemistry of Polymers - 8.5 Weathering of Polymers*, pages 121–123. RSC Publishing, 3rd edition, 2006b.

K.te Nijenhuis and D.W.van Krevelen. *Properties of polymers - Chapter 2: Typology of polymers*, pages 7–33. Elsevier, 4th edition, 2009a.

K.te Nijenhuis and D.W.van Krevelen. *Properties of Polymers - Chapter 22.7 Chemical Degradation*, page 783. 2009b.

M.A. Paltakari and J.T. Karlsson. Determination of specific heat for dry fibrematerial. *CPPA Technical Section 82nd Annual meeting*, pages B117–B120, 1996.

Sunkyu Park, Richard A. Venditti, Hasan Jameel, and Joel J Pawlak. Changes in pore size distribution during the drying of cellulose fibers as measured by differential scanning calorimetry. *Carbohydrate Polymers*, 66:97–103, 2006.

A Payen. Memoir on the composition of the tissue of plants of woody material. *CR*, 7:1052–1056, 1838.

PSEnterprise. http://www.psenterprise.com/modelbuilder.html, January 2013.

Olivier Ramalho, Anne-Laurence Dupont, Celine Egasse, and Anges Lattuati-Derieux. Emissions rates of volatile organic compounds from paper. *Preservation Sceince*, 6:53–59, 2009.

Gregory L. Rorrer, James R. Welty, Charles E. Wicks, and Robert E. Wilson. *Fundamentals of Momentum, Heat, and Mass Transfer - Fundamentals of Mass Transfer*, pages 421–456. John Wiley and Sons, 4th edition, 2001a.

Gregory L. Rorrer, James R. Welty, Charles E. Wicks, and Robert E. Wilson. *Fundamentals of Momentum, Heat, and Mass Transfer - Convective Mass Transfer*, pages 550–585. John Wiley and Sons, 4th edition, 2001b.

Gregory L. Rorrer, James R. Welty, Charles E. Wicks, and Robert E. Wilson. *Fundamentals of Momentum, Heat, and Mass Transfer - 30 Convective Mass-Transfer Correlations*, pages 605–644. John Wiley and Sons, 4th edition, 2001c.

SCAN-CM 15:88. Viscosity in Cupri-EthyleneDiamine Solution, Scandinavian pulp, paper and board testing commitee. 1988.

Gerald Scott and Dan Gilead. *Degradable Polymers: principles and applications - Chapter 3: Techniques and mechanisms of polymer degradation*, pages 29–42. Springer, 1995.

Chandru Shahani, Frank Hengemihle, and Norman Weberg. *Historic Textile and Paper Materials II, American Chemical Society - The Effect of Variation in Relative Humidity on the Accelerated Aging of Paper*, pages 63–80. 1989.

K.S.W. Sing, D.H. Everett, R.A.W. Haul, L. Moscou, R.A. Pierotti, J. Rouquerol, and T. Siemieniewska. Reporting physisorption data for gas/solid systems. *Pure and Applied Chemistry*, 57: 603–619, 1985.

Karel Soukup, Petr Schneider, and Olga Solcova. Comparison of wicke-kallenbach and graham's diffusion cells for obtaining transport characteristics of porous solids. *Chemical Engineering Science*, 63: 1003–1011, 2008.

O. Sparkman, Z. Penton, and F. Kitson. *Gas Chromatography and Mass Spectrometry - 2.2.3*, pages 36–43. Academic Press, 2nd edition, 2011.

L.E. Sparks, B.A. Tichenor, J. Chang, and Z. Guo. Gas-phase mass transfer model for predicting volatile organic compound (VOC) emission rates from indoor pollutant source. *Indoor Air*, 6:31–40, 1996.

Warren E. Stewart, Edwin N. Lightfoot, and R.Byron Bird. *Transport Phenomena - Ch17 Diffusivity and the Mechanisms of Mass Transport*, pages 513–542. John Wiley and Sons, 2nd edition, 2007a.

Warren E. Stewart, Edwin N. Lightfoot, and R.Byron Bird. *Transport Phenomena - 24.6 Mass Transport in Porous Media*, pages 793–797. John Wiley and Sons, 2nd edition, 2007b.

Warren E. Stewart, Edwin N. Lightfoot, and R.Byron Bird. *Transport Phenomena - 22.8 Transfer Coefficients at High Net Mass Transfer*, pages 703–715. John Wiley and Sons, 2nd edition, 2007c.

Warren E. Stewart, Edwin N. Lightfoot, and R.Byron Bird. *Transport Phenomena - Appendix E*, pages 864–866. John Wiley and Sons, 2nd edition, 2007d.

Warren E. Stewart, Edwin N. Lightfoot, and R.Byron Bird. *Transport Phenomena - Ch17 Diffusivity and the Mechanisms of Mass Transport*, pages 524–527. John Wiley and Sons, 2nd edition, 2007e.

M. Strlic and J. Kolar. *Ageing and stabilisation of paper - Chapter 1: Paper and Durability*, pages 3–8. 2005a.

M. Strlic and J. Kolar. *Ageing and stabilisation of paper - Figure 1.2: A simplified scheme of factors affecting paper stability*, page 7. 2005b.

M. Strlic and J. Kolar. *Ageing and stabilisation of paper - Chapter 10: Air pollution and its prevention*, pages 165–177. 2005c.

M. Strlic and J. Kolar. *Ageing and stabilisation of paper - Chapter 6: Acid-catalysed degradation*, pages 106–107. 2005d.

M. Strlic, J. Kolar, D. Kocar, T. Drnovsek, V.-S. Selih, R. Susic, and B. Pihlar. What is the pH of alkaline paper? *e-PS*, 1:35–47, 2004.

M. Strlic, I. Spulber, M. Britton, M. Cassar, and S. Maddison. Environmental monitoring with wireless intelligent sensor systems - heritage intelligence - somerset, new jersey. Eastern Analytical Symposium and Exposition, November 2009a.

Matija Strlic, Jacob Thomas, Tanja Trafela, Linda Csefalvayova, Irena Kralj Cigic, Jana Kolar, and May Cassar. Material degradomics on the smell of old books. *Analytical Chemistry*, 81:8617–8622, 2009b.

Matija Strlic, Eva Menart, Irena Kralj, Jana Kolar, Gerrit de Bruin, and May Cassar. Emission of reactive oxygen species during degradation of iron gall ink. *Polymer Degradation and Stability*, 95: 66–71, 2010.

Matija Strlic, Irena Kralj Cigic, Alenka Mozir, Gerrit de Bruin, Jana Kolar, and May Cassar. The effect of volatile organic compounds and hypoxia on paper degradation. *Polymer Degradation and Stability*, 96:608–615, 2011.

Franciska Sundholm and Maria Tahvanainen. Preparation of cellulose samples for size-exclusion chromatography analyses in studies of paper degradation. *Journal of Chromatography*, 1008:129–134, 2003.

M. Suzuki and J. M. Smith.

Swagelok. Snoop liquid leak detector. http://www.swagelok.com/products/leak-detectors-lubricants-sealants/snoop-liquid-leak-detector.aspx, March 2012.

TAPPI T 509 Om-02. Hydrogen Ion Concentration (pH) of Paper Extracts (Cold Extraction Method).

TAPPI T 553 Om-00. Alkalinity of Paper as Calcium Carbonate (Alkaline Reserve of Paper).

Ross Taylor and R. Krishna. *Multicomponent Mass Transfer - Preliminary Concepts*, pages 3–12. John Wiley and Sons, 1993a.

Ross Taylor and R. Krishna. *Multicomponent Mass Transfer - The Maxwell-Stefan Realtions*, pages 13–49. John Wiley and Sons, 1993b.

Ross Taylor and R. Krishna. *Multicomponent Mass Transfer - Fick's Law*, pages 50–66. John Wiley and Sons, 1993c.

Ross Taylor and R. Krishna. *Multicomponent Mass Transfer - Film Theory*, pages 152–219. John Wiley and Sons, 1993d.

Tenax TA information. http://www.sisweb.com/index/referenc/bv-acids.htm, May 2013.

A.L. Tiffonnet, P. Blondeau, F. Allard, and F. Haghighat. Sorption isotherms of acetone on various building materials. *Indoor+Built Environment*, 11:95–104, 2002.

ToolBase.org. Low - or No-VOC Paints, Finishes and adhesives. http://www.toolbase.org/Building-Systems/Interior-Partitions-Ceilings/low-voc-paints, January 2011.

E. Uhde, A. Borgschulte, and T. Salthammer. Characterization of the field and laboratory emission cell-FLEC: Flow field and air velocities. *Atmospheric Environment*, 32, 1998.

Josef Valus and Petr Schneider. A novel cell for gas-counterdiffusion measurements in porous pellets. *Applied Catalysis*, 1:355–366, 1981.

Vatican Library. http://www.vaticanlibrary.va, December 2010.

XinKe Wang and YinPing Zhang. General analytical mass transfer model for VOC emissions from multi-layer dry building materials with internal chemical reactions. *Chinese Science Bulletin*, 56: 222–228, 2011.

Nyoman Wistara and Raymond A. Young. Properties and treatments of pulps from recycled paper: Part 1. physical and chemical properties of pulps. *Cellulose*, 6:291–324, 1999.

P Wolkoff. Volatile organic compounds: sources, measurements, emissions and the impact on indoor air quality. *Indoor Air*, 3:9–73, 1995.

Richard Wright, Matthew Addis, and Ant Milleri. The significance of storage in the cost of risk of digital preservation. http://www.bl.uk/ipres2008, 2008.

Jianyin Xiong, Cong Liu, and Yinping Zhang. A general analytical model for formaldehyde and VOC emission/sorption in single-layer building materials and its application in determining the characteristic parameters. *Atmospheric Environment*, 47:288–294, 2012.

X. Yang, Q. Chen, J.S. Zhang, R. Magee, J. Zeng, and C.Y. Shaw. Numerical simulation of VOC emissions from dry materials. *Building and Environment*, 36:1099–1107, 2001.

Gordon R Youngquist. Diffusion and flow of gases in porous solids. *Industrial and Engineering Chemistry*, 62:52–63, 1970.

L.Z. Zhang and J.L. Niu. Modeling VOCs emissions in a room with a single-zone multi-component multi-layer technique. *Building and Environment*, 39:523–531, 2004.

X. Zou, N. Gurnagul, T. Uesaka, and J. Bouchard. Accelerated aging of papers of pure cellulose: mechanism of cellulose degradation and paper embrittlement. *Polymer Degradation and Stability*, 43:393–402, 1994.

X. Zou, T. Uesaka, and N. Gurnagul. Prediction of paper permanence by accelerated aging 1. kinetic analysis of the aging process. *Cellulose*, 3:243–267, 1996.

Appendix A

Experimental results data

In this appendix we have the experimental data from the three sets of experiments performed in Chapter 5. First we have the BET machine data, followed by the diffusion cell data and finally the adsorption data.

A.1   BET data

First we present the raw data from the BET machine and then the values after being converted using the paper samples' densities.

A.1.1   BET raw results

Time (hours)	Surface Area (m^2/g)	Pore Volume (cm^3/g)	Pore Size (Å)
3	1.7355	0.005240	120.7764
3	1.7977	0.005359	119.2465
3	1.8608	0.005475	117.6649
6	1.8657	0.006179	132.4787
6	1.8769	0.006221	132.5788
6	1.9351	0.006331	130.8696
15	3.8663	0.013581	140.5071
15	4.6473	0.015927	137.0903
15	4.1754	0.014258	136.5847

Table A.1: Sample A raw results

Time (hours)	Surface Area (m^2/g)	Pore Volume (cm^3/g)	Pore Size (Å)
3	1.7694	0.005005	113.1457
3	1.8179	0.005070	111.5585
3	1.7992	0.005170	114.9361
6	1.7312	0.004912	113.4983
6	1.8039	0.004987	110.5807
6	1.7626	0.005000	113.4584
15	1.4901	0.003944	105.8674
15	1.4572	0.003811	104.6248
15	1.4784	0.003821	103.3830

Table A.2: Sample B raw results

Time (hours)	Surface Area (m^2/g)	Pore Volume (cm^3/g)	Pore Size (Å)
3	1.7863	0.004518	101.1801
3	1.7725	0.004549	102.6538
3	1.7893	0.004462	99.7366
6	1.6737	0.004556	108.8893
6	1.6883	0.004617	109.3939
6	1.6671	0.004489	107.7083
15	1.6859	0.004613	109.443
15	1.6795	0.004553	108.4345
15	1.6837	0.004460	105.9633

Table A.3: Sample C raw results

Time (hours)	Surface Area (m^2/g)	Pore Volume (cm^3/g)	Pore Size (Å)
3	1.5201	0.004552	119.7857
3	1.5132	0.004632	122.4531
3	1.4615	0.004404	120.5250
6	x	x	x
6	1.3325	0.004025	120.8354
6	1.3648	0.004091	119.9059
15	x	x	x
15	x	x	x
15	1.5579	0.003934	101.0077

Table A.4: Sample D raw results

For Sample D in Table A.4, the "x" values represent readings that had an experimental error.

A.1.2   BET converted data

The BET raw data was converted using the information given in Table 5.1 from Chapter 5. The converted data is given with the standard deviations (S.D.).

Time (hours)	Surface Area (m^2/m^3)	Pore Volume (m^3/m^3)	Pore Size (m)
3	1353733	0.004087	1.2078E-8
3	1402251	0.004180	1.1925E-8
3	1451471	0.004271	1.1766E-8
S.D.	*48867*	*9.2E-05*	*1.6E-10*
6	1455293	0.004820	1.3248E-8
6	1464023	0.004853	1.3258E-8
6	1509426	0.004938	1.3087E-8
S.D.	*29062*	*6.1E-05*	*9.6E-11*
15	3015811	0.010594	1.4051E-8
15	3625010	0.012423	1.3709E-8
15	3256916	0.011122	1.3658E-8
S.D.	*306798*	*9.4*E-04	*2.1E-10*

Table A.5: Sample A converted results

Time (hours)	Surface Area (m^2/m^3)	Pore Volume (m^3/m^3)	Pore Size (m)
3	1431511	0.0040449	1.1315E-8
3	1470750	0.004102	1.1156E-8
3	1455620	0.004183	1.1494E-8
S.D.	*19790*	*6.7E-05*	*1.7E-10*
6	1400606	0.003974	1.1350E-8
6	1459423	0.004035	1.1058E-8
6	1426010	0.004045	1.1346E-8
S.D.	*29499*	*3.8E-05*	*1.7E-10*
15	1205547	0.003191	1.0587E-8
15	1178930	0.003083	1.0462E-8
15	1196081	0.003091	1.0338E-8
S.D.	*13492*	*6.0E-05*	*1.2E-10*

Table A.6: Sample B converted results

Time (hours)	Surface Area (m²/m³)	Pore Volume (m³/m³)	Pore Size (m)
3	1425119	0.003655	1.0118E-8
3	1414109	0.003680	1.0265E-8
3	1427512	0.003610	9.9737E-9
S.D.	*7148*	*3.6E-05*	*1.5E-10*
6	1335286	0.003686	1.0889E-8
6	1346934	0.003735	1.0939E-8
6	1330020	0.003632	1.0771E-8
S.D.	*8655*	*5.2E-05*	*8.7E-11*
15	1345019	0.003732	1.0944E-8
15	1339913	0.003684	1.0843E-8
15	1343264	0.003608	1.0596E-8
S.D.	*2594*	*6.2E-05*	*1.8E-10*

Table A.7: Sample C converted results

Time (hours)	Surface Area (m²/m³)	Pore Volume (m³/m³)	Pore Size (m)
3	964204.5	0.002887	1.1979E-8
3	959827.8	0.002938	1.2245E-8
3	927034.3	0.002793	1.2053E-8
S.D.	*20315*	*7.3E-05*	*1.4E-10*
6	x	x	x
6	845209.2	0.002553	1.2084E-8
6	865697.2	0.002595	1.1991E-8
S.D.	*14487*	*3.0E-05*	*6.6E-11*
15	x	x	x
15	x	x	x
15	988181.1	0.002495	1.0101E-8

Table A.8: Sample D converted results

A.2 Diffusion cell data

Here we have the calibration data for the Mass Flow Controllers (MFC) and the Gas Chromatography (GC) machine, followed by the recorded results of each sample. Then these results are used with the equations given in Chapter 5, Section 5.3.2 to give us the tortuosity results. Finally, these results are used to get the diffusion coefficients for acetic acid for our samples.

The MFCs are made by Bronkhorst. The GC is a Shimadzu GC-2014 with dual injector FID TCD and the software used is Shimadzu GCSolution. The column used in the GC is a Concentric dual core packed column Alltech 8700 CTR 1. The columns has two packings, one to separate permanent gases, and the other separates carbon dioxide and water. The gilibrator is a Gilian Gilibrator 2.

The equations for converting the results are given in Chapter 5, Section 5.3.2.

A.2.1 Calibration data

The MFC was set computationally, and then read using a gilibrator. The gilibrator measures the mass flow 10 times and then gives an average. The flow rates are given in standard cubic centimetres per minute (sccm). These values were then used to create the calibration curves.

Set value	Nitrogen (mixture)	Hydrogen	Nitrogen (carrier)
2.5	2.891	7.035	2.771
5	5.484	11.07	5.51
7.5	8.133	14.99	8.148
10	10.82	19.23	10.8
15	16.2	27.35	15.99
20	21.7	35.42	21.52
25	27.04	43.82	26.92
30	32.44	52.43	32.31
35	38.09	60.65	37.81
40	43.59	69.3	43.17
45	49.11	78.31	48.58
50	54.45	87.26	53.96
55	59.77	95.97	59.35
60	65.55	104.9	64.55
65	70.69	114.4	70
70	75.94	123.2	75.16
75	81.26	132.7	80.44
80	86.9	142.3	85.75
85	91.98	152.4	91.15
90	97.22	162.3	96.54
95	102.8	170.8	101.7
100	108.3	183.1	107.1

Table A.9: Mass flow controller calibration results

The GC results gave three peaks, the first peak was the nitrogen peak, the second was the hydrogen peak and the third was due the two gases not separating in one of the two packings present in the column. These results were then used to create the calibration curve.

N (set)	N (actual)	H (set)	H (actual)	Peak 1	2	3	% H
100	108.45	0	0	65185	0	194457	0
97.5	105.74	2.5	6.764	112535	157128	186053	6.0122
97	105.2	3	7.593	114530	163166	184873	6.7321
96.5	104.65	3.5	8.422	119399	180123	185160	7.4484
96	104.11	4	9.252	126872	204255	182695	8.1610
95.5	103.57	4.5	10.081	128611	210559	180959	8.8701
95	103.03	5	10.910	132861	225477	180336	9.5755
94.5	102.49	5.5	11.739	137428	240366	178652	10.2775
94	101.94	6	12.569	142382	256982	178336	10.9759
93.5	101.4	6.5	13.398	147221	272947	178010	11.6708
93	100.96	7	14.227	152030	289322	179094	12.3623
92.5	100.32	7.5	15.056	156522	303658	176215	13.0503
92	99.774	8	15.886	160845	318861	176739	13.7349
91.5	99.232	8.5	16.715	165637	334181	175395	14.4161
91	98.69	9	17.544	170230	349516	174509	15.0939
90.5	98.147	9.5	18.374	174955	364897	175525	15.7684
90	97.605	10	19.203	179594	380136	173801	16.4396

Table A.10: GC calibration area results

A.2.2 Sample results

The ratios given in the tables are the ones set computationally for the MFCs. The real values are found using the calibration curves. Sample D's 97.5/2.5 results given in Table A.14 are erroneous. The *Total*, *H* and *N* columns are in sccm.

		%H	Total	H	N
	Mix In	5.65	116	6.55	109.45
97.5/2.5	Out 1	4.84	115.4	5.59	109.81
	Out 2	0.75	56.27	0.42	55.85

		%H	Total	H	N
	Mix In	9.24	117.5	10.86	106.64
95/5	Out 1	7.96	116	9.24	106.76
	Out 2	1.66	56.66	0.94	55.72

		%H	Total	H	N
	Mix In	12.68	118.9	15.08	103.82
92.5/7.5	Out 1	10.96	117	12.82	104.18
	Out 2	2.59	56.99	1.47	55.52

		%H	Total	H	N
	Mix In	16.05	119.7	19.21	100.49
90/10	Out 1	14.03	117.8	16.52	101.27
	Out 2	3.57	57.5	2.05	55.45

Table A.11: Sample A flow rate results

		%H	Total	H	N
	Mix In	5.65	115.9	6.55	109.36
97.5/2.5	Out 1	4.84	115.6	5.59	110.01
	Out 2	0.68	56.09	0.38	55.71

		%H	Total	H	N
	Mix In	9.18	117.6	10.79	106.81
95/5	Out 1	8.00	116.3	9.31	106.99
	Out 2	1.51	56.36	0.85	55.51

		%H	Total	H	N
	Mix In	12.64	118.7	15.00	103.70
92.5/7.5	Out 1	11.06	116.9	12.93	103.97
	Out 2	2.46	57.58	1.42	56.14

		%H	Total	H	N
	Mix In	16.01	119.9	19.20	100.70
90/10	Out 1	14.09	118	16.62	101.38
	Out 2	3.43	57.92	1.99	55.93

Table A.12: Sample B flow rate results

		%H	Total	H	N
	Mix In	5.68	115.3	6.55	108.75
97.5/2.5	Out 1	4.77	114.4	5.45	108.95
	Out 2	0.93	56.92	0.53	56.39

		%H	Total	H	N
	Mix In	9.18	116.6	10.70	105.90
95/5	Out 1	7.78	115.6	9.00	106.60
	Out 2	1.94	57.62	1.12	56.50

		%H	Total	H	N
	Mix In	12.63	117.9	14.89	103.07
92.5/7.5	Out 1	10.79	116.2	12.53	103.67
	Out 2	3.02	58.02	1.75	56.27

		%H	Total	H	N
	Mix In	15.96	119.3	19.04	100.26
90/10	Out 1	13.76	117.3	16.14	101.16
	Out 2	4.07	58.47	2.38	56.09

Table A.13: Sample C flow rate results

		%H	Total	H	N
	Mix In	5.67	111	**6.29**	104.71
97.5/2.5	Out 1	3.52	109.4	**3.85**	105.55
	Out 2	1.50	52.91	**0.79**	52.12

		%H	Total	H	N
	Mix In	9.36	112.2	10.51	101.69
95/5	Out 1	7.46	110.6	8.25	102.35
	Out 2	2.81	54.07	1.52	52.55

		%H	Total	H	N
	Mix In	12.90	113.7	14.67	99.03
92.5/7.5	Out 1	10.34	110.9	11.47	99.43
	Out 2	4.46	54.31	2.42	51.89

		%H	Total	H	N
	Mix In	16.15	115.1	18.59	96.51
90/10	Out 1	13.03	111.6	14.54	97.06
	Out 2	5.75	56.56	3.25	53.31

Table A.14: Sample D flow rate results

A.2.3   Tortuosity results

As a consequence of the erroneous data in Table A.14, The first result for Sample D in Table A.15 is also erroneous.

%H	A	B	C	D
5.65	41.09	40.62	33.92	**4.92**
9.24	41.95	47.39	36.91	23.53
12.68	40.18	44.99	36.05	23.15
16.05	38.64	40.53	33.15	21.61

Table A.15: Sample A tortuosity results

A.2.4   Acetic acid diffusion results

The first line for the results in Sample D in Table A.19 are erroneous due to the problem from Table A.15.

Tortuosity	D_{ve} (m^2/s)
41.09	1.18E-10
41.95	1.16E-10
40.18	1.21E-10
38.34	1.26E-10

Table A.16: Sample A effective diffusion coefficient results

Tortuosity	D_{ve} (m^2/s)
40.62	1.12E-10
47.39	9.63E-11
44.99	1.01E-10
40.53	1.13E-10

Table A.17: Sample B effective diffusion coefficient results

Tortuosity	D_{ve} (m^2/s)
33.92	1.08E-10
36.91	9.90E-11
36.05	1.01E-10
33.15	1.10E-10

Table A.18: Sample C effective diffusion coefficient results

Tortuosity	D_{ve} (m^2/s)
4.92	**6.87E-10**
23.53	1.44E-10
23.15	1.46E-10
21.61	1.57E-10

Table A.19: Sample D effective diffusion coefficient results

A.3 Adsorption data

First we have the raw results from the adsorption experiment and then the converted data giving the gas phase and adsorbed phase concentrations for the adsorption isotherms.

A.3.1 Raw results

For each calibration results, we have the amount injected in μL, the predicted ppm of propionic acid in the jar, and the reading from the sensors in ppm in the jar. For the test results, we again have the amount injected in μL, then we have the reading in ppm, and then the converted ppm using the calibration data. Some of the calibration results sets are repeated as more than one test was done in one day and so the same calibration data was used.

Sensor 1 refers to the first jar with a sensor in it, and Sensor 2 to the second jar.

Set 1	Calibration			Test		
	Amount	**Predicted**	**Reading**	**Amount**	**Reading**	**Converted**
Sensor 1	0	0	1643.80	0	1659.67	0
	40	20.81	1837.13	40	1757.00	7.12
	80	41.62	2138.25	80	1821.17	11.82
	120	62.42	2477.95	120	1879.78	16.11
Sensor 2	0	0	1599.25	0	1636.18	0
	40	20.81	1957.14	40	1762.27	5.61
	80	41.62	2438.50	80	1881.56	10.91
	120	62.42	2985.60	120	2022.83	17.19
Set 2	**Calibration**			**Test**		
	Amount	**Predicted**	**Reading**	**Amount**	**Reading**	**Converted**
Sensor 1	0	0	1606.06	0	1628.42	0
	30	15.61	1784.17	40	1697.70	5.04
	60	31.21	2029.67	80	1744.89	8.47
	90	46.82	2237.07	120	1911.83	20.61
Sensor 2	0	0	1598.80	0	1608.63	0
	30	15.61	1868.92	40	1742.50	6.34
	60	31.21	2206.90	80	1822.36	10.13
	90	46.82	2578.70	120	1913.00	14.42
Set 3	**Calibration**			**Test**		
	Amount	**Predicted**	**Reading**	**Amount**	**Reading**	**Converted**
Sensor 1	0	0	1606.09	0	1646.00	0
	30	15.61	1757.57	40	1695.57	4.14
	60	31.21	1955.33	80	1747.50	8.47
	90	46.82	2160.44	120	1786.09	11.70
Sensor 2	0	0	1632.00	0	1625.21	0
	30	15.61	1910.90	40	1707.64	4.18
	60	31.21	2216.22	80	1792.39	8.47
	90	46.82	2554.50	120	1868.24	12.35

Table A.20: Sample A adsorption results

Set 1	Calibration			Test		
	Amount	Predicted	Reading	Amount	Reading	Converted
Sensor 1	0	0	1622.20	0	1639.82	0
	30	15.61	1738.40	40	1645.50	0.56
	60	31.21	1910.75	80	1654.00	1.39
	90	46.82	2089.13	120	1693.82	5.31
Sensor 2	0	0	1612.25	0	1677.64	0
	30	15.61	1830.80	40	1730.75	3.11
	60	31.21	2111.00	80	1768.36	5.31
	90	46.82	2404.39	120	1779.08	5.93
Set 2	Calibration			Test		
	Amount	Predicted	Reading	Amount	Reading	Converted
Sensor 1	0	0	1628.86	0	1636.80	0
	30	15.61	1774.11	40	1655.43	1.68
	60	31.21	1958.70	80	1707.38	6.35
	90	46.82	2143.67	120	1724.70	7.91
Sensor 2	0	0	1604.67	0	1658.64	0
	30	15.61	1840.42	40	1711.80	2.98
	60	31.21	2130.91	80	1753.07	5.29
	90	46.82	2435.38	120	1780.00	6.79
Set 3	Calibration			Test		
	Amount	Predicted	Reading	Amount	Reading	Converted
Sensor 1	0	0	1608.60	0	1632.10	0
	30	15.61	1726.08	40	1636.90	0.59
	60	31.21	1857.87	80	1659.88	3.43
	90	46.82	1985.20	120	1686.09	6.68
Sensor 2	0	0	1579.94	0	1622.08	0
	30	15.61	1760.93	40	1665.70	2.98
	60	31.21	2017.88	80	1688.11	4.51
	90	46.82	2252.21	120	1726.07	7.10

Table A.21: Sample B adsorption results

Set 1	Calibration			Test		
	Amount	Predicted	Reading	Amount	Reading	Converted
Sensor 1	0	0	1588.17	0	1568.33	0
	30	15.61	1664.56	40	1563.77	-0.75
	60	31.21	1774.38	80	1593.79	4.19
	90	46.82	1866.29	120	1602.05	5.55
Sensor 2	0	0	1565.75	0	1600.91	0
	30	15.61	1711.89	40	1602.23	0.012
	60	31.21	1887.72	80	1633.80	2.99
	90	46.82	2078.29	120	1664.46	5.77
Set 2	Calibration			Test		
	Amount	Predicted	Reading	Amount	Reading	Converted
Sensor 1	0	0	1588.17	0	1616.39	0
	30	15.61	1664.56	40	1613.56	-0.47
	60	31.21	1774.38	80	1630.00	2.24
	90	46.82	1866.29	120	1643.57	4.47
Sensor 2	0	0	1565.75	0	1591.33	0
	30	15.61	1711.89	40	1609.92	1.69
	60	31.21	1887.72	80	1647.39	5.09
	90	46.82	2078.29	120	1678.31	7.89
Set 3	Calibration			Test		
	Amount	Predicted	Reading	Amount	Reading	Converted
Sensor 1	0	0	1586.46	0	1599.80	0
	30	15.61	1695.07	40	1619.86	2.26
	60	31.21	1837.63	80	1655.67	6.30
	90	46.82	1996.79	120	1699.64	11.27
Sensor 2	0	0	1587.50	0	1603.33	0
	30	15.61	1813.63	40	1634.10	1.81
	60	31.21	2086.60	80	1690.83	5.15
	90	46.82	2376.80	120	1756.33	9.01

Table A.22: Sample C adsorption results

Set 1	Calibration			Test		
	Amount	Predicted	Reading	Amount	Reading	Converted
Sensor 1	0	0	1621.21	0	1605.11	0
	30	15.61	1707.83	40	1613.00	1.02
	60	31.21	1837.17	80	1645.80	5.24
	90	46.82	1977.64	120	1667.73	8.07
Sensor 2	0	0	1627.70	0	1574.25	0
	30	15.61	1795.67	40	1629.33	4.44
	60	31.21	1988.33	80	1697.31	9.92
	90	46.82	2206.89	120	1762.53	15.17

Set 2	Calibration			Test		
	Amount	Predicted	Reading	Amount	Reading	Converted
Sensor 1	0	0	1602.08	0	1625.46	0
	30	15.61	1716.33	40	1660.00	4.04
	60	31.21	1856.70	80	1701.30	8.87
	90	46.82	1998.75	120	1752.56	14.87
Sensor 2	0	0	1608.17	0	1587.14	0
	30	15.61	1809.00	40	1681.00	6.79
	60	31.21	2025.91	80	1766.85	13.00
	90	46.82	2254.43	120	1853.38	19.26

Set 3	Calibration			Test		
	Amount	Predicted	Reading	Amount	Reading	Converted
Sensor 1	0	0	1602.08	0	1581.90	0
	30	15.61	1716.33	40	1623.00	4.81
	60	31.21	1856.70	80	1674.78	10.87
	90	46.82	1998.75	120	1847.31	31.06
Sensor 2	0	0	1608.17	0	1580.33	0
	30	15.61	1809.00	40	1671.91	6.62
	60	31.21	2025.91	80	1762.39	13.17
	90	46.82	2254.43	120	1847.31	19.31

Table A.23: Sample D adsorption results

Here are the properties of the samples used for each set:

Sample A	1		2		3	
	mass (g)	m^2	mass (g)	m^2	mass (g)	m^2
Sensor 1	2.48	4.46	2.41	4.33	2.47	4.45
Sensor 2	2.52	4.52	2.51	4.51	2.51	4.52
Sample B	1		2		3	
	mass (g)	m^2	mass (g)	m^2	mass (g)	m^2
Sensor 1	2.19	3.93	2.46	4.42	2.60	4.68
Sensor 2	2.46	4.41	2.46	4.41	2.68	4.82
Sample C	1		2		3	
	mass (g)	m^2	mass (g)	m^2	mass (g)	m^2
Sensor 1	2.15	3.84	2.19	3.90	2.20	3.93
Sensor 2	2.14	3.82	2.18	3.90	2.16	3.85
Sample D	1		2		3	
	mass (g)	m^2	mass (g)	m^2	mass (g)	m^2
Sensor 1	2.48	3.71	2.47	3.69	2.51	3.76
Sensor 2	2.42	3.62	2.36	3.54	2.44	3.66

Table A.24: Sample details

A.3.2 Converted data

The converted data has first the total mols in both the gas phase and adsorbed phase in the jar, then the total mols in the gas phase, followed by the adsorbed phase. We then give the concentration in mol/m^3 in the gas phase and in mol/m^2 in the adsorbed phase.

Set 1	Total			Concentration	
	Total	Gas	Ads	Gas	Adsorbed
Sensor 1	0	0	0	0	0
	4.28E-6	1.47E-6	2.82E-6	0.00030	6.31E-7
	8.56E-6	2.43E-6	6.13E-6	0.00049	1.37E-6
	1.28E-5	3.31E-6	9.53E-6	0.00066	2.14E-6
Sensor 2	0	0	0	0	0
	4.28E-6	1.15E-6	3.13E-6	0.00023	6.92E-7
	8.56E-6	2.24E-6	6.32E-6	0.00045	1.40E-6
	1.28E-5	3.54E-6	9.31E-6	0.00071	2.06E-6
Set 2	Total			Concentration	
	Total	Gas	Ads	Gas	Adsorbed
Sensor 1	0	0	0	0	0
	4.28E-6	1.04E-6	3.24E-6	0.00021	7.50E-7
	8.56E-6	1.74E-6	6.82E-6	0.00035	1.58E-6
	1.28E-5	4.24E-6	8.60E-6	0.00085	1.99E-6
Sensor 2	0	0	0	0	0
	4.28E-6	1.31E-6	2.98E-6	0.00026	6.59E-7
	8.56E-6	2.08E-6	6.48E-6	0.00042	1.43E-6
	1.28E-5	2.97E-6	9.88E-6	0.00059	2.19E-6
Set 3	Total			Concentration	
	Total	Gas	Ads	Gas	Adsorbed
Sensor 1	0	0	0	0	0
	4.28E-6	8.51E-7	3.43E-6	0.00017	7.71E-7
	8.56E-6	1.74E-6	6.82E-6	0.00035	1.53E-6
	1.28E-5	2.41E-6	1.04E-5	0.00048	2.35E-6
Sensor 2	0	0	0	0	0
	4.28E-6	8.60E-7	3.42E-6	0.00017	7.58E-7
	8.56E-6	1.74E-6	6.82E-6	0.00035	1.51E-6
	1.28E-5	2.54E-6	1.03E-5	0.00051	2.28E-6

Table A.25: Sample A isotherm data

Set 1	Total			Concentration	
	Total	Gas	Ads	Gas	Adsorbed
Sensor 1	0	0	0	0	0
	4.28E-6	1.15E-7	4.17E-6	2.30E-5	1.06E-6
	8.56E-6	2.87E-7	8.28E-6	5.74E-5	2.10E-6
	1.28E-5	1.09E-6	1.18E-5	0.00022	2.99E-6
Sensor 2	0	0	0	0	0
	4.28E-6	6.39E-7	3.64E-6	0.00013	8.26E-7
	8.56E-6	1.09E-6	7.47E-6	0.00022	1.69E-6
	1.28E-5	1.22E-6	1.16E-5	0.00024	2.64E-6
Set 2	**Total**			**Concentration**	
	Total	Gas	Ads	Gas	Adsorbed
Sensor 1	0	0	0	0	0
	4.28E-6	3.45E-7	3.94E-6	6.9E-5	8.91E-7
	8.56E-6	1.31E-6	7.26E-6	0.00026	1.64E-6
	1.28E-5	1.63E-6	1.12E-5	0.00033	2.54E-6
Sensor 2	0	0	0	0	0
	4.28E-6	6.13E-7	3.67E-6	0.00012	8.90E-7
	8.56E-6	1.09E-6	7.47E-6	0.00022	1.69E-6
	1.28E-5	1.40E-6	1.14E-5	0.00028	2.59E-6
Set 3	**Total**			**Concentration**	
	Total	Gas	Ads	Gas	Adsorbed
Sensor 1	0	0	0	0	0
	4.28E-6	1.22E-7	4.16E-6	2.44E-5	8.90E-7
	8.56E-6	7.07E-7	7.86E-6	0.00014	1.68E-6
	1.28E-5	1.37E-6	1.15E-5	0.00028	2.45E-6
Sensor 2	0	0	0	0	0
	4.28E-6	6.13E-7	3.67E-6	0.00012	7.62E-7
	8.56E-6	9.28E-7	7.63E-6	0.00019	1.59E-6
	1.28E-5	1.46E-6	1.14E-5	0.00029	2.36E-6

Table A.26: Sample B isotherm data

Set 1	Total			Concentration	
	Total	Gas	Ads	Gas	Adsorbed
Sensor 1	0	0	0	0	0
	4.28E-6	-1.50E-7	4.44E-6	-3.10E-5	1.15E-6
	8.56E-6	8.62E-7	7.70E-6	0.00017	2.00E-6
	1.28E-5	1.14E-6	1.17E-5	0.00023	3.05E-6
Sensor 2	0	0	0	0	0
	4.28E-6	2.47E-8	4.26E-6	4.94E-6	1.12E-6
	8.56E-6	6.14E-7	7.95E-6	0.00012	2.08E-6
	1.28E-5	1.19E-6	1.17E-5	0.00024	3.06E-6

Set 2	Total			Concentration	
	Total	Gas	Ads	Gas	Adsorbed
Sensor 1	0	0	0	0	0
	4.28E-6	-9.60E-8	4.38E-6	-1.90E-5	1.12E-6
	8.56E-6	4.61E-7	8.10E-6	9.22E-5	2.08E-6
	1.28E-5	9.21E-7	1.19E-5	0.00018	3.06E-6
Sensor 2	0	0	0	0	0
	4.28E-6	3.47E-7	3.93E-6	6.94E-5	1.01E-6
	8.56E-6	1.05E-6	7.52E-6	0.00021	1.94E-6
	1.28E-5	1.62E-6	1.12E-5	0.00032	2.89E-6

Set 3	Total			Concentration	
	Total	Gas	Ads	Gas	Adsorbed
Sensor 1	0	0	0	0	0
	4.28E-6	4.66E-7	3.82E-6	9.31E-5	9.71E-7
	8.56E-6	1.30E-6	7.27E-6	0.00026	1.85E-6
	1.28E-5	2.32E-6	1.05E-5	0.00046	2.68E-6
Sensor 2	0	0	0	0	0
	4.28E-6	3.73E-7	3.91E-6	7.46E-5	1.01E-6
	8.56E-6	1.06E-6	7.50E-6	0.00021	1.95E-6
	1.28E-5	1.85E-6	1.10E-5	0.00037	2.85E-6

Table A.27: Sample C isotherm data

Set 1	Total			Concentration	
	Total	Gas	Ads	Gas	Adsorbed
Sensor 1	0	0	0	0	0
	4.28E-6	2.09E-7	4.07E-6	4.18E-5	1.10E-6
	8.56E-6	1.08E-6	7.48E-6	0.00022	20.02E-6
	1.28E-5	1.66E-6	1.12E-5	0.00033	3.01E-6
Sensor 2	0	0	0	0	0
	4.28E-6	9.13E-7	3.67E-6	0.00018	9.29E-7
	8.56E-6	2.04E-6	6.52E-6	0.00041	1.80E-6
	1.28E-5	3.12E-6	9.72E-6	0.00062	2.68E-6
Set 2	Total			Concentration	
	Total	Gas	Ads	Gas	Adsorbed
Sensor 1	0	0	0	0	0
	4.28E-6	8.23E-7	3.45E-6	0.00017	9.34E-7
	8.56E-6	1.83E-6	6.74E-6	0.00037	1.82E-6
	1.28E-5	3.06E-6	9.78E-6	0.00061	2.65E-6
Sensor 2	0	0	0	0	0
	4.28E-6	1.4E-6	2.88E-6	0.00028	8.15E-7
	8.56E-6	2.67E-6	5.89E-6	0.00054	1.66E-6
	1.28E-5	3.96E-6	8.88E-6	0.00079	2.51E-6
Set 3	Total			Concentration	
	Total	Gas	Ads	Gas	Adsorbed
Sensor 1	0	0	0	0	0
	4.28E-6	9.89E-7	3.29E-6	0.00020	8.76E-7
	8.56E-6	2.24E-6	6.33E-6	0.00045	1.68E-6
	1.28E-5	6.39E-6	6.45E-6	0.00013	1.72E-6
Sensor 2	0	0	0	0	0
	4.28E-6	1.36E-6	2.92E-6	0.00027	7.98E-7
	8.56E-6	2.71E-6	5.85E-6	0.00054	1.60E-6
	1.28E-5	3.97E-6	8.87E-6	0.00080	2.42E-6

Table A.28: Sample D isotherm data

Appendix B

gProms code

The gProms code comprises of three parts: the model, the process and the variable types.

The model includes the boundary conditions, design equations, and any initial conditions that all processes have. The model declares any constants and variables used and also defines the spatial domain.

The process gives the specifications for a simulation. It assigns values to constants which are specific to a simulation, as well as initial values for the variables. The process also defines the conditions for ending a simulation.

The variable types are where the upper and lower bounds of the variables are defined. In our case, we make sure that the variables cannot be negative.

Here we have the gProms code for the sealed fitted container at normal room conditions.

B.1 Model

```
PARAMETER

# this is a comment
# here we have the constants in the model
# the dimensions of the paper
PLength AS REAL DEFAULT 0.13 # units:  m
PWidth AS REAL DEFAULT 0.198 # units:  m
PHeight AS REAL # units:  m
# the diffusion coefficient
```

```
Dae AS REAL # units:   m2/s

# the adsorption coefficient of VOC

Kv AS REAL # units:   m

# the VOC reaction constant

kvr AS REAL

# the acid dissociation constant

Ka AS REAL

# the unit surface area

UnitSurf AS REAL # units:   m2/m3

# the porosity

Pore AS REAL # units:   m3/m3

# kDP constants

adp AS REAL DEFAULT 0.000128217

bdp AS REAL DEFAULT 0.24

# intial acidity

h0 AS REAL


DISTRIBUTION_DOMAIN


# the spatial distribution from 0 to final

Length AS (0:PLength) # z

Width AS (0:PWidth) # x

Height AS (0:PHeight) # y


VARIABLE


# the variables that change with space (and time)

Cv AS DISTRIBUTION (Length, Width, Height) OF ConcentrationVol

H AS DISTRIBUTION (Length, Width, Height) OF ConcentrationSurf

DP AS DISTRIBUTION (Length, Width, Height) OF DegreePoly

rv AS DISTRIBUTION (Length, Width, Height) OF Reaction

kdp AS DISTRIBUTION (Length, Width, Height) OF DPConst
```

```
CaCO3 AS DISTRIBUTION (Length, Width, Height) OF ConcentrationSurf

BOUNDARY

# The boundary conditions, here for a sealed fitted container
# each plane
FOR i := 0|+ TO PLength|- DO
    FOR j := 0|+ TO PWidth|- DO
        PARTIAL(Cv(i,j,0),Height)=0;
        PARTIAL(Cv(i,j,PHeight),Height)=0;
    END
END

FOR i := 0|+ TO PHeight|- DO
    FOR j := 0|+ TO PWidth|- DO
        PARTIAL(Cv(0,j,i),Length)=0;
        PARTIAL(Cv(PLength,j,i),Length)=0;
    END
END

FOR i := 0|+ TO PLength|- DO
    FOR j := 0|+ TO PHeight|- DO
        PARTIAL(Cv(i,0,j),Width)=0;
        PARTIAL(Cv(i,PWidth,j),Width)=0;
    END
END

# Edges
FOR i := 0|+ TO PLength|- DO
    PARTIAL(Cv(i,0,0),Height)=0;
    PARTIAL(Cv(i,0,PHeight),Height)=0;
    PARTIAL(Cv(i,PWidth,0),Height)=0;
```

```
        PARTIAL(Cv(i,PWidth,PHeight),Height)=0;
END

FOR i := 0|+ TO PWidth|- DO
    PARTIAL(Cv(0,i,0),Height)=0;

    PARTIAL(Cv(0,i,PHeight),Height)=0;

    PARTIAL(Cv(PLength,i,0),Height)=0;

    PARTIAL(Cv(PLength,i,PHeight),Height)=0;
END

FOR i := 0|+ TO PHeight|- DO
    PARTIAL(Cv(0,PWidth,i),Length)=0;

    PARTIAL(Cv(0,0,i),Length)=0;

    PARTIAL(Cv(PLength,0,i),Length)=0;

    PARTIAL(Cv(PLength,PWidth,i),Length)=0;
END

# Corners
PARTIAL(Cv(0,0,0),Height)=0;

PARTIAL(Cv(0,0,PHeight),Height)=0;

PARTIAL(Cv(0,PWidth,0),Height)=0;

PARTIAL(Cv(PLength,0,0),Height)=0;

PARTIAL(Cv(0,PWidth,PHeight),Height)=0;

PARTIAL(Cv(PLength,PWidth,0),Height)=0;

PARTIAL(Cv(PLength,0,PHeight),Height)=0;

PARTIAL(Cv(PLength,PWidth,PHeight),Height)=0;

EQUATION

# design equations
FOR i := 0|+ TO PLength|- DO
    FOR j := 0|+ TO PWidth|- DO
```

```
        FOR k := 0|+ TO PHeight|- DO
```

if statement for whether alkaline reserve is present at point (x,y,z)

```
            IF CaCO3(i,j,k)>0 THEN

                $Cv(i,j,k) = 0;

            ELSE

$Cv(i,j,k) = ((Dae*((Partial(Partial(Cv(i,j,k),Length),Length))

+(Partial(Partial(Cv(i,j,k),Width),Width)))

+ (Partial(Partial(Cv(i,j,k),Height),Height)))

+ (UnitSurf*rv(i,j,k))) / (Pore+(UnitSurf*Kv));

            END

        END

    END

END


FOR i := 0 TO PLength DO

    FOR j := 0 TO PWidth DO

        FOR k := 0 TO PHeight DO

            $DP(i,j,k) = -kdp(i,j,k)*(DP(i,j,k)^2);

            rv(i,j,k) = (2/(DP(i,j,k)-1))*kvr*kdp(i,j,k);

            kdp(i,j,k) = adp * (H(i,j,k)^bdp) ;

        IF CaCO3(i,j,k)>0 THEN

H(i,j,k) = h0;

$CaCO3(i,j,k) = -0.5*((Dae*((Partial(Partial(Cv(i,j,k),Length),Length))

+(Partial(Partial(Cv(i,j,k),Width),Width)))

+ (Partial(Partial(Cv(i,j,k),Height),Height)))

        ELSE

H(i,j,k) = h0 + 0.5*( -(h0+Ka) + sqrt( ((h0+Ka)^2)

+ (4*Ka*Kv*Cv(i,j,k)) ) );

$CaCO3(i,j,k) = 0;

            END

        END
```

```
        END
END

INITIAL

# the initial condition for the gas VOC concentration is always zero
# and so is specified here rather than the process
FOR i := 0|+ TO PLength|- DO
    FOR j := 0|+ TO PWidth|- DO
        FOR k := 0|+ TO PHeight|- DO
            Cv(i,j,k) = 0;
        END
    END
END
```

B.2   Process

```
UNIT

# First we define our units as our samples
# and which model they use (called ARMM here)
SampleA AS ARMM

SampleB AS ARMM

SampleC AS ARMM

SampleD AS ARMM

SET

# Here we give the values for each sample in the process
WITHIN SampleA DO
    PHeight := 0.000142;

    Dae :=0.003792395;

    Kv := 0.0032;
```

```
    kvr := 1;

    UnitSurf := 1402485;

    Pore := 0.004179;

# How the spatial domain is split and calculated

    Length := [CFDM,2,10];

    Width := [CFDM,2,10];

    Height := [CFDM,2,10];

    h0 := 7.58578E-07;

END


WITHIN SampleB DO

    PHeight := 0.000098;

    Dae := 0.003331684;

    Kv := 0.0083;

    kvr := 1;

    UnitSurf := 1452627;

    Pore := 0.004111;

    Length := [CFDM,2,10];

    Width := [CFDM,2,10];

    Height := [CFDM,2,10];

    h0 := 1.1749E-05;

END


WITHIN SampleC DO

    PHeight := 0.000108;

    Dae := 0.003297473;

    Kv := 0.0087;

    kvr := 1;

    UnitSurf := 1422247;

    Pore := 0.003648;

    Length := [CFDM,2,10];
```

```
    Width := [CFDM,2,10];

    Height := [CFDM,2,10];

    h0 := 8.51138E-09;
END


WITHIN SampleD DO

    PHeight := 0.000168;

    Dae := 0.004696568;

    Kv := 0.0031;

    kvr := 1;

    UnitSurf := 950355;

    Pore := 0.002873;

    Length := [CFDM,2,10];

    Width := [CFDM,2,10];

    Height := [CFDM,2,10];

    h0 := 0.0000001;
END

INITIAL


WITHIN SampleA DO

    FOR i := 0 TO PLength DO

        FOR j := 0 TO PWidth DO

            FOR k := 0 TO PHeight DO

                DP(i,j,k) = 1037;

                CaCO3(i,j,k) = 0;

            END

        END

    END
END


WITHIN SampleB DO
```

```
      FOR i := 0 TO PLength DO

          FOR j := 0 TO PWidth DO

              FOR k := 0 TO PHeight DO

                  DP(i,j,k) = 1330;

                  CaCO3(i,j,k) = 0;

              END

          END

      END

END


WITHIN SampleC DO

      FOR i := 0 TO PLength DO

          FOR j := 0 TO PWidth DO

              FOR k := 0 TO PHeight DO

                  DP(i,j,k) = 1916;

                  CaCO3(i,j,k) = 1618;

              END

          END

      END

END


WITHIN SampleD DO

      FOR i := 0 TO PLength DO

          FOR j := 0 TO PWidth DO

              FOR k := 0 TO PHeight DO

                  DP(i,j,k) = 2300;

                  CaCO3(i,j,k) = 0;

              END

          END

      END
```

```
END

SOLUTIONPARAMETERS

ReportingInterval := 1; # time interval recorded for

SCHEDULE

# End simulation when all samples have reached a DP of 250
CONTINUE UNTIL MIN(SampleA.DP)<250
    AND MIN(SampleB.DP)<250
        AND MIN(SampleC.DP)<250
            AND MIN(SampleD.DP)<250;
```

B.3 Variable types

Name	Lower bound	Default Value	Upper Bound
ConcentrationSurf	0.0	0.5	100000.0
ConcentrationVol	0.0	0.5	100000.0
DegreePoly	0.0	0.5	5000.0
DPconst	0.0	0.5	1E40
Reaction	0.0	0.5	1E40